University of Glasgow

Heilmann, Monika (2013) *Structure-function studies of the UV-B photoreceptor UVR8 in Arabidopsis thaliana*. PhD thesis.

http://theses.gla.ac.uk/4067/

Copyright and moral rights for this thesis are retained by the author

A copy can be downloaded for personal non-commercial research or study

This thesis cannot be reproduced or quoted extensively from without first obtaining permission in writing from the Author

The content must not be changed in any way or sold commercially in any format or medium without the formal permission of the Author

When referring to this work, full bibliographic details including the author, title, awarding institution and date of the thesis must be given

Glasgow Theses Service
http://theses.gla.ac.uk/
theses@gla.ac.uk

University of Glasgow

STRUCTURE-FUNCTION STUDIES OF THE UV-B PHOTORECEPTOR UVR8 IN *ARABIDOPSIS THALIANA*

Monika Heilmann

Submitted in fulfilment of the requirements for the degree of Doctor of Philosophy

Institute of Molecular, Cell and Systems Biology
Faculty of Biomedical and Life Sciences
University of Glasgow

January 2013

© Monika Heilmann, 2013

SUMMARY

Ultraviolet-B (UV-B) radiation is an integral component of natural sunlight reaching the Earth's surface. Although being a potentially harmful and damaging agent, UV-B is a key environmental signal for plants initiating diverse responses that affect their metabolism, development and viability. The majority of these responses involve the differential regulation of gene expression and all require accurate perception of the effective light quality by a photoreceptor. The recent identification of UV RESISTANCE LOCUS8 (UVR8) as a UV-B photoreceptor has been an important milestone in plant UV-B research (Rizzini et al., 2011; Christie et al., 2012; Wu et al., 2012). However, rather little is known yet about the precise mechanisms of photoreception and signal transduction. Therefore, the overall aim of this study was to investigate how the structure of the UVR8 protein determines its function in the UV-B response in Arabidopsis.

The mechanism of light perception by UVR8 differs from other so far characterized photoreceptors since UVR8 does not bind an external cofactor as chromophore but performs UV-B photoreception using some of its intrinsic tryptophans. To identify structurally and functionally important amino acids of UVR8, site-directed mutagenesis of a conserved and repeated motif GWRHT was carried out. The tryptophans of these motifs form the base of the postulated UV-B perceiving pyramid (Christie et al., 2012). The impact of the introduced mutations was assessed in vitro and in vivo by various methods such as size exclusion chromatography (SEC), far-UV circular dichroism (CD) spectroscopy and forms of polyacrylamide gel electrophoresis (PAGE). Results showed that in the absence of UV-B UVR8 forms a dimer that is very effectively held together by a network of cross-dimer salt bridges. Especially important for stable dimerisation were salt bridges that are located adjacent to the UV-B perceiving tryptophan pyramid, in particular those involving R286 and their disruption by mutation led to constitutive monomerisation of the photoreceptor. Several mutations resulted in a destabilized and weakened dimer which could only be detected as dimer in vitro but appeared monomeric in vivo.

The currently most upstream identified event of UV-B perception by UVR8 is its UV-B induced monomerisation which happens very rapidly and in a fluence rate dependent manner (Rizzini et al., 2011). UV-B also causes physical interaction between UVR8 and CONSTITUTIVELY PHOTOMORPHOGENIC1 (COP1) which is essential to initiate UVR8-mediated signalling (Favory et al., 2009). Stable transgenic Arabidopsis lines expressing various UVR8 salt bridge mutants as GFP-fusions in the *uvr8-1* background

were generated to analyse structural requirements of UVR8 for its interaction with COP1 and to test the photomorphogenic response with respect to UV-B induction of *ELONGATED HYPOCOTYL5* (*HY5*) and *CHALCONE SYNTHASE* (*CHS*) gene expression and suppression of hypocotyl extension. The results established that, in vivo, constitutive monomerisation and constitutive interaction with COP1 are not sufficient to initiate a UVR8-mediated response in the absence of UV-B. Furthermore, a constitutively monomeric mutant that still showed a photomorphogenic response in the presence of UV-B could be identified, suggesting that dimerisation is not required for UV-B perception and UVR8-mediated signalling in vivo.

One characteristic feature of the UV-B perceiving tryptophan pyramid is that the close proximity of the aromatic side chains allows overlap of their electronic orbitals resulting in exciton coupling of the tryptophans which could be monitored by far-UV CD spectroscopy (Christie et al., 2012). Exciton coupling was absent after UV-B induced monomerisation and was reduced in several salt bridge mutants. The close proximity of UV-B perceiving tryptophan residues to essential dimer maintaining salt bridges led to the hypothesis that electron transfer may occur between the tryptophans and adjacent salt-bridging arginines leading to charge neutralization and thus dimer destabilization and monomerisation (Christie et al., 2012). Fourier transform infrared (FTIR) spectroscopy was employed to detect UV-B induced changes in the chemical structure of the amino acid side chains and the overall conformation of the protein. However, the signals obtained in the light-induced difference spectra could not be clearly assigned to a specific process and require further experiments. Changes in the local environment of the tryptophan chromophore could be detected by fluorescence spectroscopy. Here, a UV-B induced red shift of the protein's emission spectrum was observed which shows that the initially buried tryptophan pyramid becomes solvent exposed, which is consistent with UV-B induced monomerisation. UV-B induced conformational changes of the photoreceptor's C-terminus were revealed by limited proteolysis experiments. The pattern of peptides produced by mild trypsin digestion of UVR8, which are derived from the C-terminus, changes after UV-B exposure suggesting that UV-B not only induces monomerisation but also conformational changes in the C-terminus that lead to changes in its accessibility. Those changes are required for activation of the signalling pathway as seen in vivo.

Finally, to allow regulation of UVR8 signal transduction and an optimally balanced UV-B response, the activated monomeric form must return to its homodimeric ground state once UV-B is no longer present. This process had so far not been investigated and therefore the kinetics of dimer regeneration were analysed in various Arabidopsis genotypes and under

influence of a protein synthesis inhibitor as well as an inhibitor of proteasomal activity. The level of total UVR8 protein remained unchanged in the presence of these inhibitors and also the kinetics of dimer regeneration were only slightly affected, which suggests that regeneration of dimeric UVR8 occurs by reversion from the monomer to the dimer. Regeneration of the UVR8 dimer was also possible in vitro with illuminated plant extract or purified UVR8 but was considerably slower, suggesting that the presence of intact cells is required. The absence of the C-terminus, which is known to interact with COP1 and REPRESSOR OF UV-B PHOTOMORPHOGENESIS (RUP) 1 and 2 (Cloix et al., 2012), had the greatest effect in slowing regeneration of the dimer in vivo but did not completely prevent it.

The present study has extended our understanding of UV-B perception and signal transduction by UVR8 in plants in several respects and even if many questions still remain to be answered, slowly, the position and role of UVR8 in the great network of light signal transduction is emerging.

TABLE OF CONTENTS

FIGURES AND TABLES ____ *vii*

PREFACE ____ *x*

ACKNOWLEDGMENTS ____ *xi*

ABBREVIATIONS ____ *xii*

1. INTRODUCTION ____ **1**

1.1 Impact of the sunlight spectrum on plants ____ 1

1.2 Visible light perception and signalling responses in Arabidopsis ____ 2

1.3 UV-B radiation and its biological effects ____ 7

1.4 UVR8 – a UV-B photoreceptor ____ 12

1.5 COP1 – a central switch of light signal transduction ____ 18

1.6 Negative feedback regulation of light signalling pathways ____ 21

1.7 Conclusion ____ 23

1.8 Aims of this study ____ 24

2. MATERIAL AND METHODS ____ **26**

2.1 Materials ____ 26

2.2 Preparation of media and solutions ____ 27

2.3 Plant material ____ 28

2.4 Treatments ____ 29

2.5 Bacterial transformation ____ 31

2.6 DNA and RNA methods ____ 32

2.7 Semi-quantitative Reverse Transcriptase PCR (RT-PCR) ____ 35

2.8 Protein methods ____ 36

2.9 Generation of stable transgenic Arabidopsislines ____ 42

2.10 Transient expression of gene constructs in *N. benthamiana* ____ 43

2.11 Yeast two-hybrid methods ____ 43

2.12 Protein expression in *E. coli* ____ 44

2.13 Spectroscopy ____ 47

3. DIMER-MONOMER STATE OF UVR8 SALT BRIDGE MUTANTS 50

3.1 Introduction 50

3.2 The UVR8 dimer is held together by a complex network of salt bridges 50

3.3 The salt bridge formed through R286 is essential to maintain the UVR8 dimer 52

3.4 R338 and D44 form a second important salt bridge to stabilize the dimer 54

3.5 R146 and E182 form a second double hydrogen bonded salt bridge 56

3.6 Native gel electrophoresis reveals various conformations of UVR8 mutants 58

3.7 Semi-native SDS-PAGE shows constitutive monomerisation of all salt bridge mutants 60

3.8 The UVR8 dimer shows exciton coupling 60

3.9 Exciton coupling is reduced in the monomeric mutants 62

3.10 Analysis of the UVR8 homodimer in plants 63

3.11 Dimer-monomer state of UVR8 salt bridge mutants expressed in plants analysed by PAGE 66

3.12 Dimer-monomer state of UVR8 salt bridge mutants expressed in plants analysed by SEC 68

3.13 Discussion 72

4. FUNCTIONAL ANALYSIS OF UVR8 SALT BRIDGE MUTANTS 78

4.1 Introduction 78

4.2 The evolutionarily conserved reoccurring motif GWRHT 78

4.3 UV-B dependent interaction of UVR8 mutants and COP1 in yeast 80

4.4 UV-B dependent interaction of UVR8 mutants and COP1 in Arabidopsis 82

4.5 The positive charge of R286 is essential for UVR8 function 84

4.6 The monomeric mutant GFP-UVR8$^{D96N/D107N}$ is functional in Arabidopsis 86

4.7 Influence of various mutations on functionality of GFP-UVR8 in Arabidopsis 88

4.8 Limited proteolysis of purified UVR8 shows UV-B induced conformational changes 91

4.9 Discussion 95

5. REGENERATION OF THE UVR8 DIMER AFTER PHOTORECEPTION 100

5.1 Introduction 100

5.2 Regeneration of the UVR8 dimer is rapid in vivo 100

5.3 Protein synthesis is required for rapid regeneration of the dimer 103

5.4 No evidence of targeted proteolysis of UVR8 via the proteasome 105

5.5 The C-terminus of UVR8 is required for rapid regeneration of the photoreceptor in vivo 107

5.6 COP1 is required for rapid dimer regeneration in vivo 110

5.7 Discussion 112

6. BIOPHYSICAL ANALYSIS OF UVR8 PHOTORECEPTION 117

6.1 Introduction 117

6.2 FTIR spectroscopy reveals UV-B induced conformational changes in UVR8 118

6.3 FTIR spectra of UVR8 salt bridge mutants 120

6.4 UV-B induced changes in UVR8 fluorescence 122

6.5 Ultrafast transient absorption spectroscopy of UVR8 128

6.6 Discussion 133

7. FINAL DISCUSSION 139

7.1 Introduction 139

7.2 The salt bridge network and the tryptophan pyramid 139

7.3 UV-B induced monomerisation 141

7.4 The UVR8-COP1 interaction 143

7.5 Integration of signals from different photoreceptors by COP1 144

7.6 Regeneration of the photoreceptor 146

7.7 Conclusions 147

7.8 Future Work 149

APPENDIX* *151

REFERENCES* *154

FIGURES AND TABLES

CHAPTER 1:

FIG 1-1: *Photomorphogenesis during the life cycle of Arabidopsis* 1

FIG 1-2: *Photoreceptor families that mediate plant photomorphogenic responses in response to visible light* 3

FIG 1-3: *COP1 at the centre of light signal transduction* 20

CHAPTER 2:

FIG 2-1: *Spectra of the light sources used in this study* 30

TAB 2-1: *Working concentrations of used antibiotics* 26

TAB 2-2: *Used plasmid DNA vectors* 27

TAB 2-3: *Primers used for site-directed mutagenesis* 34

TAB 2-4: *Primers used for RT-PCR* 36

TAB 2-5: *Primary antibodies used for immunoblotting* 40

CHAPTER 3:

FIG 3-1: *View of the UVR8 dimer* 51

FIG 3-2: *The salt bridge formed through R286 is essential to maintain the UVR8 dimer* 53

FIG 3-3: *R338 is also important for stable dimerisation of UVR8* 55

FIG 3-4: *R146 and E182 form the second double hydrogen bonded salt bridge further distanced from the tryptophan pyramid* 56

FIG 3-5: *Mutation of salt bridge forming residues alters the mobility of UVR8 mutants on native gels in various ways* 59

FIG 3-6: *Salt bridge mutants are constitutively monomeric under semi-native SDS-PAGE conditions* 60

FIG 3-7: *The UVR8 dimer shows exciton coupling and a UV-B response* 61

FIG 3-8: *Exciton coupling is reduced in the monomeric UVR8 mutants* 63

FIG 3-9: *Expression levels of GFP-UVR8 in transgenic lines* 64

FIG 3-10: *UVR8 forms a homodimer in plants* 65

FIG 3-11: *Semi-native SDS-PAGE to show dimer-monomer state of UVR8 in whole cell extracts* 67

FIG 3-12: *Native PAGE to show dimer-monomer state of UVR8 in whole cell extracts* 68

FIG 3-13: *Dimerisation of GFP-UVR8 expressed in* N. benthamiana *plants* 70

FIG 3-14: *Constitutive monomerisation of GFP-UVR8 salt bridge mutants expressed in* N. benthamiana *plants* 71

CHAPTER 4:

FIG 4-1: *The GWRHT motif is conserved among UVR8 orthologs in higher and lower plants* 79

FIG 4-2: *Yeast two-hybrid assay showing UV-B dependent interaction between UVR8 and COP1* 80

FIG 4-3: *Yeast two-hybrid assay showing UV-B dependent interaction between UVR8 and COP1 and loss of interaction between mutant forms of UVR8 and COP1* 81

FIG 4-4: *Effect of salt bridge mutations on UVR8 and COP1 interaction in Arabidopsis* 83

FIG 4-5: *The positive charge of R286 is essential for UVR8 function* 85

FIG 4-6: *Plants expressing GFP-UVR8^{R286K} show UV-B induced suppression of hypocotyl extension* 86

FIG 4-7: *The monomeric mutant GFP-UVR8$^{D96N/D107N}$ is functional in plants* 87

FIG 4-8: *Plants expressing GFP-UVR8^{D96N} or GFP-UVR8$^{D96N/D107N}$ show UV-B induced suppression of hypocotyl extension* 88

FIG 4-9: *Mutation of R234 neighbouring the tryptophan pyramid has more severe effects on functionality then mutation of R146 forming a cross-dimer salt bridge* 89

FIG 4-10: *The monomeric mutant GFP-UVR8^{R338A} is non-functional in plants* 90

FIG 4-11: *Mutation of H287 has no effect on UVR8 functionality* 91

FIG 4-12: *Limited proteolysis of purified UVR8 protein with trypsin reveals conformational changes after UV-B exposure* 93

FIG 4-13: *Limited proteolysis of non-functional monomeric mutant UVR8 proteins shows no conformational change after UV-B exposure* 94

CHAPTER 5:

FIG 5-1: *Regeneration of the UVR8 dimer after UV-B exposure is much more rapid in vivo than in vitro* 101

FIG 5-2: *Kinetics of the loss of UVR8 monomer in darkness following UV-B exposure* 102

FIG 5-3: *Protein synthesis is required to maximize the rate of dimer regeneration* 104

FIG 5-4: *Monomeric UVR8 is not degraded via the proteasome* 106

FIG 5-5: *The C-terminus of UVR8 is required for rapid regeneration of the dimer in vivo* 107

FIG 5-6: *The C27 region of UVR8 is required for rapid regeneration of the dimer in vivo* 108

FIG 5-7: *The in vitro regeneration rate of UVR8 is unaffected by the C-terminus* 109

FIG 5-8: *Protein synthesis is probably not required to maximize the rate of dimer regeneration if the C-terminus is absent* 110

FIG 5-9: *Rapid dimer regeneration in vivo requires intact COP1* 111

CHAPTER 6:

FIG 6-1: *FTIR spectroscopy reveals UV-B induced conformational changes in UVR8* 119

FIG 6-2: *Dimeric UVR8 salt bridge mutants and wild-type UVR8 show comparable light-minus-dark difference FTIR spectra* 121

FIG 6-3: *Monomerisation of wild-type UVR8 causes a red shift in its emission spectrum* 123

FIG 6-4: *UVR8 salt bridge mutants show shifted emission spectra* 125

FIG 6-5: *The shifted emission spectrum can be partially reversed after at least 24 h of dark recovery in wild-type UVR8 and UVR8^{D107N} but not in UVR8^{R286A}* 127

FIG 6-6: *Excitation of tryptophan in solution with 266 nm pulses leads to formation of a photoproduct with an absorption band at 425 nm* 129

FIG 6-7: *Excitation of the UVR8 dimer and monomer with 266 nm pulses generates a long lived photoproduct* 131

FIG 6-8: *Comparison of the formed photoproduct between UVR8 wild-type dimer and monomer* 132

TAB 6-1: *Emission maxima of UVR8 wild-type and salt bridge mutants before and after exposure to UV-B* 124

CHAPTER 7:

FIG 7-1: *Proposed model of UVR8 photoreception and signalling* 148

APPENDIX:

FIG A-1: *Calibration curve for SEC column Superdex 200* 151

FIG A-2: *Near-UV CD spectra of salt bridge mutants compared to wild-type UVR8* 152

FIG A-3: *Stability of wild-type UVR8 protein compared to dimeric mutant UVR8^{R286K} and monomeric mutants UVR8^{R286A} and UVR8$^{R146A/R286A}$* 153

PREFACE

Parts of the experimental work of this thesis have been published in the following two publications:

Christie JM, Arvai AS, Baxter KJ, Heilmann M, Pratt AJ, O'Hara A, Kelly SM, Hothorn M, Smith BO, Hitomi K, Jenkins GI, Getzoff ED (2012) Plant UVR8 photoreceptor senses UV-B by tryptophan-mediated disruption of cross-dimer salt bridges. *Science* 335:1492-1496.

Heilmann M and Jenkins GI (2013) Rapid reversion from monomer to dimer regenerates the Ultraviolet-B photoreceptor UV RESISTANCE LOCUS8 in intact Arabidopsis plants. *Plant Physiology* 161:547-555.

ACKNOWLEDGMENTS

I would like to thank my supervisor Prof. Gareth I. Jenkins for the advice, constant support and encouragement throughout the time of my Ph.D. at the University of Glasgow. I highly appreciated all the fruitful discussions we had throughout the three years about the design of experiments and the outcomes of them. Many thanks also to Prof. John M. Christie who also greatly supported me throughout my Ph.D. with inspiring discussions, many helpful suggestions to trouble-shoot my experiments and by making me aware what it means to be successful in science.

I would also like to thank Dr. Catherine Cloix and Dr. Katherine Baxter for teaching me many techniques and always having time to discuss any matters, work or personal related. Furthermore, thanks to Dr. Bobby Brown and Peggy Ennis who have, especially in the beginning of my studies, provided me with many useful protocols. Thanks to Lisa Blackwood, Chris Velanis, Kirsty McInnes and Kirsten Findlay for all the small favours they have done for me throughout the years and for all the jokes and the good atmosphere in the lab. I am also especially grateful to everybody working in the Bower Building for their support and their assistance on any matter, making the Bower Building a great working environment.

Thanks to Dr. Brian Smith and Dr. Sharon Kelly for letting me use their facilities which contributed a lot to this thesis and always taking time to answer my questions. This thesis benefited from two great collaborations: Firstly, the elucidation of the crystallographic structure by Prof. John M. Christie with members of Prof. Elizabeth D. Getzoff group at the Scripps Research Institute in La Jolla, CA, USA which gave us the opportunity to jointly publish a high impact paper, whose development was a great learning experience. The second collaboration with Dr. John M. Kennis and Dr. Tilo Mathes at the Vrije Universiteit in Amsterdam delivered me insights into a number of new techniques to explore the structure and function of proteins and I would like to thank both of them as well as Dr. Jingyi Zhu for the very instructive time I had during my two visits to their lab in Amsterdam.

Last, but not least I would like to thank the Leverhulme Trust for funding my work and my boyfriend who has been my greatest support during this work by cheering me up in difficult times and for always being there to help me to sort out any problems.

ABBREVIATIONS

35S	Cauliflower mosaic virus *35S* promoter
ABCB	ATP-binding cassette B
AD	activation domain
ADO	Adagio
ATP	Adenosine triphosphate
BBX	b-box zinc finger protein
BD	DNA binding domain
BLUF	blue light sensing using flavin
BSA	bovine serum albumin
bZIP	basic leucine zipper
CD	circular dichroism
CFP	cyan fluorescent protein
CHS	chalcone synthase
CHX	cycloheximide
CO	constans
COP	constitutively photomorphogenic
CPD	cyclobutane pyrimidine dimers
CRY	cryptochrome
CUL	cullin
CV	column volume
DASH	Drosophila Arabidopsis Synechocystis Homo
DDB1	damaged DNA binding protein 1
DMSO	dimethyl sulfoxide
dNTP	deoxyribonucleotide triphosphate
DTT	1,4-Dithiothreitol
EADS	evolution associated difference spectra
EDTA	ethylenediaminetetraacetic acid
EFO	early flowering by overexpression
ELIP	early light induced proteins
ESA	excited state absorption
FAD	flavin adenine dinucleotide
FHY	far-red elongated hypocotyl
FKF	flavin-binding Kelch Repeat F-box
FMN	flavin mononucleotide
FTIR	Fourier transform infrared spectroscopy
GEF	guanine nucleotide exchange factor
GFP	green fluorescent protein

GI	gigantea
HFR	long hypocotyl in far-red
HKRD	histidine kinase related domain
HRP	horseradish peroxidase
HS	high salt
HY	elongated hypocotyl
HYH	HY5 homolog
IPTG	isopropyl-beta-D-thiogalactopyranoside
IR	infrared
IRF	instrument response function
kDa	kilo dalton
L&L	lyse and load buffer
LAF	long after far-red
LB	Luria broth medium
LKP	LOV Kelch Protein
LOV	Light oxygen voltage
LS	low salt
MALS	multi-angle laser light scattering
MAPK	mitogen-activated protein kinase
MES	2-(*N*-morpholino)ethanesulfonic acid
MKP	MAPK phosphatase
MS	Murashige and Skoog salts
NASC	The European *Arabidopsis* Stock Centre
NMR	nuclear magnetic resonance
NO	nitric oxide
NOS	nitric oxide synthase
NPH	non-phototropic hypocotyl
OD	optical density
PAGE	polyacrylamide gel electrophoresis
PAR	photosynthetically active radiation
PAS	Per-ARNT-Sim
PCR	polymerase chain reaction
PEG	polyethylene glycole
Pfr	far-red light absorbing form of phytochrome
PHOT	phototropin
PHR	photolyases related domain
PHY	phytochrome
PIF	phytochrome interacting factor
PMSF	phenylmethysulphonylfluoride
Pr	red light absorbing form of phytochrome

PR	pathogenesis-related
Pro	promoter
PVPP	polyvinyl-polypyrrolidone
rbcL	ribulose-1,5-bisphosphate carboxylase large subunit
RBX	ring-box
RCC1	regulator of chromatin condensation
ROS	Reactive oxygen species
RT-PCR	reverse transcriptase polymerase chain reaction
RUP	repressor of UV-B photomorphogenesis
SAXS	small angle X-ray scattering
SDS	sodium dodecyl sulfate
SE	standard error
SEC	size exclusion chromatography
SPA	suppressor of phyA
STO	salt tolerance
SUMO	small ubiquitin-related modifier
TAE	Tris-acetate EDTA
TBS-T	Tris buffered saline triton-X
TBS-TT	Tris buffered saline triton-X Tween
TEMED	N,N,N',N'-tetramethylethane-1,2-diamine
TF	transcription factor
TPCK	N-tosyl-L-phenylalanyl chloromethyl ketone
Tris	Tris(hydroxymethyl)aminomethane
UGPase	UDP-glucose pyrophosphorylase
uli	UV-B light insensitive
UV	ultraviolet
UVR	UV resistance locus
v/v	volume / volume
w/v	weight / volume
WT	wild-type
YPD	yeast extract peptone dextrose
ZTL	Zeitlupe

1. INTRODUCTION

1.1 Impact of the sunlight spectrum on plants

Light has profound effects on the development of plants and acts throughout their entire lifecycle. Being photoautotrophic and sessile organisms, light is the plants' source of energy driving photosynthesis and ensuring biomass production. However, light is also a source of information and regulates the important process of photomorphogenesis (Fig 1-1). The most striking effects of light mediated changes in plant growth and development are observed when a germinating seedling emerges from the soil and is exposed to light for the first time. Numerous changes are triggered in the plant shoot, such as inhibition of hypocotyl growth, stimulation of cotyledon expansion and chloroplast development to prepare the plant for photosynthesis (Taiz and Zeiger, 2002). The induction of these photomorphogenic processes is only possible because plants have evolved sophisticated perception systems to sense different parameters of the light environment. Those photoreceptors are coupled to networks of signal transduction pathways triggering a massive reprogramming of the plant transcriptome in response to light (Jiao et al., 2007).

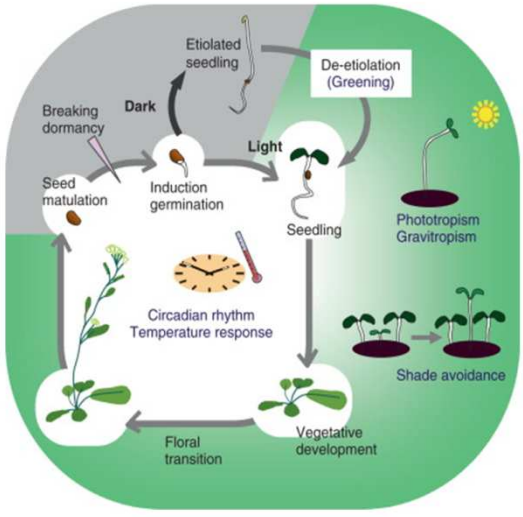

FIGURE 1-1: Photomorphogenesis during the life cycle of Arabidopsis.
Light affects growth and development of plants at every stage throughout their life cycle (Kami et al., 2010).

Light is therefore essential for plant survival but also comprises harmful radiation that has an extensive effect on the biosphere. Due to the stratospheric ozone layer, the non-visible damaging ultraviolet-B (UV-B) radiation accounts for less than 0.5% of the sun's energy

reaching the Earth's surface (Caldwell et al., 2003). However, UV-B radiation has the highest energy of the daylight spectrum that reaches the Earth and therefore, although only small quantities of UV-B are involved, it is notorious for being a ubiquitous and potent environmental carcinogen affecting human skin cells (Gilchrest et al., 1999). Organisms have therefore evolved mechanisms to protect themselves against UV-B and to repair UV damage (Rozema et al., 1997). The systems of UV-protection and repair in plants are evidently very effective because in the natural environment they rarely show any signs of UV damage. Nevertheless, UV-B is not simply a damaging agent for plants. Just like the other spectral parts of the daylight spectrum, UV-B is a key environmental signal for plants affecting plant morphology, gene regulation and changes in the plants metabolism accounting for UV-B acclimation and protection (Brosche and Strid, 2003; Frohnmeyer and Staiger, 2003; Ulm and Nagy, 2005; Jenkins, 2009). To be able to generate such responses the plant has to be able to 'see the invisible' (Gardner and Correa, 2012). Several action spectra for photomorphogenic UV-B responses have been published and most show maxima between 280 and 300 nm suggesting involvement of a UV-B photoreceptor (Yatsuhashi et al., 1982; Takeda and Abe 1992; Ensminger 1993). Decades of research on the postulated presence of a UV-B photoreceptor have finally been successful by identifying, characterising and also elucidating the crystal structure of UV RESISTANCE LOCUS8 (UVR8) as a plant UV-B photoreceptor (Hahlbrock and Grisebach, 1979; Kliebenstein et al., 2002; Brown et al., 2005; Rizzini et al., 2011; Christie et al., 2012; Wu et al., 2012).

1.2 Visible light perception and signalling responses in Arabidopsis

Photoreceptors are proteins responsible for light perception and they are able to initiate a signalling cascade resulting in a light specific response. Today, this conversion of light of different wavelengths into biochemical signals is well understood for photoreceptors sensitive to visible light (400 - 700 nm). Since the polypeptide backbone and the amino acid side chains do not absorb in the visible light range, the primary site of photon absorption is a non-protein, organic component, the so-called chromophore. The energy of light causes photoisomerization or photoreduction of the chromophore, a physical change perceived by the apoprotein which initiates the light signal transduction (Taiz and Zeiger, 2002). The chemical nature and the photochemistry of the chromophore form the basis of photoreceptor classification and at present three different classes of visible light photoreceptors are known in plants: phytochromes, cryptochromes and light-oxygen-voltage (LOV) sensors including phototropins and zeitlupe proteins (Fig 1-2).

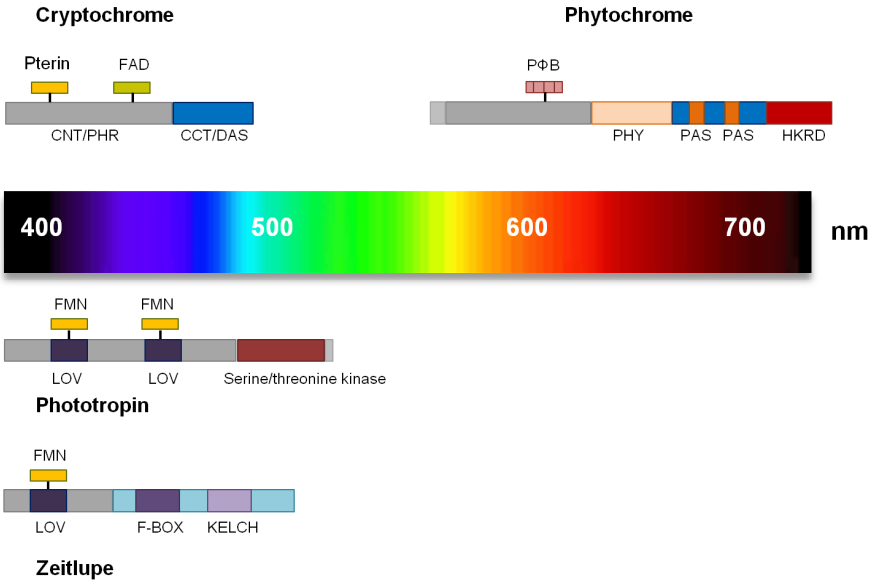

FIGURE 1-2: Photoreceptor families that mediate plant photomorphogenic responses in response to visible light. Cryptochromes, phototropins and zeitlupe proteins perceive blue light and UV-A wavelengths whereas phytochromes predominately absorb in the red and far-red region of the spectrum. **Cryptochromes**: N-terminal photolyase-related (PHR) domain (CNT); less-conserved, intrinsically unstructured C-terminal DAS domain (CCT); flavin adenine dinucleotide (FAD). **Phytochromes**: N-terminal photosensory domain covalently binding the chromophore, a phytochromobilin (PϕB); C-terminal domain containing several motifs and functioning in dimerisation: Per-ARNT-Sim (PAS) domain, histidine kinase related domain (HKRD). **Phototropins**: Photosensory N-terminal half consists two light-oxygen-voltage (LOV) domains with flavin mononucleotide (FMN), C-terminal half contains serine/threonine kinase function. **Zeitlupe:** Photosensory N-terminal half consists of LOV domain with FMN followed by an F-Box motif and six Kelch repeats (KELCH) in the C-terminal region. Adapted from Jiao et al., 2007.

1.2.1 Phytochromes

The red and far-red light sensing phytochrome family in Arabidopsis consists of five members (phyA to phyE) with unique and overlapping characteristics and functions during photomorphogenesis. Phytochromes were the first plant photoreceptors that were identified over 50 years ago (Butler et al., 1959). Control of seed germination and the shade avoidance response are two major photomorphogenic responses that are exclusively mediated by the phytochrome family (Franklin and Quail, 2010). Structurally, phytochromes consist of two domains whereupon the N-terminal photosensory domain covalently binds the chromophore, a phytochromobilin and the C-terminal regulatory region includes a histidine-kinase-related domain (Fig 1-2; Rockwell et al., 2006).

Phytochromes share the characteristic that red light (R) irradiation converts the R-absorbing Pr form into the metastable, biologically active, far-red light (FR)-absorbing Pfr form. This photoconversion is reversible, with Pfr returning to Pr either upon absorption of an FR photon or upon prolonged incubation in the dark via a thermal process

known as dark reversion (Rockwell et al., 2006). The biological active Pfr form is translocated into the nucleus, localises to speckles or nuclear bodies and triggers a transcription cascade that leads to the regulation of a large number of light-responsive genes (Yamaguchi et al., 1999; Kircher et al., 1999; Chen et al., 2003).

The five members of the phytochrome family differ in their light stabilities and fluence rate requirements. Four of the five, phyB, phyC, phyD and phyE, are light-stable in Arabidopsis and function primarily in regulation of responses to low-fluence red light and to the R:FR light ratio. In contrast, phyA is rapidly degraded in its Pfr form and controls plant responses to very low fluence rates and high-irradiance (Nagy and Schaefer, 2002). A further characteristic of some of the light stable phytochromes is their ability to heterodimerise. Whereas phyA, phyB and phyD form homodimers, phyC and phyE are present in seedlings only as heterodimers with phyB and phyD (Sharrock and Clack, 2004; Clack et al., 2009).

Yeast two-hybrid screening has identified a number of phytochrome-interacting proteins as well as transcription factors, such as for example PHYTOCHROME INTERACTING FACTOR3 (PIF3) (Leivar and Quail, 2011). Although PIF3 was originally considered as a positive regulator of phytochrome-induced signalling, recent evidence shows that upon continued red light exposure, signalling by the Pfr form is terminated by PIF promoted CONSTITUTIVELY PHOTOMORPHOGENIC1 (COP1) -mediated degradation suggesting that PIF3 is also a negative regulator of phy-induced signalling (Castillon et al., 2007; Jang et al., 2010). Furthermore, phytochromes interact with the UV-A/blue light photoreceptors cryptochromes 1 and 2 (Ahmad et al., 1998; Mas et al., 2000), the clock proteins ZEITLUPE/ADAGIO1 (ZTL/ADO1) (Jarillo et al., 2001) as well as phototropins (Jaedicke et al., 2012) allowing photoreceptor regulation and integration of other light signal transduction pathways.

1.2.2 Cryptochromes

The blue part of the visible light spectrum is absorbed and utilized by the cryptochromes (cry) which are members of a larger blue light-absorbing chromoprotein superfamily present in plants, animals, fungi and bacteria (Batschauer et al., 2007). This family also includes the DNA photolyases which catalyze the repair of UV light-damaged DNA and are postulated to be the ancestors of cryptochromes (Chaves et al., 2011). All members of the cry/photolyase family share an amino-terminal photolyase-related (PHR) domain that is responsible for binding the chromophores, both a primary/catalytic flavin and a second light-harvesting deazaflavin or pterin (Fig 1-2; Liscum et al., 2003). However,

cryptochromes lack DNA repair activity and also differ from photolyases by the presence of a carboxyl-terminal extension (CCT) beyond the PHR domain which was shown to be important for protein interactions and mediation of signalling processes (Cashmore et al., 1999; Yang et al., 2000).

The cryptochrome family in Arabidopsis currently consists of three members: cryptochrome 1 and 2 (cry1 and cry2) entrain the circadian clock and trigger developmental processes such as de-etiolation and flower induction (Moeglich et al., 2010). Cryptochrome 3 (cry3), belonging to the cry-DASH (Drosophila, Arabidopsis, Synechocystis and Homo) class of cryptochromes is the only plant cryptochrome with clear DNA-binding and also DNA-repair activities (Brudler et al., 2003). Evolutionarily, it therefore forms an intermediate between cryptochromes and photolyases. Furthermore, Arabidopsis cry3 also lacks the CCT and is localized in chloroplasts and mitochondria (Kleine et al., 2003).

In terms of subcellular localization cry1 and cry2 greatly differ: whereas cry1 is nuclear in the dark but largely cytoplasmic under light, cry2 is constitutively nuclear localized (Jiao et al., 2007). In the nucleus, homodimers of cry1 and cry2 both constitutively interact with COP1, an E3 ubiquitin ligase which forms a central switch in plant photomorphogenesis (see also section 1.5; Yang et al., 2001; Yi and Deng, 2005). Perception of UV-A or blue light causes photoexcitation of cry1 and cry2 which in turn leads to rapid phosophorylation and conformational change of the C-terminal domains of the receptors which is considered to be an important step in the signalling pathway (Shalitin et al., 2002; Bouly et al., 2003; Liu et al., 2010). Rapid phosphorylation-based cryptochrome activation results in COP1 deactivation, thus preventing the degradation of activators of the light response by polyubiquitination, such as ELONGATED HYPOCOTYL5 (HY5), LONG AFTER FAR-RED1 (LAF1), and LONG HYPOCOTYL IN FAR-RED1 (HFR1), which is an important event during seedling de-etiolation processes (Osterlund et al., 2000; Wang et al., 2001; Seo et al., 2003; Jang et al., 2005).

1.2.3 Phototropins and Zeitlupe proteins

Besides the cryptochrome family, a second family of blue light sensors that utilizes LOV domains for light perception is present in plants. LOV domains were first discovered as tandem sensor domains in plant phototropins (Christie et al., 1998) and have since been found in several plant, fungal and bacterial proteins (Crosson et al., 2003). In Arabidopsis, phototropins (phot1 and phot2) mediate a variety of relatively fast, light-induced responses

that serve to optimize photosynthetic performance, including phototropism, chloroplast and leaf movements and stomatal opening (Christie, 2007).

Phototropins are plasma-membrane associated serine/threonine kinases with an N-terminal photosensory input region which contains two LOV domains, LOV1 and 2, each non-covalently binding a flavin mononucleotide acting as chromophore (Fig 1-2) (Briggs and Christie, 2002). Upon excitation with blue light, a reversible photocycle is activated that involves the formation of a covalent adduct between the flavin and a conserved cystein residue within the LOV domain (Salomon et al., 2000). This subsequently induces conformational changes in the protein (Harper et al., 2003) which relieves repression of the kinase activity resulting in rapid fluence rate dependent autophosphorylation of the photoreceptor required for phototropin signalling (Chen et al., 2004).

In contrast to phytochromes and cryptochromes, the contribution of phototropins to transcriptional regulation is relatively small and only a limited number of genes are under their control (Jiao et al., 2007). Several proteins essential for phototropin signalling have been identified to date (Inada et al., 2004; de Carbonnel et al., 2010). Among them is a phot1-interacting protein, NON-PHOTOTROPIC HYPOCOTYL3 (NPH3) that is essential for lateral auxin redistribution and phototropism (Motchoulski and Liscum, 1999). New insights into auxin redistribution during phototropism are provided by a recent study that identified the auxin efflux transporter ATP-BINDING CASSETTE B19 (ABCB19) as a phosphorylation target of phot1 (Christie et al., 2011). This process inhibits the efflux activity of ABCB19, thereby redistributing auxin to halt vertical growth and prime lateral fluxes that are subsequently channelled to the elongation zone by PIN-FORMED3 (PIN3). Light-mediated polarization of PIN3 has also recently been demonstrated to be essential for phototropic responses (Ding et al., 2011).

A second group of blue light receptors utilizing LOV domains for light sensing are the proteins of the ZEITLUPE family which currently comprises three members: Zeitlupe (ZTL, also known as Adagio, ADO), Flavin-binding Kelch Repeat F-box 1 (FKF1) and LOV Kelch Protein 2 (LKP2) (Demarsy and Fankhauser, 2009). All three proteins contain only one LOV domain with an FMN chromophore followed by an F-box domain and several Kelch repeats (Fig 1-2). These proteins mediate ubiquitin-dependent protein degradation in a light-controlled manner (Mas et al., 2003), ultimately leading to photoperiodic expression and/or accumulation of key proteins involved in flowering onset and entrainment of the circadian clock, after which they were named (Kim et al., 2007).

1.3 UV-B radiation and its biological effects

1.3.1 UV-B radiation

Plants in their natural environment are not only exposed to visible light wavelengths but also to UV-A and UV-B-radiation which are integral parts of the sunlight reaching the surface of the Earth. By definition, UV-B radiation comprises wavelengths between 280 and 315 nm, though only wavelengths greater than 290 nm can reach the Earth's surface due to effective absorption of even shorter wavelengths by the stratospheric ozone layer. The intensity of solar UV-B radiation incident on organisms and ecosystems is influenced by a range of factors, making it a highly dynamic component of the environment (McKenzie et al., 2003). In particular, large scale effects are due to latitude, altitude and the seasons that affect the solar angle and hence the thickness of the atmosphere that UV-B must penetrate (Paul and Gwynn-Jones, 2003). Short term changes that also affect the level of UV-B present are the time of the day, the degree of cloud cover and the dispersal of atmospheric aerosols and pollutants that can absorb UV-B (Jenkins, 2009). Overall, the effects of UV-B radiation on plants can be broadly divided into two classes reflecting the function of the response: firstly, UV-B damage causing an acute stress response that will help the plant to survive exposure to elevated levels of UV-B and secondly UV-B causing a photomorphogenic response in the plant, a non-damage response that establishes UV-B protection and modifies development (Jenkins, 2009). Examples of both responses will be described in the following two sections.

1.3.2 UV-B as a damaging agent

In general, the damaging nature of UV-B radiation is due to the high energy per photon of such short wavelengths combined with the ability of a wide range of biologically active molecules including nucleic acids, aromatic acids and lipids to absorb it. DNA damage can occur in several ways; however UV-B exposure most prevalently induces the formation of cyclobutane pyrimidine dimers (CPD) and to a lesser extent pyrimidine [6-4] pyrimidinone dimers (6-4 photoproduct) (Britt, 2004). The presence of these photoproducts leads to inhibition of replication and transcription, mutation, growth arrest and finally cell death. In order to cope with these damages, most organisms have developed DNA repair mechanisms, which involve photoreactivation, excision repair and homologous recombination (Ulm, 2006). Pyrimidine dimers are mainly repaired by photoreactivation which is mediated by photolyases in the presence of UV-A/blue light (Britt, 2004). Functional photolyases are critical for plant survival under UV-B and several mutants

hypersensitive to UV-B due to deficiencies in DNA repair have been identified (Britt et al., 1993; Jiang et al., 1997; Landry et al., 1997).

One response to UV-B radiation as an environmental stress involves mitogen-activated protein kinase (MAPK) signalling cascades (Jenkins, 2009). UV-B dependent activation of the two best-characterized stress activated MAPKs of Arabidopsis, MPK3 and MPK6, is initiated by pyrimidine dimers resulting from UV-B damage (González Besteiro and Ulm, 2013). MPK3 and MPK6 are negatively regulated by becoming dephosphorylated by MAPK phosphatase1 (MKP1), which is required to cope with UV-B stress but is not involved in UV-B acclimation (González Besteiro et al., 2011). DNA damage signalling in response to UV-radiation (UV-C and UV-B) has also been characterized in other systems. Although no UV-B photoreceptor has yet been identified in mammalian systems, UV radiation initiates DNA damage signalling pathways that arrest cell cycle progression and promote DNA repair in mammalian cells (Sancar et al., 2004). Exposure to UV also triggers a transcriptional induction response including the activation of transcription factors such as AP-1 and nuclear factor-κB (NF-κB) as well as the initiation of signal-transduction events mediated by receptor tyrosine kinases (Devary et al., 1992).

In addition to the effects on survival, UV-B mediated DNA damage in plants induces, for example, the expression of a pathogenesis-related (PR) protein (β-1,3-glucanase) in bean (Kucera et al., 2003) and promotes isoflavonoid synthesis in leguminous plants (Beggs et al., 1985).

At the whole-plant level, extensive exposure to UV-B results in reduced plant biomass and crop yield, mainly due to growth inhibition as well as tissue destruction (Casati and Walbot, 2004 a; Caldwell et al., 2007). Further damage by UV-B is caused by crosslinking of ribosomes and ribosome oxidation which subsequently inhibits protein synthesis (Casati and Walbot, 2004 b). UV-B also impinges on various aspects of photosynthesis whereby its damaging effects on photosystem II caused by triggering the rapid degradation of the D1 and D2 proteins from photosystem II, are the best characterized effect (Jansen et al., 1998). Inhibition of photosynthetic electron transport due to UV-B can be one source of increased accumulation of reactive oxygen species (ROS) observed after UV-B exposure of plants (Mackerness et al., 2001; Barta et al., 2004; Hideg et al., 2002). ROS accumulate in response to various abiotic and biotic stresses and cause oxidative damage to cellular components, and their levels therefore need to be controlled by the plant. Oxidative stress is reduced by increased activity of ROS-scavenging enzymes, such as ascorbate peroxidase and superoxide dismutase, which is observed following UV-B treatments, although mostly only under very high doses (Foyer et al., 1994; Rao et al., 1996). Another UV-B induced

stress response that overlaps with other environmental stimuli is the activation of wound and defence signalling pathways due to UV-B dependent accumulation of signal molecules such as ROS, jasmonic acid or ethylene that mediate wound/defence mechanisms (Mackerness et al., 1999, Brosche and Strid, 2003). The signalling pathways and target genes involved in these high fluence UV-B responses are however not UV-B specific.

1.3.3 UV-B mediated photomorphogenesis

Clearly distinguishable from the non specific UV-B signalling pathways under high UV-B fluence rate are the photomorphogenic UV-B signalling pathways that act at low and very low fluence rates of UV-B to regulate UV protection and morphogenesis. The phenotypic responses evoked in plants by those fluence rates are diverse, ranging from hypocotyl growth inhibition, cotyledon expansion, phototropic growth and regulation of stomatal opening to the induction of UV protective secondary metabolites such as flavonoids and sinapic acid esters (Ballare et al., 1995; Frohnmeyer et al., 1999; Shinkle et al., 2004; Wargent et al., 2009). The fact that mutants defective in DNA repair mechanisms, which would be expected to show increased levels of responses mediated by DNA damage signalling, do not show an alteration of any of the above processes, is evidence that distinct photomorphogenic signalling processes exist. The two most extensively studied responses are the suppression of hypocotyl extension (Kim et al., 1998; Shinkle et al., 2004) and the UV-B induced induction of genes involved in flavonoid biosynthesis especially CHALCONE SYNTHASE (CHS) (Feinbaum and Ausubel, 1988; Jenkins et al., 2001). Both phenotypes have been successfully used to identify specific UV-B-photomorphogenic mutants. A screen for mutants lacking a UV-B mediated suppression of hypocotyl extension led to the isolation of the UV-B light insensitive (*uli*) mutants (Suesslin and Frohnmeyer 2003). These mutants were also impaired in UV-B induced expression of *CHS* and *PR1* compared to the response in wild-type plants. The *ULI3* gene is predicted to encode a cytoplasmic protein with homology to human diacylglycerol kinases but lacking the conserved kinase domain; thus, its exact biochemical function remains to be determined (Suesslin and Frohnmeyer, 2003).

Moving from morphogenesis towards UV-protection in the photomorphogenic UV-B signalling pathway, the most effective protection mechanism stimulated under such light conditions is the biosynthesis of flavonoids and other UV-B-absorbing phenolic compounds (Frohnmeyer and Staiger, 2003). The flavonoid biosynthesis pathway is a branch of the phenylpropanoid pathway that results in the production of several important secondary metabolites such as for example anthocyanins, flavones and flavonols (Winkel,

2006). The basic flavonols kaempferol and quercetin are further glycosylated by a number of glycosyltransferases and accumulate mainly in the upper epidermal cell layer and selectively absorb only harmful UV-B wavelengths, allowing photosynthetically active radiation to penetrate into the cells below thus not diminishing photosynthetic yields (Jansen et al., 1998). Mutants devoid of these photoprotective pigments are hypersensitive to UV-B (Li et al., 1993; Landry et al., 1995; Casati and Walbot, 2004 b) whereas mutants with enhanced flavonoid levels show increased resistance to UV-B (Bieza and Lois, 2001). Additionally, flavonoids can act as scavengers of free radicals allowing further protection against high levels of UV-B (Rice-Evans et al., 1997). Regulation of the flavonoid biosynthesis pathway largely takes place at the level of transcription by a network of transcription factors including the PRODUCTION OF FLAVONOL GLYCOSIDES (PFG) family of R2R3-MYB TFs (Stracke et al., 2007). PFG gene expression is up regulated by UV-B in a HY5 dependent manner and they contribute to the establishment of UV-B tolerance as shown by loss of function mutants and overexpressor lines (Stracke et al., 2007). These findings demonstrate the physiological relevance of flavonoids as UV-B sunscreens during the acclimation response allowing plants to inhabit high latitudes and altitudes and to endure extensive exposure to UV-B (Jordan, 1996).

The regulation of *CHS* transcripts has been the focus of many studies. CHS, encoded by a single gene in Arabidopsis, is the first enzyme in the flavonoid specific branch of the phenylpropanoid biosynthesis pathway and therefore a key enzyme in the secondary metabolism and regulated by a variety of environmental stimuli (Weisshaar and Jenkins, 1998). The transcriptional regulation of *CHS* has become a well-established model system to analyse the interplay of UV-B radiation with other wavelengths of the daylight spectrum since it relies on complex interactions within a network of phytochrome-, cryptochrome- and UV-B-signalling pathways (Jenkins et al., 2001). In brief, distinct UV-A and blue light pathways interact synergistically with the UV-B pathway to enhance *CHS* expression, whereas phyB is a negative regulator of the UV-B inductive pathway (Fuglevand et al., 1996; Wade et al., 2001). This extensive signalling network is just one example of ‘crosstalk’ between signal transduction pathways highlighting how plants are able to integrate information of a wide range of environmental stimuli, UV-B radiation being one of them.

1.3.4 UV-B signal transduction

An indispensable requirement for all of the above described UV-B induced responses is the ability of the plant to specifically sense UV-B. The long-lasting search and finally the successful identification of a UV-B photoreceptor will be described in the next section. Nevertheless, after UV-B perception, signal transduction pathways must be recruited to generate responses such as gene activation or repression. It still remains elusive how many different UV-B signalling pathways a plant possesses as well as how they actually work (Jenkins, 2009). Over the years, a number of signalling intermediates have been linked to the UV-B signalling pathways including ROS, Ca^{2+}/calmodulin, nitric oxide (NO), reversible protein phosphorylation and various plant hormones (Frohnmeyer and Staiger, 2003; Ulm, 2006).

Pharmacological studies suggest that the generation of ROS, from multiple sources, is required for the induction and repression of a number of UV-B responsive genes such as *PR1* or *PDF1.2* (Mackerness et al., 2001). In contrast, UV-B mediated induction of *CHS* expression is independent of ROS confirming the existence of several signal transduction pathways (Mackerness et al., 2001, Jenkins et al., 2001). Further pharmacological approaches using NO scavenger or NO synthase (NOS) inhibitors indicate that the up regulation of *CHS* expression by UV-B requires NO (Mackerness et al., 2001). A study by Tossi et al. (2011) in maize and Arabidopsis demonstrates that UV-B perception increases NO concentration, which is an important step in UV-B protection by the ability of NO to scavenge ROS and also to up-regulate expression of some transcription factors that are involved in the phenylpropanoid pathway. The involvement of Ca^{2+}, calmodulin and protein phosphorylation in UV-B signal transduction pathways was demonstrated by inhibitor studies with cell suspension cultures. Millisecond UV-B pulses caused an immediate rise of cytosolic calcium correlating with the subsequent stimulation of *CHS* expression (Frohnmeyer et al., 1999). The effects of calcium-channel antagonists and Ca^{2+}-ATPase inhibitors suggest the involvement of an intracellular calcium pool rather than flux across the plasma membrane (Christie and Jenkins, 1996; Long and Jenkins, 1998).

The output of these still rather poorly understood signal transduction pathways is a transcriptional response with altered levels of gene expression. Genome-wide gene expression profiling via microarrays has shown that UV-B leads to profound changes in gene expression and these changes can account to some extent for the effects observed at the physiological level (Brosche et al., 2002; Casati and Walbot, 2003; Izaguirre et al., 2003; Casati and Walbot, 2004; Ulm et al., 2004, Brown et al., 2005). One of the most extensive transcript profilings was performed in 2004 by Ulm and co-workers which

identified a robust set of early low-level UV-B responsive genes that were postulated to comprise a UV-B photoreceptor readout. Perhaps the most significant finding of this microarray study was that among the UV-B induced transcriptional regulators is the basic leucine zipper (bZIP) transcription factor HY5 which is known as a key player regulating the transition from growth in complete darkness to growth in light (Osterlund et al., 2000). The importance of UV-B mediated gene expression changes will be discussed further in the following section.

1.4 UVR8 – a UV-B photoreceptor

1.4.1 Isolation and characterisation of the uvr8 mutant

The *UV resistance locus 8-1* (*uvr8-1*) was first identified by Kliebenstein and co-workers in 2002 in a screen for UV-B sensitive plants. The *uvr8-1* mutant displayed necrosis of the leaves and cotyledons after the exposure of the plants to UV-B radiation. The *uvr8-1* mutant also showed lack of UV-B induced accumulation of flavonoids and *CHS* transcripts as well as CHS protein (Kliebenstein et al., 2002). The inhibition of CHS induction in the mutant was not caused by a general loss of stress responsive gene expression since stress-induced proteins like PR1 and PR5 as well as ROS scavengers like manganese SOD 1 (MSD1) were still induced and even more rapidly and to a higher level than in wild-type plants (Kliebenstein et al., 2002). Loss of UVR8 therefore subjects the plants to increased stress under UV-B, allowing the conclusion that UVR8 transduces a UV-B signal initiating UV-protection of the plant. The UV-B specificity of the inhibition of *CHS* induction in the *uvr8* mutant was further established by Brown and co-workers showing that CHS gene expression is still induced by cold, sucrose, UV-A radiation and far red light in UVR8 mutant plants (Brown et al., 2005). This was a key discovery as it identified *UVR8* as the first gene exclusively involved in UV-B responses and ever since made it the most promising candidate for being a UV-B photoreceptor. Further screens for mutants lacking specifically the UV-B induction of *HY5* or *CHS* gene expression identified several additional *uvr8* alleles and a mutation in the *COP1* gene (Brown et al., 2005; Favory et al., 2009). Failure to identify any UV-B specific components upstream of UVR8 by these screens also supports the idea of UVR8 being a UV-B photoreceptor. The *uvr8* mutant is further impaired in other important photomorphogenic responses, the suppression of hypocotyl elongation under UV-B (Favory et al., 2009) as well as regulation of leaf expansion (Wargent et al., 2009). In line with the loss of function mutants, overexpression of UVR8 leads to enhanced expression of *HY5* and *CHS* genes resulting in increased UV-B

tolerance but also causing a dwarfed and dark green phenotype (Favory et al., 2009). These overexpressor lines illustrate that a major role of the UV-B induced photomorphogenic response is the acclimation of plants to finally establish UV-B tolerance essential for survival.

The ultimate breakthrough in proving that UVR8 is the long sought UV-B photoreceptor was achieved by Rizzini and co-workers in 2011. They revealed by co-immunoprecipitation of endogenous UVR8 with CFP-UVR8 only under dark conditions that UVR8 undergoes a UV-B light dependent conversion from a dark state dimer to a lit-state monomer (Rizzini et al., 2011). This UV-B induced monomerisation is very rapid, fluence rate dependent and shows a reciprocal relationship between treatment duration and fluence rate (Rizzini et al., 2011). The ability of UVR8 to directly perceive UV-B was shown through an in-gel UV-B illumination assay of the protein leading to accessibility of an antibody epitope to detect the dark-state dimer. This UV-B induced change in conformation is linked to the observed in vivo monomerisation of the UVR8 dimer and finally established UVR8 as a UV-B photoreceptor. Further proof that UVR8 has photoreceptor properties was given by examining monomerisation in heterologous systems. UV-B induced monomerisation can be observed in transformed yeast cells as well as in transfected human embryonic kidney cells demonstrating activation of the receptor (Rizzini et al., 2011).

1.4.2 UVR8 regulated genes

In addition to the UV-B specific induction of *CHS* transcripts, microarray analyses have shown that UVR8 regulates the expression of a large number of genes involved in photoprotection and photomorphogenesis in a UV-B dependent manner (Brown et al., 2005; Favory et al., 2009). Amongst those regulated genes is for example the one coding for the photolyase *PHR1*, which is required for photoreactivating DNA repair. Furthermore, UVR8 regulates genes concerned with protection against oxidative stress (e.g. glutathione peroxidases) and photooxidative damage (e.g. EARLY LIGHT INDUCED PROTEINS (ELIP)) ensuring UV-protection of the plant. An important role of the HY5 transcription factor in the UV-B response was already highlighted by Ulm et al. (2004). Extension of the microarray analysis of the *uvr8* mutant to a *hy5* mutant clearly revealed that the HY5 transcription factor functions downstream of UVR8 and regulates about half of the genes that are also regulated by UVR8 (Brown et al., 2005). Therefore, HY5 is a main effector of the UVR8 pathway and the *hy5* mutant shows greatly reduced viability when exposed to UV-B (Brown et al., 2005; Oravecz et al., 2006). In Arabidopsis,

HY5 has a close homolog, HYH (HY5 HOMOLOG), which is 49% identical to HY5 containing the critical functional domains and also acting redundantly with HY5 particularly under blue light (Holm et al., 2002). Unsurprisingly, HY5 and HYH also have overlapping roles in the UV-B pathway; however, *hyh* is less sensitive to UV-B than *hy5* indicating that HYH is of secondary importance (Brown and Jenkins, 2008).

Transcriptome analysis also identified a large number of UV-B regulated genes that were not regulated by UVR8, indicating the presence of a UVR8 independent signalling pathway (Brown et al., 2005). RT-PCR analyses of individual genes produced two genetically distinct UV-B signalling pathways that stimulate gene expression, but only the UVR8-dependent pathway operates at low UV-B fluence rates (Brown and Jenkins, 2008). Analysis of UV-B induced transcript levels of various UV-B regulated genes in *hy5* and *hyh* mutant plants also showed that the presence of HY5 and HYH is only required for the UVR8-dependent pathway (Brown and Jenkins, 2008). UV-B photoreception by UVR8 and downstream signalling via HY5/HYH emerges as one important photomorphogenic signalling pathway, but variation in responsiveness to different wavelengths of UV-B suggest that multiple, yet unidentified pathways might exist (Kalbina et al., 2008; Ulm et al., 2004).

1.4.3 Localisation of UVR8

The role of UVR8 in UV-B induced regulation of transcription was further examined by localisation studies of the UVR8 protein. UVR8 is expressed throughout the whole plant in all stages of development at a constant level (Rizzini et al., 2011). GFP-UVR8 fusion proteins can be detected in the cytoplasm as well as in the nucleus in the absence of UV-B (Brown et al., 2005), but exposure of plants to low fluence rates of UV-B causes a rapid nuclear accumulation of the protein (Kaiserli and Jenkins, 2007). Furthermore, UVR8 was found to associate with chromatin fragments containing the *HY5* promoter (Brown et al., 2005) and therefore suggesting a general mechanistic basis for the involvement of UVR8 in the transcriptional regulation of target genes. However, UVR8 was only found to interact with chromatin containing promoter regions of some of the genes it regulates, such as *MYB12* (encodes a TF that regulates *CHS* and flavonol biosynthesis genes) or *CRYD* (encodes a putative chloroplast photolyases) but not for example with promoter regions of *CHS* or *HYH* (Cloix and Jenkins, 2008). These interactions can already be observed in the absence of UV-B suggesting that UVR8 might be part of a multi-protein complex that associates with chromatin but so far unidentified components are responsible for UV-B signal transduction to mediate UV-B induced gene expression (Cloix and Jenkins, 2008).

Additionally, nuclear localisation of UVR8 is required for function, but constitutively nuclear localized UVR8 is insufficient to cause expression of target genes in the absence of UV-B (Kaiserli and Jenkins, 2007). A 23 amino acid deletion at the N-terminus greatly impairs the ability of UVR8 to accumulate in the nucleus as well as its ability to induce *HY5* or *CHS* expression in response to UV-B (Kaiserli and Jenkins, 2007). The nuclear fraction nevertheless is still able to bind to chromatin indicating that it still has the potential to function in transcriptional regulation.

Regulation of gene expression is closely connected to specific posttranslational modifications of particular histones that facilitate the remodelling of chromatin structure. UVR8 interacts with chromatin via histones and competition experiments have identified preferential interaction with histone H2B (Cloix and Jenkins, 2008). Following UV-B treatment, the promoter regions of some UV-B regulated genes were enriched in chromatin containing diacetyl-histone H3 (K9/K14) suggesting that histone modification might result in increased transcriptional activity in response to UV-B (Cloix and Jenkins, 2008). Histone acetylation and chromatin remodelling was also shown to be required for UV-B dependent transcriptional activation of regulated genes in maize (Casati et al., 2008). Microarray analysis further indicated that among UV-B responsive transcripts are several genes implicated in chromatin remodelling which were also generally transcribed at higher levels in maize lines adapted to higher altitudes with increased levels of UV-B (Casati et al., 2006). Thus, chromatin remodelling seems to be an important process in acclimation to UV-B.

1.4.4 UVR8 – a member of the WD40 protein family

Before the very recent elucidation of the UVR8 crystal structure, structural modelling of UVR8 was based on the structurally related human REGULATOR OF CHROMATIN CONDENSATION1 (RCC1) protein. UVR8 and RCC1 are 35% identical and 50% similar in their amino acid sequences and a number of amino acids, mostly glycines, which are required for the structural integrity of RCC1 are well conserved within UVR8 (Kliebenstein et al., 2002). RCC1 is a guanine nucleotide exchange factor (GEF) for the small GTP-binding protein Ran, which is involved in nucleocytoplasmic transport, regulation of the cell cycle and mitosis (Seki et al., 1996). Despite their sequence similarities, UVR8 and RCC1 are not functional homologues since UVR8 only displays insignificant GEF activity and is also unable to interact with Ran (Brown et al., 2005). Moreover, UVR8 mutants are indistinguishable from wild-type in the absence of UV-B, whereas *rcc1* mutants in yeast and mammalian cells fail to grow (Brown et al., 2005).

Structurally, RCC1 belongs to the large family of WD40 proteins and folds into a seven bladed β-propeller whereby each blade consists of four anti-parallel β-sheets with loops in between (Renault et al., 1998). UVR8 also has a seven bladed β-propeller fold, but unlike canonical WD-40 repeats, each blade in UVR8 comprises only three β-strands, whereby the third strand is followed by an extended loop (Wu et al., 2012; Christie et al., 2012). It is remarkable that all three β-strands in all seven blades exhibit a nearly identical main chain conformation which is very similar to the conformation of RCC1 (Wu et al., 2012). Further structural differences between the majority of WD40 proteins including RCC1 and UVR8 can be observed in the topology of the blades. Usually, β-propeller proteins have a "velcro" closure meaning that one of the blades is formed from β-strands from both the most N-terminal and the most C-terminal parts of the sequence (Smith et al., 1999). This arrangement is supposed to further stabilize the β-propeller fold in addition to the extensive hydrophobic interactions between the β-sheets (Xu and Min, 2011). Nevertheless it is not essential, since the "velcro" closure is for example absent in AipI (Actin-interacting protein 1, Voegtli et al., 2003) and in the yeast polarity protein Sro7 where the terminal blades associate only via hydrophobic interactions (Hattendorf et al., 2007). The same is true for UVR8, where each blade is contiguous in sequence with the N and C termini in the first and last blades, respectively, potentially permitting greater conformational flexibility (Christie et al., 2012).

In general, WD40 proteins perform diverse cellular functions by acting as hubs in cellular networks (Stirnimann et al., 2012). Proteins of this family are especially well suited to serve as interaction platforms because they offer three distinct surfaces for interactions with other proteins: the top and the bottom region of the propeller as well as the circumference (Stirnimann et al., 2012). The general scaffolding role of WD40 proteins is also supported by the fact that no WD40 domain has been found yet with intrinsic enzymatic activity which also fits for UVR8 so far (Stirnimann et al., 2012). Most interacting peptides bind to the top region of the propeller which also forms the dimerisation surface of UVR8 (Christie et al., 2012). So far only a small number of UVR8 interacting proteins are known (Oravecz et al., 2006; Gruber et al., 2010; Cloix et al., 2012) but the general scaffolding role of WD40 proteins suggests that further unknown interactors are very likely.

1.4.5 UV-B photoreception

The discovery of UV-B induced monomerisation of UVR8 immediately evoked the question how this protein can specifically act as a UV-B photoreceptor since in general all proteins can absorb UV-B radiation. Amongst the aromatic amino acids, tryptophan is particularly well suited as a UV-B chromophore since its absorption maximum in solution lies at 280 nm extending towards 300 nm (Lakowicz, 2006). An action-spectrum based on the UV-B induced accumulation of *HY5* transcripts mediated by UVR8 suggests maximum photon effectiveness at 280 nm but with still significant action at longer UV-B wavelengths (Brown et al., 2009). The high abundance of tryptophan residues in UVR8 (14 in total) has always been striking leading to the hypothesis that unlike other known photoreceptors, UV-B photoreception does not rely on a bound chromophore but is mediated by aromatic amino acids of the receptor itself (Jenkins, 2009).

The mutation of selected tryptophan residues of UVR8 and the analysis of their impact on UV-B induced monomerisation provided first evidence for a tryptophan-based perception mechanism, with one tryptophan as a key residue (Rizzini et al., 2011). The recently reported x-ray crystallographic structure finally proved that photoactive UVR8 lacks any bound co-factor and that UV-B induced monomerisation is a property intrinsic to the protein (Christie et al., 2012; Wu et al., 2012). The crystal structure also revealed that the UVR8 dimer is very effectively maintained by a network of salt bridges formed via charged side chains positioned on the dimer interface (Christie et al., 2012; Wu et al., 2012). The role of these salt bridges for structure and function of the photoreceptor is analysed in detail in Chapter 3 and 4 of this thesis. Further biophysical characterisation of the purified photoreceptor mainly by far-UV circular dichroism (CD) spectroscopy has shown that four tryptophan residues which form a pyramid within the UVR8 dimer are key to photoperception (Christie et al., 2012). The close proximity of the aromatic side chains allows overlap of electronic orbitals resulting in exciton coupling of the tryptophans which will be described in detail in Chapter 3. Of the four tryptophans, W285 and W233 seem to play more crucial roles, whereas the other two, W94 and W337, are of auxiliary nature (Christie et al., 2012). The importance of tryptophan residues for UV-B photoperception has not only been shown in vitro but has also been reported in vivo (O'Hara and Jenkins, 2012). Mutational studies of three of the four pyramid forming tryptophans showed different extents of impaired photomorphogenic responses in plants, leading to the conclusion that also in vivo one specific tryptophan seems absolutely essential for UVR8 function (Christie et al., 2012; O'Hara and Jenkins, 2012). Each of the three tryptophans forming the base of the UV-B perceiving tryptophan pyramid is flanked by an arginine

residue. Two of these arginines participate in important dimer maintaining cross-dimer salt bridges and are essential for function of the photoreceptor (Chapter 3). Analysis of various tryptophan and arginine mutants suggests that the proximity and coupling of arginines and tryptophans provides a specific mechanism whereby photoreception leads to monomerisation (Christie et al., 2012). However, the precise primary response of UVR8 to UV-B at a structural level still remains elusive and needs further investigation (Chapter 6).

1.5 COP1 – a central switch of light signal transduction

1.5.1 COP1 as a negative regulator

One of the central components in light signal transduction is the now long known and extensively studied COP1 protein. It was established early on that COP1 negatively regulates light-mediated development in seedlings since *cop1* mutant seedlings undergo photomorphogenic development in the dark and *cop1* null alleles are lethal (Deng and Quail, 1992). Research in the past years has expanded the role of COP1 beyond seedling photomorphogenesis indicating a role of COP1 for example in flowering, circadian rhythm and plant defence (Liu et al., 2008; Yu et al., 2008; Jeong et al., 2010; Lau and Deng, 2012).

COP1 is an E3 ubiquitin ligase with three structural domains conserved in higher plants and vertebrates: a RING finger domain, a coiled-coil domain and seven WD40 repeats at the C-terminus. All three domains play a role in protein-protein interactions between COP1 and its substrates and the coiled-coil domain has also been shown to mediate self-dimerization of COP1 (Yi and Deng, 2005). COP1 is part of a multimeric E3 ubiquitin ligase complex that includes CULLIN4 (CUL4), DAMAGED DNA-BINDING PROTEIN1 (DDB1), RING-BOX1 (RBX1), and SUPPRESSOR OF PHYA (SPA) proteins (Chen et al. 2010). Through its E3 ubiquitin ligase activity, COP1 targets photomorphogenesis-promoting transcription factors of different families, such as HY5, LAF1 or HFR1 for ubiquitination and degradation in the dark to suppress their activities (Fig 1-3; Osterlund et al., 2000; Seo et al., 2003; Jang et al., 2005). The four SPA proteins act in concert with COP1 to suppress photomorphogenesis in the dark as shown by several mutant studies (Laubinger et al., 2004). Although the SPA proteins mostly act redundantly, they have distinct roles during plant development and the regulated abundance of SPA family members possibly leads to different COP1/SPA complexes with distinct functions (Fittinghoff et al., 2006; Chen et al., 2010)

COP1 activity has long been postulated to be primarily regulated by its nucleocytoplasmic partitioning controlled by light (von Arnim and Deng, 1994). Nuclear COP1 depletes upon light exposure and therefore nuclear-localized transcription factors can re-accumulate and activate the transcription of downstream genes required for photomorphogenesis. Since the nuclear abundance change of COP1 is rather slow this mechanism may represent only long-term suppression of COP1 under extended light conditions (von Arnim et al., 1997). A more rapid mechanism for down-regulation of COP1 by phytochromes and cryptochromes is believed to exist because far-red, red and blue light can initiate changes in the transcriptome observable within one hour (Jiao et al., 2007; Tepperman et al., 2001). Furthermore, COP1 has been detected in the cytoplasm as well as in the nucleus of etiolated seedlings or seedlings exposed to red light, which shows that the regulation of COP1 activity is far more complex than a simple spatial distribution of the protein (Jang et al., 2010). Recently, several studies revealed how cryptochromes inactivate the COP1 complex in response to blue light to allow accumulation of transcription factors required for photomorphogenesis. Here, blue light leads to interaction between CRY1 and SPA1 inhibiting at the same time COP1-SPA1 binding which is essential for COP1-mediated protein degradation (Lian et al., 2011). The interplay between CRY2, SPA1 and COP1 functions slightly different but also results in rapid inactivation of COP1 activity. The light-regulated CRY2-SPA1 interaction does not affect the interaction between COP1 and SPA1 but rather strengthens the CRY2/COP1 complex which suppresses the proteolytic activity of the COP1/SPA1 complex (Liu et al., 2011; Zuo et al., 2011). This allows accumulation of CONSTANS (CO) and initiates flowering under long day conditions. COP1 does not only interact with cryptochromes, it also interacts with phytochromes placing COP1 as a central regulator between photoreceptors and transcription factors. However, the mechanism by which phytochromes rapidly inhibit COP1 in response to red or far-red light is still largely unknown.

1.5.2 COP1 as a positive regulator of the UV-B response

The involvement of COP1 in the UV-B response was first reported by Oravecz and co-workers in 2006 when they observed that the *cop1-4* mutant is impaired in flavonoid accumulation and that the expression of as much as 75% of UV-B induced genes, including *HY5*, depends on the presence of functional COP1 (Oravecz et al., 2006). Combined with the microarray analyses of the *uvr8* mutant, this strongly indicates that almost all genes of the photomorphogenic UV-B pathway are activated in a UVR8- and COP1-dependent manner (Favory et al., 2009). COP1 and HY5 both accumulate in the nucleus under white

light supplemented with UV-B and act together as positive regulators of the UV-B response, whereas COP1 degrades HY5 in the nucleus in darkness (Fig 1-3; Oravecz et al., 2006; Favory et al., 2009). This observed nuclear accumulation contrasts with the current dogma of COP1 nuclear exclusion in response to light and suggests that under natural light conditions COP1 is located in the nucleus. However, nuclear accumulation of COP1 is also slow under UV-B and the much quicker induction of gene expression by UV-B indicates that processes other than nucleocytoplasmic partitioning are involved in the regulation, as also proposed for the other photoreceptors.

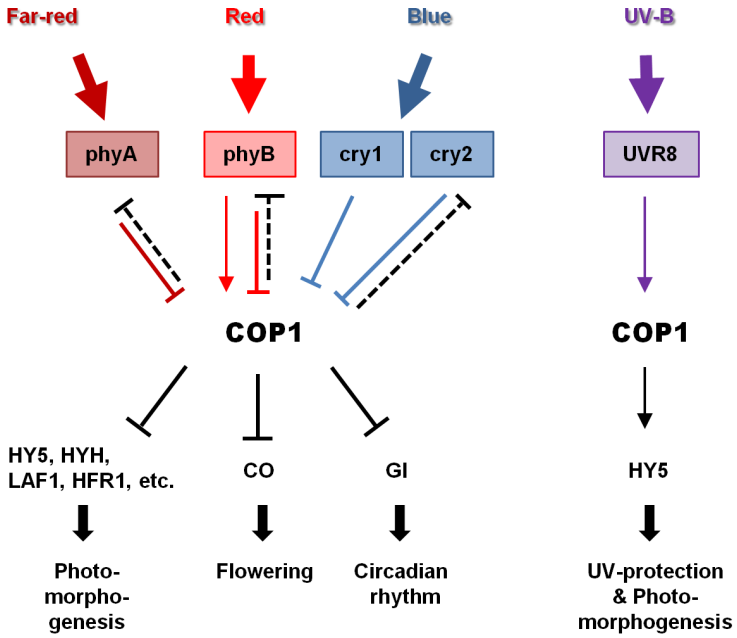

FIGURE 1-3: COP1 at the centre of light signal transduction.
COP1 acts downstream from multiple plant photoreceptors such as cryptochromes, phytochromes, and the UV-B receptor, and controls the light-regulated abundance of numerous transcription factors. Phytochrome and cryptochrome-mediated suppression of COP1 activity allows accumulation of the effectors, resulting in the specific light responses. Phytochrome and cryptochrome signalling is regulated through COP1 mediated degradation of the photoreceptors (dashed lines). Under UV-B, COP1 acts as a positive regulator in the signalling pathway by directly interacting with UVR8 (arrow) and promoting transcription of *HY5*. COP1 also acts positively in red light signalling mediated by phyB. CO: CONSTANS, GI: GIGANTEA (adapted from Lau and Deng, 2012).

UV-B stimulates the interaction between the UVR8 monomer and COP1 which is essential to initiate signal transduction and also one of the very upstream events in the signalling cascade (Favory et al., 2009; Cloix et al., 2012). The interaction is mediated by a region of 27 amino acids from the C-terminus of UVR8 and the WD40 domain of COP1 and has been demonstrated in plants as well as in the yeast two-hybrid system (Rizzini et al., 2011; Cloix et al., 2012). Despite growing knowledge about UVR8 as a UV-B photoreceptor, the

precise mechanism of COP1 function in the signalling pathway still remains elusive. However, the positive role of COP1 appears not to be specific to UV-B because a positive relationship between COP1 and photomorphogenic responses mediated via phyB has been observed (Boccalandro et al., 2004). Weak alleles of *cop1* show reduced rather than enhanced cotyledon unfolding under red light compared to darkness and conversely COP1 overexpressor lines show enhanced de-etiolation under red light (Boccalandro et al., 2004). Very recently, it has been reported that *COP1* is a UV-B inducible gene, whose full activation requires binding of the two transcription factors HY5 and FAR-RED ELONGATED HYPOCOTYL3 (FHY3) to its promoter region establishing a positive feedback loop that maintains the activated UVR8-COP1-HY5 signalling pathway (Huang et al., 2012). So far, it cannot be excluded that COP1 acts as a positive regulator in other light responses as well. Also whether COP1 functions in the UV-B response as an E3 ubiquitin ligase degrading so far unidentified negative regulators of the pathway or whether COP1 may act via a yet undiscovered mechanism remains to be seen.

1.6 Negative feedback regulation of light signalling pathways

Equally important to activation of a signalling pathway is the negative regulation of signalling to ensure that a response to a single stimulatory event is not perpetuated indefinitely. One of the most important post-translational regulatory events is the degradation of receptor proteins and other signalling components through ubiquitination and proteolysis (Henriques et al., 2009). Over the years, COP1 and associated proteins of the E3 ubiquitin ligase complex have been implicated in light regulated feedback mechanisms that control the level of activated photoreceptors.

The first photoreceptor that was described as a degradation substrate for COP1 was the light labile photoreceptor phyA (Seo et al., 2004). COP1 and phyA interaction and subsequent ubiquitination of phyA was shown in vitro and phyA accumulated to higher levels in *cop1* mutant plants after exposure to light compared to wild-type (Seo et al., 2004). More recently it was discovered that the light stable phytochromes B-E are also subject to degradation to prevent over-activation of their signalling pathways. Several studies using various single and double *pif*-mutant combinations revealed that upon continued exposure to red light, signalling by the Pfr form of phyB is terminated by COP1-mediated degradation, which is promoted by PIFs (Leivar et al., 2008; Al-Sady et al., 2008; Jang et al., 2010). Possibly, the binding of PIFs to both phyB and COP1 increases the affinity of the photoreceptor for COP1, thereby increasing ubiquitination and its

degradation. However, in contrast to the nuclear turnover of phyB, the cytosolic pool of phyB has shown to be rather stable dampening the overall decay rate and justifying its designation as a light-stable photoreceptor (Jang et al., 2010).

For the cryptochromes, so far only degradation of the light labile cry2 has been observed. Irradiation of seedlings with blue lights leads to cry2 phosphorylation and poly-ubiquitination (Shalitin et al., 2002; Yu et al., 2007). Higher levels of cry2 can be observed in *cop1* mutant plants under blue light compared to wild-type (Shalitin et al., 2002). Furthermore, cycloheximide and proteasome inhibitor studies have shown that the decrease in cry2 is due to 26S-proteasome mediated degradation in the nucleus (Yu et al., 2009). The stability of cry2 is further controlled by phyA and SPA1, which reveals another molecular mechanism of interaction between cryptochromes and phytochrome photoreceptors (Weidler et al., 2012).

Limited knowledge yet exists about negative feedback regulation of the UVR8-dependent UV-B signalling pathway. UVR8 seems to be light stable with unchanged protein levels after exposure to UV-B (Kaiserli and Jenkins, 2007; Rizzini et al., 2011). The SPA proteins, which have been shown to be important regulators of COP1 activity in all light qualities (Laubinger et al., 2004) are not required for COP1 function in the UV-B response since UV-B responsive gene activation is still possible in a *spa1 spa2 spa3 spa4* quadruple mutant (Oravecz et al., 2006). The enhanced UV-B photomorphogenic response in UVR8 overexpressor lines suggests that a balanced UV-B response also requires negative regulation. Recently, two highly related WD40-repeat proteins, REPRESSOR OF UV-B PHOTOMORPHOGENESIS1 (RUP1) and RUP2, were identified as potent repressors of UV-B signalling (Gruber et al., 2010). RUP1 and RUP2 were identified and described in parallel as EARLY FLOWERING BY OVEREXPRESSION1 (EFO1) and EFO2, overexpression of which leads to an early flowering phenotype (Wang et al., 2011). Transcript levels of EFO1 and EFO2 are regulated by the circadian clock showing high expression levels at night peaking at daybreak and declining during the day (Wang et al., 2011). Transcriptional activation of both genes requires functional COP1, UVR8 and HY5 and is observed under UV-B but also under other light qualities (Gruber et al., 2010). The r*up1 rup2* double mutants showed an enhanced response to UV-B and elevated UV-B tolerance after acclimation. Conversely, overexpression of RUP2 reduced UV-B induced photomorphogenesis and impaired acclimation, leading to UV-B hypersensitivity of the mutant. Importantly, UVR8 levels were not affected by altered RUP1 and RUP2 accumulation. The role of RUP1 and RUP2 in the UV-B signalling pathway is far from being understood especially since both proteins are able to interact with UVR8 in the

presence and absence of UV-B (Gruber et al., 2010) and the interaction is mediated by the C-terminal C27 region of UVR8 which is also the site of interaction between UVR8 and COP1 (Cloix et al., 2012).

Negative regulation of the UV-B signalling pathway also seems to be possible through regulation of HY5 activity. The UV-B inducible STO/BBX24 (SALT TOLERANCE/B-BOX ZINC FINGER PROTEIN24) protein interacts with COP1 and HY5 in a UV-B dependent manner and negatively regulates UV-B induced HY5 accumulation (Yan et al., 2011; Jiang et al., 2012). However, the precise role of BBX4 in the UV-B response and its relationship to UVR8 and COP1 needs further investigation. The fact that BBX24 has been described as a negative regulator in phytochrome and cryptochrome signalling (Indorf et al., 2007) reveals once more the connectivity of visible light and UV-B signalling pathways since UV-B is an integral component of natural sunlight and plants constantly have to cope with this environmental factor.

1.7 Conclusion

Research within the last decade has produced major breakthroughs in the area of light perception and signal transduction and has widened our understanding of how plants can cope with their ever changing environment. The very recent discoveries in UV-B photoperception finally establish a further class of plant photoreceptors, extending photoreception of plants beyond the visible part of the electromagnetic spectrum. Elucidation of the crystal structure of UVR8 as well as the discovery of UV-B induced monomerisation of the protein has led to rapid advances in the field of UV-B signalling within the time period of producing this thesis. Remarkably, UV-B photoreception is distinct from other known photoreceptors in exploiting the UV-B absorbance of UVR8's intrinsic tryptophans, rather than a bound chromophore. To fully understand the mechanism of UVR8 photoreception and downstream signalling will be a future challenge and will reveal a new mechanism of light perception. The so far known UVR8 signalling pathway shares similarities with visible light signalling but also shows some major differences. The study of central interactors of all pathways will shed light on the crosstalk and integration of UVR8 signalling pathways with visible light photoreceptor pathways extending the light signalling network beyond the visible part of sunlight.

1.8 Aims of this study

The key aspect of this study was to investigate how the structure of the UVR8 protein determines its function in the UV-B response in Arabidopsis. Several regions of the protein have been shown to be essential for UVR8 function (Kaiserli and Jenkins, 2007; Kaiserli, Ph.D. thesis, 2007) but prior to the present study, no specific single amino acids involved in the UV-B response had been identified. Sequence analysis of UVR8 showed a conserved and repeated motif GWRHT that surrounds three tryptophans that were postulated to be involved in UV-B perception. This motif was chosen as a starting point for the undertaken structure-function studies in Chapters 3 and 4.

In order to identify the role of specific amino acids in this motif, a site-directed mutagenesis approach was applied. Stable transgenic Arabidopsis lines expressing various mutant forms of GFP-UVR8 were generated and were assessed for functionality by testing complementation of the *uvr8-1* phenotype with respect to *HY5* and *CHS* gene expression, occurrence of a photomorphological UV-B response, i.e. suppression of hypocotyl extension, as well as interaction between UVR8 and COP1. This interaction can also be seen in yeast and therefore a yeast two-hybrid system was used as well.

An abundance of structural information became available with elucidation of the crystal structure of UVR8 (Christie et al., 2012). Furthermore, the discovery that UVR8 exists as a homodimer and UV-B induces monomerisation (Rizzini et al., 2011) opened another way of characterizing mutant forms of UVR8 and assigning function to single amino acids. It was possible to extend the mutagenesis approach to previously unidentified interacting amino acids spanning across the dimer interface. The key question arising from these studies was whether monomeric UVR8 is sufficient for photoreception and function.

Another focus of this study was the important issue of regeneration of the functional UVR8 photoreceptor following photoreception. Since UV-B photoreception converts the UVR8 dimer into a monomer, the dimeric photoreceptor has to be restored at some point. Two possible ways of regeneration were investigated - de novo synthesis following degradation of the monomer and regeneration by reversion from monomer to dimer.

Finally, a biophysical approach was pursued to gain first insights into the mechanism of the very initial steps of UV-B photoreception through the tryptophan pyramid and its adjacent arginine salt bridges. Fourier transform infrared (FTIR) spectroscopy was applied to detect photo-induced changes in the protein structure and amino acid side chains. To investigate a possible electron transfer between tryptophans and arginines ultrafast transient absorption spectroscopy was used to detect possible tryptophan radicals formed following UV-B absorption.

In summary, the aim of this study is to contribute to the understanding of how UVR8 regulates UV-B initiated responses in plants. Therefore, it is essential to have a detailed knowledge of the structural properties of the photoreceptor and its early signalling mechanism to understand how UV-B perception initiates signal transduction.

2. MATERIAL AND METHODS

2.1 Materials

2.1.1 Chemicals

The chemicals used for all experiments described were obtained from Fisher Scientific UK Ltd. (Loughborough, Leicestershire, UK), VWR International Ltd. (Poole, Dorset, UK) and Sigma Aldrich Ltd. (Poole, Dorset, UK) unless stated otherwise.

2.1.2 Antibiotics

Ampicillin and gentamycin were purchased from Melford Ltd. (Ipswich, Suffolk, UK). Kanamycin was obtained from Sigma-Aldrich and chloramphenicol from Duchefa Biochemie B.V. (Haarlem, The Netherlands). Working concentrations of the antibiotics are given in the following table:

TABLE 2-1: Working concentrations of used antibiotics.

Antibiotic	Solvent	Working Concentration
Ampicillin	H_2O	100 µg/ml
Chloramphenicol	EtOH	34 µg/ml
Gentamycin	H_2O	30 µg/ml
Kanamycin (*E. coli*)	H_2O	50 µg/ml
Kanamycin (plants)	H_2O	75 µg/ml

2.1.3 Enzymes

Enzymes used for DNA restriction digests, ligations, synthesis and DNA/RNA modifications were purchased from Promega (Southampton, Hampshire, UK), New England Biolabs (Hitchin, Hertfordshire, UK) as well as Ambion Inc. (Huntigdon, Cambridgeshire, UK) and were used according to the manufacturer's instructions.

2.1.4 Vectors

The following plasmid DNA vectors were used in this study:

TABLE 2-2: Used plasmid DNA vectors.

Plasmid Vector	Application	Source
pEZR(K)L-C	GFP tagged transgenic Arabidopsis lines	Dr. Gert-Jan de Boer
pGBKT7	Yeast two-hybrid	Clontech
pGADT7	Yeast two-hybrid	Clontech
pHS	*E. coli* protein expression/purification	Michael Hothorn

2.1.5 Bacterial and yeast strains

E. coli strains TOP10, XL1-Blue and Gold (Agilent Technologies, California, USA) and Rosetta 2 (DE3) pLysS (Novagen, Merck KGaA, Darmstadt, Germany) were transformed with various plasmid vector constructs for sub-cloning and protein expression. *A. tumefaciens* strain GV3101 was used for Arabidopsis transformation with the pEZR(K)L-C vector containing various constructs of mutant UVR8. *S. cerevisiae* strain AH109 (Clontech) was used for the yeast two-hybrid assay transformed with bait and prey vectors (pGBKT7 and pGADT7 respectively)

2.1.6 Other reagents

All reagents required for protein work (electrophoresis and immunoblotting) were purchased from Bio-Rad Laboratories (California, USA) unless stated otherwise.

2.2 Preparation of media and solutions

2.2.1 Measurement of pH

The pH of solutions and media was measured using either a glass electrode connected to a Jenway 3320 pH meter (Jenway, Felsted, Essex, UK) or pH Indicator Strips (BDH, Poole, Dorset, UK).

2.2.2 Autoclave sterilisation

Solutions and equipment were sterilised using a benchtop autoclave (Prestige Medical, Model 220140).

2.2.3 Filter sterilisation

Heat sensitive solutions or solutions of small volume were sterilised by filtration through a 0.2 µm pore diameter Nalgene filter.

2.3 Plant material

2.3.1 Seed stocks

Wild-type *A. thaliana* cv. Landsberg *erecta* (L*er*) and Wassilewskija (W*s*) seeds were obtained from The European Arabidopsis Stock Centre (NASC, Nottingham, UK). Prof. Daniel Kliebenstein (UC Davis, CA, USA) provided the *uvr8-1* mutant (L*er*), Dr. Bobby Brown the *uvr8-2* mutant (L*er*) (Brown et al., 2005) and Prof. Roman Ulm (University of Geneva, Switzerland) the *cop1-4* (W*s*) mutant. The *hy5-ks50*, *hyh* and *hy5-ks50-hyh* mutants (all in W*s*) were supplied by Prof. Xing Wang Deng (Yale University, CT, USA). The GFP-UVR8 and GFP-ΔC27UVR8 lines were generated in the Jenkins lab by Eirini Kaiserli (Kaiserli and Jenkins, 2007; Cloix et al., 2012).

2.3.2 Growth of plants on soil

Arabidopsis seeds were sown on the surface of pots containing compost soaked in insecticide solution (0.2 g/l Intercept® (Scotts, Ipswich, Suffolk, UK)). The pots were kept under a humidifier during a vernalisation period of 2-4 days and for one week after germination in the growth chamber at 20°C. In general, plants grown on soil were either used for transformation with Agrobacterium or for seed collection of transgenic lines. In both cases, plants were grown under high fluence rate of white light (100 µmol m^{-2} s^{-1}) until flowering or until dried out. Plants used for treatments and experiments were generally grown on agar plates with ½ MS medium (see 2.3.4).

2.3.3 Surface sterilisation of Arabidopsis seeds

Arabidopsis seeds were surface sterilised for growth of plants on agar plates with ½ MS medium by a 5 min incubation in a sodium hypochlorite solution (50% (v/v)) followed by three washes in sterile dH_2O.

2.3.4 Growth of Arabidopsis plants on agar plates

Sterilised Arabidopsis seeds were sown on 0.8% agar plates containing 2.15 g/l Murashige and Skoog salts (½ MS) with the pH adjusted to 5.7. For segregation studies of transgenic Arabidopsis lines 75 µg/ml kanamycin was added. Seeds were cold-treated on the plates in

the dark at 4°C for 2-4 days and then grown under high fluence rate of white light (100 µmol m^{-2} s^{-1}) for the required period of time. Plants for RT-PCR experiments were grown for ten days under high fluence rate of white light and then transferred for 4 days under low fluence rate of white light (20 µmol m^{-2} s^{-1}). Protein extractions were performed on 7-14 d old seedlings grown under high white light.

2.4 Treatments

2.4.1 Light sources

Light treatments were carried out in growth chambers at 20°C. Warm white fluorescent tubes L36W/30 (Osram, Munich, Germany) were used for white light (Fig 2-1 A). Two UV-B sources were used in this study: either narrowband UV-B tubes, Philips TL20W/01RS (Philips, Aachen, Germany; Fig 2-1 B) or broadband UVB-313 fluorescent tubes (Q-Panel Co., USA; Fig 2-1 C). The broadband UVB-313 fluorescent tubes were covered by cellulose acetate filter (Cat No. FLM400110/2925, West Design Products, Nathan Way, London) which was changed every 24 h in order to eliminate any UV-C. This source has a maximal emission at 313 nm and emits very low levels of UV-A and blue light, which have been found to be insufficient to induce CHS expression (Christie and Jenkins, 1996). The narrowband UV-B source has a maximal emission at 311 nm. The use of various cut-off filters in combination with this UV-B source has also shown that the very low levels of UV-A and blue light that are emitted are insufficient to induce a UV-A/blue light specific response (Ulm et al., 2004).

2.4.2 Light fluence rate measurements

Fluence rates of white light were measured using a LI-250A light meter with a LI-190 quantum sensor (LI-COR, Lincoln, NE, USA). UV-B fluence rates were measured using either a RS232 meter or a Spectro Sense 2 SKL904 meter fitted with a UV-B Sensor (SKU 430/SS2) (Skye Instruments, Powys, UK). For detailed spectral measurements a Macam Spectroradiometer Model SR9910 (Macam Photometrics Ltd., Livingston, UK) recording wavelengths of light between 240 and 800 nm was used.

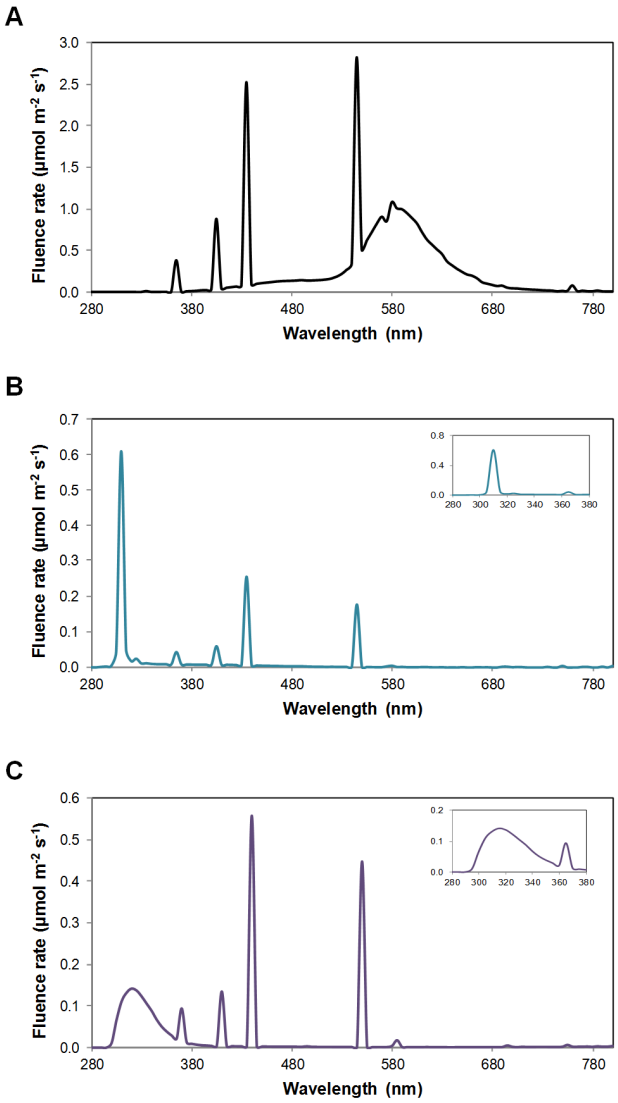

FIGURE 2-1: Spectra of the light sources used in this study. (A) Spectrum of the white light fluorescent tubes L36W/30 **(B)** Spectrum of the narrowband UV-B tubes, Philips TL20W/01RS **(C)** Spectrum of the broadband UV-B-313 fluorescent tubes, Q panel.

2.4.3 UV-B

Plants were put in darkness overnight before the start of the UV-B treatment. Plants were exposed to 3 µmol m^{-2} s^{-1} narrowband UV-B (Philips TL20W/01RS) for 3 h if not indicated otherwise. Plant extracts were exposed on ice to 4 µmol m^{-2} s^{-1} narrowband UV-B for 30 min. Plants used for RT-PCR experiments were treated with 3 µmol m^{-2} s^{-1} broadband UV-B for 4 h. Purified protein was exposed to 1.5 µmol m^{-2} s^{-1} narrowband UV-B for 1 h.

For measurements of hypocotyl length, seedlings were grown for 4 d under 1.5 µmol m^{-2} s^{-1} white light supplemented with 1.5 µmol m^{-2} s^{-1} narrowband UV-B. A UV-B cut-off filter ('Clear 130' mylar filter, Lee Filters, Andover, UK) was used for control plants grown under ' -UV-B' conditions. For reversion studies, plants were moved back in darkness after exposure for ascertained times before preparation of protein extracts.

2.4.4 Cycloheximide and MG132

For cycloheximide and MG132 treatments, plants were transferred to liquid ½ MS medium containing cycloheximide (100 µM, dissolved in dimethyl sulfoxide (DMSO); Sigma) or MG132 (100 µM, dissolved in DMSO; Calbiochem) and were incubated for 1 h or 11 h respectively prior to the UV-B treatment. Control plants were equally treated with 0.1% DMSO.

2.5 Bacterial transformation

2.5.1 Preparation of competent E. coli cells for electroporation

A colony of *E. coli* TOP10 cells was inoculated in a 5 ml subculture of Luria broth (LB) medium and grown overnight at 37˚C with constant shaking (200 rpm). The following day, 250 ml LB medium was inoculated with the subculture and grown until it reached an OD_{600} of ~ 0.4. Cells were then pelleted at 4,000 g for 10 min at 4°C. The supernatant was discarded and the pellet was washed 3 times with 50 ml ice cold water and once with 20 ml CCMB80 buffer (10 mM KOAc pH 7.0, 80 mM $CaCl_2 \cdot 2H_2O$, 20 mM $MnCl_2 \cdot 4\ H_2O$, 10 mM $MgCl_2 \cdot 6\ H_2O$, 10% glycerol, adjust pH to 6.4 with 0.1 N HCl). The pellet was finally resuspended in 5 ml CCMB80 buffer. Aliquots of 100 µl were snap frozen in liquid nitrogen and stored at -80°C.

2.5.2 Transformation of chemically competent E. coli cells

Various strains of chemically competent *E. coli* cells TOP10, Rosetta 2 (DE3) pLysS (Novagen, Merck KGaA, Darmstadt, Germany), XL1-Blue and XL10-Gold (Agilent Technologies, CA, USA) were used. All strains were transformed according to the manufacturer's instructions with a heat shock at 42°C and plated onto agar plates containing LB medium and the appropriate antibiotic for the selection of the plasmid. Plates were incubated at 37°C overnight.

2.5.3 Preparation of competent A. tumefaciens cells for electroporation

An aliquot of Agrobacterium strain GV3101 was inoculated in a 10 ml subculture of LB medium containing 30 µg/ml gentamycin and grown for 20-24 h at 28°C with constant shaking (200 rpm). The following day, one litre of LB medium with rifampicillin and gentamycin was inoculated with the subculture to approximately an OD_{600} of 0.1 and grown until it reached an OD_{600} of 0.5 - 0.8. Cells were then pelleted at 2,000 g for 10 min at 4°C. The supernatant was discarded and the pellet was gently resuspended in 100 ml

cold sterile 10% (v/v) glycerol. Centrifugation and resuspension was repeated twice only changing the volume of 10% glycerol used to 10 ml and finally 1 ml. Aliquots of 50 µl were frozen on dry ice and stored at -80°C.

2.5.4 Transformation of electroporation competent A. tumefaciens *cells*

To competent cells of Agrobacterium (2.5.3) 1-2 µl of plasmid DNA were added and incubated on ice for 20-30 min. Cells were then transferred into a chilled electroporation cuvette (Bio-Rad) and pulsed with 2.2 kV using a MicroPulser™ Electroporator (Bio-Rad). Immediately after, 950 µl of LB medium was added to the cells which were then transferred to a 15 ml Falcon® tube and incubated at 28°C at constant shaking (200 rpm) for 3 h (expression of antibiotic resistance genes). To ensure colonies with good separation from each other on the plates were obtained, 50 µl of 1/10 and 1/1000 dilutions were spread onto LB agar plates containing appropriate selective antibiotics. Plates were incubated at 28°C for 2 days and colonies for further use tested using colony PCR with the appropriate primers.

2.6 DNA and RNA methods

2.6.1 Isolation of genomic DNA from Arabidopsis plants

Genomic DNA from Arabidopsis plant tissue was isolated using the DNeasy® Plant Mini Kit (Qiagen, Crawley, West Sussex, UK) according to the manufacturer's instructions. Approximately 100 mg of tissue were ground to fine powder under liquid nitrogen using a mortar and pestle and then transferred into an Eppendorf tube. Cell lysis and genomic DNA purification was carried out as described in the Qiagen DNeasy® Plant Mini Kit. Purified genomic DNA was eluted from the DNeasy membrane by adding 50 µl of pre-heated buffer AE. Genomic DNA samples were stored at 4°C.

2.6.2 Isolation of plasmid DNA

Small and large-scale plasmid DNA purifications from *E. coli* were performed using the Qiagen® Plasmid Mini or QIAfilter™ Plasmid Maxi Kit respectively. A single bacterial colony was inoculated into 10 ml (small-scale) or 250 ml (large-scale) of LB medium containing the appropriate antibiotics for plasmid selection. The cultures were incubated overnight at 37°C with constant shaking (200 rpm). Cells were pelleted at 6,000 g for 10 min and the supernatant was discarded. Cell lysis and plasmid DNA purification was carried out according to the manufacturer's instructions. Plasmid DNA was stored at -20°C.

2.6.3 Isolation of total RNA from Arabidopsis plants

Total RNA from Arabidopsis leaf tissue was isolated using the RNeasy® Plant Mini Kit (Qiagen) according to the manufacturer's instructions. Approximately 100 mg of tissue were ground to fine powder under liquid nitrogen using a mortar and pestle and then transferred into an Eppendorf tube. Cell lysis was performed with RLT buffer and β-mercaptoethanol. The procedure described in the Qiagen manual was followed in order to obtain purified RNA, which was eluted from the RNeasy spin column with 30 µl of RNase free water. RNA samples were stored at -80°C.

2.6.4 Quantification of DNA and RNA

To quantify purified nucleic acids, 2 µl of DNA or RNA were diluted in 70 µl of dH_2O and the absorbance at 260 nm as well as 280 nm was measured (Eppendorf Bio Photometer) against a dH_2O blank sample. An absorbance of 1 at 260 nm corresponds to a concentration of 50 µg/ml double-stranded DNA or 40 µg/ml of single-stranded DNA or RNA (Sambrook and Russell, 2001). The ratio of the absorbance 260/280 indicates the purity of the sample (1.8 for DNA, 2.0 for RNA).

2.6.5 Restriction digest

For restriction digests 0.5 to 1 µg of DNA were digested using the appropriate restriction enzymes and buffers at concentrations and incubation conditions according to the manufacturer's instructions.

2.6.6 DNA ligation

Digested and purified DNA derived from PCR amplifications or plasmid DNA with appropriate restriction sites were used for subsequent DNA ligations. An aliquot of plasmid vector and DNA insert was separated on an agarose gel to estimate quantities. An approximate 3:1 ratio of insert:vector was calculated. Reactions were done in a total volume of 10 µl containing 1 x ligation buffer and 1 µl of T4 DNA ligase (Promega). The ligation mix was incubated either at room temperature for 3 h or at 4°C overnight. 2-5 µl of the ligation mix was used for transformation of competent *E. coli* cells (TOP10).

A second ligation method using polyethylene glycol (PEG) as a crowding reagent was also applied in some cases. PEG alters the distribution of ligation products thereby suppressing intramolecular ligation and favouring intermolecular joining events even at concentrations of DNA that favour circularisation. PEG 6000 was used in a final concentration of 2.5% together with 1 x ligation buffer and 1 µl of T4 DNA ligase and a 1:1 ratio of vector:insert accounting for 8.6 µl of the total 12 µl reaction volume. The ligation mix was incubated at

room temperature for 1 h followed by a 30 min inactivation period at 68°C. Two µl of the ligation was used for transformation of competent *E. coli* cells.

2.6.7 Site-directed mutagenesis

Specific mutations in the UVR8 gene were introduced by site-directed mutagenesis using *Pfu* Polymerase (Promega) and extension times of 2 min per kb at 68˚C. Primers that were used are listed in the table below. All constructs were verified by DNA sequencing.

TABLE 2-3: Primers used for site-directed mutagenesis.

Mutation		Primer Sequence
D96N	**F**	5'-ACAGTTGGGGATGGGGTAATTTTGGGAGATTAGGC-3'
	R	5'-GCCTAATCTCCCAAAATTACCCCATCCCCAACTGT-3'
D107N	**F**	5'-GCCATGGTAACTCAAGCAACTTGTTTACTCCGCTA-3'
	R	5'-TAGCGGAGTAAACAAGTTGCTTGAGTTACCATGGC-3'
R146A	**F**	5'-GTCCAGAGTTGGGGCGCCAACCAGAATGGTCA-3'
	R	5'-TGACCATTCTGGTTGGCGCCCCAACTCTGGAC-3'
R234A	**F**	5'-AATGGTTGCTTGTGGATGGGCGCACACAATATCAGTTTCC-3'
	R	5'-GGAAACTGATATTGTGTGCGCCCATCCACAAGCAACCATT-3'
H235A	**F**	5'-GTTGCTTGTGGATGGCGGGCCACAATATCAGTTTCCTAC-3'
	R	5'-GTAGGAAACTGATATTGTGGCCCGCCATCCACAAGCAAC-3'
R286A	**F**	5'-CCAGATTTCGGGAGGTTGGGCACATACAATGGCATTGACT-3'
	R	5'-AGTCAATGCCATTGTATGTGCCCAACCTCCCGAAATCTGG-3'
R286K	**F**	5'-CCAGATTTCGGGAGGTTGGAAACATACAATGGCATTG-3'
	R	5'-CAATGCCATTGTATGTTTCCAACCTCCCGAAATCTGG-3'
R286E	**F**	5'-CCAGATTTCGGGAGGTTGGGAACATACAATGGCATTGACT-3'
	R	5'-AGTCAATGCCATTGTATGTTCCCAACCTCCCGAAATCTGG-3'
H287A	**F**	5'-GATTTCGGGAGGTTGGAGAGCTACAATGGCATTGACTTCA-3'
	R	5'-TGAAGTCAATGCCATTGTAGCTCTCCAACCTCCCGAAATC-3'
T288A	**F**	5'-CGGGAGGTTGGAGACATGCAATGGCATTGACTTCA-3'
	R	5'-TGAAGTCAATGCCATTGCATGTCTCCAACCTCCCG-3'
R338A	**F**	5'-CAAGTCTCATGTGGATGGGCACATACCTTGGCTGTCAC-3'
	R	5'-GTGACAGCCAAGGTATGTGCCCATCCACATGAGACTTG-3'
H339A	**F**	5'-GTCTCATGTGGATGGAGAGCTACCTTGGCTGTCACTGA-3'
	R	5'-TCAGTGACAGCCAAGGTAGCTCTCCATCCACATGAGAC-3'

2.6.8 Electrophoresis of DNA

Gel electrophoresis of DNA was performed on 1% agarose gels with 0.2 µg/ml ethidium bromide (1% (w/v) agarose melted in 1 x TAE buffer (40 mM Tris-HCl, 1 mM EDTA)). DNA samples were mixed with 6 x loading buffer (Promega) and separated by agarose gel electrophoresis in TAE buffer at 100 V.

2.6.9 Extraction and purification of DNA from agarose gels

From DNA separated on 1% agarose ethidium bromide-stained gels, bands of the expected size were excised under a UV-illuminator. The DNA was then purified according to the instructions of the QIAquick® Gel Extraction Kit (Qiagen).

2.6.10 DNA sequencing

Sequencing of DNA was carried out by the Dundee Sequencing Service (University of Dundee, UK) or by GATC Biotech (Konstanz, Germany) according to the service's instructions. Sequencing was always performed after a series of sub-cloning reactions to verify the sequence of the DNA insert in every vector used in this study.

2.7 Semi-quantitative Reverse Transcriptase PCR (RT-PCR)

2.7.1 DNase treatment of RNA

Following extraction of total RNA, a DNase treatment (DNA-free, Ambion) was used to eliminate contamination with genomic DNA. Approximately 5 µg of RNA were incubated with 4 units of DNase I and 1 x DNase buffer at 37° C for 1 h. The reaction was terminated by adding DNase Inactivation Reagent to the samples and incubating for 2 min at room temperature before pelleting the inactivation reagent by microcentrifugation. Efficiency of the DNase treatment was tested by a 35 cycle PCR reaction using primers for *ACTIN2*. If no PCR product was detected, DNase treated samples were used for cDNA synthesis. Otherwise the DNase treatment was repeated until no PCR product due to genomic DNA contamination could be detected.

2.7.2 Synthesis of cDNA

Synthesis of cDNA was performed according to Brown et al. (2005). 20 µl of the DNA-free RNA samples were incubated with 0.24 µM oligo dT (dTTP15) at 70°C for 10 min. The mixtures were cooled down on ice and 1 x AMV Reverse Transcriptase Reaction Buffer (Promega), 20 units of AMV Reverse Transcriptase (Promega), 1 mM of dNTPs (Promega) and 50 units of RNase inhibitor (Promega) were added. The reactions were allowed to proceed at 48°C for 45 min followed by 5 min at 95°C to inactivate the enzyme. The cDNA samples were stored at -20°C.

2.7.3 RT-PCR primers

ACTIN2, *HY5* and *CHS* transcripts were assayed by RT-PCR with gene-specific primers as used in Brown and Jenkins (2008). Primers were synthesised by Invitrogen and are listed in the table below.

TABLE 2-4: Primers used for RT-PCR.

Gene		Primer Sequence	Fragment size (bp)
ACTIN2 (at3g18780)	**F**	5'-CTTACAATTTCCCGCTCTGC-3'	500
	R	5'-GTTGGGATGAACCAGAAGGA-3'	
HY5 (at5g11260)	**F**	5'-GCTGCAAGCTCTTTACCATC-3'	404
	R	5'-AGCATCTGGTTCTCGTTCTG-3'	
CHS (at5g13930)	**F**	5'-ATCTTTGAGATGGTGTCTGC-3'	337
	R	5'-CGTCTAGTATGAAGAGAACG-3'	

2.7.4 RT-PCR conditions

Equivalent amounts of cDNA, estimated using reactions with *ACTIN2* primers, were used as template for semi-quantitative RT-PCR reactions with the following PCR conditions: 2.5 min at 94˚C, 1 min at 55˚C, 2 min at 72˚C for one cycle, then 45 s at 94˚C, 1 min at 55˚C, 1 min at 72˚C for 24 cycles (*ACTIN2*) and 28 cycles for *CHS* and *HY5* followed by 5 min at 72˚C. Each PCR reaction contained 1x PCR buffer (New England Biolabs), 0.1 mM dNTPs, 0.5 µM of each gene-specific primer and 0.625 units Taq DNA polymerase (New England Biolabs) in a final volume of 25 µl. PCR products were visualized by electrophoresis on agarose gels containing ethidium bromide.

2.8 Protein methods

2.8.1 Protein extraction from Arabidopsis plants

For protein extractions, Arabidopsis plants were ground on ice with a mortar and pestle in micro-extraction buffer (20 mM HEPES pH 7.8, 450 mM NaCl, 50 mM NaF, 0.2 mM EDTA, 25% (v/v) glycerol, 0.5 mM PMSF, 1 mM DTT and protease inhibitor mix (Complete Mini, Roche)). The homogenate was then centrifuged at 16,000 g for 10 min at 4°C and the supernatant was transferred to a fresh tube.

2.8.2 *Protein extraction from* N. benthamiana *plants*

For protein extractions from *N. benthamiana* plants, leaf parts were frozen in liquid nitrogen and ground with a mortar and pestle. *N. benthamiana* is rich in phenolic compounds and to avoid interference of those with downstream applications a spatula of polyvinyl-pyrrolidone (PVP), an effective absorbent for phenolic compounds, was added as soon as the liquid nitrogen had evaporated. Once ground, the plant material was transferred to a microcentrifuge tube and approximately one volume of extraction buffer (25 mM Tris-HCl pH 7.5, 1 mM EDTA, 10% glycerol, 5 mM DTT, 0.1% Triton) was added and vortexed to mix homogenously. Samples were then centrifuged at 16,000 g for 15 min at 4°C and the supernatant was transferred to a fresh tube.

2.8.3 *Quantification of protein concentrations*

The protein concentration of obtained samples was determined by the Bradford colorimetric method using bovine serum albumin (BSA) as a standard. Bradford assay solution (Bio-Rad, UK) was diluted five-fold with distilled water and filter sterilized to remove any particles. 1 µl of protein extract was added to 1 ml of Bradford solution and mixed well to obtain a homogenous colour. The absorbance at 595 nm was recorded with a spectrophotometer (Eppendorf, Germany) against a blank sample (Bradford solution without added protein). The concentration of each sample was calculated based on the equation of a standard curve that was generated using a serial dilution of BSA standards of known concentrations (1, 2, 4, 6, 8, 10 µg/µl).

2.8.4 *Immunoprecipitation of GFP-tagged proteins from plant extracts*

Total protein extracts from either Arabidopsis or *N. benthamiana* plants were used for immunoprecipitation of GFP-tagged proteins using magnetic anti-GFP micro-beads (µMac^{TM} beads, 130-091-370, Miltenyi Biotech). Per IP reaction, 1.5 mg (Arabidopsis cell extract) or 7.5 mg protein (*N. benthamiana* extract) was used. The protein samples were incubated on ice in the dark or under UV-B with 50 µl micro-beads for 30 min. A microcolumn was equilibrated with 200 µl lysis buffer (450 mM NaCl, 1% (v/v) Triton-X, 50 mM Tris-HCl pH 8) before the lysate containing the anti-GFP micro beads was applied on the column. Non-GFP tagged proteins were allowed to flow through the column and the GFP-tagged proteins together with any interacting proteins were retained on the column via magnetic interaction through the micro-breads. The column was washed four times with 200 µl high salt lysis buffer and once with 100 µl wash buffer 2 (300 mM NaCl, Tris-HCl pH 7.5). To elute, 20 µl of elution buffer (0.1 M triethylamine pH 11.8, 0.1% (v/v)

Triton X) was applied on the column and incubated for 5 min at room temperature. An extra 50 µl of elution buffer were added and the eluate was collected in a microcentrifuge tube containing 3 µl of 1 M MES pH 3 in order to neutralise the pH of the samples to avoid abnormalities during migration on SDS-PAGE.

Immunoprecipitated samples that were used for subsequent size exclusion chromatography were buffer exchanged into wash buffer II (50 mM Tris-HCl pH 7.5, 150 mM NaCl, 1 mM β-mercaptoethanol) or wash buffer II HS (50 mM Tris-HCl pH 7.5, 500 mM NaCl, 1 mM β-mercaptoethanol) using spin concentrators with a MWC of 30,000 kD.

2.8.5 SDS-Polyacrylamide gel electrophoresis (SDS-PAGE)

Protein samples were denatured by adding required amounts of 4 x SDS protein sample buffer (250 mM Tris-HCl pH 6.8, 2% (w/v) SDS, 20% (v/v) β-mercaptoethanol, 40% (v/v) glycerol, 0.5% (w/v) bromophenol blue) and subsequent boiling of the samples for 5 min at 95°C. Depending on the size of the protein of interest either a 7.5%, 10% or a 12.5% polyacrylamide separating gel with a 4% polyacrylamide stacking gel was used (Separating: 7.5%, 10% or 12.5% (w/v) polyacrylamide, 0.38 M Tris-HCl pH 8.8, 0.1% (w/v) SDS, 0.05% (w/v) APS, 0.07% (v/v) TEMED; Stacking: 4% (w/v) polyacrylamide, 132 mM Tris-HCl pH 6.8, 0.1% (w/v) SDS, 0.05% (w/v) APS, 0.15% (v/v) TEMED). Proteins were separated according to their size in SDS running buffer (25 mM Tris-HCl pH 8.5, 190 mM glycine and 0.1% (w/v) SDS) at 200 V for approximately 40 min. Protein molecular weights were determined using a prestained molecular weight marker (P7708, New England Biolabs)

2.8.6 Semi-native SDS-PAGE

To investigate the dimeric state of UVR8 proteins semi-native SDS-PAGE gels were used. SDS-PAGE gels with the respective percentages were used as described in 2.8.5. Required amounts of 4 x SDS protein sample buffer were added to the samples and loaded on a SDS-PAGE gel without boiling. The following protein separation was carried out as described in 2.8.5.

2.8.7 Native PAGE

To analyze protein samples under non denaturing conditions on PAGE gels, 2x native sample buffer (Invitrogen, LC0725) was added to samples and separated on 7.5% native PAGE gels (7.5% (w/v) polyacrylamide, 0.38 M Tris-HCl pH 8.8, 0.05% (w/v) APS, 0.07% (v/v) TEMED). Proteins were separated according to their charge and conformation in running buffer (25 mM Tris-HCl pH 8.5, 190 mM glycine) at 120 V for approximately

100 min in the cold room. Molecular weight of proteins was estimated by using NativeMark™ unstained Protein standard (LC0725, Invitrogen).

2.8.8 Coomassie Blue staining

Gels were stained for approximately 10 min at room temperature in 0.1% Coomassie Brilliant Blue R250 (Bio-Rad), 45% methanol and 10% acetic acid and subsequently destained in 45% methanol and 10% acetic acid. To completely remove all background stain, gels were left in rehydration buffer (10% ethanol and 5% acetic acid) overnight before gels were scanned and dried under vacuum onto 3M paper.

2.8.9 Western Blot transfer

Protein extracts separated by SDS-PAGE were transferred onto nitrocellulose membranes (Bio-Rad, UK) at 400 mA for 45 min in transfer buffer (25 mM Tris-HCl pH 8.5, 190 mM glycine and 20% (v/v) methanol). Membranes were then stained with Ponceau solution (0.1% (w/v) Ponceau S, 1% (v/v) acetic acid) to reveal protein bands and thus determine if equal loading of protein samples had been achieved. Membranes were blocked using 8% (w/v) non-fat dried milk in TBS-T (25 mM Tris-HCl pH 8, 150 mM NaCl, 2.7 mM KCl, 0.1% (v/v) Triton-X) to prevent non-specific binding of the antibodies.

2.8.10 Immunolabelling

Primary antibodies were either used in concentrations shown in the table below in TBS-T with 8% or 5% (COP1 and CHS) non-fat dried milk. Incubation was preferably done overnight; if not feasible, the incubation time was shortened to 1 h at room temperature. Between primary and secondary antibody incubations, membranes were washed 4 times with TBS-TT (25 mM Tris-HCl pH 8, 150 mM NaCl, 2.7 mM KCl, 0.1% (v/v) Triton-X, 0.05% (v/v) Tween) and one time with TBS-T for a total of 25 min. Secondary anti-rabbit, anti-mouse (both Promega), anti-rat (Dako Denmark A/S, Glostrup, Denmark) or anti-goat HRP conjugated antibodies (Sigma) were used either in 1:5000, 1:10000 or 1:20000 dilutions in TBS-T with 8% non-fat dried milk. The incubation time of 1 h was followed by five washes with TBS-TT and 2 washes with TBS for a total of 35 min.

TABLE 2-5: Primary antibodies used for immunoblotting.

Primary antibody	Dilution	Source
anti-CHS (N-20)	1:1000	Santa Cruz
anti-c-myc	1:1000	Roche
anti-COP1	1:1000	X.W. Deng
anti-GFP	1:5000	Clontech
anti-HA	1:5000	Roche
anti-Ubiquitin	1:2500	Agrisera (A. Sadanandom)
anti-UVR8 (C-terminal)	1:5000	E. Kaiserli (Kaiserli and Jenkins, 2007)
anti-UVR8 (N-terminal)	1:1000	E. Kaiserli (Cloix and Jenkins, 2008)

2.8.11 Immunodetection

For chemiluminescent detection of the protein bands the ECL Plus™ Western Blotting Detection Reagent (Amersham or Pierce Fisher) was used according to the manufacturer's instructions. After incubation with the ECL reagents, the membranes were placed between two sheets of clear plastic and subsequently placed into an X-ray cassette. Under safe red light conditions sheets of X-ray film (Kodak) were applied on top of the membranes in the cassettes. Films were developed by the X-OMAT developing system.

2.8.12 Stripping of immunolabelled protein membrane

A stripping procedure is necessary for complete antibody removal from an already immunolabelled protein membrane in order to re-probe with different antibodies. Membranes developed by chemiluminescence were washed in TBS and then incubated in stripping buffer (100 mM β-mercaptoethanol, 2% (w/v) SDS, 62.5 mM Tris-HCl pH 6.8) at 50°C for 30 min with gentle agitation (30 rpm). Membranes were then washed at least three times with TBS-T for at least 15 min in total at room temperature followed by blocking with 8% non-fat dried milk in TBS-T for 1 h. Immunolabelling and immuno-detection were carried out as described in 2.8.10 and 2.8.11.

2.8.13 Quantification of Western Blots

Quantification of UVR8 monomer loss in darkness following UV-B exposure was undertaken for representative Western blots from three independent experiments. The immunodetected UVR8 bands were quantified using Image J. Data were corrected for background and normalized against the value of the monomer after UV-B illumination, taken as 100%. Points were plotted and fitted using Curve Fitting Toolbox in MATLAB (Version 7.12.0). The type of fit that gave an R^2 value closest to 1 ($R^2 = 1.0$ would represent a perfect fit) was chosen and a 95% confidence level of the fit is shown. To facilitate comparison between treatments and genotypes, the time taken for loss of 50% of the monomer was calculated.

2.8.14 Analytical Size-Exclusion Chromatography

To assess dimer monomer status of purified protein or immunoprecipitated GFP-UVR8 derived from *N. benthamiana* plants before and after UV-B treatment gel filtration experiments were performed on a Superdex 200 HR10/30 column (GE Healthcare). The column was equilibrated with wash buffer II (50 mM Tri-HCl pH 7.5, 150 mM NaCl, 1 mM β-mercaptoethanol, 0.02% sodium azide) and run at a flow rate of 0.5 ml/min at 4°C on an AKTA FPLC system. For size and shape approximation the standard proteins aldolase, albumin, ovalbumin, chymotrypsinogen A and ribonuclease A were used.
Collected fractions from gel filtration runs of immunoprecipitated GFP-UVR8 and mutants derived from *N. benthamiana* plants were concentrated with Strata Clean Resin (Agilent) before separation by SDS-PAGE and immunoblotting.

2.8.15 Trypsin digests

Limited proteolysis with trypsin was used to probe conformational changes of purified UVR8 and mutants before and after UV-B treatment. About 5 µg of protein was digested on ice with 0.02 µg of trypsin (TPCK treated trypsin (Sigma), dissolved at 10 mg/ml in 25 mM Tris-HCl pH 7.5, 150 mM NaCl). Samples were taken before trypsin was added and after 5 and 30 min incubation respectively. The reaction was stopped by adding PMSF and 4 x SDS protein sample buffer. The samples were boiled and separated on a 10% SDS-PAGE gel and stained with Coomassie Blue.

2.9 Generation of stable transgenic Arabidopsis lines

2.9.1 Generated constructs

A number of selected point mutations in UVR8 were chosen to generate stable transgenic lines to examine functionality of these mutant proteins in Arabidopsis plants. All constructs were cloned at restriction sites 5' *EcoR*I and 3' *Sal*I in the pEZR(K)L-C vector at the C-terminal region of *e*GFP and are expressed under the control of the constitutive *35S* promoter of the Cauliflower Mosaic Virus. The following point mutations were chosen: D96N, D96N/D107N, R146A, R234A, R286A, R286K, H287A, R338A, R286A/R338A, and R146A/R286A.

2.9.2 Agrobacterium mediated transformation of Arabidopsis by floral dip

The transgenic lines described in this study were either generated in the *uvr8-1* mutant or in WT background by Agrobacterium mediated transformation. Arabidopsis plants for transformation were grown in high white light until flowers developed (4-5 weeks). A single colony of Agrobacterium containing the plasmid construct of interest was inoculated in 500 ml of LB medium with appropriate antibiotics for selection and grown at 28°C under constant shaking (200 rpm) until the culture reached an OD_{600} of approximately 1.5 - 2.0. The cells were then pelleted by centrifugation at 2,000 g for 15 min and resuspended in infiltration medium (2.2 g/l MS salts, 50 g/l sucrose, 0.5 g/l MES and 200 µl/l Silwet L-77) to an OD_{600} of approximately 0.8. Upper parts of the plants were immersed in the Agrobacterium solution described for 1 min with gentle agitation. Plants were kept under humid conditions in autoclave bags overnight and were returned into the growth room the next day. Two to four days later plants were once again immersed in the Agrobacterium solution. Plants were then allowed to develop seeds.

2.9.3 Screen for homozygous lines

Transgenic seeds were grown on 0.8% agar plates containing ½ MS and 75 µg/ml kanamycin for selection. 20-30 surviving T1 seedlings were transferred to soil and allowed to set seeds. T2 generation plants showing a 3:1 segregation on selective plates and a satisfying GFP expression (checked by confocal microscopy) were carried on. Finally, at least three independent homozygous T3 lines exhibiting 100% resistance to kanamycin and showing satisfying expression levels were used for complementation and protein characterisation studies.

2.9.4 Confocal microscopy

The expression of GFP-UVR8 fusions was visualised by a confocal laser scanning microscope (Zeiss LSM 510) under water with a 20 x objective lens. The GFP fluorescent tag was excited using an argon laser at 488 nm. GFP emission was collected between 505-530 nm to avoid cross-talk with chloroplast autofluorescence.

2.10 Transient expression of gene constructs in *N. benthamiana*

A single colony from freshly transformed Agrobacterium cells with the desired plasmid DNA was inoculated in 10 ml of LB medium with appropriate antibiotics and grown overnight at 28°C under constant shaking (200 rpm). When cultures had reached an OD_{600} of about 0.6 - 1.0, cells were pelleted by centrifugation at 2,000 g for 10 min. The cells were then resuspended in 10 mM $MgCl_2$, 10 mM MES pH 6.5 and 200 µM acetosyringone at an OD_{600} of 0.2 and incubated at room temperature for 3 hours. The Agrobacterium medium was infiltrated in *N. benthamiana* plants at the lower side of the leaves using a syringe. The infiltrated plants were moved back into the growth room at 28°C and left for 2-3 days before examining gene expression by confocal microscopy or protein extracts were prepared.

2.11 Yeast two-hybrid methods

2.11.1 Yeast transformation and yeast two-hybrid assay

Several colonies of yeast strain AH109 grown on YPD agar plates (20 g/l peptone, 10 g/l yeast extract, 20 g/l glucose, 20 g/l agar) were resuspended in 30 µl dH_2O. For cotransformation 30-50 µg of each plasmid DNA and 270 µl of transformation solution containing 40% (w/v) PEG, 0.1 M lithium acetate and 10 mM TE buffer pH 8.0 were added to the cell suspension followed by vigorously vortexing and an incubation at 42°C for 15 min vortexing every 5 min. Cells were then pelleted by centrifugation at 1,000 g for 5 min. The supernatant was discarded and the cells resuspended in 500 µl of YPD medium and incubated at room temperature for 2-3 h. Cells were then pelleted again and resuspended in 0.8% NaCl and incubated overnight. The next day cells were once again pelleted, resuspended in 100 µl of 0.8% NaCl and plated on agar plates with double dropout medium (46.7 g/l Minimum SD Agar Base, (63041; Clontech) 0.64 g/l $L^- W^-$ DO Supplements (630417; Clontech)). The plates were incubated at 30°C for 2 to 3 days until colonies developed.

A single colony was then taken from each plate, resuspended in 100 µl of 0.8% NaCl and 5 µl aliquots were spotted on agar plates containing quadruple dropout medium (46.7 g/l Minimum SD Agar Base, 0.60 g/l L^- W^- A^- H^- DO Supplements (630428; Clontech)) to test for interaction of prey and bait protein. Plates were incubated at 30°C in the dark or under narrowband UV-B (0.1 µmol m^{-2} s^{-1}) for 3 to 4 days.

2.11.2 Isolation of protein from yeast

A colony of transformed yeast was inoculated in 10 ml of liquid SD-L^- W^- and grown over night at 30˚C under constant shaking (200 rpm) until the OD_{600} reached about 1. Then 2 ml of overnight culture were harvested (16,000 g for 2 min) and resuspended in lyse and load buffer (L&L) containing 50 mM Tris-HCl pH 6.8, 4% SDS, 8 M urea, 30% glycerol, 0.1 M DTT and 0.005% bromophenol blue whereby the amount of L&L buffer added to the sample in µl corresponded to the OD x 100 of the sample (e.g. OD_{600} 0.95, add 95 µl L&L buffer). Samples were heated for 20 min at 65˚C before separation on a 10% SDS-PAGE gel and subsequent immunoblotting.

2.12 Protein expression in *E. coli*

2.12.1 Generated constructs

The cDNA encoding Arabidopsis UVR8 was cloned at restriction sites 5' *Nco*I and 3' *Not*I into a modified pET (Novagen) expression vector providing N-terminal 7 x His and StrepII affinity tags for purification (pHS vector, obtained from Michael Hothorn). Because UVR8 contains an internal *Nco*I restriction site, the isoschizomer *BspH*I was used to digest the PCR fragment. The protein is expressed as a SUMO (small ubiquitin-related modifier) fusion protein, where the SUMO is used to cleave off the affinity tags after purification of the protein by incubation with a SUMO protease. Several UVR8 mutants were generated in this vector by site-directed mutagenesis with primers and conditions as described under 2.6.7.

2.12.2 Culture growth

A starter culture of 100 ml LB medium with appropriate antibiotics was inoculated with a single colony of transformed Rosetta (DE3) pLysS cells and incubated overnight at 37°C with constant shaking (200 rpm). The next morning, one litre of Terrific Broth medium (ForMedium™, Hunstanton, UK) with appropriate antibiotics was inoculated with 10 ml of the overnight culture. The culture was incubated on a shaking incubator at 37°C until its

density reached an OD_{600} of 1.0. Cultures were then transferred to a 16°C shaker and allowed time to adapt before protein expression was induced by adding isopropyl-beta-D-thiogalactopyranoside (IPTG) to a final concentration of 60 µM. The cultures were then incubated overnight at 16°C with constant shaking. Cells were pelleted the next morning by centrifugation at 4,000 rpm at 4°C for 20 min. Pellets were flash frozen in liquid nitrogen and stored at -80°C until proteins were purified.

2.12.3 Protein purification

Cells were resuspended in wash buffer I (50 mM Tris-HCl pH 8.0, 500 mM NaCl, 20 mM imidazole, 1 mM β-mercaptoethanol, 10% glycerol, EDTA free protease inhibitor tablets (Roche)) at a 3:1 ratio of buffer to cells. Cells were lysed by sonication at 4˚C until viscosity of the lysate decreased. To remove nucleic acids 2 µl Benzonase®Nuclease (Novagen) per 100 ml of lysate was added. Cell debris was pelleted by centrifugation at 20,000 rpm at 4°C for 30 min and the supernatant was collected.

All steps of the following purification were carried out in the cold room at 4°C. 0.8 ml nickel charged resin (Ni-NTA Super flow, 30401, Qiagen) per 1l TB culture was equilibrated by washing with 10 column volumes (CV) of wash buffer I. Equilibrated resin was transferred to a beaker and incubated with the supernatant collected in 2.13.1 for one hour with mixing. The mixture was then transferred back into the column, the supernatant allowed to flow through followed by a wash step with 10 CV of wash buffer I. Subsequently, the ends of the column were capped and the resin with the bound proteins resuspended in 3 CV of incubation buffer (50 mM Tris-HCl pH 8.0, 500 mM NaCl, 10 mM MgATP, 2.5 mM $MgCl_2$, 1 mM β-mercaptoethanol) to remove bound chaperone proteins. After a 15 min incubation period on a rolling shaker, the cap was removed and the buffer allowed flowing through followed by a final wash step with 10 CV of wash buffer II (50 mM Tris-HCl pH 7.5, 150 mM NaCl, 1 mM β-mercaptoethanol). To elute the His tagged protein five one CV fractions were collected after addition of elution buffer (50 mM Tris-HCl pH 7.5, 150 mM NaCl, 250 mM imidazole, 1 mM β-mercaptoethanol). Fractions two to four were pooled and used for the second purification step.

0.35 ml strep resin (*Strep*-Tactin® Superflow®, 2-1208-002, IBA, Goettingen, Germany) per 1l TB culture was equilibrated with 5 CV wash buffer II. Equilibrated resin was transferred to a beaker and incubated with the pooled elution fractions from the first purification step for one hour with mixing. Again the mixture was transferred back to the column, the supernatant allowed to flow through and the resin washed with 5 CV of wash buffer II. For the on-column cleavage of the tags, the ends of the column were capped, the

resin resuspended in 2 CV of wash buffer II and SUMO protease was added. The mixture was incubated on a rolling shaker overnight. The next morning, the column was uncapped and the flow through collected. Subsequently the column was washed 3 times with one CV of wash buffer II. All three wash steps were collected and pooled with the flow through. Purified proteins were flash frozen in liquid nitrogen and stored at -80˚C.

2.12.4 Purification of SUMO protease

Cleavage of the affinity tags of purified UVR8 was done via incubation with SUMO protease. SUMO protease is a highly active cysteinyl protease also known as Ulp which cleaves in a highly specific manner, recognizing the tertiary structure of the ubiquitin-like protein, SUMO rather than an amino acid sequence. A recombinant fragment of Ulp1 (Ubl-specific protease 1) from *S. cerevisiae* (ScUlp1 residues 403-621) was cloned into a vector with a non cleavable N-terminal 6 x His and StrepII tag (construct obtained from Michael Hothorn) and expressed in Rosetta (DE3) pLysS cells. Culture growth, induction of protein expression as well as harvesting of the culture was essentially done as described under 2.12.2.

Thawed cell pellets were resuspended in a 3:1 ratio buffer:pellet in lysis and wash buffer (25 mM Tris-HCl pH 7.6, 1 M NaCl , 2 mM β-mercaptoethanol, 10 mM imidazole) and sonicated as described under 2.12.3. The lysate was then centrifuged as described under 2.12.3. Cobalt resin (2 ml resin per 1 l TB medium used for culture growth) was equilibrated with lysis and wash buffer as described under 2.12.3, incubated with the clarified cell lysate, washed and incubated with incubation buffer containing ATP to wash off chaperone proteins (50 mM Tris-HCl pH 7.6, 1 M NaCl, 10 mM MgATP, 2.5 mM $MgCl_2$, 1 mM β-mercaptoethanol). After another wash step, the SUMO protease was eluted from the column with 4 CV of elution buffer (25 mM Tris-HCl pH 7.6, 1 M NaCl, 2 mM β-mercaptoethanol, 200 mM imidazole). The purified protease was then desalted with a Sephadex G-25 M column (GE-Healthcare) and concentrated to a final concentration of 3 mg/ml (final storage buffer: 25 mM Tris-HCl pH 8, 350 mM NaCl, 2 mM β-mercaptoethanol). Aliquots of 100 µl were snap frozen in liquid nitrogen and stored at -80ºC.

2.13 Spectroscopy

2.13.1 Circular Dichroism spectroscopy

2.13.1.1 Far- and near-UV measurements

Wild type and mutant UVR8 proteins were analyzed in the far- and near-UV region before and after UV-B treatment (1 h, 1.5 µmol m^{-2} s^{-1} narrowband UV-B). Circular Dichroism (CD) spectra were recorded on a Jasco J-810 spectropolarimeter. Spectra in the far-UV (190 nm - 260 nm) were measured in a 0.2 cm path length cell using a scan speed of 50 nm/min, a 0.5 s response and a bandwidth of 1 nm. Spectra in the near-UV (260 nm - 320 nm) were recorded in a 0.2 cm path length cell using a scan speed of 10 nm/min, a 2 s response and a bandwidth of 1 nm. Eight scans were accumulated and averaged. Spectra were corrected by subtraction of a buffer blank spectrum and respective sample concentration. Data were expressed in units of molar ellipticity [θ] (degrees cm^2 $dmol^{-1}$).

2.13.1.2 Thermal melt

Wild type and mutant UVR8 proteins were analyzed at different temperatures in a wavelength range between 220 and 320 nm. A Peltier thermal device was used to increase the starting temperature of 5°C in 5°C steps up to 60°C. Spectra were recorded in a 0.2 cm path length cell using a scan speed of 10 nm/min, a 2 s response and a bandwidth of 1 nm. One scan was performed for each temperature step.

2.13.2 Ultrafast transient absorption spectroscopy

Time-resolved transient absorption measurements were performed on a visible pump-visible probe setup in the LaserLab facilities at the Vrije Universiteit Amsterdam. The system uses a Coherent Libra Titanium:Sapphire amplifier oscillator (1 kHz), providing a light source with a central wavelength of 800 nm, bandwidth of 30 nm at full-width half-maximum, with an energy of >3.5 mJ/pulse and a duration of ~40 fs. The 800 nm pulse was split into two parts: one part was used for third harmonic generation to create a 266 nm pump beam to trigger the photoreaction. The second part was focused on a rotating CaF_2 crystal to generate a white light continuum that was used as the probe beam. The polarization between pump and probe beam was set to magic angle (54.7°). The probe pulse was focused on the sample by parabolic mirrors. Parabolic mirrors and an achromatic lens (fl: 200 mm) were used to focus the pump beam on the sample. The pump pulse was progressively delayed with respect to the probe using a 60 cm long delay stage (Newport IMS-6000) to cover a time window up to 3.7 ns. The sample, placed in a quartz flow cell of 2 mm optical path, was fixed in the focal plane of the two focusing elements (achromatic

lens and parabolic mirror) and circulated by a peristaltic pump. Pump and probe beams were spatially separated after the sample. The probe beam was collimated and focused on the entrance slit of a spectrograph (Oriel Instruments, Newport Corporation, USA) and spectrally dispersed across a home-built camera equipped with a 256 element photodiode array (Hamamatsu Photonics, Japan). This 256 pixel array is read out by a computer to calculate the transient absorption. Out of the thousand pulses per second, 500 pump pulses were blocked by a synchronized chopper in order to calculate the difference in absorption of the white light between pumped and non-pumped sample. The transient absorption setup is described in detail in Berera et al. (2009)

The resulting data was corrected for pre-time-zero signals by calculating the average signal at each wavelength before time-zero and subtracting the result from the corresponding time trace. The pre-treated data was analyzed by global analysis using the Glotaran software package (Snellenburg et al., 2012). The time-resolved data can be described in terms of a parametric model in which some parameters, such as those descriptive of the instrument response function (IRF), are wavelength-dependent, whereas others, such as the lifetime of a certain spectrally distinct component underlay the data at all wavelengths. This allows the application of global analysis techniques, which model wavelength-invariant parameters as a function of all available data. The spectral evolution was investigated using a compartmental model, in which so-called evolution associated difference spectra (EADS) sequentially interconvert with increasing lifetimes (1->2->3->…; $\tau 1 < \tau 2 < \tau 3 <$…).

2.13.3 Fourier Transform Infrared (FTIR) spectroscopy

The differential FTIR spectra were recorded at room temperature using a FTIR spectrometer (IFS 66s Bruker) equipped with a nitrogen cooled photovoltaic MCT detector (20 MHz, KV 100, Kolmar Technologies, Inc., USA) at the LaserLab facilities of the VU Amsterdam. A UV-LED light (Photon systems, Covina, CA, USA) emitting at 280 nm was used to convert UVR8 and its mutant forms to their light activated states. The light minus dark FTIR data was obtained, by subtracting an initially over one minute recorded dark state spectrum from the light activated protein spectrum also recorded over the duration of one minute but under continuous UV illumination. Background and sample interferogram data were averaged from 100 interferogram scans, at 3 cm^{-1} spectra resolution. Light-minus-dark difference spectra were corrected for experimental drift by subtraction of the corresponding dark-minus-dark difference spectrum. Measurements were repeated after a 24 h recovery of the sample. The FTIR samples were prepared by using 10-15 µl sample at OD_{280} of ~70 (in 50 mM Tris-HCl pH 7.5, 150 mM NaCl, 1 mM β-mercaptoethanol) and

spread between two tightly fixed CaF_2 windows. The sample can be considered as a hydrated film.

2.13.4 Fluorescence spectroscopy

The fluorimeter (Fluorolog, Horiba Jobin-Yvon) was set to 280 nm excitation with an excitation bandpass of 1 nm. Emission spectra were recorded with an emission bandpass of 5 nm between 285 nm and 500 nm with steps of 2 nm. The light intensity of the excitation source was determined to be 40 µW. Protein samples were diluted to OD_{280} ~ 0.04 - 0.06 in a 1x1 cm quartz fluorescence cuvette. Two times 100 emission spectra were recorded with an acquisition time of each spectrum of about 38 s. The excitation shutter was closed during the resetting procedure between the spectra. The samples were continuously stirred. Excitation and absorption spectra were recorded before and after each measurement. For analysis of the UVR8 WT monomer, the sample was preilluminated for ~ 10 min by an UV-LED emitting at 280 nm (Photon systems, Covina, CA, USA).

3. DIMER-MONOMER STATE OF UVR8 SALT BRIDGE MUTANTS

3.1 Introduction

The UV-B induced monomerisation of UVR8 is an important property of the photoreceptor and requires stable dimerisation of the protein in the absence of UV-B. To investigate the importance of ionic interactions in maintaining the UVR8 dimer, site-directed mutagenesis was used to mutate residues predicted to participate in cross-dimer salt bridges. UVR8 mutants were generated for two main approaches: Firstly, to test their dimer-monomer state *in vitro* by using recombinantly expressed protein purified from *E. coli* and, secondly, to test effects of mutations *in vivo* by generating transgenic Arabidopsis lines with the respective mutation (see Chapter 4). Three methods were applied for each approach respectively: size-exclusion chromatography (SEC), native polyacrylamide gel electrophoresis (PAGE) and semi-native SDS-PAGE. The last method was established by Rizzini and coworkers (2011), whereby samples in SDS loading buffer are not heat denatured and therefore the highly stable UVR8 dimer can be detected on a SDS-PAGE gel. Purified protein was also analysed by far- and near-UV circular dichroism (CD) spectroscopy to assess exciton coupling of tryptophans and also indirectly the dimer-monomer state of the protein. The major findings of this chapter are that the UVR8 dimer is very effectively held together by cross-dimer salt bridges and mutation of involved residues can lead to constitutive monomerisation. Especially important for stable dimerisation are salt bridges that are located adjacent to the UV-B perceiving tryptophan pyramid, in particular those involving R286.

3.2 The UVR8 dimer is held together by a complex network of salt bridges

Elucidation of the crystal structure of UVR8 revealed the forces and residues that are involved in stable dimerisation of the photoreceptor in the absence of UV-B. Remarkable is the high content of aromatic residues (seven tryptophans, three phenylalanines and two tyrosines) and charged side chains across the dimer interface. The latter ones will be the focus of this chapter. Distinct regions of complementary electrostatic potential are formed within each monomer and the dimer offset and the two-fold symmetry align arginine and

carboxylate side chains to form a complex network of salt bridges across the dimer interface (Fig 3-1 A). These ionic interactions are the dominating force to hold the dimer together whereas hydrophobic interactions play a negligible role.

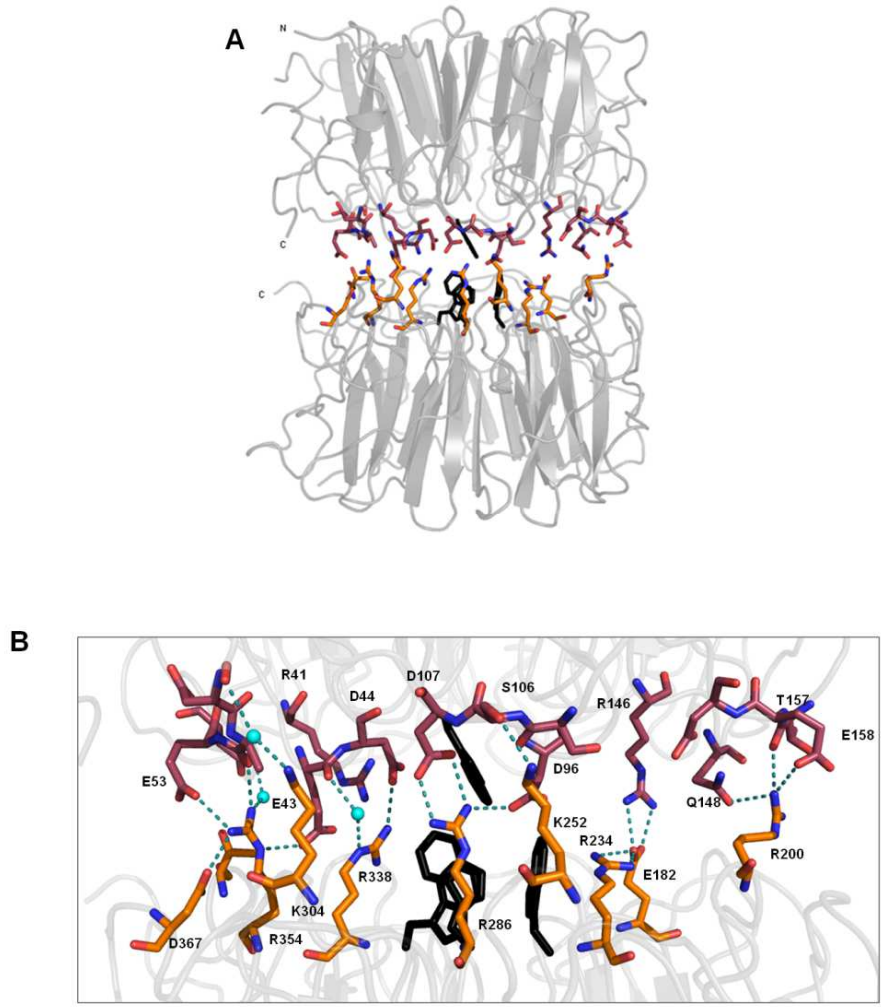

FIGURE 3-1: View of the UVR8 dimer (A) and close-up view of residues forming salt bridges across the dimer interface (B). Hydrophilic residues are located along the entire periphery of each disk-like monomer and are shown in red (top subunit) and orange (bottom). Positive charges are shown in blue, negative charges in red. The tryptophan pyramid is colored in black, hydrogen bonds and water molecules are shown in turquoise. For clarity, residues from only one half of the interface are displayed (adapted from Christie et al., 2012).

The crystallographic structure allowed the identification of individual residues involved in ionic interactions (Fig 3-1 B). Two strong double hydrogen bonded salt bridges are formed between R286 and D107 and between R146 and E182. Single hydrogen bonded salt bridges are formed between a number of residues such as R286 and D96, R354 and E53 and E43 as well as between R338 and D44 and also between R200 and E158. By using site-directed mutagenesis, the importance of a number of these residues was examined in the present chapter.

3.3 The salt bridge formed through R286 is essential to maintain the UVR8 dimer

Several mutations were carried out to test the importance of the double hydrogen bonded salt bridge involving R286 and D107 as well as D96 (Fig 3-2 A). This salt bridge is positioned directly adjacent to the UV-B perceiving tryptophan pyramid which will be described in more detail later on. To completely interrupt the ionic interaction, R286 was mutated to alanine and in a second mutant the two aspartic acid residues (D96 and D107) were replaced by asparagines. The proteins were expressed as SUMO fusion proteins in *E. coli* cells and purified through an N-terminal 7x His and Strep II affinity tag. To assess the dimerisation state of the mutant protein, SEC was used as first method of choice. Wild-type UVR8 protein shows UV-B induced monomerisation when it is exposed to 1.5 µmol m^{-2} s^{-1} narrowband UV-B for 1 h (Fig 3-2 B). Elution volumes of the non-treated and UV-B treated wild-type protein correspond to approximately 96 and 58 kDa respectively, showing the dimer and monomer states of UVR8 (for calibration curve see Fig A-1 Appendix). In contrast, the $UVR8^{D96N/D107N}$ and $UVR8^{R286A}$ mutants both show constitutive monomerisation under non UV-B conditions and remain unchanged after exposure to UV-B (Fig 3-2 B). The elution volumes are slightly different in both cases compared to the monomeric wild-type form; however, size exclusion chromatography is greatly influenced not only by size but by the hydrodynamic radius, i.e. the shape of the protein, which might well be altered due to the introduced mutations. To be able to exclude concentration dependency of the elution volumes, a range of concentrations was tested with the $UVR8^{D96N/D107N}$ mutant. Fig 3-2 C shows absence of concentration dependence of the elution volume and therefore strengthens the finding that the two mutants are constitutive monomeric forms of UVR8.

To test the importance of the positively charged side chain, a conserved mutation of R286 was carried out as well, replacing the arginine by lysine. The elution profile of the $UVR8^{R286K}$ mutant shows a UV-B induced dimer to monomer shift (Fig 3-2 D). A positively charged side chain in this position is therefore essential for dimerisation. However, the elution volume of the $UVR8^{R286K}$ dimer differs from wild-type UVR8 suggesting most likely a different overall shape of the protein. To further investigate the variability of dimer shapes the behaviour of the $UVR8^{R286K}$ mutant was tested under 500 mM NaCl conditions (HS). Under non UV-B high salt conditions the elution volume of the $UVR8^{R286K}$ dimer is shifted towards the wild-type dimer and about a third of the protein elutes at the position of the monomer. Complete monomerisation was observed

after UV-B treatment with the same elution volume for the UVR8^{R286K} monomer as under low salt conditions.

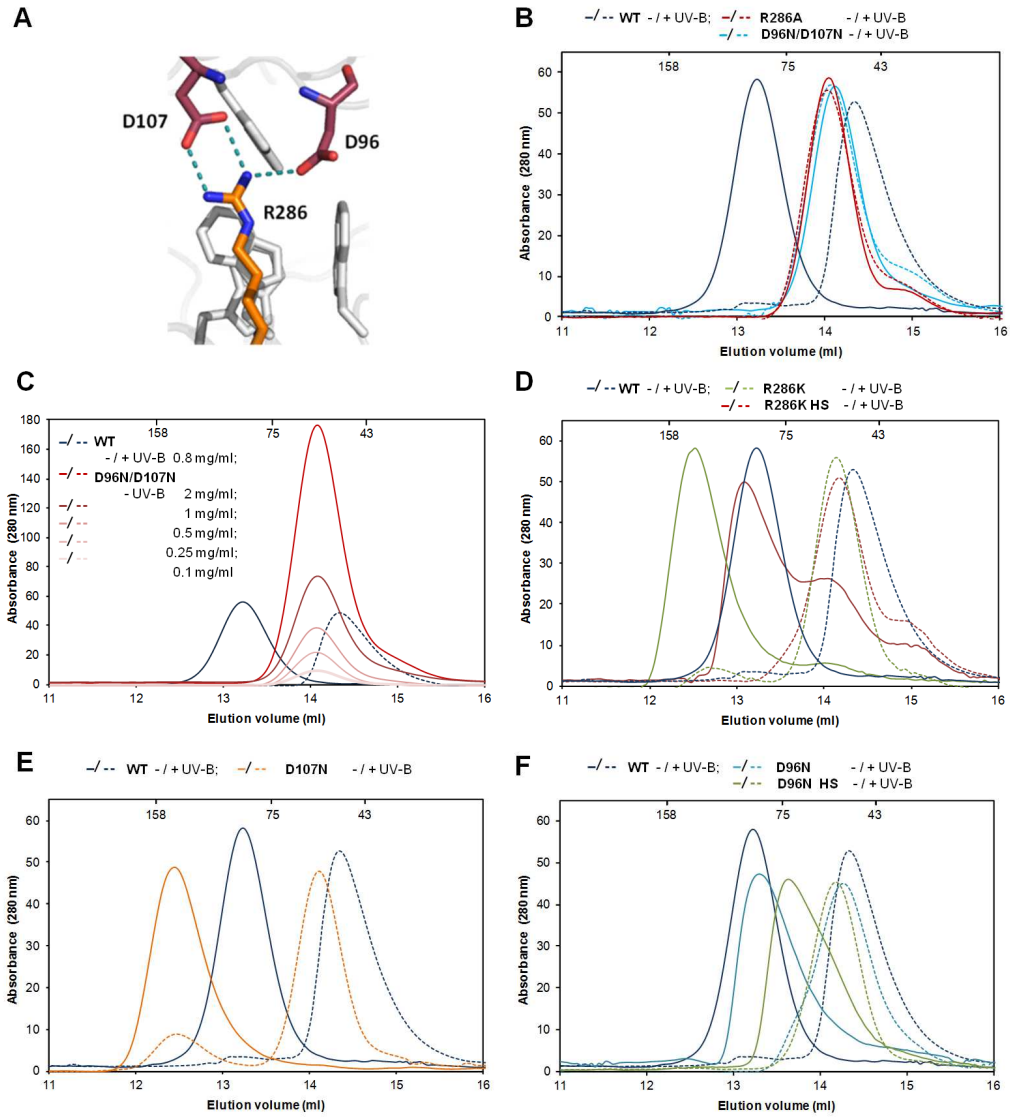

FIGURE 3-2: The salt bridge formed through R286 is essential to maintain the UVR8 dimer. Purified proteins exposed or not (-UV-B, solid line) to 1.5 µmol m^{-2} s^{-1} narrowband UV-B for 1 h (+UV-B, dotted line) were run on a Superdex 200 column (GE Healthcare) which was calibrated using the low molecular weight calibration Kit (GE Healthcare). Elution points of aldolase (158 kDa), albumin (75 kDa) and ovalbumin (43 kDa) are indicated in the top of each diagram. **(A)** Close up view of the salt bridge formed between R286 and D107 and D96. **(B)** SEC of wild-type UVR8, UVR8$^{D96N/D107N}$ and UVR8^{R286A} mutants. The two mutants show constitutive monomerisation. **(C)** Constitutive monomerisation of UVR8$^{D96N/D107N}$ is independent of protein concentration. **(D), (E)** and **(F)** Dimerisation is still possible in the UVR8^{R286K} mutant and in the two single mutants UVR8^{D107N} and UVR8^{D96N} (HS = high salt conditions: 500 mM NaCl). Data shown in B, C and D are representative of three independent experiments. Data shown in E and F are representative of two independent experiments.

The negatively charged aspartic acids were investigated further by introducing only a single point mutation to asparagine at a time. Both mutant forms, UVR8^{D96N} and UVR8^{D107N} are still able to dimerize under non UV-B conditions and monomerise after exposure to UV-B (Fig 3-2 E and F). The elution volume of the UVR8^{D107N} dimer differs

again from wild-type UVR8, which is also most likely due to an overall change in the shape of the protein. A likely scenario would be a minor reorientation of R286 to form a tighter interaction with the remaining D96. Removing only the single hydrogen bonded salt bridge between R286 and D96 has the least effect on shape alteration, resulting in close to wild-type elution volumes during size exclusion chromatography. To further test the strength of cross-dimer salt bridges in the UVR8^{D96N} dimer, chromatography runs were performed under high salt conditions as well. In contrast to UVR8^{R286K}, where high salt condition lead to partial monomerisation, UVR8^{D96N} still mainly elutes as a single peak under non UV-B conditions close to the wild-type dimer. The elution volume has changed slightly; however changes in compactness and shape of the dimer are most likely responsible for this behaviour. As expected, the UVR8^{D96N} monomer remains unaffected by high salt conditions and elutes in the same position as under low salt conditions.

It can be concluded from these mutations that the salt bridge formed through R286 is essential to maintain the UVR8 dimer. The ionic interactions and UV-B induced monomerisation will only be sustained as long as either side can participate with a positively and at least one negatively charged side chain.

3.4 R338 and D44 form a second important salt bridge to stabilize the dimer

R338 forms a cross-dimer salt bridge with D44 adjacent to the above described double hydrogen bonded salt bridge and also in close proximity to the tryptophan pyramid (Fig 3-3 A). R338 also forms a second much weaker salt bridge via a water molecule with E43. The contribution of the salt bridges to maintain the dimer was again examined by mutagenesis, changing R338 to alanine to eliminate the positive charge. The SEC elution profile of the UVR8^{R338A} mutant shows monomer-dimer equilibrium under low salt conditions but UVR8^{R338A} becomes constitutively monomeric independent of exposure to UV-B if examined under high salt conditions (Fig 3-3 B). R338 is therefore less crucial for dimerisation than R286 since complete monomerisation in the UVR8^{R338A} mutant only occurs if enough counterions in solution are present to prevent charged residues pairing up across the dimer interface.

Besides the UVR8^{R338A} single mutant, the double mutant UVR8$^{R286A/R338A}$ and the triple mutant UVR8$^{R234A/R286A/R338A}$ were generated. The main purpose hereby was to determine the combined effect of the loss of arginines on the enclosed tryptophan pyramid. However, both mutants showed partial proteolytic cleavage during protein expression and

purification and therefore analysis of these mutants was limited. Due to the effect of the R286A mutation causing constitutive monomerisation, UVR8$^{R286A/R338A}$ and UVR8$^{R234A/R286A/R338A}$ are monomeric as well. However, the elution volume is greater than for wild-type UVR8, caused by the proteolytic cleavage as well as probably major alterations in their shape (Fig 3-3 C and D). Exposure of UVR8$^{R286A/R338A}$ to UV-B leads to a mixed species of protein; whereas one species coincides with the monomeric form observed in the absence of UV-B, the second species elutes earlier from the column. Most likely, this second monomeric species has a changed conformation induced by UV-B. To possibly narrow down the region of conformational change, the UVR8$^{R286A/R338A}$ mutant was treated with trypsin before SEC, which eliminates the last 40 amino acids of the C-terminus (Christie et al., 2012). Trypsin treated UVR8$^{R286A/R338A}$ remains unchanged after UV-B exposure, suggesting a changed conformation of the C-terminus in the full length UVR8$^{R286A/R338A}$ protein induced by UV-B.

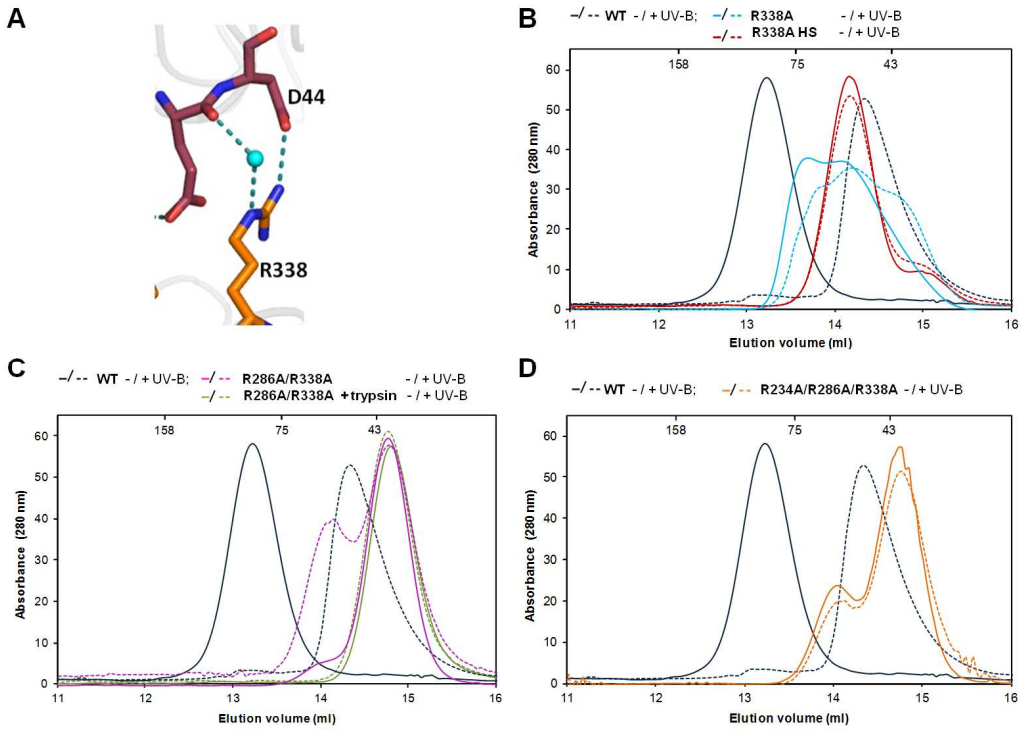

FIGURE 3-3: R338 is also important for stable dimerisation of UVR8.
Purified proteins exposed or not (-UV-B, solid line) to 1.5 µmol m^{-2} s^{-1} narrowband UV-B for 1 h (+UV-B, dotted line) were run on a Superdex 200 column (GE Healthcare) which was calibrated using the low molecular weight calibration Kit (GE Healthcare). Elution points of aldolase (158 kDa), albumin (75 kDa) and ovalbumin (43 kDa) are indicated in the top of each diagram. **(A)** Close up view of the salt bridge formed between R338 and D44. **(B)** SEC of wild-type UVR8 protein compared to UVR8^{R338A} shows constitutive monomerisation under low and high salt conditions (HS: 500 mM NaCl). **(C)** SEC of UVR8$^{R286A/R338A}$ shows a UV-B response which is lost after trypsin treatment of the protein. **(D)** SEC of UVR8$^{R234A/R286A/R338A}$. Data shown in B and C are representative of two experiments. Experiment shown in D has not been repeated.

3.5 R146 and E182 form a second double hydrogen bonded salt bridge

The contribution to dimerisation of a third cross-dimer salt bridge was investigated by mutagenesis of R146. The second double hydrogen bonded salt bridge formed between R146 and E182 is not directly adjacent to the tryptophan pyramid but lies close to the symmetry axis of the protein (Fig 3-4 A). E182 also forms an intermolecular salt bridge with R234 which contributes little to dimerisation but is still a remarkable arrangement: it connects the cross-dimer salt bridge between R146 and E182 to the tryptophan pyramid, since R234 neighbours W233 of the tryptophan triad. To completely prevent formation of the R146 and E182 salt bridge, R146 was mutated to alanine. The SEC elution profile shows dimerisation of UVR8^{R146A} in the absence of UV-B and monomerisation after exposure to UV-B (Fig 3-4 B).

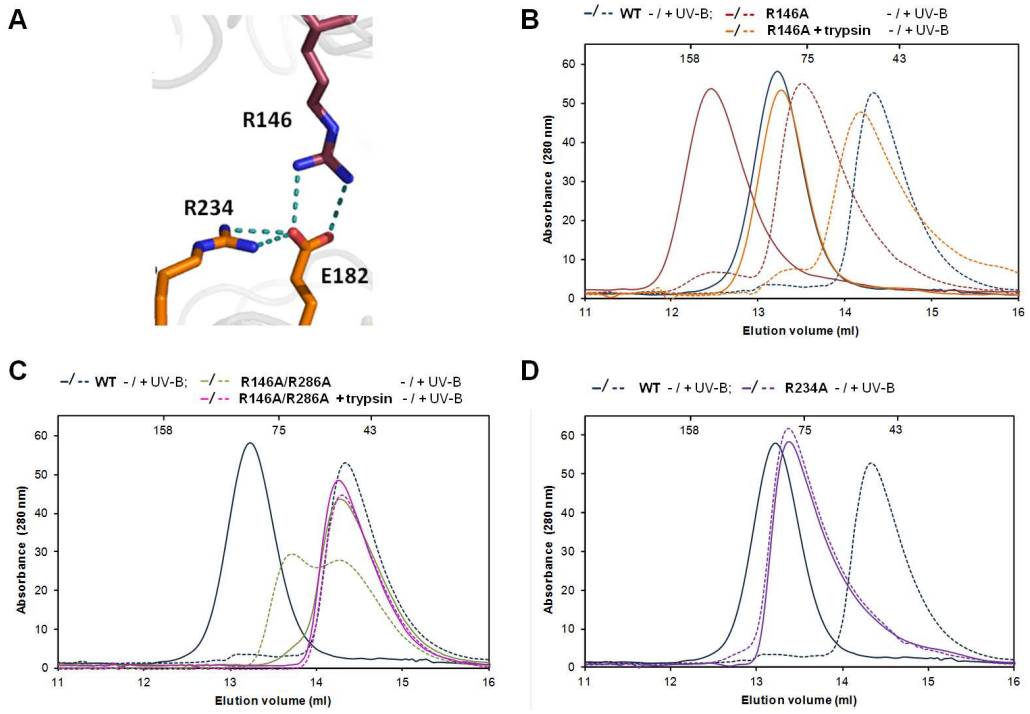

FIGURE 3-4: R146 and E182 form the second double hydrogen bonded salt bridge further distanced from the tryptophan pyramid. Purified proteins exposed or not (-UV-B, solid line) to 1.5 µmol m^{-2} s^{-1} narrowband UV-B for 1 h (+UV-B, dotted line) were run on a Superdex 200 column (GE Healthcare) which was calibrated using the low molecular weight calibration Kit (GE Healthcare). Elution points of aldolase (158 kDa), albumin (75 kDa) and ovalbumin (43 kDa) are indicated in the top of each diagram. **(A)** Close up view of the cross-dimer salt bridge formed between R146 and E182 and its interaction with R234. **(B)** SEC of wild-type UVR8 protein compared to UVR8^{R146A} shows a dimer to monomer shift after UV-B exposure with an altered shape of the mutant protein. Trypsin treated UVR8^{R146A} shows similar behavior to wild-type protein. **(C)** SEC of UVR8$^{R146A/R286A}$ shows a UV-B response which is lost after trypsin treatment of the protein. **(D)** SEC of UVR8^{R234A} shows no response to UV-B and appears to be dimeric. Data shown is representative of two independent experiments. The trend of the data shown in C has been observed several times but with slightly differing elution volumes.

However, the elution volumes of this mutant differ greatly from wild-type UVR8, but nevertheless two distinct states are visible before and after exposure to UV-B. To investigate whether an altered shape of $UVR8^{R146A}$ causes the shift in elution volume, the protein was treated with trypsin as described before. The elution profile of trypsin treated $UVR8^{R146A}$ closely resembles the elution profile of wild-type UVR8 before and after exposure to UV-B suggesting that the mutation of R146 to alanine somehow affects the conformation of the C-terminus. Nevertheless, $UVR8^{R146A}$ is not impaired in dimerisation and it responds to UV-B by monomerisation.

The last cross-dimer salt bridge mutant that was generated and characterized was $UVR8^{R146A/R286A}$ effectively lacking the two double hydrogen bonded salt bridges. Size exclusion chromatography shows constitutive monomerisation of $UVR8^{R146A/R286A}$ (Fig 3-4 C) but exposure to UV-B shows a similar effect of generation of two mixed species as observed for the $UVR8^{R286A/R338A}$ mutant in Fig 3-3 C. Similarly, treatment of $UVR8^{R146A/R286A}$ with trypsin before the chromatography run eliminated the shape change after exposure to UV-B leading to a constitutively monomeric form of UVR8 unresponsive to UV-B. It should be mentioned at this point that reproducibility of elution profiles of the two double mutants $UVR8^{R146A/R286A}$ and $UVR8^{R286A/R338A}$ have been problematic during this study. Both mutants always showed elution volumes close to the wild-type monomer and therefore these mutants are clearly monomeric. However, the shape of both proteins can be altered greatly by the conformation of the C-terminus as shown by the treatment with trypsin. Shape alterations have especially been problematic under low salt conditions where the charged residues of the C-terminus may interact with the dimer interface of the same subunit. Differences in protein concentrations under these circumstances may result in differing C-terminal conformations leading to different shapes and elution volumes. Conclusions drawn from the SEC data of these two mutants, besides the fact that they are constitutively monomeric, have to be considered were carefully.

Finally, the intermolecular salt bridge between R234 and E182 was investigated by mutation of R234 to alanine. Fig 3-4 D suggests that $UVR8^{R234A}$ mainly exists as a dimer under non-UV-B conditions, however the broadening of the peak towards the right hand side shows a less tight conformation of the dimer compared to the wild-type protein. Remarkable is the loss of UV-B induced monomerisation of this mutant. Most likely the rather drastic mutation from arginine to alanine adjacent to the tryptophan pyramid has altered the tryptophan arrangement and therefore disabled the UV-B sensing mechanism. Nevertheless, the dimeric state of this mutant has to be investigated further especially by trypsin treatment of the protein. The elution volume of $UVR8^{R146A}$ after exposure to UV-B

is very similar to the elution volume of $UVR8^{R234A}$, and $UVR8^{R146A}$ is supposedly monomeric after UV-B treatment with conformational differences in the C-terminus as shown by trypsin treatment. It can therefore not be excluded that mutation of R234 to alanine even if not directly involved in a cross-dimer salt bridge also leads to constitutive monomerisation with an altered shape of the C-terminus by disturbing the arrangement of surrounding amino acids.

To summarize, comparing effects of salt bridge breaking mutations between the two double hydrogen bonded salt bridges spanning the interface, the interaction between R146 and E182 contributes less to dimerisation then the interactions formed through R286.

3.6 Native gel electrophoresis reveals various conformations of UVR8 mutants

Alongside size exclusion chromatography, the dimerisation state of UVR8 salt bridge mutants was also analyzed by native PAGE. Native or non-denaturing gel electrophoresis is run in the absence of SDS and therefore the mobility of proteins does not only depend on the proteins' size, as in SDS-PAGE, but on their charge and their hydrodynamic radii. The electric charge driving the electrophoresis is determined by the intrinsic charge of the protein at the pH of the running buffer and depends on the amino acid composition of the protein. Separation of purified wild-type UVR8 protein before and after exposure to 1.5 µmol m^{-2} s^{-1} of narrowband UV-B for 1 h on a 7.5 % native gel reveals only a very small shift between the dimeric and monomeric form of the wild-type (Fig 3-5 A).

The dimeric mutant $UVR8^{R286K}$, where the total charge of the protein remains unchanged, runs in a comparable position to wild-type under non-UV-B conditions, but UV-B induced monomerisation results in a much more mobile monomer then seen for wild-type. A similar effect can be observed for the two single mutants $UVR8^{D96N}$ and $UVR8^{D107N}$, whereas here the mutation has an effect on the charge of the protein (Fig 3-5 B). This clearly demonstrates that the monomeric form of these three mutants is present in a different conformation to the wild-type monomer under the native gel conditions. Further changes in the mobility of monomeric forms can be seen for $UVR8^{R286A}$ and $UVR8^{D96N/D107N}$ (Fig 3-5 A).

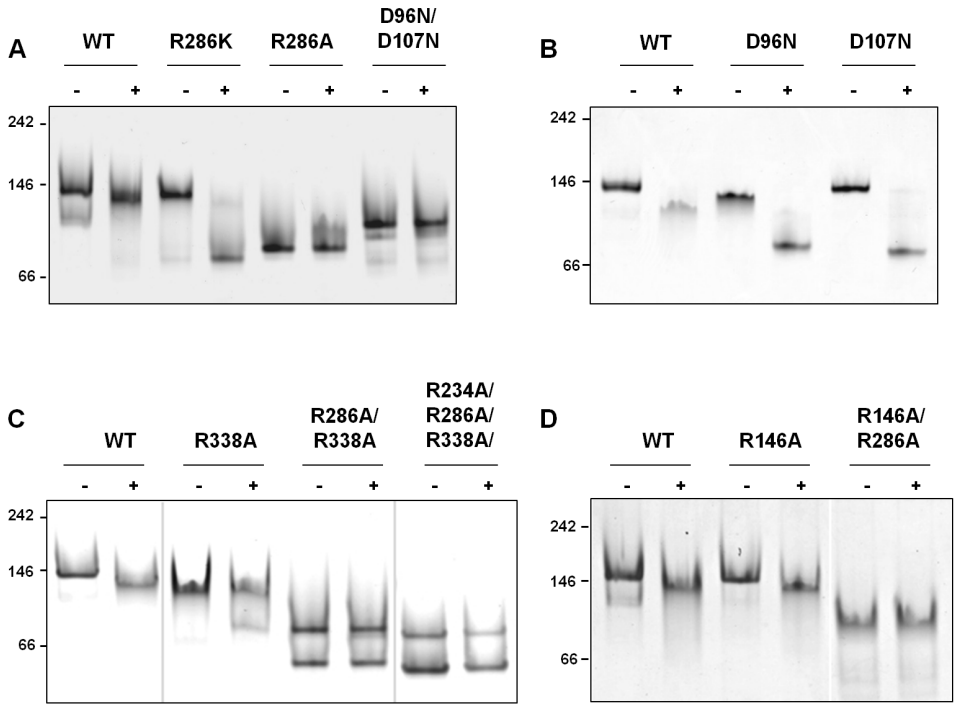

FIGURE 3-5: Mutation of salt bridge forming residues alters the mobility of UVR8 mutants on native gels in various ways. Purified proteins were exposed (+) or not (-) to 1.5 µmol m^{-2} s^{-1} narrowband UV-B for 1 h. Samples were separated on a 7.5% native gel and stained with Coomassie Blue.

Whereas size exclusion chromatography suggests the same size and shape for these two mutants, their behaviour differs under native PAGE conditions resulting in bands in different positions. In accordance to the SEC data, both mutants however show no response to exposure to UV-B. $UVR8^{R338A}$ and $UVR8^{R146A/R286A}$ also show no response to UV-B as seen before; however, their mobilities suggest two further variations in the conformation of monomeric mutants. Finally, the conformation and mobility of the double mutant $UVR8^{R286A/R338A}$ and the triple mutant $UVR8^{R234A/R286A/R338A}$ also remain unchanged after exposure to UV-B (Fig 3-5 D). However, the proteolytic cleavage of the two proteins which has been described earlier becomes clearly visible. The only mutation that results in a mutant form showing wild-type characteristics under native PAGE conditions is R146 to alanine (Fig 3-5 D), where a similar small shift between unexposed and UV-B exposed protein can be observed.

The conclusion that can be drawn from this set of experiments is that the mobility of the protein is altered after exposure to UV-B if the mutant is still responsive to UV-B and this coincides with UV-B induced monomerisation observed by size exclusion chromatography. This method however does not allow clear assignment of dimer or monomer state to mutants if compared to the wild-type form.

3.7 Semi-native SDS-PAGE shows constitutive monomerisation of all salt bridge mutants

Finally, a third method was applied to test the contributions of individual salt bridges to dimer stability. Purified proteins were analysed by semi-native SDS-PAGE hereby taking advantage of the observation that interactions that maintain the dimer are sufficiently strong to resist denaturation by SDS if samples are not heat denatured (Rizzini et al., 2011). As shown in Figure 3-6, this approach is rather debatable for salt bridge mutant forms of UVR8. Whereas wild-type UVR8 is dimeric before exposure to 1.5 µmol m^{-2} s^{-1} of narrowband UV-B for 1 h, no dimer can be detected for $UVR8^{R286K}$, $UVR8^{R146A}$ or $UVR8^{D96N}$, even though dimerisation was observed by SEC. It should also be noted that the wild-type UVR8 dimer runs at a much lower size than a protein of an approximate size of 100 kDa would be expected according to the molecular weight marker. However, omitting denaturation of the protein by boiling leads to 'semi-native' conditions and as described above, the conformation of the proteins greatly influences separation behaviour under such conditions. This matter was also investigated with UVR8 whole plant cell extract and will be described later in this chapter.

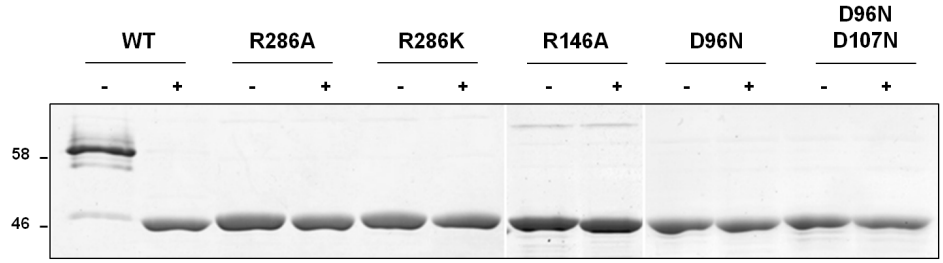

FIGURE 3-6: Salt bridge mutants are constitutively monomeric under semi-native SDS-PAGE conditions. Purified proteins were exposed (+) or not (-) to 1.5 µmol m^{-2} s^{-1} of narrowband UV-B for 1h. Unboiled samples in SDS-loading buffer were run on a 7.5% SDS-PAGE gel and stained with Coomassie Blue.

3.8 The UVR8 dimer shows exciton coupling

Besides the use of SEC, far-UV CD spectroscopy has also been established during this study as an important tool to assess the dimer-monomer state as well as the UV-B responsiveness of UVR8 and its mutant forms. The monomer interaction surface includes seven tryptophans, of which W233, W285 and W337 form a closely packed triad in one monomer facing W94 on the other monomer. This arrangement constitutes the earlier mentioned tryptophan pyramid which is responsible for photoreception (Christie et al.,

2012). These four tryptophans are less than 5Å apart which is sufficiently close that electronic orbitals would overlap, permitting exciton coupling as seen in other proteins (Kuwajima et al., 1991; Vuilleumier et al., 1993; Andersson et al., 2001). Three more pairs of aromatic residues from the surface W198 - Y201, W250 - Y253 and W302 - F305 create a perimeter fence of aromatic residues that isolates the tryptophan triad from solvent. Exciton coupling of tryptophans gives rise to signals in the far-UV CD spectra of proteins (Grishina and Woody, 1994; Kelly et al., 2005). The far-UV CD spectrum of UVR8 shows a strong peak at 234 nm and a trough at 221 nm which is characteristic of exciton coupling between tryptophans (Fig 3-7 A). Exposure of wild-type UVR8 to 1.5 µmol m^{-2} s^{-1} narrowband UV-B for 1 h strongly diminishes these far-UV CD features, indicating that tryptophan exciton coupling is greatly reduced, presumably by separation and possibly disordering of the tryptophan cluster upon dimer dissociation. The near-UV CD spectrum is dominated by the signal of all 14 tryptophans present in UVR8 giving a main peak close to 290 nm with fine structures between 290 and 305 nm (Fig 3-7 B). Overall the near-UV CD spectrum shows integrity of the protein with a nicely folded tertiary structure with no major changes after exposure to UV-B.

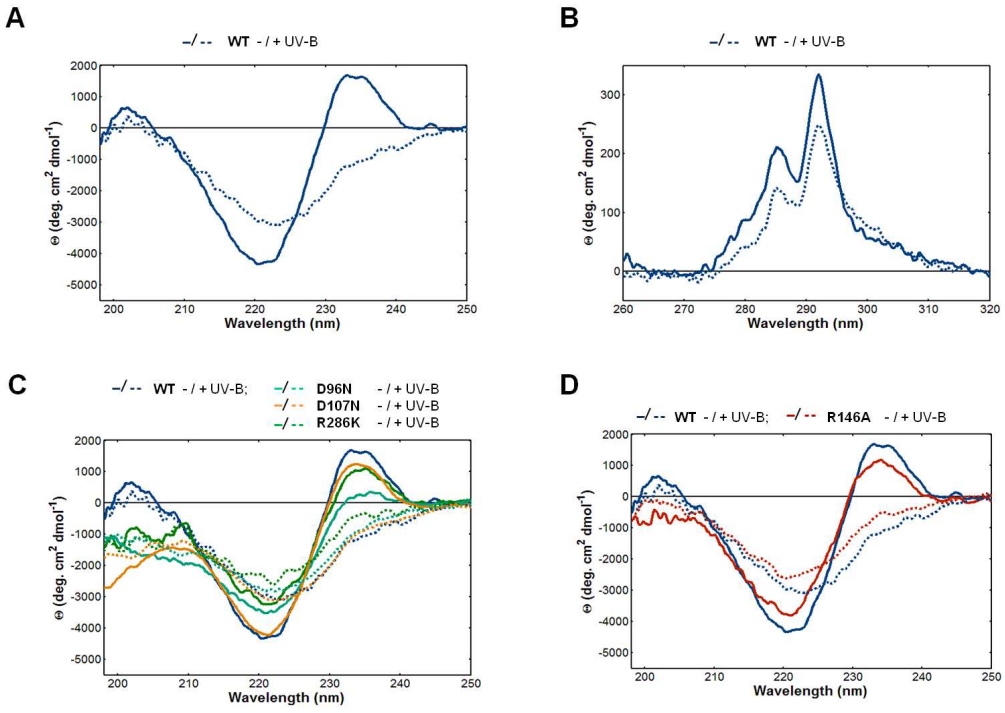

FIGURE 3-7: The UVR8 dimer shows exciton coupling and a UV-B response.
(A) and **(B)** Far- and near-UV CD spectra of wild type UVR8 protein exposed or not (-UV-B, solid line) to 1.5 µmol m^{-2} s^{-1} narrowband UV-B for 1 h (+UV-B, dotted line) **(C)** Far-UV CD spectra of dimeric $UVR8^{D96N}$, $UVR8^{D107N}$ and $UVR8^{R286K}$ mutants with same treatment as in (A) **(D)** Far-UV CD spectra of dimeric $UVR8^{R146A}$ mutant with same treatment as in (A).

The presence of exciton coupling in the UVR8 dimer was next examined in those mutants that were characterized as dimeric by size exclusion chromatography. $UVR8^{D107N}$, $UVR8^{R286K}$ and $UVR8^{R146A}$ show only a very small reduction in exciton coupling under non UV-B conditions compared to wild-type UVR8 (Fig 3-7 C and D). This is most likely due to minor changes in side chain orientations around the tryptophan pyramid caused by the mutations, which will influence distances of overlapping orbitals and thus the intensity of exciton coupling. All three mutants respond to UV-B by showing the same loss in exciton coupling as wild-type. The $UVR8^{D96N}$ mutant shows the greatest reduction of exciton coupling amongst the dimeric mutants; however, exposure to UV-B still flattens the signal even further like in the wild-type protein (Fig 3-7 C). Near-UV CD spectra were also recorded for all UVR8 mutants. All spectra are fairly similar compared to wild-type UVR8 and are therefore shown in the appendix (Fig A-2).

3.9 Exciton coupling is reduced in the monomeric mutants

To test whether exciton coupling requires an intact UVR8 dimer, the monomeric mutants were investigated by far-UV CD spectroscopy (Fig 3-8). None of the spectra recorded for the monomeric mutants resembles that of the monomeric wild-type protein after exposure to UV-B. This observation suggests that a change of the tryptophan arrangement can only be achieved by UV-B induced monomerisation and not through monomerisation by mutagenesis. The far-UV CD spectrum of $UVR8^{D96N/D107N}$ shows the greatest reduction in exciton coupling amongst the monomeric mutants (Fig 3-8 A). Exciton coupling seems to be reduced slightly further after exposure of the protein to UV-B; however, the overall shape of the curve has not changed as seen for wild-type UVR8. A similar observation can be made for $UVR8^{R286A}$, except exciton coupling is less reduced at 234 nm but more at 221 nm. The far-UV CD spectrum of $UVR8^{R338A}$ is comparable in height to the 234 nm exciton coupling peak and also shows subtle changes after exposure to UV-B (Fig 3-8 B). The two double mutants $UVR8^{R286A/R338A}$ and $UVR8^{R146A/R286A}$ show similar strength of exciton coupling as the other monomeric mutants but remain unchanged after exposure to UV-B (Fig 3-8 C). Interestingly, exciton coupling is greatly reduced in the $UVR8^{R234A}$ mutant in respect to the 234 nm peak but not the 221 nm trough (Fig 3-8 D). However, whether this mutation truly leads to monomerisation or not needs to be investigated further.

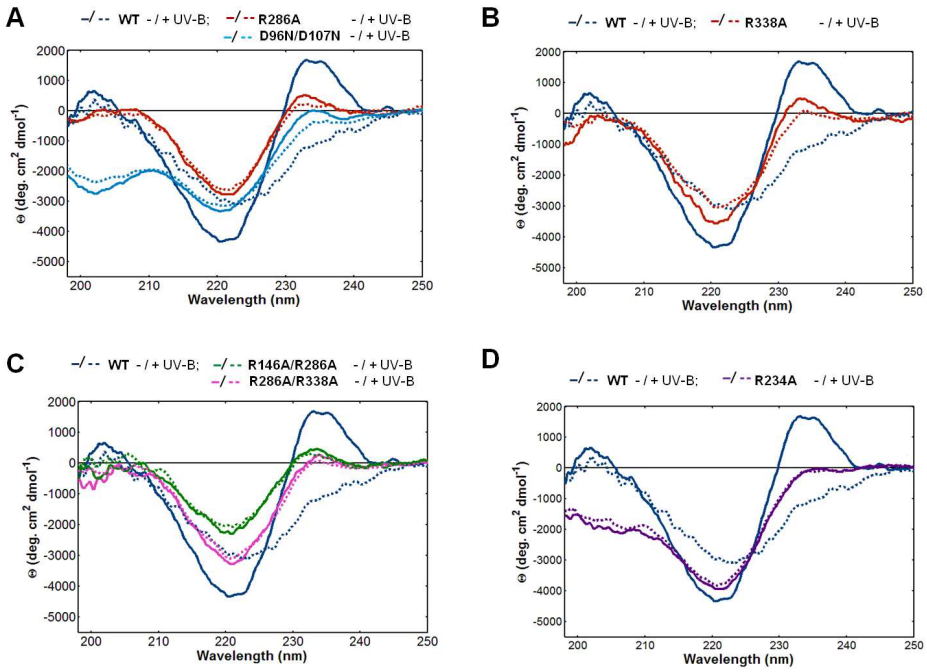

FIGURE 3-8: Exciton coupling is reduced in the monomeric UVR8 mutants.
(A) Far-UV CD spectra of monomeric UVR8$^{D96N/D107N}$ and UVR8^{R286A} mutants exposed or not (-UV-B, solid line) to 1.5 µmol m^{-2} s^{-1} narrowband UV-B for 1 h (+UV-B, dotted line) **(B)** Far-UV CD spectra of monomeric UVR8^{R338A} with same treatment as in (A) **(C)** Far-UV CD spectra of monomeric UVR8$^{R146A/R286A}$ and UVR8$^{R286A/R338A}$ mutants with same treatment as in (A) **(D)** Far-UV CD spectra of dimeric UVR8^{R234A} mutant with same treatment as in (A).

3.10 Analysis of the UVR8 homodimer in plants

Besides the in vitro studies of the dimer-monomer state of UVR8 salt bridge mutants, effects of mutations were also tested in transgenic *uvr8-1* Arabidopsis lines expressing GFP-UVR8 with the respective mutation under control of the CaMV *35S* promoter. The *uvr8-1* allele has a 15 bp deletion in the middle of the gene which includes an among RCC1 homologues highly conserved glycine residue and leads to complete absence of the protein (Kliebenstein et al., 2002). Fig 3-9 shows the expression levels of GFP-UVR8 in the generated mutant lines used during this study. Three independent homozygous T3 lines (numbered) were selected for each GFP-UVR8 mutant except for GFP-UVR8^{R146A} and line 4 for GFP-UVR8$^{D96N/D107N}$ where plants of the T2 generation were used.

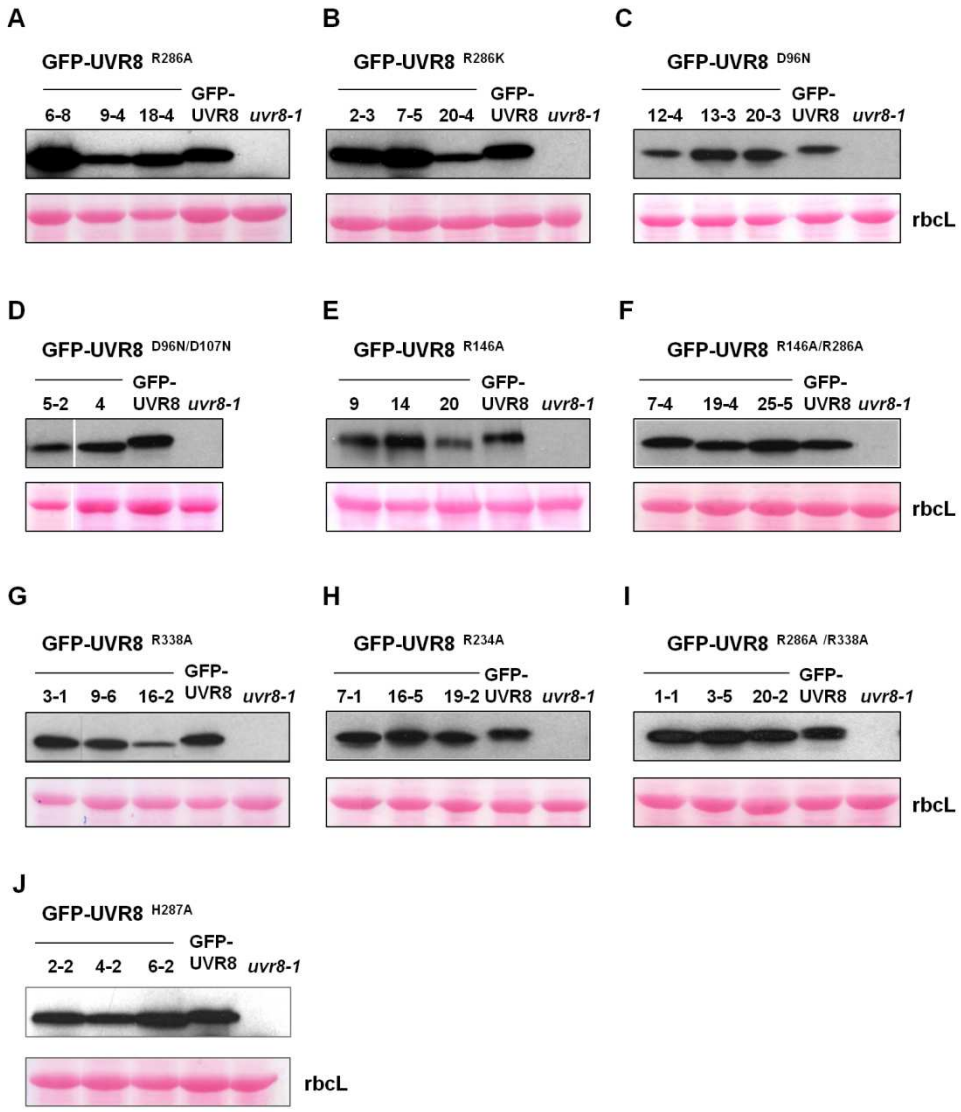

FIGURE 3-9: Expression levels of GFP-UVR8 in transgenic lines.
Immunoblot analysis of plant cell extracts of transgenic lines expressing the indicated GFP-UVR8 fusions. Extracts were separated by SDS-PAGE and immunoblots were probed with anti-GFP antibody. Ponceau S staining of Rubisco large subunit (rbcL) is shown as a loading control. Three independent homozygous T3 lines (numbered) were selected for each GFP-UVR8 mutant (except T2 generation for GFP-UVR8^{R146A} and line 4 for GFP-UVR8$^{D96N/D107N}$). The level of expression in each line was compared to that in GFP-UVR8 line 6-2, in which the level of GFP-UVR8 expression is sufficient to functionally complement *uvr8-1 (*Kaiserli and Jenkins, 2007).

UV-B-dependent monomerisation of UVR8 in plants was first shown by undertaking a co-immunoprecipitation assay. Whole cell extracts were obtained from wild-type plants expressing GFP-UVR8 treated or not with 3 μmol m^{-2} s^{-1} narrowband UV-B for 4 h. Subsequently, a co-immunoprecipitation assay with anti GFP-beads was carried out under the same conditions. Figure 3-10 A shows that native UVR8 protein interacts with GFP-UVR8 forming a heterodimer under non-UV-B conditions. The interaction is lost after exposure to UV-B since the native UVR8 protein is no longer pulled down by GFP-UVR8.

This demonstrates UV-B induced monomerisation in plants. However, this kind of experiment can only be used for the wild-type form of UVR8, since transformation of plants with a GFP-tagged and an untagged mutant form of UVR8 at the same time is not easily accomplished.

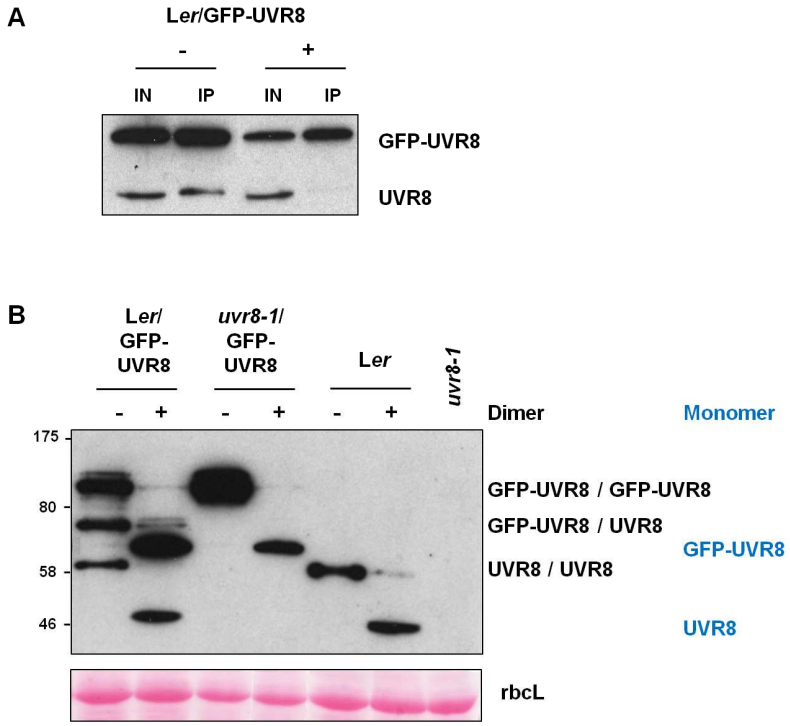

FIGURE 3-10: UVR8 forms a homodimer in plants.
(A) UV-B induces monomerisation of GFP-UVR8 and UVR8 dimers. Whole cell extracts obtained from wild-type L*er* plants transformed with GFP-UVR8 treated (+) or not (-) with 3 µmol m^{-2} s^{-1} UV-B for 4 h. A co-immunoprecipitation assay was performed with anti-GFP beads and the immunoblot was probed with anti-UVR8 antibody. **(B)** Whole cell extracts obtained from *uvr8-1* and L*er* plants transformed with GFP-UVR8 and extracts from L*er* wild type plants were exposed (+) or not (-) to 4 µmol m^{-2} s^{-1} narrowband UV-B for 30 min. SDS-loading buffer was added to the extracts, and unboiled samples were run on a 7.5% SDS-PAGE gel. The immunoblot was probed with anti-UVR8 antibody. GFP-UVR8/UVR8 heterodimers and homodimer as well as monomeric forms are indicated. Ponceau S staining of Rubisco large subunit (rbcL) is shown as a loading control.

In vivo studies of the dimer-monomer state of UVR8 and GFP-UVR8 using semi-native SDS-PAGE were already in progress before expression and purification of the recombinant protein was achieved in *E. coli*. Since very little was known at that time about any proteins interacting with UVR8 under non UV-B conditions, concerns arouse whether the band detected by the UVR8 antibody in plant cell extract in the dark state really was a UVR8 homodimer since it was running much lower than its expected molecular weight. Interestingly, the fact that the proteins are separated under semi-native conditions and therefore protein conformation greatly influences their separation behaviour only seems to

be true for the dimer but not for the monomer since a band around the expected 46 kDa marker band is detected for the monomer.

To prove that UVR8 is indeed forming a homodimer in plants that can be maintained during semi-native SDS-PAGE conditions and detected by immunoblotting, whole cell extracts obtained from *uvr8-1* and L*er* plants transformed with GFP-UVR8 and extracts from L*er* wild-type plants were analyzed. Fig 3-10 B shows that in wild-type plants expressing GFP-UVR8 three bands can be detected by the UVR8 antibody in the dark state. These correspond to the GFP-UVR8 and UVR8 homodimers and the intermediate corresponds to the heterodimer formed between GFP-UVR8 and UVR8. In the absence of UV-B, the intermediate band is only present if GFP-UVR8 is expressed in the wild-type background but not if expressed in the *uvr8-1* mutant background proving that this is indeed a heterodimer formed between the tagged and the endogenous form of UVR8. Upon exposure of the extract to 4 μmol m^{-2} s^{-1} narrowband UV-B for 30 min, the GFP-UVR8 and the UVR8 monomers can be detected. The experiment therefore demonstrates that even if the UVR8 dimer runs at a rather unexpected low molecular weight, it is a homodimer and not an interaction with another protein. This ties in with the analysis of purified protein as shown in Fig 3-6 where a band of the same size appears under in vitro conditions excluding possible interactions with other proteins and only allowing homodimerisation.

3.11 Dimer-monomer state of UVR8 salt bridge mutants expressed in plants analysed by PAGE

To find an appropriate technique to reliably investigate the dimer-monomer state of the salt bridge mutants expressed in plants has been rather difficult. As already shown for the purified UVR8 salt bridge mutants, the very convenient method of semi-native SDS-PAGE does not rigorously show whether a UVR8 mutant is monomeric or dimeric if compared to data gained from SEC experiments. The limitations of native PAGE in this respect have been described earlier on as well. Furthermore, due to limited amount of plant material and presumably unknown interacting proteins, as well as possible complex formations in vivo, the method of choice for purified UVR8 protein, size exclusion chromatography, is not as straight forward to apply as one might wish for an in vivo analysis of UVR8 dimerisation state.

Nevertheless, semi-native SDS-PAGE was undertaken with whole cell extracts obtained from *uvr8-1* plants transformed with GFP-UVR8 or GFP-UVR8 salt bridge mutant forms.

Extracts were exposed or not to 4 µmol m^{-2} s^{-1} narrowband UV-B for 30 min before separation on a SDS-PAGE gel. All transgenic lines that were generated in this study (Fig 3-9) were tested by semi-native SDS-PAGE and immunoblotting using an anti-UVR8 antibody and not unexpectedly all salt bridge mutants were detected as constitutive monomers (Fig 3-11).

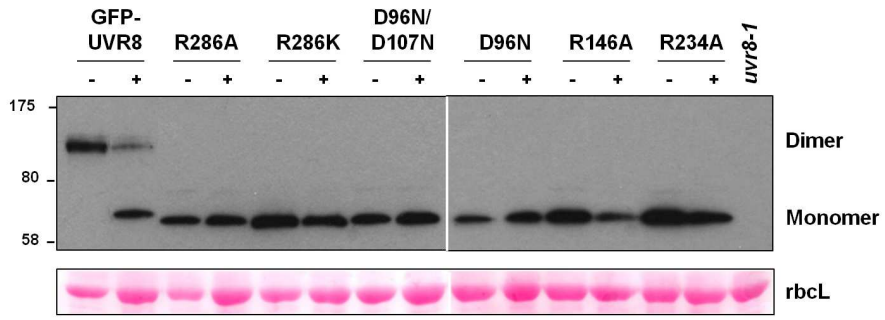

FIGURE 3-11: Semi-native SDS-PAGE to show dimer-monomer state of UVR8 in whole cell extracts obtained from *uvr8-1* plants transformed with GFP-UVR8 or GFP-UVR8 salt bridge mutant forms. Extracts were exposed (+) or not (-) to 4 µmol m^{-2} s^{-1} narrowband UV-B for 30 min. SDS sample buffer was added to the extracts and unboiled samples were run on a 7.5% SDS-PAGE gel. An immunoblot was probed with anti-UVR8 antibody. GFP-UVR8 dimer and monomer bands are indicated. Ponceau S staining of Rubisco large subunit (rbcL) is shown as a loading control.

The same extracts were also separated by native PAGE and UVR8 was again revealed by immunoblotting with an anti-UVR8 antibody (Fig 3-12). The shift between the dimeric and monomeric form of endogenous UVR8 obtained from wild-type L*er* plants (Fig 3-12 A) is once again very subtle whereas also a smear below the monomeric band is observed especially on longer exposed immunoblots (not shown). A similar observation can be made for GFP-UVR8 (Fig 3-12 B) thus making it very difficult to distinguish between the two states and assess effects of mutations. Comparison between the native PAGE of purified UVR8 mutant forms and the native PAGE of whole cell extract reveals one major difference: whereas the various purified mutants show great differences in mobility, the GFP-UVR8 mutants expressed in plants show bands in the same position suggesting rather similar conformations and charges (Fig 3-12 B-D). Especially the putative dimeric bands of the $UVR8^{D96N}$ and $UVR8^{R286K}$ mutants visible in Fig 3-5 A and B are not detected in the whole cell extract samples. The only exception is GFP-$UVR8^{R146A}$ which shows a close to GFP-UVR8 wild-type behaviour with a very small shift visible after UV-B treatment and also a smear below the supposedly monomeric form of GFP-$UVR8^{R146A}$. Overall, the native PAGE results of whole cell extract shed very little light on the dimer-monomer state of salt bridge mutants and a further approach had to be considered.

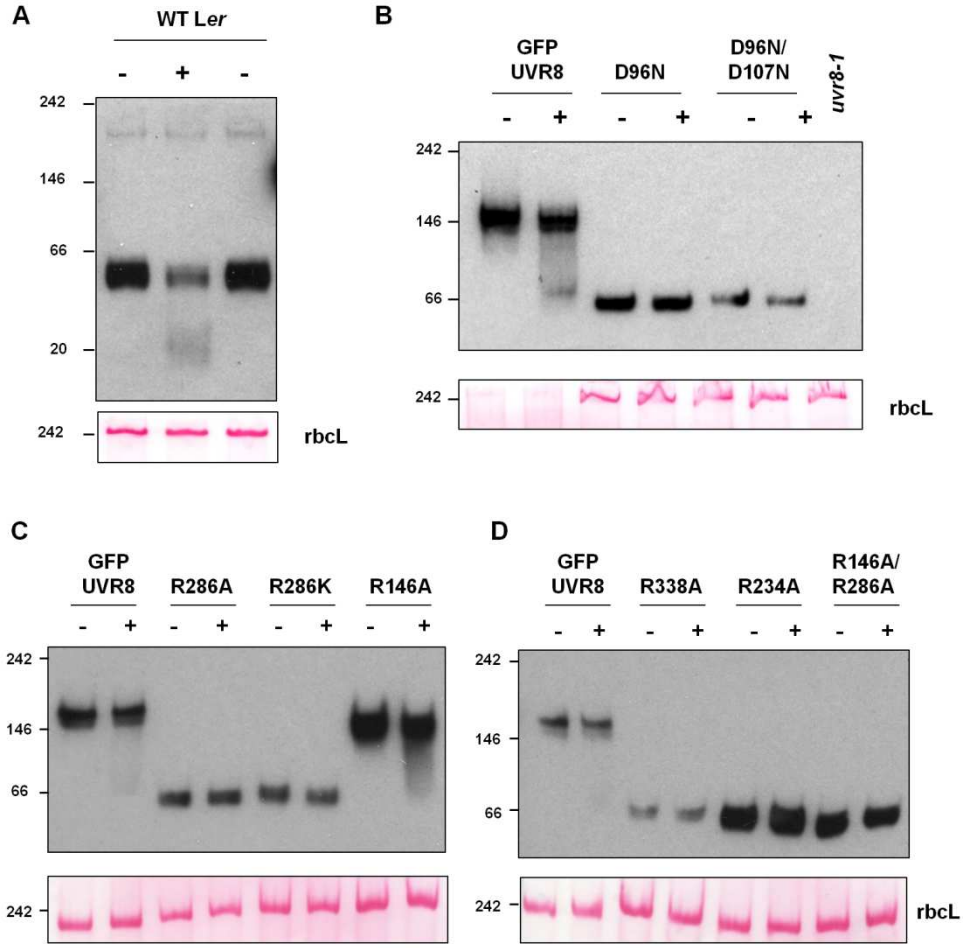

FIGURE 3-12: Native PAGE to show dimer-monomer state of UVR8 in whole cell extracts of WT L*er* and several transgenic GFP-UVR8 salt bridge mutant lines. Whole cell extracts were exposed (+) or not (-) to 4 µmol m^{-2} s^{-1} of narrowband UV-B for 30 min. Samples were separated on a 7.5% native gel and immunoblots were probed with anti-UVR8 antibody. Ponceau S staining of Rubisco large subunit (rbcL) is shown as a loading control.

3.12 Dimer-monomer state of UVR8 salt bridge mutants expressed in plants analysed by SEC

Since size exclusion chromatography served as the most instructive approach for dimer-monomer analysis of purified protein, it was ultimately tested for plant derived UVR8. Due to limited amounts of plant material and several homozygous transgenic lines still in progress, GFP-UVR8 and GFP-UVR8 salt bridge mutants were transiently expressed in *N. benthamiana* plants. GFP-UVR8 transiently expressed in *N. benthamiana* monomerises in response to UV-B and this approach was therefore suitable in generating sufficient amounts of plant cell extract containing UV-B responsive GFP-UVR8 (data not shown). However, it is unclear if Arabidopsis UVR8 can interact with COP1 or other so far unidentified interactors in *N. benthamiana*. Information about possible complex formation

is lacking as well. Nevertheless, it was hoped that GFP-UVR8 under control of the *35S* promoter would be expressed at such high levels in the plant that even if any of the above interactions were formed, enough cytosolic UVR8 would still be available to analyse the dimerisation state of the protein. To purify the protein, GFP-UVR8 was immunoprecipitated under native conditions before being applied to the SEC column. GFP-UVR8 was then detected by SDS-PAGE of the collected chromatography fractions followed by immunoblotting using an anti-GFP-antibody.

Fig 3-13 A shows a clearly distinguishable shift in elution volumes between immunoprecipitated wild-type GFP-UVR8 derived from *N. benthamiana* plants before and after exposure to 4 µmol m^{-2} s^{-1} narrowband UV-B for 30 min. The main peak of non UV-B exposed GFP-UVR8 is detected around 160-260 kDa. After UV-B exposure, monomerisation becomes visible, resulting in a peak at approximately 75 kDa, the expected size of a GFP-tagged UVR8 monomer. Even if the assigned size of the GFP-UVR8 dimer is higher than predicted, conformational contributions have to be considered as described above. However, the most important observation is that with this method a clear shift between the dimeric and the monomeric form is visible which is necessary for subsequent analysis and classification of the respective mutants.

Next, the two monomeric mutants GFP-UVR8^{R286A} and GFP-UVR8$^{D96N/D107N}$ were tested in the established system. Fig 3-13 A and B show similar elution volumes for GFP-UVR8^{R286A}, GFP-UVR8$^{D96N/D107N}$ and for UV-B exposed wild-type GFP-UVR8 confirming the constitutive monomerisation of the two mutants. It was now of interest to test whether the GFP-UVR8^{R286K} dimer detected by size exclusion chromatography of purified protein was also present in plant derived GFP-UVR8^{R286K}. However, the mutant form could only be detected in elution fractions assigned to the monomeric form (Fig 3-13 C). Since the immunoprecipitation assay contains several high salt washes and as seen before higher salt conditions favour monomerisation of the UVR8^{R286K} mutant, washes were performed with low salt buffers resulting in a small shift towards higher molecular weight of the GFP-UVR8^{R286K} elution profile. Nevertheless, the elution profile did not match the profile of dimeric wild-type GFP-UVR8.

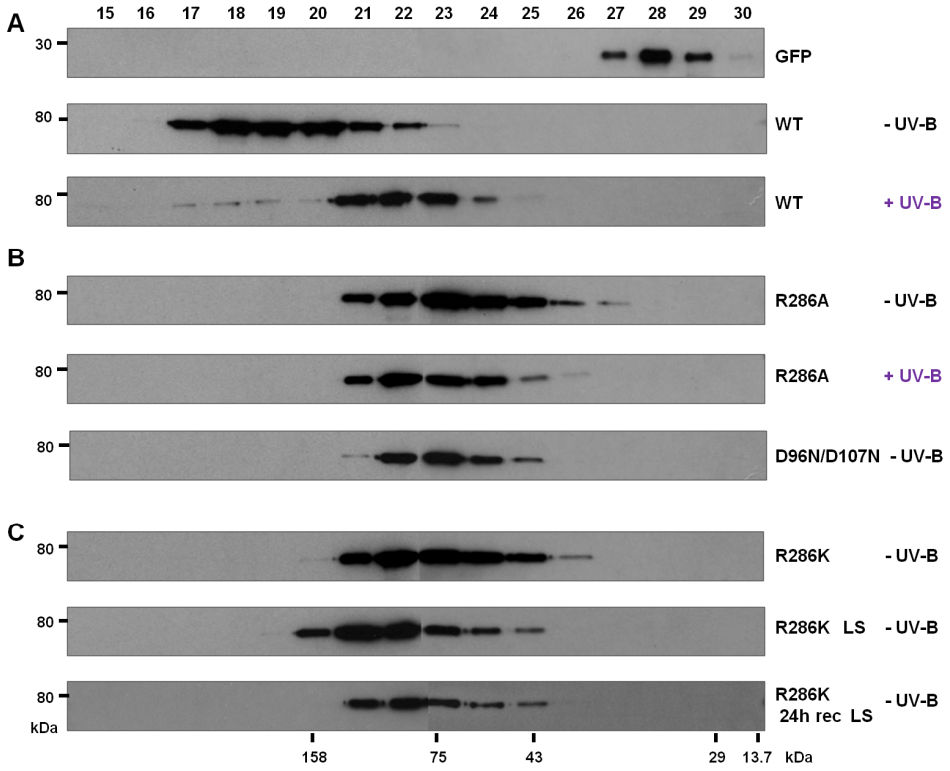

FIGURE 3-13: Dimerisation of GFP-UVR8 expressed in *N. benthamiana* plants.
(A) SEC profiles of immunoprecipitated GFP-UVR8 (WT) expressed in *N. benthamiana* plants before and after UV-B treatment (30 min, 4 µmol m^{-2} s^{-1} narrowband UV-B). Empty vector just containing GFP was used as a control. Eluates of immunoprecipitation assays with anti-GFP beads were loaded onto a Superdex 200 column and fractions 15 to 30 were used for SDS-PAGE and immunoblotting with an anti-GFP antibody. The column was calibrated using a low molecular weight calibration Kit (GE Healthcare). **(B)** SEC profiles of immunoprecipitated GFP-$UVR8^{D96N/D107N}$ and GFP-$UVR8^{R286A}$ before and after UV-B treatment (30 min, 4 µmol m^{-2} s^{-1} narrowband UV-B). **(C)** SEC profiles of GFP-$UVR8^{R286K}$ immunoprecipitated under low and high salt conditions (150 mM NaCl (LS) and 500 mM NaCl (HS)) and after a 24 h recovery period between immunoprecipitation and SEC.

The observed constitutive monomerisation for the $UVR8^{R286K}$ mutant might be due to the combined effect of $UVR8^{R286K}$ forming a destabilized dimer, as seen by semi-native SDS-PAGE and the fact that the elution step of the immunoprecipitation assay involves a drastic change in pH up to 11.8. The highly stable wild-type dimer can be maintained during this step, which is followed by immediate neutralization of the eluate, but possibly not a by mutation-weakened dimer as for example $UVR8^{R286K}$. Knowing that monomerisation is reversible, immunoprecipitation of GFP-$UVR8^{R286K}$ was carried out and a 24 h recovery period of the eluate at room temperature was allowed before SEC was performed to facilitate possible regeneration of the dimer. However, once again the elution profile showed GFP-$UVR8^{R286K}$ being monomeric (Fig 3-13 C). Due to time restraints none of the other dimeric mutants were tested in this system.

A number of other mutants were also tested in an attempt to gain information about whether different conformations of the monomeric mutants are present in plant derived UVR8. GFP-UVR8^{R234A}, GFP-UVR8^{R338A}, GFP-UVR8$^{R286A/R338A}$ and GFP-UVR8$^{R146A/R286A}$ all showed monomeric behaviour under non UV-B conditions matching what has been observed in vivo but without any further gain of information on conformation (Fig 3-14 B). Notably, the double mutant UVR8$^{R286A/R338A}$ only showed proteolytic cleavage when expressed in *E. coli* but not when expressed in either Arabidopsis or *N. benthamiana* plants as GFP fusion proteins.

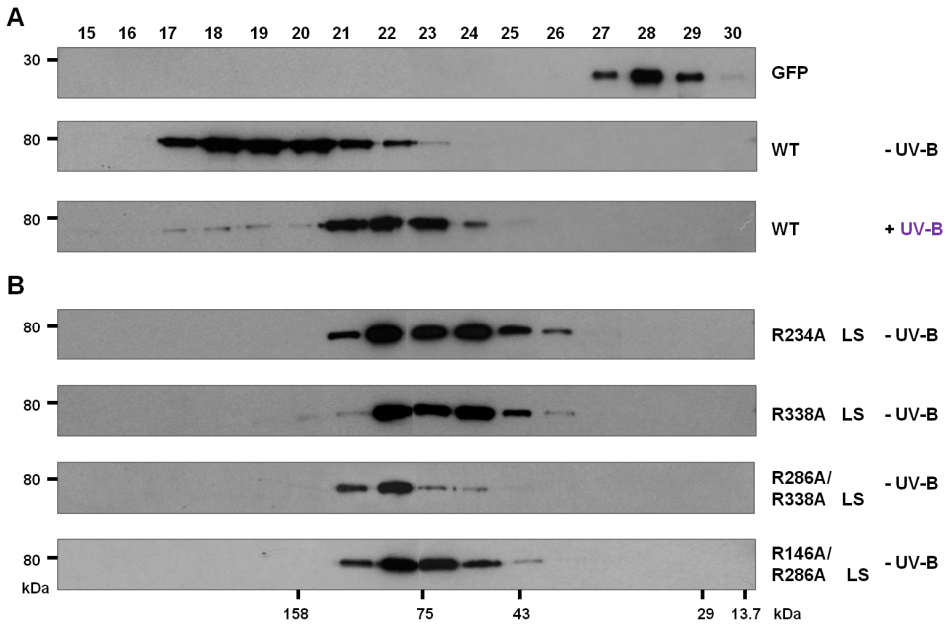

FIGURE 3-14: Constitutive monomerisation of GFP-UVR8 salt bridge mutants expressed in *N. benthamiana* plants. (A) SEC profiles of immunoprecipitated GFP-UVR8 (WT) expressed in *N. benthamiana* plants before and after UV-B treatment (30 min, 4 µmol m^{-2} s^{-1} narrowband UV-B). Empty vector just containing GFP was used as a control. Eluates of immunoprecipitation assays with anti-GFP beads were loaded onto a Superdex 200 column and fractions 15 to 30 were used for SDS-PAGE and Western Blotting with anti-GFP antibody. The column was calibrated using a low molecular weight calibration Kit (GE Healthcare). **(B)** SEC profiles of GFP-UVR8^{R234A}, GFP-UVR8^{R338A}, GFP-UVR8$^{R286A/R338A}$, GFP-UVR8$^{R146A/R286A}$, immunoprecipitated under low salt conditions (LS: 150 mM NaCl).

To conclude, results from SEC of immunoprecipitated plant derived GFP-UVR8 salt bridge mutants could not confirm the dimeric state of UVR8^{R286K} observed when the protein was expressed in vitro. Even modifications of the most critical steps of the immunoprecipitation assay did not lead to detection of a GFP-UVR8^{R286K} dimer. It remains therefore to be established whether salt bridge mutants, in particular GFP-UVR8^{R286K}, GFP-UVR8^{D96N}, GFP-UVR8^{D107N} and GFP-UVR8^{R146A} are indeed able to dimerize when expressed in plants.

3.13 Discussion

3.13.1 Dimerisation of plant photoreceptors

The current chapter is focused on the characterisation of the dimer maintaining forces of UVR8 with respect to individual contributions of amino acid side chains present on the dimer interface. Homodimerisation is a common feature of plant photoreceptors but activation of the receptor by light induced monomerisation of the protein is unique to UVR8. All currently characterized phytochromes act as dimer whereby phyA is mostly found as homodimer and the light-stable phytochromes (phyB-E) can also form tightly bound heterodimers (Sharrock and Clack, 2004). Formation of such heterodimeric photoreceptors increases the potential complexity of R/FR light sensing and signalling mechanisms of phytochromes. Remarkably, there is no evidence for homodimerization of phyC or phyE, indicating that these two forms are present in cells only as heterodimers with phyB or phyD (Clack et al., 2009). In clear contrast to UV-B induced monomerisation of UVR8, light regulated subunit-subunit dissociation is not the signalling mechanism used by plant phytochromes.

For cryptochromes, homodimerisation mediated by the cryptochrome N-terminal domain is required for function (Sang et al., 2005). Activation of the photoreceptor is achieved by rapid phosphorylation upon irradiation with blue light and a subsequent conformational change of the C-terminal domains (Yang et al., 2000). However, during this process of activation the cryptochrome dimer is still maintained. Dimerisation of the second class of blue light receptors, the phototropins, still needs to be fully proven. It has been reported that the LOV1 domain may promote dimerisation of the phototropins based on size exclusion chromatography in addition to x-ray crystallography studies of purified LOV1 (Salomon et al., 2004; Nakasako et al., 2008). Furthermore, a fully active version of phot1 can transphosphorylate a kinase-dead version of phot1 in planta, suggesting that homodimerization is likely and the dimer is maintained in the active state of the receptor (Kaiserli et al., 2009). As for phytochromes and cryptochromes, monomerisation is not the underlying mechanism of phototropin signalling.

In summary, it still has to be determined what precise functional role dimerisation plays in regulating photosensing activity of the visible light photoreceptors. Likewise, the role of dimerisation of UVR8 is not sufficiently characterised yet but several implications of the homodimeric ground state of the receptor will be described and discussed throughout this thesis. Regardless, the UV-B induced dimer to monomer transition of UVR8 to activate the receptor is a new and unique feature in plant photoreceptor responses described so far.

3.13.2 Constitutive monomerisation of several UVR8 salt bridge mutants

Elucidation of the crystal structure revealed an extensive salt bridge network very effectively stitching together the two monomers in the absence of UV-B. Site directed mutagenesis of charged amino acids, especially arginine residues, along the dimer interface has demonstrated their important contributions to dimerisation. This is in accordance with studies for example by Clackson and Wells (1995) showing that single residues can contribute a large fraction of the binding free energy of proteins. Free energies are not uniformly distributed across protein interfaces; instead, certain critical residues contribute the most to the binding free energy and are therefore called 'hot spots'. These 'hot spots' are enriched in tryptophan, tyrosine and arginine residues (Bogan and Thorn, 1998). The abundance of arginine in protein interfaces relates to the versatility of its side chain as a contributor to multiple types of intermolecular interactions (Bogan and Thorn, 1998). Arginine has the ability to form a hydrogen bond network with up to five hydrogen bonds and a salt-bridge with its positively charged guanidinium motif, while the methylene groups can contribute favourably to the hydrophobic effect. Mutations of R286 to alanine or lysine highlight some of these features, causing UVR8 monomerisation or a destabilized dimer, respectively (Fig 3-2 A and 3-6). Furthermore, cation-π interactions between arginines and aromatic side chains are another potentially beneficial interaction at the protein-protein interface (Crowley and Golovin, 2005). Cation-π interactions for R286 within the monomer have been identified by Wu and co-workers (2012) confirming and extending the structural importance of this residue. R286 is surrounded by four aromatic residues (W285, W302, Y253 and W250) which are sufficiently close to allow cation-π interactions which are of structural relevance. The salt bridge formed through R286 is therefore essential for structural integrity as seen by constitutive monomerisation of UVR8^{R286A} and UVR8$^{D96N/D107N}$ and also has major influence on the function of the photoreceptor, as will be described in Chapter 4.

The identification of constitutive monomeric mutant forms of UVR8 is a very valuable tool for elucidation of the UV-B perception mechanism and to investigate the function of dimerisation during this process. Monomerisation of purified UVR8 mutants was assessed by SEC using the wild-type protein as reference point (Fig 3-2 B). However, variation of elution volumes of the UVR8 mutant proteins due to putative shape alterations caused by the mutations had to be addressed to ensure genuine monomerisation and to rule out concentration-dependent or buffer-condition-dependent monomerisation (Fig 3-2 C). Our collaborators (E. Getzoff, The Scripps Research Institute, La Jolla, CA, USA) analysed three monomeric mutants UVR8$^{D96N/D107N}$, UVR8$^{R146A/R286A}$ and UVR8$^{R286A/R338A}$ by multi-

angle laser light scattering (MALS) to determine their molecular masses. UV-B treated wild-type and constitutive monomeric mutants eluted with similar monomeric molecular masses however, distinct hydrodynamic radii were also observed by peak shifts in the elution profiles during MALS confirming the SEC results (Christie et al., 2012).

Variation of the ionic strength in the buffer also caused shifts in the elution volumes, in particular for UVR8^{R286K} and UVR8^{R338A} (Fig 3-2 D and 3-3 B). This observation fits the model of ionic interactions maintaining the dimer since increasing the salt concentration reduces the strength of ionic interactions across the dimer interface by providing competing ions for the charged residues. Thus monomerisation will occur. The shifted dimer peak also suggests that the compactness of the protein is greatly influenced by its ionic environment. Conformational changes were also caused by altered arrangements of the C-terminus as shown by treatments of the mutants with trypsin (Fig 3-4). The C-terminus contains a high number of charged residues (11 out of 42: three arginines, two lysines, four aspartic acids and two glutamic acids) which might cause artefacts in vitro interfering with counter ions in solution.

Besides the identification of monomeric mutants, a second set of mutants comprising UVR8^{R286K}, UVR8^{D96N}, UVR8^{D107N} and UVR8^{R146A} was characterised (Fig 3-2 and 3-4). Here, mutation of an interface residue did not prevent dimerisation under SEC conditions. However, monomerisation was observed under semi-native SDS-PAGE conditions (Fig 3-6). It can therefore be concluded that mutation of any of the salt bridges results in a destabilized or weakened dimer that monomerizes if buffer conditions become harsher as for example during semi-native SDS-PAGE. In the case of UVR8^{R286K}, where no salt bridge is removed in contrast to the other three mutants, the destabilized dimer is most likely caused by the fact that lysine only contains a single amino group, meaning it is more limited in the number of hydrogen bonds it can form. It can therefore only partially substitute for the double hydrogen bonded salt bridge formed through R286.

The monomeric as well as the weakened dimeric forms of UVR8 identified in the in vitro studies were ultimately tested in transgenic Arabidopsis plants as GFP fusion proteins. Dimerisation of wild-type GFP-UVR8 could be shown by semi-native SDS-PAGE and also by SEC of immunoprecipitated GFP-UVR8 derived from *N. benthamiana* plants (Fig 3-11 and 3-13). Dimerisation however, could not be shown for GFP-UVR8^{R286K}, GFP-UVR8^{D96N} or GFP-UVR8^{R146A}. The semi-native SDS-PAGE of these purified mutants reveals a weakened or destabilized dimer compared to wild-type UVR8 and most likely this dimer cannot be maintained under the immunoprecipitation conditions. Immunoprecipitation of GFP-UVR8 before SEC analysis is nevertheless essential, since

SEC of whole plant cell extract omitting immunoprecipitation has led to the detection of GFP-UVR8 in a rather big complex at roughly 300 kDa. This unidentified complex remains more or less unchanged after exposure to UV-B making this an unsuitable technique for mutant analysis (Headland, Ph.D. thesis, 2009). It can also not be excluded that discrepancies might exist between UVR8 expressed in vitro and UVR8 expressed in vivo. A weakened dimer in vivo might allow interaction with so far unknown proteins pushing the dimer-monomer equilibrium towards monomerisation. Also the cytosolic pH might favour monomer formation. These possibilities have to be kept in mind for the functional analysis of the generated Arabidopsis salt bridge mutant lines undertaken in Chapter 4.

3.13.3 The influence of dimerisation on exciton coupling

Many interactions involving aromatic residues have the potential to contribute to CD features of a protein. Exciton coupling between tryptophan residues has been observed in several proteins before, including the dihydrofolate reductase (DHFR) of *E. coli* (Kuwajima et al., 1991) and the bacterial ribonuclease barnase (Vuilleumier et al., 1993). The utilization of far-UV CD spectroscopy to investigate exciton coupling in wild-type UVR8 and tryptophan mutants has given first insights into a possible mechanism of UV-B perception (Christie et al., 2012). In respect to the salt bridge mutants, it was now of interest to test whether dimer formation is essential for exciton coupling, since a complete loss of it is observed after UV-B exposure of the protein. However, CD spectra of proteins are quite complex and difficult to unravel, as they represent the sum of contributions of backbone peptide groups in different conformations, aromatic side chains and coupling of electronic transitions arising from interactions involving aromatic residues and side-chain amide as well as charged groups in an asymmetric environment (Strickland, 1974).

The contribution of single tryptophans to the observed exciton coupling of UVR8 has been investigated by site directed mutagenesis revealing that W285A causes the greatest loss of exciton coupling, with its far-UV CD spectrum closely resembling that of the triple-mutant $UVR8^{W233A/W285A/W337A}$ and UV-B treated wild-type (Christie et al., 2012). None of the monomeric mutants show such a profound loss of exciton coupling, only different levels of reduction were observed (Fig 3-8). This suggests that dimerisation maximises the extent of exciton coupling but is not a requirement for it to occur. This hypothesis is supported by the fact that mutation of W94A, the apex of the UV-B perceiving pyramid on the opposing monomer, still allows exciton coupling but is similarly reduced as, for example, in $UVR8^{R286A}$ or $UVR8^{R338A}$. Amongst the mutations that only lead to a destabilized dimer

but not to a constitutive monomer, UVR8^{D96N} is strikingly different in respect to its ability of exciton coupling. UVR8^{D96N} shows the greatest reduction of exciton coupling amongst the dimeric mutants comparable to the monomeric mutant UVR8^{R286A}. However, exposure of UVR8^{D96N} to UV-B still flattens the signal even further like in the wild-type protein (Fig 3-7 C) indicating that UV-B photoreception does not necessarily require intensive exciton coupling. One should be aware that conclusions drawn from these experiments have to be considered very carefully since the basic requirement for exciton coupling is sufficient proximity of the chromophores (Grishina and Woody, 1994). Thus, a specific feature of a spectrum including intensity of signals is very sensitive to changes in the tertiary structure of the protein. Those will be created more or less severely by the introduced mutation and can lead to unpredictable rearrangements of essential residues.

3.13.4 The role of the salt bridges during photoreception

To understand the role of the salt bridges during photoreception the overall structural arrangement of the arginine residues within the dimer interface has to be considered. Several bulky aromatic residues are tightly packed around the key charged residues, in particular R286. R338 and R234 are positioned as ‘book ends’ flanking W285 and W233 of the tryptophan pyramid (Christie et al., 2012). The proximity and coupling of arginines and tryptophans suggest a specific mechanism whereby photoreception leads to disruption of the salt bridges (Christie et al., 2012). The closely packed central W285-R286 pair is possibly the linker between UV-B photoreception and salt-bridge status. The impact of the W-R arrangement on structure as well as on function can be characterized by comparison of the UVR8^{R286A} and the UVR8$^{D96N/D107N}$ mutants, since both mutants are monomeric but the latter mutation does not directly alter the tryptophan-arginine arrangement. Unfortunately, the far-UV CD spectrum only reveals a small difference in the occurrence of exciton coupling which does not allow a more specific assignment on the role of R286 (Fig 3-8). Nevertheless, the native PAGE of purified protein reveals two different conformations for the two mutants (Fig 3-5). In respect to function, the two mutants can be clearly distinguished, which will be described in the following chapter. So far the photoreception mechanism remains hypothetical and needs further experimental proof. A possible scenario would be that photoreception by the tryptophan pyramid, predominantly W285 and W233, results in the effective transfer of an excited electron from a tryptophan to a neighbouring arginine, leading to charge neutralization followed by breakage of cross-dimer salt bridges and dissociation of the two subunits (Christie et

al. 2012). Once monomerisation is achieved, interaction with COP1 is the next defined step in the UVR8 signalling pathway which will be analysed in the next chapter.

4. FUNCTIONAL ANALYSIS OF UVR8 SALT BRIDGE MUTANTS

4.1 Introduction

UV-B induced dissociation of the UVR8 dimer into monomers is one of the very early events of UV-B signalling that ultimately leads to the expression of a range of genes essential for UV-B protection. A great number of UVR8-regulated genes are controlled by the transcription factor HY5 and UVR8 regulates transcript levels of HY5 (Brown et al., 2005). Another known essential process to initiate signal transduction is the interaction between UVR8 and COP1 (Favory et al., 2009). The objective of this chapter was to determine the effect of UVR8 salt bridge mutations in respect to functionality of the mutant in plants. To do so, the interaction between UVR8 and COP1 was assayed alongside with RT-PCR experiments to test UV-B induced *HY5* and *CHS* gene expression, analysis of CHS protein levels and assessment of a photomorphological UV-B response mediated by UVR8. The site-directed mutagenesis was also extended towards residues in a conserved and repeated motif GWRHT that embeds the tryptophan triad and the main salt bridge formed through R286. The major findings of this chapter are firstly that constitutive monomerisation and interaction with COP1 are not sufficient to initiate a UVR8-mediated response in the absence of UV-B in vivo and secondly that dimerisation is not required for UVR8-mediated signalling in vivo.

4.2 The evolutionarily conserved reoccurring motif GWRHT

Initial sequence analysis before the crystal structure of UVR8 became available resulted in identification of an evolutionarily conserved and three times repeated motif (GWRHT) which was used as a starting point for the structure-function studies. Looking at orthologs of UVR8 in other higher plants, e.g. the poplar (*Populus trichocarpa*) or rice (*Oryza sativum*), protein sequences show a high degree of conservation being about 75% identical (Fig 4-1). Extending the comparison from higher to lower plants like the moss *Physcomitrella patens* or the green algae *Chlamydomonas reinhardtii*, sequences are still 67% and 49% identical respectively, raising the possibility that UVR8 has evolved because plants needed to be exposed to sun light required for photosynthesis but have to be protected against UV radiation at the same time especially during land plant evolution (Wolf et al., 2010). As shown before, stretches containing the 14 tryptophans and also the

structurally important glycines which maintain the blade structure are especially conserved throughout the plant kingdom (Christie et al., 2012; O'Hara and Jenkins 2012). Likewise conserved even in lower plants is the GWRHT motif which embeds the tryptophan triad. This suggests that this motif has an important role in the function of the protein. Furthermore, the crystal structure shows that these pentapeptides, occurring in blades 5, 6 and 7 form protruding tight turns that project tryptophan and arginine residues outward and histidine residues (in all seven blades) inward to form a buried ring of so far unknown function (Christie et al., 2012).

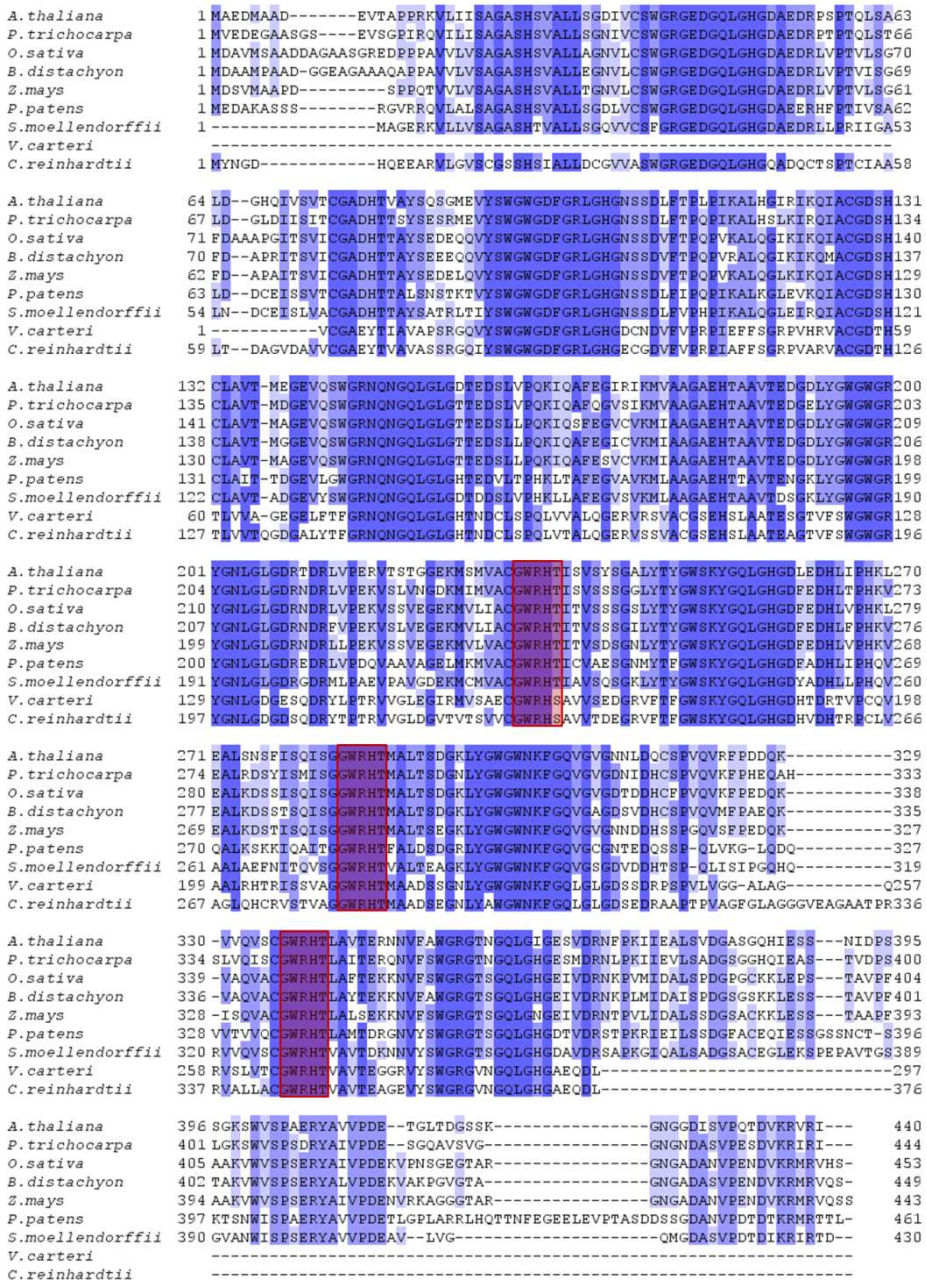

FIGURE 4-1: The GWRHT motif is conserved among UVR8 orthologs in higher and lower plants. Multiple sequence alignment of full length *Arabidopsis* UVR8 with UVR8 sequences from various higher and lower plant species. The plant species shown are: *Brassica rapa, Populus trichocarpa, Oryza sativum* (subspecies japonica), *Brachypodium distachyon, Zea mays, Physcomitrella patens, Selaginella moellendorfii, Volvox carteri* and *Chlamydomonas reinhardtii*. The arginines of the three motifs are R234, R286 and R338 respectively.

4.3 UV-B dependent interaction of UVR8 mutants and COP1 in yeast

The effects of mutations within the GWRHT motif on UVR8 function were first investigated by application of a yeast two-hybrid system in *S. cerevisiae* to test for UVR8 and COP1 interaction. The suitability of this system to investigate UV-B dependent interaction of the two proteins has been shown before (Rizzini et al., 2011; Cloix et al. 2012; O'Hara and Jenkins 2012). It is possible since yeast does not contain a COP1 homolog (Yi and Deng, 2005) or a UVR8 protein. Furthermore, the observed interaction between UVR8 and COP1 is UV-B specific and is not mediated by the yeast DNA damage signalling pathway (Cloix et al., 2012).

Yeast strain AH109 was co-transformed with a vector expressing the DNA binding domain (BD) of the yeast GAL4 transcription factor fused to UVR8 wild-type or a mutant form and a vector expressing the GAL4 activation domain (AD) fused to COP1. Successfully transformed yeast colonies were then spotted on plates lacking essential amino acids; growth requires activation of reporter genes which is only possible through reconstitution of the full-length GAL4 transcription factor by interaction of the fused proteins. UVR8 and COP1 interaction is observed when yeast are grown under 0.1 μmol m^{-2} s^{-1} narrowband UV-B at 30°C but not if grown in darkness (Fig 4-2).

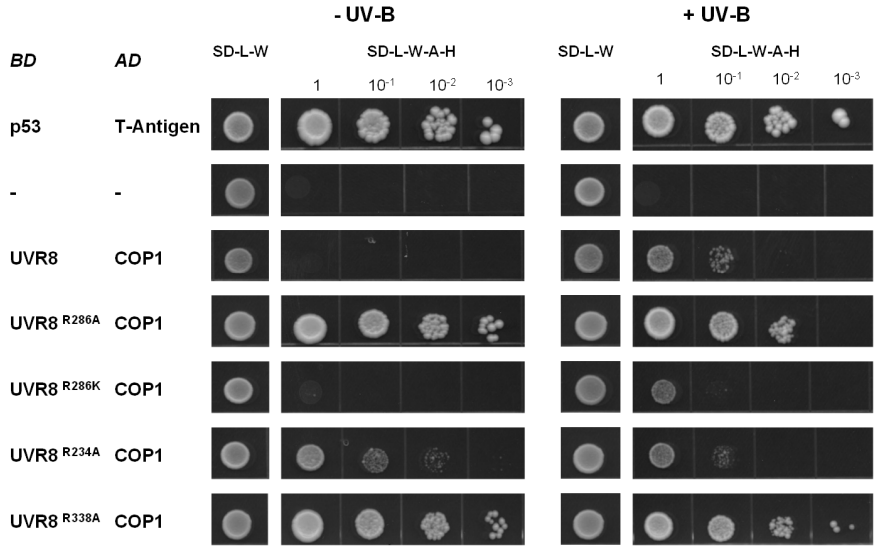

FIGURE 4-2: Yeast two-hybrid assay showing UV-B dependent interaction between UVR8 and COP1 and $UVR8^{R286K}$ and COP1 as well as constitutive interaction between $UVR8^{R286A}$, $UVR8^{R234A}$ and $UVR8^{R338A}$ and COP1. Yeast strain AH109 was either transformed with pGBKT7-p53 and pGADT7-T-antigen (positive control), pGBKT7-UVR8 and pGADT7-COP1 or pGBKT7-UVR8 (mutations indicated) and pGADT7-COP1. The empty vectors (-) were used as a negative control. Yeast were left to grow in darkness (- UV-B) or under 0.1 μmol m^{-2} s^{-1} narrowband UV-B (+) at 30°C on fully selective plates (SD-L-W-A-H) in serial dilutions or undiluted on non-selective plates (SD-L-W) for 4 days.

Next, each of the three arginines in the GWRHT repeats were mutated to alanine and a UV-B independent constitutive interaction between COP1 and UVR8^{R234A}, UVR8^{R286A} and UVR8^{R338A} respectively occurs. To test whether the strength of interaction differs under dark and UV-B conditions, a serial dilution of yeast spots was carried out showing a slightly stronger interaction in the dark. The interaction between UVR8^{R286A} and COP1 as well as UVR8^{R338A} and COP1 seems to be stronger then between UVR8^{R234A} and COP1. When R286 was replaced by lysine, the UV-B dependent interaction as see for wild-type UVR8 can be restored between UVR8^{R286K} and COP1. However, complete loss of the interaction was observed if the negatively charged amino acid glutamate was introduced at position 286 (Fig 4-3 A).

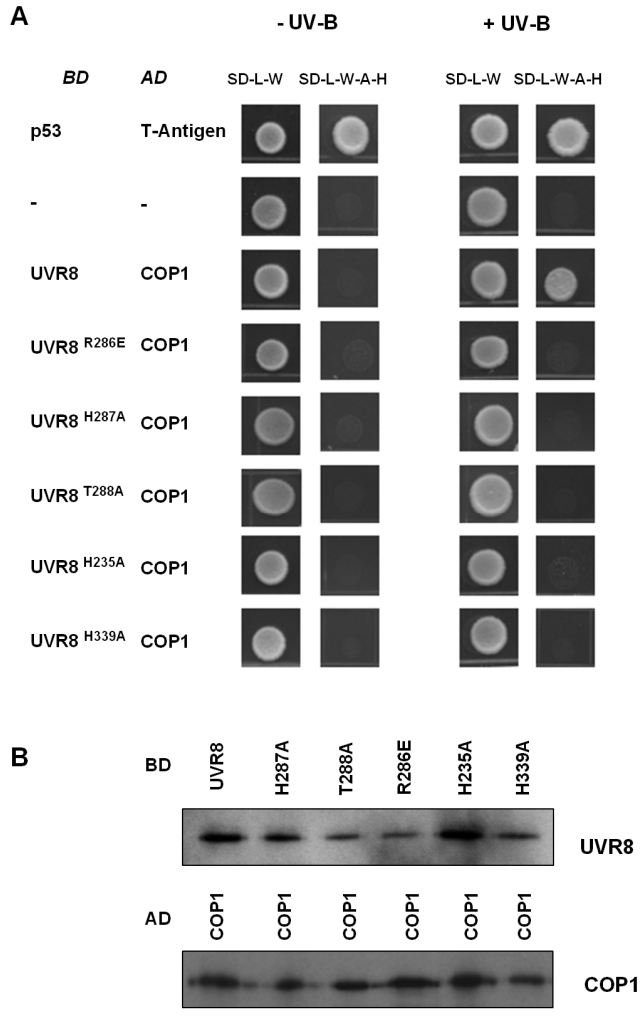

FIGURE 4-3: Yeast two-hybrid assay showing UV-B dependent interaction between UVR8 and COP1 and loss of interaction between mutant forms of UVR8 and COP1.
(A) Yeast strain AH109 was either transformed with pGBKT7-p53 and pGADT7-T-antigen (positive control), pGBKT7-UVR8 and pGADT7-COP1 or pGBKT7-UVR8 (mutations indicated) and pGADT7-COP1. The empty vectors (-) were used as a negative control. Yeast were left to grow in darkness (− UV-B) or under 0.1 µmol m^{-2} s^{-1} narrowband UV-B (+) at 30°C on fully selective plates (SD-L-W-A-H) or on non-selective plates (SD-L-W) for 4 days. **(B)** Expression of proteins from yeast two-hybrid vectors shown in (A) to detect the presence of fusion proteins expressed from the BD and AD vectors. Yeast cells were grown in liquid SD-L-W medium at 30°C overnight. Adequate volumes of the culture were resuspended in lyse and load buffer and samples were separated on a 10% SDS-PAGE gel. Western blots were probed with anti-myc or anti-HA antibodies, respectively.

Similar to the arginines, all three histidines of the GWRHT motifs were mutated to alanine and tested in the yeast two-hybrid system. Fig 4-3 A shows a loss of interaction between the three mutants UVR8^{H235A}, UVR8^{H287A} and UVR8^{H339A} and COP1 respectively. The

lack of interaction is not due to failure of the yeast cells to express the proteins, as each protein was detectable in an immunoblot probed for UVR8 or COP1 with anti-myc or anti-HA antibodies (Fig 4-3 B). Finally, one of the conserved threonines was mutated to alanine (UVR8^{T288A}) which also results in a loss of interaction with COP1 even though the protein was expressed at similar levels to wild-type UVR8 (Fig 4-3 A and B).

4.4 UV-B dependent interaction of UVR8 mutants and COP1 in Arabidopsis

Following the UVR8-COP interaction study in yeast, a co-immunoprecipitation assay with transgenic GFP-UVR8 Arabidopsis lines was established to test the interaction in plants. Co-immunoprecipitation of UVR8 and COP1 has been carried out before by Favory and co-workers (2009), however, mutant lines expressing YFP-COP1 were generated in a *cop1* background and therefore allowed immunoprecipitation with an anti-YFP antibody and detection of UVR8 in the immunoprecipitate with an anti-UVR8 antibody. To be able to analyse the generated GFP-UVR8 salt bridge mutant lines described in Chapter 3 (Fig 3-9), GFP-UVR8 had to be immunoprecipitated with an anti-GFP antibody and the immunoprecipitate had to be analysed for the presence of COP1 using an anti-COP1 antibody. Immunoprecipitation of GFP-UVR8 from whole cell extract of plants kept in darkness or exposed to 3 μmol m^{-2} s^{-1} narrowband UV-B for 3 h was carried out with anti-GFP microbeads (μMacs) pulling down GFP-UVR8 and any associated proteins. Immunoblot analysis of the immunoprecipitate using an anti-COP1 antibody shows UV-B dependent interaction between GFP-UVR8 and COP1 (Fig 4-4 A).

Having established the method for wild-type UVR8, transgenic lines expressing mutant forms of UVR8 could be tested. The constitutive interaction reported in yeast between UVR8^{R234A}, UVR8^{R286A} and UVR8^{R338A} with COP1 can only be observed for GFP-UVR8^{R234A} and GFP-UVR8^{R338A} in plants (Fig 4-4 H, I). Mutation of R286 to alanine in plants shows a loss of interaction between GFP-UVR8^{R286A} and COP1 (Fig 4-4 B). Thus, combined mutation of R286 as well as R338 to alanine results in constitutive interaction between GFP-UVR8$^{R286A/R338A}$ and COP1 (Fig 4-4 J). Yeast and in planta data show further discrepancies when comparing the results of the mutants GFP-UVR8^{H287A} and GFP-UVR8^{R286K}. Whereas mutation of H287 to alanine showed a loss of interaction in the yeast two-hybrid system (Fig 4-3 A), wild-type behaviour regarding COP1 interaction can be observed in plants (Fig 4-4 D). Differences between yeast and plant data are less severe for the GFP-UVR8^{R286K} mutant, since UV-B dependent interaction with COP1 is present in

both systems; however, in plants, the interaction with COP1 is also detectable in darkness, thus the amount of COP1 pulled down is considerably lower than following the UV-B treatment (Fig 4-4 C). A similar pattern of UVR8-COP1 interaction with a seemingly weaker interaction in darkness and a much stronger interaction after exposure of the plants to UV-B can be observed for three of the salt bridge mutants introduced in Chapter 3, i.e. GFP-UVR8^{D96N}, GFP-UVR8$^{D96N/D107N}$ and GFP-UVR8^{R146A} (Fig 4-4 E-G).

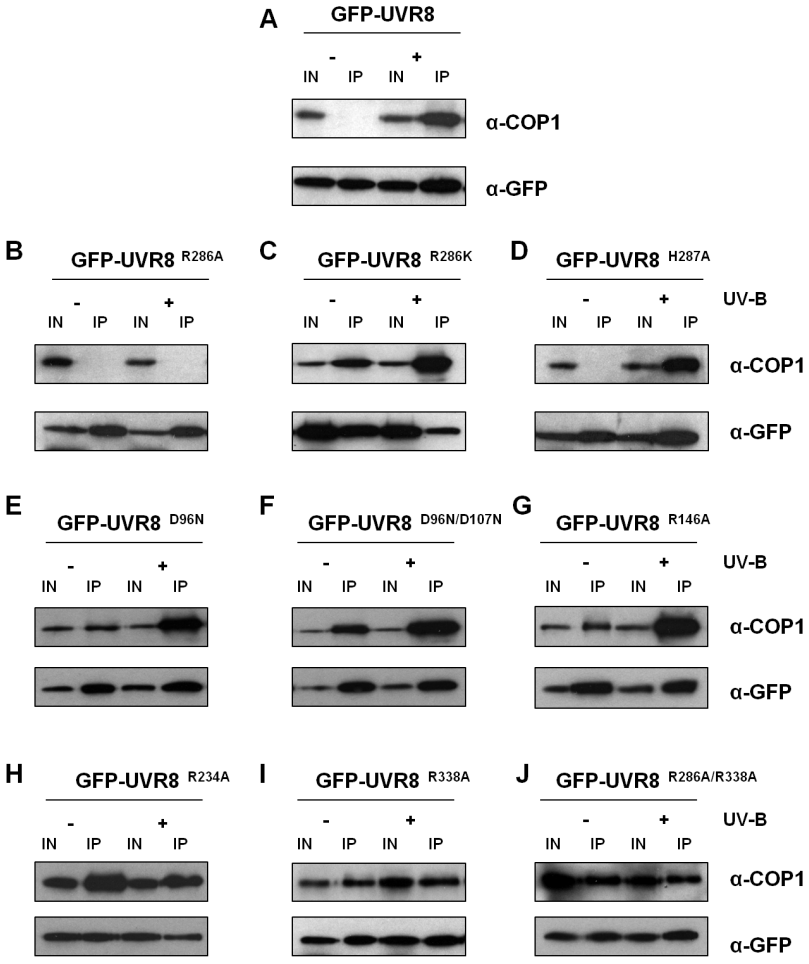

FIGURE 4-4: Effect of salt bridge mutations on UVR8 and COP1 interaction in Arabidopsis. Co-immunoprecipitation of GFP-UVR8 and COP1 in whole plant cell extracts obtained from *uvr8-1* plants transformed with GFP-UVR8 or a GFP-UVR8 salt bridge mutant form exposed (+) or not (-) to 3 µmol m^{-2} s^{-1} of narrowband UV-B for 3 h. Co-immunoprecipitation assays were performed under the same conditions. Input samples (15 µg, IN) and eluates (IP) were loaded on a SDS-PAGE gel, and the immunoblot was probed with anti-COP1 and anti-GFP antibodies. The following transgenic lines were used for the assay: **(A)** GFP-UVR8 6-2, **(B)** GFP-UVR8^{R286A} 6-8, **(C)** GFP-UVR8^{R286K} 2-3, **(D)** GFP-UVR8^{H287A} 2-2 , **(E)** GFP-UVR8^{D96N} 13-3, **(F)** GFP-UVR8$^{D96N/D107N}$ 5-2, **(G)** GFP-UVR8^{R146A} 9, **(H)** GFP-UVR8^{R234A} 16-5, **(I)** GFP-UVR8^{R338A} 9-3 and **(J)** GFP-UVR8$^{R286A/R338A}$ 20-2. The data is representative of at least two repeats for each mutation.

To conclude, the yeast two-hybrid assay and the co-immunoprecipitation assay using Arabidopsis whole cell extract are two valuable and informative tools to investigate the UVR8-COP1 interaction. Four different interaction patterns between mutant forms of GFP-UVR8 and COP1 were identified: behaviour like wild-type, a complete loss of the interaction, constitutive interaction or constitutive interaction followed by an increase of the interaction after UV-B treatment. An interpretation of these results will be provided in the Discussion in combination with the functional studies of the mutants, as well as possible explanations for the observed discrepancies between the yeast and plant system.

4.5 The positive charge of R286 is essential for UVR8 function

The findings of Kliebenstein et al. (2002) and Brown et al. (2005) that Arabidopsis *uvr8* mutant plants are hypersensitive to UV-B and deficient in the induction of *HY5* and *CHS* gene expression in response to UV-B provided the basics for establishing a complementation assay to test the functionality of UVR8 mutants (Kaiserli and Jenkins 2007). Therefore, RT-PCR analysis of the induction of *HY5* and *CHS* gene expression in response to UV-B of three independent homozygous transgenic lines expressing a GFP-UVR8 mutant form in the *uvr8-1* background was carried out. Figure 4-5 A shows that there is an increase in *HY5* and *CHS* mRNA but not in control *ACTIN2* transcript levels when wild-type plants are exposed for 4 h to 3 μmol m^{-2} s^{-1} broadband UV-B. In contrast, *uvr8-1* mutant plants show no induction of *HY5* or *CHS* gene expression in response to UV-B and therefore serve as a negative control. Expression of GFP-UVR8^{R286A} in the *uvr8-1* background is not able to restore *HY5* and *CHS* gene expression after UV-B treatment even if there is some basal *HY5* expression visible under both light conditions. If the positive charge at position 286 is conserved by replacing the arginine by lysine, a functional mutant is created showing similar *HY5* and *CHS* expression levels after UV-B treatment like wild-type.

To extend the analysis from transcript levels to protein accumulation, a plant cell extract of five day old seedlings expressing GFP-UVR8 with the respective mutations as well as control plants were tested for CHS protein accumulation. Plants were grown in 1.5 μmol m^{-2} s^{-1} white light to avoid CHS induction by high white light and treated plants were additionally supplemented with 1.5 μmol m^{-2} s^{-1} narrowband UV-B. In accordance to UV-B induced accumulation of *CHS* transcript levels in wild-type and GFP-UVR8^{R286K} plants, accumulation of CHS protein can be detected in an immunoblot of respective plant cell extract probed with anti-CHS antibody (Fig 4-5 B). Seedlings expressing GFP-

UVR8^{R286A} showed a very weak induction of CHS protein compared to wild-type, which was also detectable in the *uvr8-1* mutant even if slightly lower.

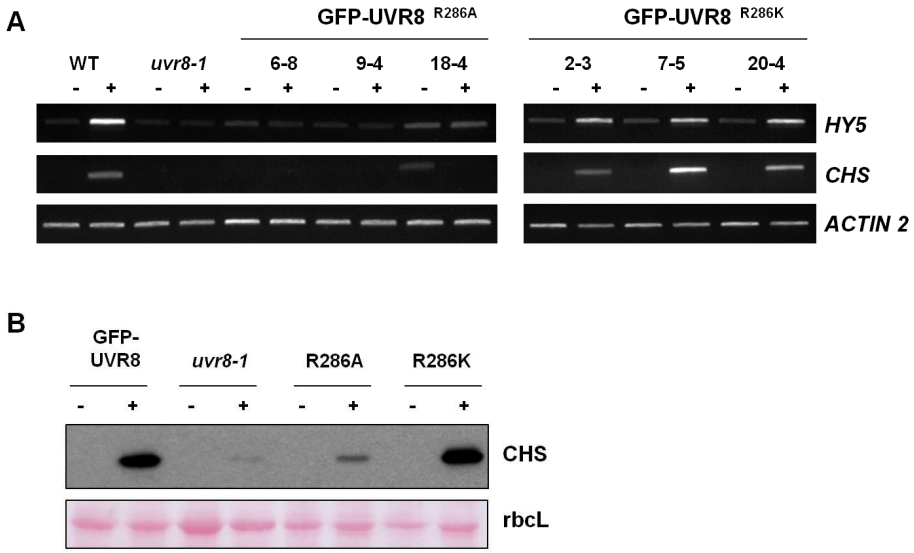

FIGURE 4-5: The positive charge of R286 is essential for UVR8 function.
(A) RT-PCR assays of *HY5*, *CHS* and control *ACTIN2* transcripts in L*er*, *uvr8-1*, *uvr8-1*/*35S*pro:GFP-UVR8^{R286A} (lines 6-8, 9-4, and 18-4) and *uvr8-1*/*35S*pro:GFP-UVR8^{R286K} (lines 2-3, 7-5, and 20-4) plants grown under 20 μmol m^{-2} s−1 white light (−) and exposed to 3 μmol m^{-2} s^{-1} broadband UV-B for 4 h (+). **(B)** Immunoblot of plant cell extract of 5 d old *uvr8-1*/*UVR8*pro:GFP-UVR8, *uvr8-1*/*35S*pro:GFP-UVR8^{R286A} (line 18-4), *uvr8-1*/*35S*pro:GFP-UVR8^{R286K} (line 2-3) and *uvr8-1* plants grown in 1.5 μmol m^{-2} s^{-1} white light (−) supplemented with 1.5 μmol m^{-2} s^{-1} narrowband UV-B (+) probed with anti-CHS antibody. Ponceau S staining of Rubisco large subunit (rbcL) is shown as a loading control.

Another way of assessing functionality of UVR8 mutants is by testing their morphological response to UV-B. Although details of the effects of UV-B on morphogenesis remain elusive, some of the genes regulated by UVR8 seem to be involved in morphogenesis, since the *uvr8* mutant is altered in the UV-B induced suppression of hypocotyl extension (Favory et al., 2009) and regulation of leaf expansion (Wargent et al., 2009). The UV-B induced suppression of hypocotyl extension was measured using seedlings of various genotypes grown under 1.5 μmol m^{-2} s^{-1} white light alone or supplemented with 1.5 μmol m^{-2} s^{-1} narrowband UV-B for four days. *uvr8-1* mutant plants expressing GFP-UVR8^{R286K} exhibit hypocotyl suppression under UV-B, similar to wild-type, whereas those expressing GFP-UVR8^{R286A} have similar hypocotyl lengths to *uvr8-1* (Fig 4-6), demonstrating that the positive charge of R286 is essential to mediate the UV-B induced response. Hypocotyl growth suppression by UV-B is mediated by HY5/HYH as seen in the long hypocotyl of the *hy5/hyh* mutant under UV-B. Therefore the lack of response in *uvr8-1* plants and in *uvr8-1* plants expressing GFP-UVR8^{R286A} ties in with the RT-PCR results shown in Fig 4-5 A where a lack of *HY5* gene induction is observed.

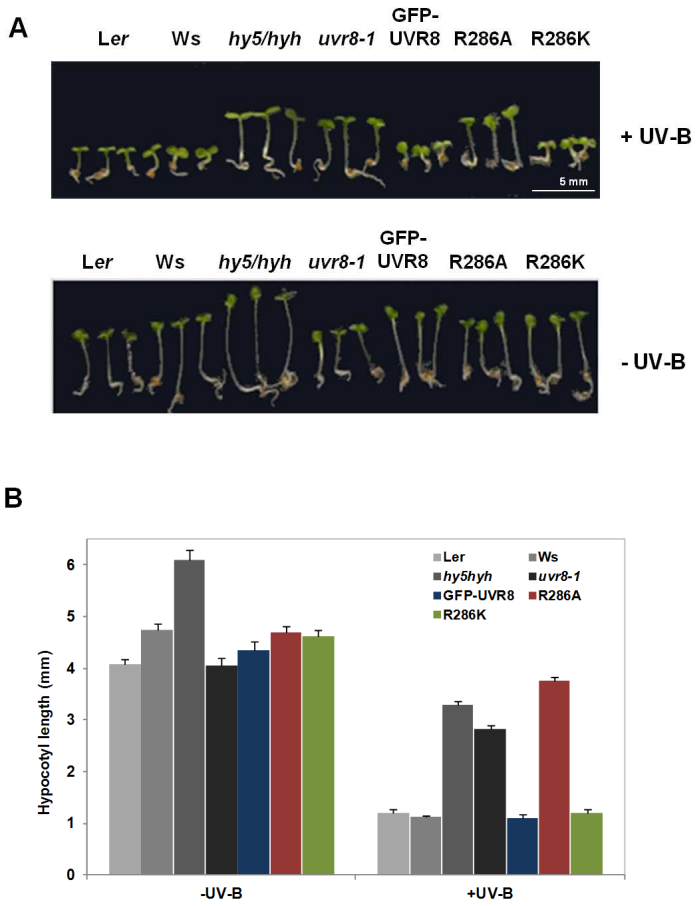

FIGURE 4-6: Plants expressing GFP-UVR8^{R286K} show UV-B induced suppression of hypocotyl extension. (A) Four day-old wild-type L*er*, wild-type W*s*, *hy5-ks50 hyh* (W*s* background) , *uvr8-1*, *uvr8-1*/*UVR8*pro:GFP-UVR8, *uvr8-1*/*35S*pro:GFP-UVR8^{R286A} (line 9-4), and *uvr8-1*/*35S*pro:GFP-UVR8^{R286K} (line 2-3) plants grown in 1.5 µmol m^{-2} s^{-1} white light (-UV-B) supplemented with 1.5 µmol m^{-2} s^{-1} narrowband UV-B (+UV-B). **(B)** Hypocotyl lengths (±SE, n = 10) of plants shown in (A). Data are representative of three independent experiments.

4.6 The monomeric mutant GFP-UVR8$^{D96N/D107N}$ is functional in Arabidopsis

By applying the three above described methods to determine the functionality of UVR8 mutants, a number of mutations introduced in Chapter 3 were now investigated in respect to their function. RT-PCR analysis of *uvr8-1* plants expressing either the single mutant GFP-UVR8^{D96N} or the double mutant GFP-UVR8$^{D96N/D107N}$ show a UV-B induced induction of *HY5* and *CHS* transcripts similar to wild-type plants (Fig 4-7 A). In accordance, CHS protein accumulation can also be observed in the two transgenic lines whereas it is absent in the *hy5/hyh* mutant (Fig 4-7 B).

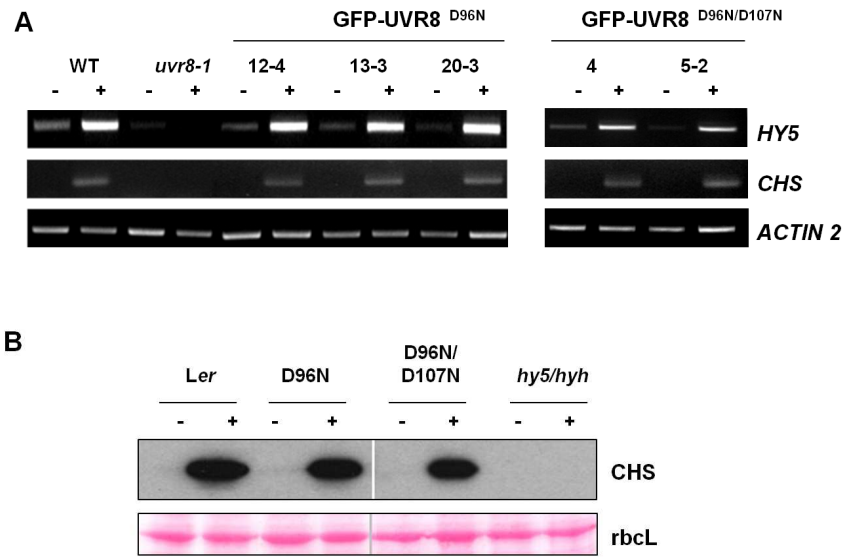

FIGURE 4-7: The monomeric mutant GFP-UVR8$^{D96N/D107N}$ is functional in plants.
(A) RT-PCR assays of *HY5*, *CHS* and control *ACTIN2* transcripts in L*er*, *uvr8-1*, *uvr8-1*/*35S*pro:GFP-UVR8^{D96N} (lines 12-4, 13-3, and 20-3) and *uvr8-1*/*35S*pro:GFP-UVR8$^{D96N/D107N}$ (lines 4, and 5-2) plants grown under 20 µmol m^{-2} s−1 white light (−) and exposed to 3 µmol m^{-2} s^{-1} broadband UV-B for 4 h (+). **(B)** Immunoblot of plant cell extract of 4 d old wild-type L*er*, *uvr8-1*/*35S*pro:GFP-UVR8^{D96N} (line 12), *uvr8-1*/*35S*pro:GFP-UVR8$^{D96N/D107N}$ (line 5) and *hy5/hyh* plants grown in1.5 µmol m^{-2} s−1 white light (−) supplemented with 1.5 µmol m^{-2} s^{-1} narrowband UV-B (+) probed with anti-CHS antibody. Ponceau S staining of Rubisco large subunit (rbcL) is shown as a loading control.

Furthermore, the gene expression data is supported by the morphological characterisation of GFP-UVR8^{D96N} and GFP-UVR8$^{D96N/D107N}$ since both mutations do not impair the UV-B induced suppression of hypocotyl extension resulting in wild-type like growth under UV-B (Fig. 4-8). As will be discussed later, the double mutant UVR8$^{D96N/D107N}$ is consistently seen as a constitutive monomer in various assays in vitro and in vivo (see Chapter 3) but still retains its function in inducing gene expression leading to UV-B protection of the plant.

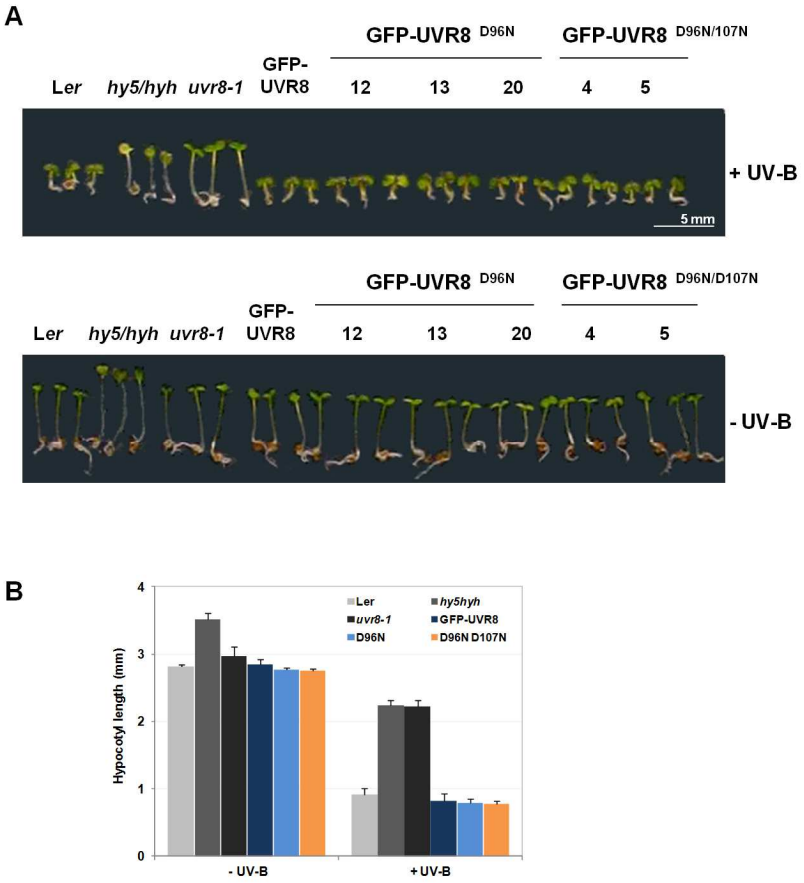

FIGURE 4-8: Plants expressing GFP-UVR8^{D96N} or GFP-UVR8$^{D96N/D107N}$ show UV-B induced suppression of hypocotyl extension. (A) Four day-old wild-type L*er*, *hy5-ks50 hyh* (W*s* background) , *uvr8-1*, *uvr8-1*/*UVR8*pro:GFP-UVR8, *uvr8-1*/*35S*pro:GFP-UVR8^{D96N} (T2 lines 12, 13 and 20), and *uvr8-1*/*35S*pro:GFP-UVR8$^{D96N/D107N}$ (T2 lines 4 and 5) plants grown in 1.5 µmol m^{-2} s^{-1} white light (−UV-B) supplemented with 1.5 µmol m^{-2} s^{-1} narrowband UV-B (+UV-B). **(B)** Hypocotyl lengths (± SE, n = 10) of plants shown in (A). Mean values of the three or two T2 lines *uvr8-1*/*35S*pro:GFP-UVR8^{D96N} and *uvr8-1*/*35S*pro:GFP-UVR8 $^{D96N/D107N}$ respectively are shown. Data are representative of three independent experiments.

4.7 Influence of various mutations on functionality of GFP-UVR8 in Arabidopsis

Apart from mutations affecting the salt bridge formed through R286, the importance of other salt bridges for UVR8 functionality was tested. The GFP-UVR8^{R146A} mutant, where formation of the second double hydrogen bonded cross-dimer salt bridge is prevented shows no impairment in function (Fig 4-9). UV-B induction of *HY5* and *CHS* transcripts similar to wild-type plants is observed as well as UV-B induced suppression of hypocotyl extension.

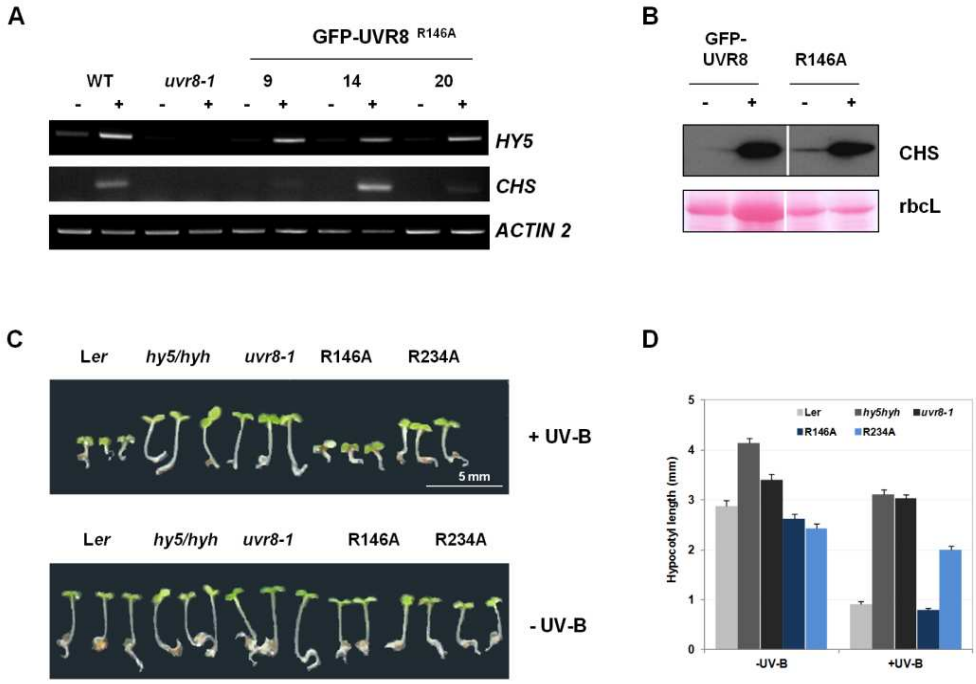

FIGURE 4-9: Mutation of R234 neighbouring the tryptophan pyramid has more severe effects on functionality then mutation of R146 forming a cross-dimer salt bridge. (A) RT-PCR assays of *HY5*, *CHS* and control *ACTIN2* transcripts in L*er*, *uvr8-1* and *uvr8-1*/*35S*pro:GFP-UVR8^{R146A} (T2 lines 9, 14 and 20) plants grown under 20 µmol m^{-2} s−1 white light (−) and exposed to 3 µmol m^{-2} s^{-1} broadband UV-B for 4 h (+). **(B)** Immunoblot of plant cell extract of 5 day old *uvr8-1*/*UVR8*pro:GFP-UVR8 and *uvr8-1*/*35S*pro:GFP-UVR8^{R146A} (line 14) grown under 20 µmol m^{-2} s^{-1} white light (−) and exposed to 3 µmol m^{-2} s^{-1} narrowband UV-B for 4 h (+) probed with anti CHS antibody. Ponceau S staining of Rubisco large subunit (rbcL) is shown as a loading control. **(C)** Four day old wild-type L*er*, *hy5/hyh*, *uvr8-1*, *uvr8-1*/*35S*pro:GFP-UVR8^{R146A} (line 14) and *uvr8-1*/*35S*pro:GFP-UVR8^{R234A} (line 16-5) plants grown in1.5 µmol m^{-2} s^{-1} white light (−UV-B) supplemented with 1.5 µmol m^{-2} s^{-1} narrowband UV-B (+UV-B). **(D)** Hypocotyl lengths (± SE, n = 10) of plants shown in (C). Data are representative of three independent experiments.

Mutation of the two arginines in each of the two remaining GWRHT motifs, R234 and R338, to alanine has severe effects on function. GFP-UVR8^{R338A} is unable to complement the *uvr8-1* phenotype in the morphological UV-B response and the UV-B induced induction of *HY5* and *CHS* transcripts is also absent (Fig 4-10). Therefore, no UV-B induced accumulation of CHS protein can be detected either (Fig 4-10 B). The double mutant GFP-UVR8$^{R286A/R338A}$ was only tested for UV-B induced CHS protein accumulation since the results of the two single mutants already suggested that the mutation would lead to a loss of function phenotype. As expected from the phenotypes of the single mutants, CHS protein accumulation was not induced after UV-B treatment of GFP-UVR8$^{R286A/R338A}$ plants (Fig 4-10 B).

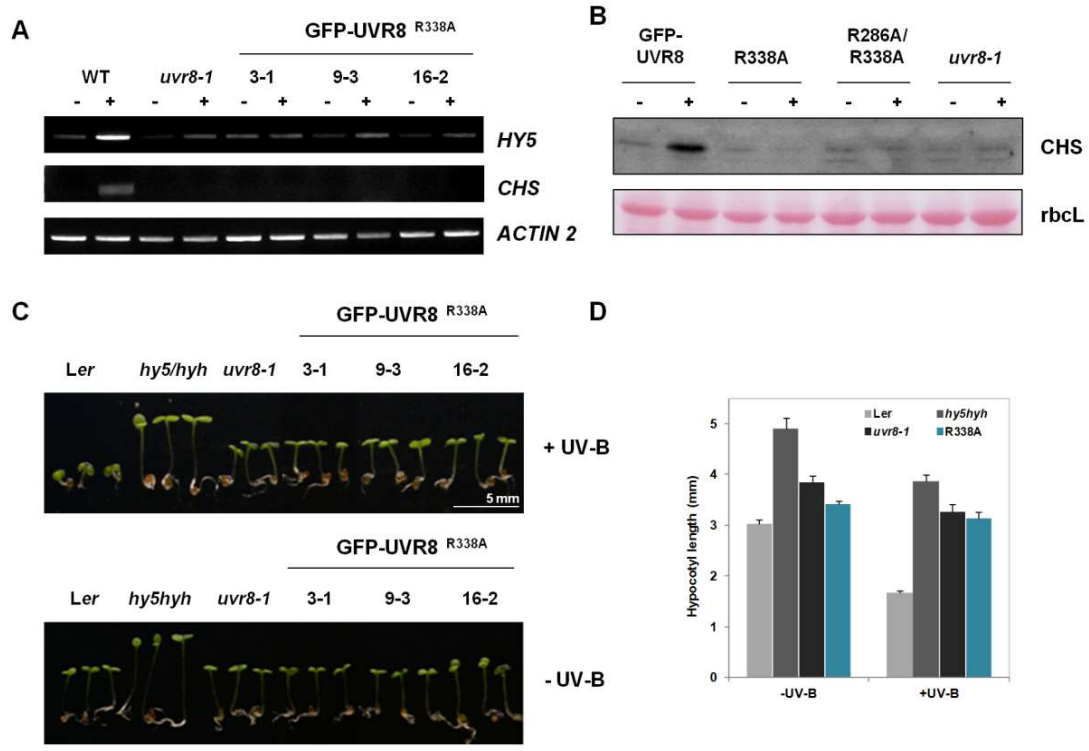

FIGURE 4-10: The monomeric mutant GFP-UVR8^{R338A} is non-functional in plants.
(A) RT-PCR assays of *HY5*, *CHS* and control *ACTIN2* transcripts in L*er*, *uvr8-1*, *uvr8-1*/*35S*pro:GFP-UVR8^{R338A} (lines 3-1, 9-3, and 16-2) plants grown under 20 µmol m^{-2} s^{-1} white light (−) and exposed to 3 µmol m^{-2} s^{-1} broadband UV-B for 4 h (+). **(B)** Immunoblot of plant cell extract of 10 day old *uvr8-1*/*UVR8*pro:GFP-UVR8, *uvr8-1*/*35S*pro:GFP-UVR8^{R338A} (line 3-1), *uvr8-1*/*35S*pro:GFP-UVR8$^{R286A\ /R338A}$ (line 1-1) and *uvr8-1* plants grown under 20 µmol m^{-2} s^{-1} white light (−) and exposed to 3 µmol m^{-2} s^{-1} narrowband UV-B for 4 h (+) probed with anti-CHS antibody. Ponceau S staining of Rubisco large subunit (rbcL) is shown as a loading control. **(C)** Four day old wild-type L*er*, *hy5-ks50 hyh* (W*s* background), *uvr8-1* and *uvr8-1*/*35S*pro:GFP-UVR8^{R338A} (lines 3-1, 9-3, and 16-2) plants grown in 1.5 µmol m^{-2} s^{-1} white light (−UV-B) supplemented with 1.5 µmol m^{-2} s^{-1} narrowband UV-B (+UV-B). **(D)** Hypocotyl lengths (± SE, n = 10) of plants shown in **(C)**. Mean value of the three *uvr8-1*/*35S*pro:GFP-UVR8^{R338A} lines is shown. Data are representative of three independent experiments.

Another mutant that is unable to complement the *uvr8-1* phenotype is GFP-UVR8^{R234A}. Disruption of the intermolecular salt bridge formed adjacent to the tryptophan pyramid has more severe effects on functionality than, for example, mutation of R146 which forms a cross-dimer salt bridge. However, functionality of this mutant was only tested via the hypocotyl extension assay. GFP-UVR8^{R234A} consistently shows a much longer hypocotyl than wild-type plants under UV-B; however it seems as if there is some partial activity of hypocotyl growth suppression left since the length of the *uvr8-1* mutant is not quite reached (Fig 4-9 B and C). This observation however is preliminary and needs much further investigation, especially by applying qPCR analysis to detect if a reduced response is present.

Finally, one mutation concerning the histidine ring was also tested for function in plants. GFP-UVR8^{H287A} shows no impairment in function as shown by UV-B induced induction of *HY5* and *CHS* transcripts similar to wild-type plants as well as the UV-B induced suppression of hypocotyl extension (Fig 4-11).

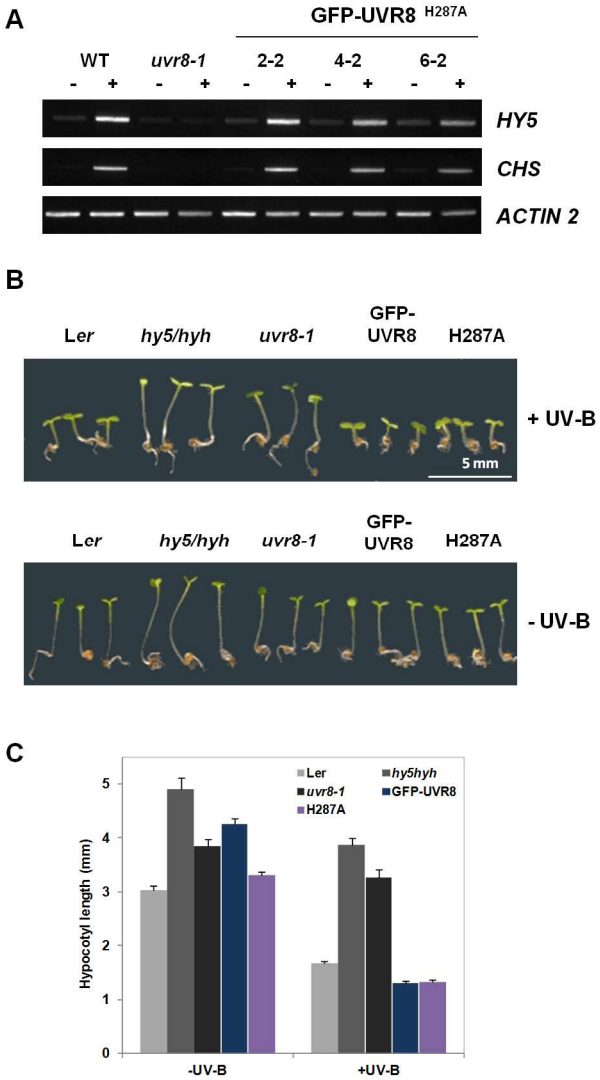

FIGURE 4-11: Mutation of H287 has no effect on UVR8 functionality. (A) RT-PCR assays of *HY5*, *CHS* and control *ACTIN2* transcripts in L*er*, *uvr8-1* and *uvr8-1*/*35S*pro:GFP-UVR8^{H287A} (lines 2-2, 4-2, and 6-2) plants grown under 20 µmol m^{-2} s^{-1} white light (−) and ex-posed to 3 µmol m^{-2} s^{-1} broadband UV-B for 4 h (+). **(B)** Four day old wild-type L*er*, *hy5-ks50 hyh*, *uvr8-1*, *uvr8-1*/*UVR8*pro:GFP-UVR8 and *uvr8-1*/*35S*pro:GFP-UVR8^{H287A} (line 2-2) plants grown in 1.5 µmol m^{-2} s^{-1} white light (−UV-B) supplemented with 1.5 µmol m^{-2} s^{-1} narrowband UV-B (+UV-B). **(C)** Hypocotyl lengths (± SE, n = 10) of plants shown in (B). Data is representative of three independent experiments.

4.8 Limited proteolysis of purified UVR8 shows UV-B induced conformational changes

To be able to test the effect of a mutation on UVR8 function beyond just monomerisation, a transgenic line expressing the mutant form must be generated as described extensively in the present chapter. The generation of transgenic lines is a lengthy and tedious process and an in vitro method to test the functionality of a recombinantly expressed UVR8 mutant would therefore be advantageous. The above described results lead to the hypothesis that UV-B does not only induce monomerisation of UVR8 but also induces further

conformational changes within the monomer necessary for function. This ties in with in-gel illumination assays of UVR8 where UV-B exposure causes UVR8 to become accessible to antibodies that specifically recognise a C-terminal peptide (Rizzini et al., 2011).

This hypothesis was tested by carrying out a proteolysis experiment with the purified protein and trypsin, since limited proteolysis experiments have been used successfully to probe conformational features of a protein (Cui and Somerville, 1993; Fontana et al., 1997). Proteolysis of a protein substrate can only occur if the polypeptide chain can bind and adapt to the specific stereochemistry of the protease's active site (Fontana et al., 2004). Therefore, the native rigid structure of a globular protein generally cannot act as substrate for a protease, as shown by the fact that folded proteins under physiological conditions are rather resistant to proteolysis. Trypsin cleaves peptide chains mainly at the carboxyl side of lysine or arginine, except when either is followed by a proline. In total, 35 theoretical trypsin cleavage sites are present in the UVR8 protein. A treatment of the protein with trypsin results only in the loss of the approximately last 45 amino acids of the C-terminus, whereas the protein core remains resistant to proteolysis (Christie et al., 2012; Wu et al., 2012). Hence, limited proteolysis occurs preferentially at those loops which display inherent conformational flexibility and are therefore accessible to the protease. Cleavage of the C-terminus suggests that parts of it are flexible which allows to hypothesize that a change in its conformation might play a role in UVR8 signalling.

Purified wild-type UVR8 exposed for 1 h to 1.5 μmol m^{-2} s^{-1} narrowband UV-B or kept unexposed was treated with trypsin for 5 or 30 minutes before samples were taken and separated by SDS-PAGE. Coomassie staining of the protein bands reveals a different pattern of peptides when comparing UV-B treated and untreated wild-type protein (Fig 4-12 A). The most prominent difference can be observed after five minutes incubation with trypsin where only two or possibly three products are formed in the dark state but six products are distinguishable in the UV-B exposed state. The smallest product formed in the UV-B exposed sample is also smaller than the one in the dark control. These observations suggest that changes in chain flexibility, i.e. conformational changes must be induced by UV-B to allow differing cleavage by the protease. These conformational changes most likely involve the C-terminus since the UVR8 core is fairly resistant to proteolysis (Christie et al., 2012).

Subsequently, various mutants were analysed by this method. The four dimeric mutants $UVR8^{D96N}$, $UVR8^{D107N}$, $UVR8^{R286K}$ and $UVR8^{R146A}$ show quite similar proteolysis products with and without UV-B treatment as seen for wild-type UVR8 (Fig 4-12 B). This

is consistent with the findings in plants, where these mutants showed no impairment in function (no information is available for UVR8^{D107N} since no transgenic line was generated for this mutation).

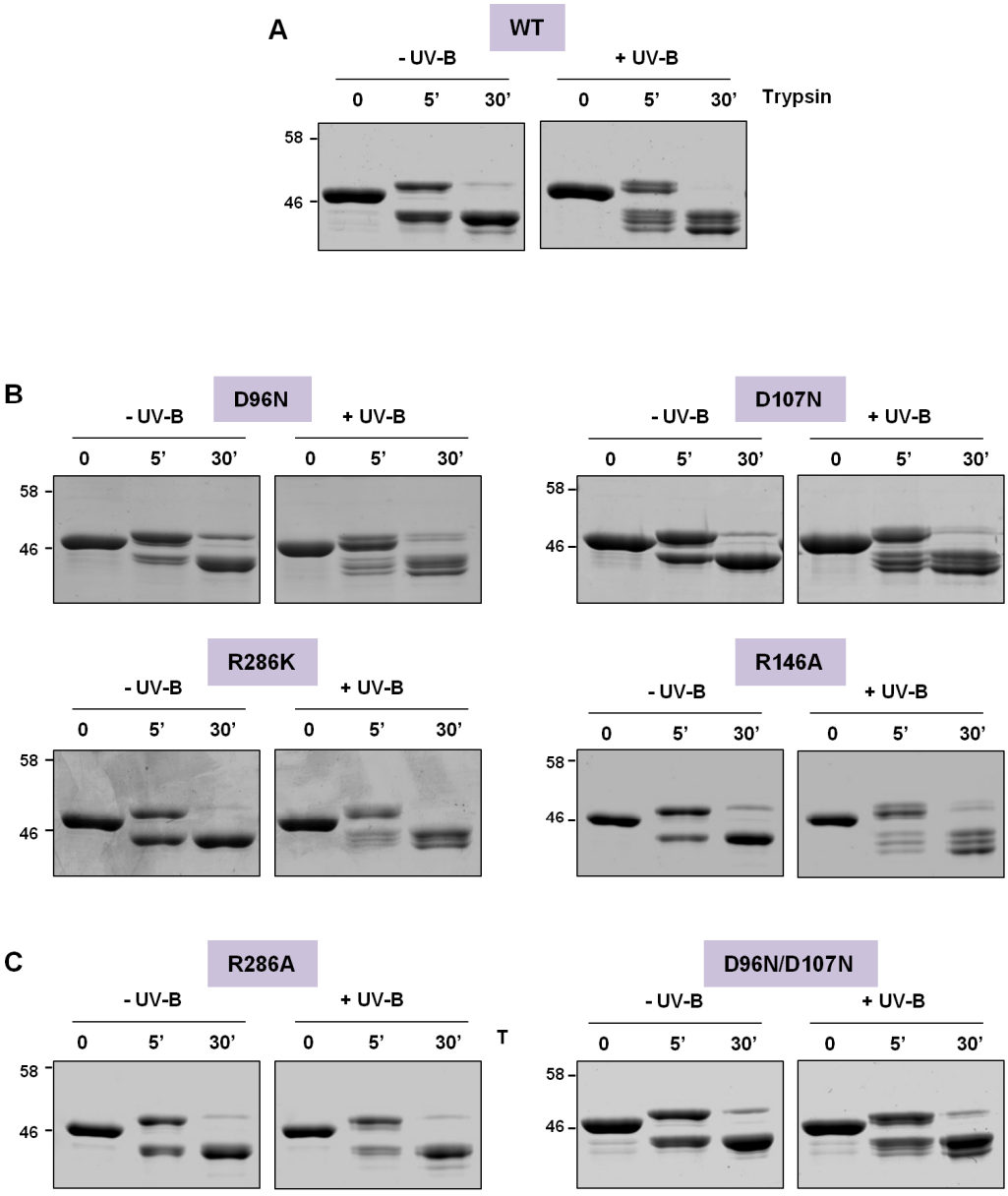

FIGURE 4-12: Limited proteolysis of purified UVR8 protein with trypsin reveals conformational changes after UV-B exposure. (A) Wild-type UVR8 protein exposed (+) or not (-) to 1.5 µmol m^{-2} s^{-1} narrowband UV-B for 1 h before digestion with trypsin (0) and after 5 and 30 min incubation with trypsin. Products were separated on 10% SDS-PAGE gels and stained with Coomassie Blue. **(B)** Trypsin treatment as described in (A) of dimeric mutants UVR8^{D96N}, UVR8^{D107N}, UVR8^{R286K} and UVR8^{R146A}. **(C)** Trypsin treatment as described in (A) of monomeric mutants UVR8^{R286A} and UVR8$^{D96N/D107N}$. Data in A and C is representative of at least three independent experiments. Data in B is representative of two independent expreiments.

Limited proteolysis of the two constitutively monomeric mutants UVR8^{R286A} and UVR8$^{D96N/D107N}$ only partially resembles the findings for wild-type (Fig 4-12 C). Whereas the proteolysis products of both mutants unexposed to UV-B match the wild-type pattern,

accessibility of cleavage sites seems to be different in the UVR8^{R286A} mutant after exposure to UV-B since two of the lower bands detected in wild-type are absent. The proteolysis banding profile of the UVR8$^{D96N/D107N}$ mutant matches the wild-type in regard of presence of all bands, however the major product after 30 min incubation with trypsin seems to be the one with the highest molecular weight, whereas in wild-type and in the other dimeric mutants the three end products are present in more or less equal amounts. In plants, mutation of R286 to alanine leads to a non-functional form of GFP-UVR8 whereas GFP-UVR8$^{D96N/D107N}$ is able to complement the *uvr8-1* phenotype. For these two mutants, the similarities of the observed banding pattern do not correlate with function of the protein as shown for the mutants in Fig 4-12 B.

Limited trypsin proteolysis was also undertaken with UVR8^{R338A}, UVR8^{R234A} and UVR8$^{R146A/R286A}$ as shown in Fig 4-13. The proteolysis pattern is unaffected by exposure of the proteins to UV-B indicating absence of conformational changes induced by UV-B. This corresponds with the data obtained from plants where at least GFP-UVR8^{R338A} and GFP-UVR8^{R234A} were impaired in their functionality (Fig 4-9 and 4-10). Only preliminary experiments were undertaken with GFP-UVR8$^{R146A/R286A}$ mutant lines, which nevertheless suggest inability of the mutant to complement the *uvr8-1* phenotype.

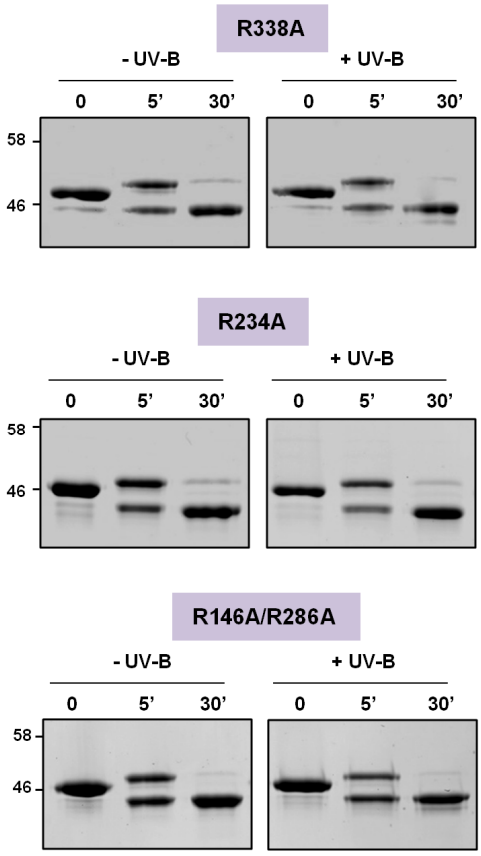

FIGURE 4-13: Limited proteolysis of non-functional monomeric mutant UVR8 proteins shows no conformational change after UV-B exposure.
UVR8^{R338A}, UVR8^{R234A} and UVR8$^{R146A/R286A}$ protein exposed (+) or not (-) to 1.5 µmol m^{-2} s^{-1} narrowband UV-B for 1 h before digestion with trypsin (0) and after 5 and 30 min incubation with trypsin. Products were separated on 10% SDS-PAGE gels and stained with Coomassie Blue. Data is representative of two independent experiments.

Limited proteolysis was also undertaken with chymotrypsin. However, a quite similar digestion pattern to that seen with trypsin was observed since trypsin and chymotrypsin cleavage sites in the C-terminus occur rather close to each other. Theoretical cleavage sites of other proteases were also investigated but seemed unsuitable for such an approach.

In summary, the different observed proteolysis patterns support the idea of UV-B induced conformational changes leading to flexible or unstructured chain regions in vitro. Those mutants showing a proteolysis banding pattern similar to wild-type are functional in plants, but mutants showing banding patterns unaffected by UV-B exposure of the proteins are non-functional.

4.9 Discussion

4.9.1 Constitutive monomerisation and COP1 interaction is not sufficient for a UVR8 mediated response

To be able to understand how UV-B mediated signalling by UVR8 and thus UV-B protection is achieved it is necessary to understand the structure of the photoreceptor and also structural requirements for e.g. interactions with other proteins. Therefore, this chapter focused on the functional analysis of the UVR8 mutants, whose structures were characterised in the previous chapter.

The current model (Heijde and Ulm, 2012) proposes that UV-B induces monomerisation of UVR8 which then allows COP1 binding to initiate signalling. The yeast two-hybrid assay with the two monomeric mutants UVR8^{R286A} and UVR8^{R338A} showing constitutive interaction with COP1 and the dimeric mutant UVR8^{R286K} requiring UV-B for monomerisation to allow COP1 interaction, seems to support this model. The model then already becomes challenged by the observed discrepancies between the yeast and the plant system. GFP-UVR8^{R286A} is constitutively monomeric in plants, however rather surprisingly it is unable to interact with COP1 in plants. Furthermore, the dimeric mutant GFP-UVR8^{R286K} shows constitutive interaction with COP1 followed by an apparent increase of the interaction after UV-B treatment. A plausible explanation for this behaviour is that UVR8^{R286K} is indeed able to dimerize but the dimer is destabilized and weakened compared to the wild-type dimer as seen by semi-native SDS-PAGE analysis. The conformation of the destabilized dimer seems to be affected in such way that the COP1 binding region becomes exposed thus allowing COP1 binding in darkness. This assumption is strengthened by the COP1 interaction pattern of the GFP-UVR8^{H287A} mutant, being the only mutant to display wild-type like behaviour (Fig 4-4 D). GFP-

UVR8^{H287A} is the only mutant generated in this study that can be detected as a dimer under semi-native SDS-PAGE conditions, thus forming a tight wild-type like dimer that prevents interaction between UVR8 and COP1 in the dark.

It has been established now that UVR8 and COP1 interaction takes place via a stretch of 27 amino acids of the UVR8 C-terminus and the WD40 domain of COP1 (Cloix et al., 2012). The hypothesis that the conformation of the C-terminus is influenced if a destabilized UVR8 dimer is formed is supported by the size exclusion chromatography results shown in Chapter 3. The destabilized dimers UVR8^{R286K} and UVR8^{R146A} show interaction with COP1 in the dark (Fig. 4-4 C and G) and both elute earlier from the SEC column than the wild-type dimer, suggesting a somehow inflated shape which can be reduced by a treatment with trypsin that leads to cleavage of the C-terminus. Interaction between these mutants and COP1 in the absence of UV-B therefore seems justifiable and can be regarded almost as an artefact, only appearing due to an altered conformation of the C-terminus but independent of UV-B. However, none of the experimental data generated so far is sufficient to define the position of the C-terminus in these mutants more precisely. The only information so far available on the position of the C-terminus derives from molecular envelope data generated from small angle X-ray scattering (SAXS) on the full length protein (Christie et al., 2012). Those data match the information generated by crystallography regarding the dimer assembly and diameter and locate the missing C-terminus at the distal ends of the dimer. Further experiments are required to understand how mutation of the dimeric interface can thus lead to changes in the C-terminus if the SAXS data, which suggest no direct contact between the interface and the C-termini, proves to be correct.

Moving on to the next step in the proposed model now, namely that the interaction between UVR8 and COP1 is essential to initiate UV-B mediated signalling one has to assume constitutive signalling if constitutive interaction is observed. However, this is not the case, as observed for example with the GFP-UVR8^{R286K} or GFP-UVR8^{R146A} mutants. Exposure of the plants to UV-B is still required to induce *HY5* and *CHS* gene expression (Fig 4-5 A and 4-9 A) even though there is interaction with COP1 in the absence of UV-B (Fig 4-4 C and G). However, functional UVR8 mediated signalling does coincide with a change in the apparent strength of interaction between UVR8 mutants and COP1. Compared to non-UV-B conditions, elevated levels of COP1 are detected in the eluates of the co-immunoprecipitation assays after UV-B exposure for all the functional mutants (Fig 4-4 C, E, F and G). Constitutive interaction also takes place between COP1 and the two monomeric mutants GFP-UVR8^{R338A} and GFP-UVR8$^{R286A/R338A}$ but, as with the other

mutants, interaction in the absence of UV-B does not lead to an induction of *HY5* and *CHS* gene expression or a photomorphological phenotype. Further examination of the GFP-UVR8^{R338A} and GFP-UVR8$^{R286A/R338A}$ mutants nevertheless shows that both mutations lead to non-functional forms of UVR8, which is also visible in the co-immunoprecipitation assay where the detected amount of COP1 is similar with and without exposure of the plant to UV-B.

In summary, the functional analysis of the salt bridge mutants in combination with the structural data allows to extend the proposed model of UVR8 function in UV-B photoreception. UV-B does not only induce monomerisation of the photoreceptor but also seems to initiate a conformational change in the protein that is essential for function. Therefore, neither constitutive monomerisation nor constitutive interaction with COP1 is sufficient to initiate a UVR8 mediated response in the absence of UV-B.

4.9.2 Dimerisation is not required for UVR8-mediated signalling

The identification of several constitutively monomeric mutants allowed to test whether dark state dimerisation is required for UV-B photoreception and subsequent UVR8-mediated signalling, which is a further part of the proposed model. The analysis of the exciton coupling phenomena in Chapter 3 has shown that dimerisation maximises the extent of exciton coupling but is not a requirement for it to occur. In respect to function, the monomeric mutant GFP-UVR8$^{D96N/D107N}$, showing relatively little exciton coupling (Fig 3-8 A), is able to complement the *uvr8-1* phenotype (Fig 4-7 A). The GFP-UVR8$^{D96N/D107N}$ monomer is able to interact constitutively with COP1, although an increase in the interaction is observed after UV-B exposure, as described for the destabilized dimer mutants (Fig 4-4 F). The GFP-UVR8$^{D96N/D107N}$ mutant shows that a UVR8 monomer is able to sense UV-B and to induce the proposed conformational changes required for UVR8 to initiate signalling, since GFP-UVR8$^{D96N/D107N}$ becomes active only after exposure to UV-B (Fig 4-7 A). The UV-B induced conformational changes are evident through the limited proteolysis of purified UVR8$^{D96N/D107N}$, in that this mutant shows a changed proteolysis pattern after UV-B exposure more similar to that observed for wild-type UVR8 than for the non-functional mutants (compare Fig 4-12 C to Fig 4-13). In this case, the in vitro data nicely link up with the observations on functionality made in plants.

The observation that none of the other monomeric arginine mutants are functional is most likely due to the fact that the mutation has impaired the UV-B sensing mechanism and not because the mutants are monomeric. By replacing the two aspartates by two asparagines

very little structural disturbance should take place because of the close similarity of the two amino acids. Additionally, and maybe even more important, the mutation has apparently not perturbed the tryptophan-arginine arrangement of the monomer, allowing UV-B perception and subsequent signalling. The much more disruptive mutation of arginine to alanine, for example in UVR8^{R338A}, leads to a protein that cannot perceive UV-B, since limited proteolysis does not reveal any conformational changes which would be necessary for UVR8 mediated signalling to induce *HY5* and *CHS* gene expression.

The results that are most difficult to interpret are those of the monomeric mutant UVR8^{R286A}. The limited proteolysis suggests that the protein has not fully lost its ability to perceive UV-B and some sort of conformational change still takes place (Fig 4-12 C). The inability of GFP-UVR8^{R286A} to complement the *uvr8-1* phenotype is due to the inability of the mutant to interact with COP1 (Fig 4-4 B). However, none of the experimental data generated so far suggests why the mutant is impaired in COP1 binding, also taking into consideration that the mutant can bind COP1 in the yeast two-hybrid system. For a better understanding of this behaviour, more detailed information is needed on the mechanism of UVR8 and COP1 interaction.

A last point that should not be disregarded during this analysis of mutant function is the difficulty of detecting any of the mutant dimers in plants, as described in Chapter 3. Even if the main findings of this chapter are not affected by this difficulty it would be desirable for the overall understanding of the mechanism to know whether these destabilized dimers are present in plants or not. The constitutive interaction of, for example, GFP-UVR8^{R286K} with COP1 might simply be due to the protein being monomeric in the plant and hence the dimerisation of the purified UVR8^{R286K} can be regarded more as an artefact caused by the in vitro conditions. The most suitable approach to clarify this matter in plants in a future project would probably be bimolecular fluorescence complementation (BiFC) (e.g. Grefen et al., 2010).

4.9.3 Why does UVR8 form a dimer?

The discovery of a functional monomeric mutant inevitably leads to the question of the purpose of initial dimerisation, if the monomeric form can functionally substitute for the dimer. Perhaps rather like the dimer maximises the extent of exciton coupling, the functional response is maximised by initial dimerisation. The functional studies undertaken here were focused on getting a yes or no answer in respect to functionality of the mutations and therefore did not include for example a dose-response analysis. A detailed qPCR analysis of the UV-B induced gene expression under different doses of UV-B might show

subtle differences in the strength of response between the dimeric wild-type and the monomeric GFP-UVR8$^{D96N/D107N}$ mutant, suggesting a purpose for dimerisation of the protein.

Dimerisation also generates a shielding effect in regard to the dimer interface under non-signalling conditions. The mechanism of exposing the interface and thereby exposing possible interaction sites for other proteins is a tempting model and not unreasonable if one considers the signalling mechanism of other WD40 proteins. WD40 proteins often act as scaffolds in many multi protein complexes and one preferred site of interaction is the surface that UVR8 uses for dimerisation (Stirnimann et al., 2012). However, the only so far known interactors of UVR8 interact via the C-terminus of UVR8 and not the dimerisation interface (Cloix et al., 2012). Since the current crystal structure of UVR8 does not include the C-terminal 40 amino acids a more detailed understanding of the mechanism of interaction between UVR8 and COP1 is greatly limited at the moment. It is therefore crucial to determine where the C27 region resides in the protein and what conformation it adopts after exposure to UV-B allowing COP1 interaction. A conceivable model would be that the UV-B activated conformation of the C-terminus is stabilized through interactions with the interface. One possibility is that charged residues on the surface interact with the numerous polar residues in the C-terminus. To test this hypothesis further rather complex experiments will be required. Since crystallisation is impaired by the C-terminus and also has so far been unsuccessful under UV-B conditions, the implementation of nuclear magnetic resonance (NMR) spectroscopy might allow examination of the location of the C-terminus and conformational changes induced by UV-B. Furthermore, NMR can provide information on conformational changes that occur in the protein ‘core’ following photoreception. To be able to ultimately accomplish protein interaction studies between UVR8 and COP1 in vitro, to generate, for example, a co-crystal structure of the complex, recombinant COP1 has to be expressed successfully in any in vitro system in sufficient amounts which so far has not been achieved.

5. REGENERATION OF THE UVR8 DIMER AFTER PHOTORECEPTION

5.1 Introduction

Elucidation of an unknown signalling mechanism is firstly concerned with characterisation of pathways and processes that are involved in generating the active signalling state. Equally important is the question of how initial conditions are restored once the activation signal is no longer present. Since UV-B photoreception leads to monomerisation of the photoreceptor which activates the signalling pathway, how is the dimeric photoreceptor subsequently restored to re-establish the initial conditions? In principle, two mechanisms are conceivable: Firstly, the monomer could be degraded after signalling and the dimer could be replaced via protein synthesis in the cell meaning quite rapid and continual turnover of the UVR8 protein. Second, reversion from the monomer to the dimer could reconstitute the functional photoreceptor without any requirement for synthesis and degradation. Hence, the aim of this chapter was to investigate the kinetics and mechanism of regeneration of the UVR8 dimer in vitro and in vivo.

5.2 Regeneration of the UVR8 dimer is rapid in vivo

To establish the kinetics of UVR8 dimer regeneration in vivo, wild-type plants were exposed for 3 h to 2.5 μmol m^{-2} s^{-1} narrowband UV-B. Fig 5-1 A shows that prior to the UV-B treatment, UVR8 is present as a dimer as shown by semi-native SDS-PAGE and immunoblotting using an anti-UVR8 antibody. UV-B then induces conversion of the dimeric to the monomeric form. When plants are subsequently transferred to darkness, a decrease in the amount of monomer and a concomitant increase in the amount of dimer is seen within 30 minutes. Virtually all the UVR8 protein is present again as a dimer after one hour of darkness following the UV-B treatment. The total amount of UVR8 also does not appear to change significantly over the observed time course.

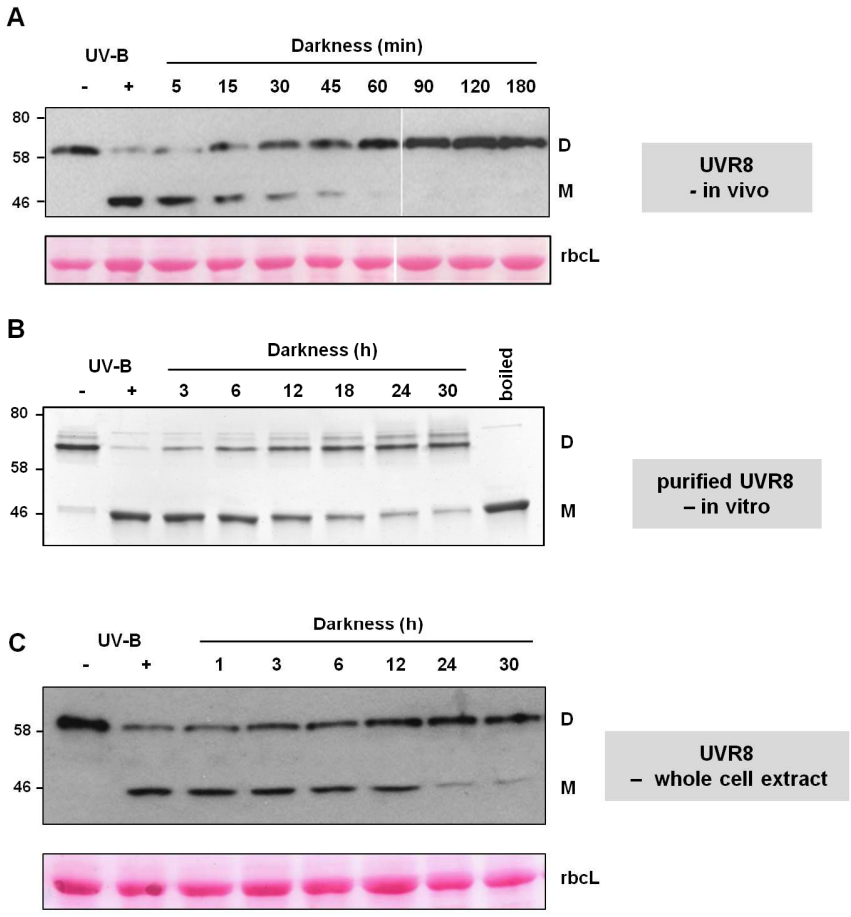

FIGURE 5-1: Regeneration of the UVR8 dimer after UV-B exposure is much more rapid in vivo than in vitro. (A) Immunoblot of whole cell extracts from wild-type L*er* plants probed with anti-UVR8 antibody. Plants were exposed to 2.5 µmol m^{-2} s^{-1} narrowband UV-B for 3 h (UV-B +) and then transferred to darkness for the indicated time periods before extracts were prepared. Extract samples were prepared for electrophoresis without boiling and resolved on a 7.5% SDS-PAGE gel prior to immunoblotting. The UVR8 dimer (D) and monomer (M) are indicated. Ponceau staining of Rubisco large subunit (rbcL) is shown as a loading control. **(B)** Coomassie stained SDS-PAGE gel of purified UVR8 protein exposed to 1.5 µmol m^{-2} s^{-1} UV-B for 1 h (UV-B +) and then transferred to darkness at room temperature for the indicated times. Samples were analyzed without boiling on a 7.5% SDS-PAGE gel. A non-UV-B treated boiled sample is shown as a control. **(C)** Immunoblot of UV-B treated whole cell extract from WT L*er* plants probed with anti-UVR8 antibody. The extract was exposed to 1.5 µmol m^{-2} s^{-1} UV-B for 1 h (UV-B +) and then transferred to darkness at room temperature for the indicated times. Samples were analyzed without boiling on a 7.5% SDS-PAGE gel prior to immunoblotting. Ponceau staining of Rubisco large subunit (rbcL) is shown as a loading control.

In contrast, reappearance of the dimer in darkness following exposure of purified UVR8 protein to 1.5 µmol m^{-2} s^{-1} narrowband UV-B for 1 h is considerably slower (Fig 5-1 B). Although partial reversion to the dimer is detectable 3 hours after transfer to darkness, most of the protein is still in the monomeric form 6 hours after the end of UV-B illumination, and approximately 30 hours are required to see near complete dimer regeneration (see also Christie et al., 2012; Wu et al., 2012). Similarly slow regeneration kinetics are also seen if whole cell extract obtained from wild-type Arabidopsis plants is

exposed to 1.5 µmol m^{-2} s^{-1} narrowband UV-B for 1 h (Fig 5-1 C). A rather large percentage of the protein can still be detected in its monomeric form 12 hours after the end of UV-B illumination.

To be able to show reproducibility of the results and to compensate for the fact that ordinary Western blots are not ideally used for quantification, the decay of the monomeric state was quantified by measuring the band intensities of the monomer in Western blots from three independent experiments. The value for the monomer at each time point was normalized against that after UV-B illumination, which was taken as 100%. Values of % monomer were plotted against time and a best fit line was generated to visualise the kinetics.

A

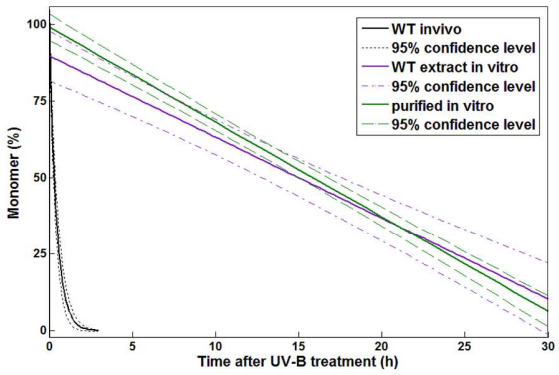

B

	50% monomer	R^2	Type of fit
UVR8 in vivo	18 min (-3/ +4)*	0.94	exponential
UVR8 whole cell extract	15 h (+/- 2)*	0.85	linear
UVR8 purified in vitro	15 h (+/- 1)*	0.98	cubic polynomial

* 95% confidence level

FIGURE 5-2: Kinetics of the loss of UVR8 monomer in darkness following UV-B exposure. (A) Best fit curves of the decay of the monomeric state of UVR8 in wild-type L*er* plants in vivo (black), wild-type L*er* whole cell extract analysed in vitro (purple) and purified UVR8 protein in vitro (green). UVR8 protein bands were quantified in three representative Western blots of each experiment using Image J software. The value for the monomer at each time point was normalized against that after UV-B illumination, taken as 100%. Values of % monomer with time were plotted and the best fit was chosen using Curve Fitting Toolbox in MATLAB (Version 7.12.0). **(B)** Time points when the monomer reached 50% are shown +/- the 95% confidence values at that point. The type of fit that produced a R^2 value closest to 1.0 was chosen. The R^2 value indicates how well the line fits the data points, where 1.0 would represent a perfect fit.

In vivo, the monomer declines exponentially in darkness following UV-B exposure whereas in vitro for purified UVR8 as well as for whole cell extract the conversion rates are much slower and rather linear (Fig 5-2 A). To obtain values for each experiment that can be used for significant comparison, the mean time required for 50% loss of the monomer was calculated from the graphical data with 95% confidence limits (Fig 5-2 B). In vivo, 50% monomer is lost within approximately 18 minutes whereas in vitro it takes about 15 hours. Therefore, if the UVR8 dimer is regenerated by reversion, the process is greatly accelerated in intact plants compared to in vitro conditions. However, if there is monomer degradation and resynthesis in the plant, both must occur rapidly and must be carefully coordinated to maintain a constant amount of UVR8.

5.3 Protein synthesis is required for rapid regeneration of the dimer

Next, it was investigated whether protein synthesis is required for regeneration of the initial dimer state. Plants were treated with the protein synthesis inhibitor cycloheximide (CHX) and the effects of the treatment were analysed by semi-native SDS-PAGE and immunoblotting monitoring dimer and monomer state of UVR8. Plants were transferred to liquid MS medium containing 100 µM CHX or DMSO for the control group one hour before the start of UV-B exposure to ensure that the chemical entered the cells. Subsequently, plants were exposed to 2.5 µmol m^{-2} s^{-1} narrowband UV-B for 3 h and then transferred to darkness for recovery. Fig 5-3 A shows that UV-B induced conversion of the UVR8 dimer to monomer is unaffected by the CHX treatment. Nevertheless, CHX was active in the tissue because UV-B induced accumulation of CHS protein is prevented (Fig 5-3 B) as revealed by immunobloting with a CHS specific antibody. UV-B induced accumulation of CHS protein serves as a suitable positive control for the treatment since it was shown previously that protein synthesis is required for the initiation of CHS expression by UV-B (Christie and Jenkins, 1996). If protein synthesis is required to regenerate the UVR8 dimer following hypothetical rapid degradation of the monomer, treatment with CHX should lead to a substantial decrease of total UVR8 protein present in the plant. However, Fig 5-3 A shows that CHX treatment did not affect the total amount of UVR8 up to at least 3 hours following the end of UV-B exposure, when the dimeric form is fully regenerated. This result indicates that the UVR8 dimer is not newly synthesized once UV-B induced monomerisation has taken place.

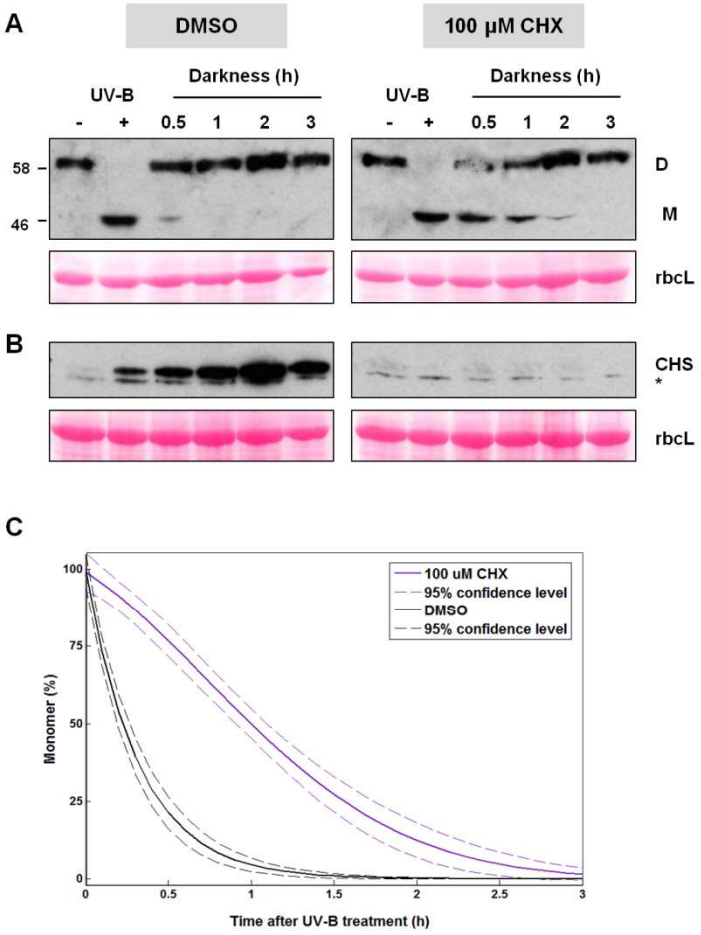

D

	50% monomer	R^2	Type of fit
DMSO	14 min (-3 / +2)*	0.99	exponential
CHX	60 min (+/- 6)*	0.99	gaussian

* 95% confidence level

FIGURE 5-3: Protein synthesis is required to maximize the rate of dimer regeneration. (A) Immunoblots of whole cell extracts from WT L*er* plants probed with anti-UVR8 antibody. Plants were placed in medium containing 0.1% DMSO with or without cycloheximide 1 h before exposure to 2.5 µmol m^{-2} s^{-1} UV-B for 3 h (UV-B +), and then transferred to darkness for the indicated times before extracts were prepared. Samples were prepared for electrophoresis without boiling and resolved on a 7.5% SDS-PAGE gel prior to immunoblotting. Ponceau staining of Rubisco large subunit (rbcL) is shown as a loading control. **(B)** Immunoblots from the experiment shown in (A) probed with anti-CHS antibody. The asterisk (*) indicates a non-specific band recognized by the antibody. **(C)** Kinetics of the loss of UVR8 monomer in darkness following treatment with cycloheximide and UV-B exposure. Data was obtained as described in Fig 5-2. **(D)** Time points when the monomer reached 50% are shown +/- the 95% confidence values at that point. The type of fit that produced a R^2 value closest to 1.0 was chosen. The R^2 value indicates how well the line fits the data points, where 1.0 would represent a perfect fit.

Nevertheless, Fig 5-3 A shows that the rate of dimer reappearance is slowed down in plants treated with CHX; whereas very little monomer remains in control plants 30 minutes after transfer to darkness following UV-B treatment, a substantial amount of monomer remains in the CHX treated plants after 1 hour and is still detectable after 2 hours of darkness. The slower kinetics of monomer loss after CHX treatment are clear if comparing the two 50% loss of monomer values: whereas control plants show loss of 50% monomer already after 14 min, 60 min are required if plants are treated with CHX (Fig 5-3 C and D).

5.4 No evidence of targeted proteolysis of UVR8 via the proteasome

To complement the experiments with CHX, the amount and state of UVR8 following UV-B exposure and dark recovery was investigated in the presence of MG132, an inhibitor of protein degradation via the proteasome. Wild-type plants were transferred to liquid medium containing 100 µM MG132 eleven hours before the start of UV-B illumination since prolonged pre-incubation with MG132 to see inhibition of the proteasome was reported in several previous studies (e.g. Yang et al., 2005; Jang et al., 2005; Dong et al., 2006). The treatment with MG132 did not impair UV-B induced conversion of the UVR8 dimer to the monomer (Fig 5-4 A). Furthermore, there was no effect visible on regeneration of the dimer following transfer to darkness and no quantitative difference in the kinetics for monomer loss in MG132 treated and control plants (Fig 5-4 D and E). To ensure that MG132 had entered the tissue and was effective the accumulation of polyubiquitylated proteins in the cell resulting from inhibition of proteasomal degradation was visualized by an immunoblot with an antibody to ubiquitin. Fig 5-4 B shows that increased amounts of polyubiquitylated proteins could be detected in plants treated with the inhibitor compared to the control. Finally, the total amount of UVR8 remained unchanged over the time course of illumination and dimer regeneration in darkness (Fig 5-4 A and C). It can therefore be concluded that UVR8 is not subject to proteasomal degradation following UV-B exposure.

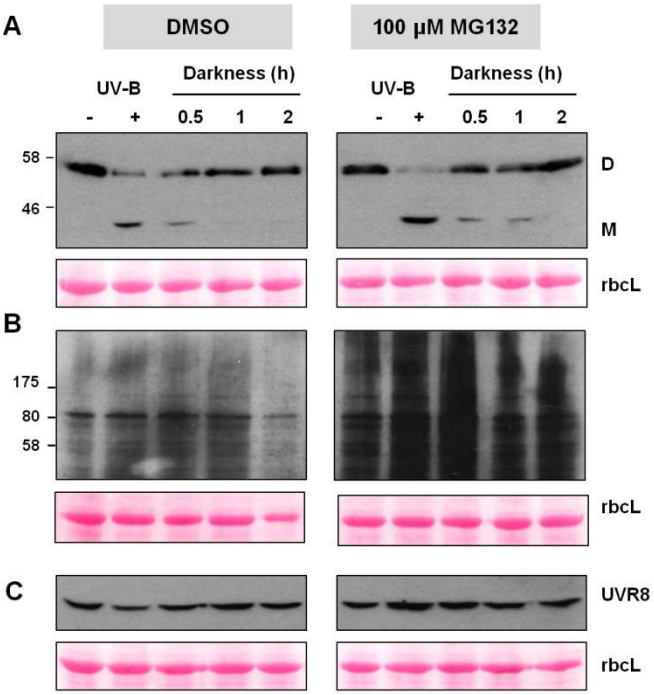

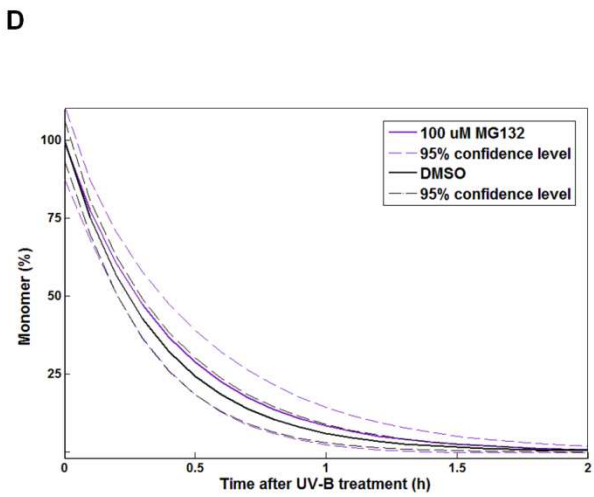

E

	50% monomer	R^2	Type of fit
DMSO	15 min (+/- 2)*	0.99	exponential
MG132	17 min (-4 / +6)*	0.95	cubic polynomial

* 95% confidence level

FIGURE 5-4: Monomeric UVR8 is not degraded via the proteasome. (A) Immunoblots of whole cell extracts from WT L*er* plants probed with anti-UVR8 antibody. Plants were placed in medium containing 0.1% DMSO with or without MG132 11 h before exposure to 2.5 µmol m^{-2} s^{-1} UV-B for 3 h (UV-B +), and then transferred to darkness for the indicated times before extracts were prepared. Samples were prepared for electrophoresis without boiling and resolved on a 7.5% SDS-PAGE gel prior to immunoblotting. Ponceau staining of Rubisco large subunit (rbcL) is shown as a loading control. **(B)** Immunoblots from the experiment shown in (A) probed with anti-ubiquitin antibody. **(C)** Immunoblots pre-pared as in (A) probed with anti-UVR8 antibody, but with samples of whole cell extract boiled prior to electrophoresis on a 7.5% SDS-PAGE gel. **(D)** Kinetics of the loss of UVR8 monomer in darkness following treatment with MG132 and UV-B exposure. Data was obtained as described in Fig 5-2. **(E)** Time points when the monomer reached 50% are shown +/- the 95% confidence values at that point. The type of fit that produced a R^2 value closest to 1.0 was chosen. The R^2 value indicates how well the line fits the data points, where 1.0 would represent a perfect fit.

5.5 The C-terminus of UVR8 is required for rapid regeneration of the photoreceptor in vivo

The role and the importance of the C-terminus in UVR8 mediated signalling has been described in the previous chapters. To test whether the C-terminus is also involved in regeneration of the dimer, two different Arabidopsis genotypes were examined. First, a natural allele of UVR8, *uvr8-2*, was analysed. The *uvr8-2* mutant lacks the final 40 amino acids of the C-terminus due to an introduced stop codon at position 400 (Brown et al., 2005; Cloix et al., 2012). As shown in Figure 5-5, normal UV-B induced monomerisation is observed in the *uvr8-2* mutant, but regeneration of the dimer in subsequent darkness is much slower compared to the wild-type; the monomer is still detectable 4 hours after the end of illumination.

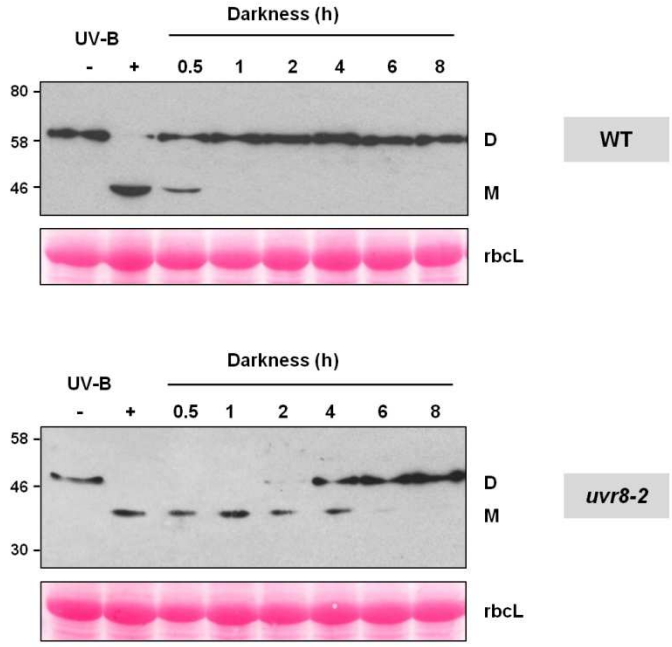

FIGURE 5-5: The C-terminus **of UVR8 is required for rapid regeneration of the dimer in vivo.** Immunoblots of whole cell extracts from WT L*er* and *uvr8-2* plants probed with anti-UVR8 antibody (N-terminal). Plants were exposed to 3 µmol m^{-2} s^{-1} UV-B for 3 h (UV-B +) and then transferred to darkness for the indicated times before extracts were prepared. Extract samples were prepared for electrophoresis without boiling and resolved on a 10% SDS-PAGE gel prior to immunoblotting. Ponceau staining of Rubisco large subunit (rbcL) is shown as a loading control.

The second genotype that was analysed was a transgenic *uvr8-1* line expressing a GFP-UVR8 fusion lacking 27 amino acids within the C-terminus (*uvr8-1*/GFP-ΔC27UVR8; Cloix et al., 2012). This particular stretch of amino acids (residues 397 to 423, termed C27) has shown to be necessary and essential for interaction with the WD40 region of COP1 and can also interact with other WD40 proteins, i.e. RUP1 and RUP2 (Cloix et al., 2012). Plants expressing wild-type UVR8 fused to GFP were used as control plants. Both lines

show UV-B induced monomerisation, but regeneration of the dimer is much slower in plants lacking the C27 region compared to plants expressing wild-type full length UVR8 (Fig 5-6 A). Quantification of the data results in two clearly distinguishable 50% loss of monomer values: whereas approximately 1 h is needed in the GFP-UVR8 line, 5.5 h are required for 50% loss of monomer if the C27 region is absent (Fig 5-6 B and C). These findings suggest that the C27 region is required to maximize the rate of UVR8 dimer regeneration in vivo.

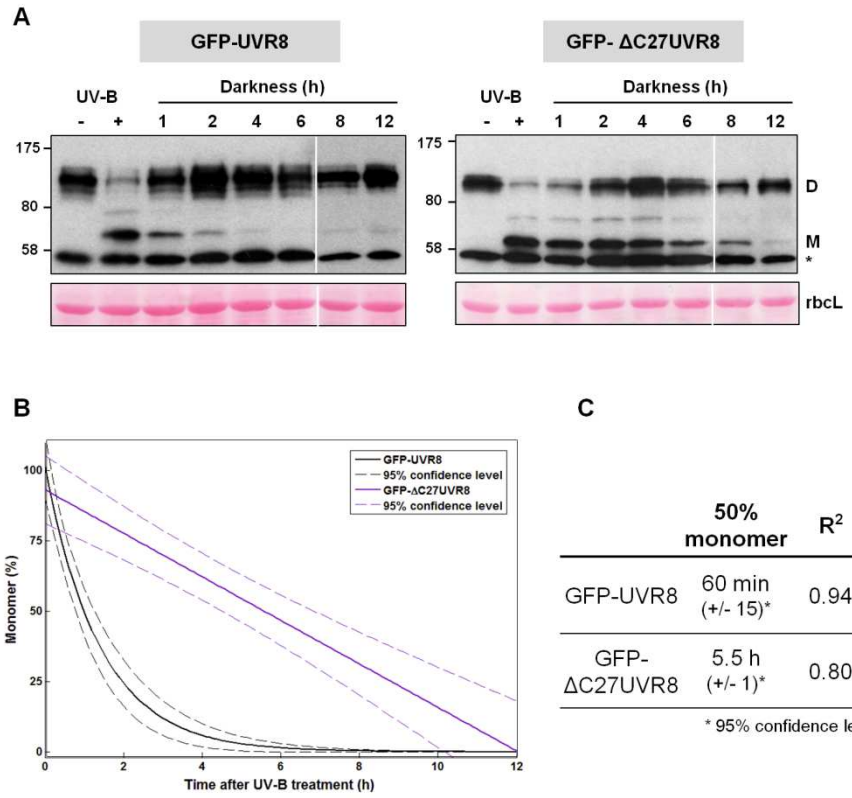

FIGURE 5-6: The C27 region of UVR8 is required for rapid regeneration of the dimer in vivo. (A) Immunoblots of whole cell extracts from *uvr8-1*/GFP-UVR8 and *uvr8-1*/GFP-ΔC27UVR8 plants probed with anti-GFP antibody. Plants were exposed to 3 μmol m^{-2} s^{-1} UV-B for 3 h (UV-B +) and then transferred to darkness for the indicated times before extracts were prepared. Extract samples were prepared for electrophoresis without boiling and resolved on a 10% SDS-PAGE gel prior to immunoblotting. Ponceau staining of Rubisco large subunit (rbcL) is shown as a loading control. The asterisk (*) indicates a non-specific band recognized by the anti-GFP antibody. **(B)** Kinetics of the loss of UVR8 monomer in darkness following UV-B exposure. Data was obtained as described in Fig 5-2. **(C)** Time points when the monomer reached 50% are shown +/- the 95% confidence values at that point. The type of fit that produced a R^2 value closest to 1.0 was chosen. The R^2 value indicates how well the line fits the data points, where 1.0 would represent a perfect fit.

It was now also of interest whether the C-terminus affected the rate of dimer regeneration of purified UVR8 in vitro. The very convenient trypsin treatment could be applied to remove the last 40 amino acids from the C-terminus. This C-terminally truncated protein undergoes normal UV-B induced dimer to monomer conversion, as reported previously (Christie et al., 2012). However, in contrast to the above described in vivo situation, the rate of dimer regeneration in darkness following UV-B exposure was not slower for C-terminally truncated UVR8 compared to the wild-type protein. The kinetics of regeneration were indistinguishable for the two proteins (compare Fig 5-7 A with Fig 5-1 B) and quantification of the data resulted in similar times within the 95% confidence limit required for loss of 50% monomer (15 h, Fig 5-7 B and C).

A

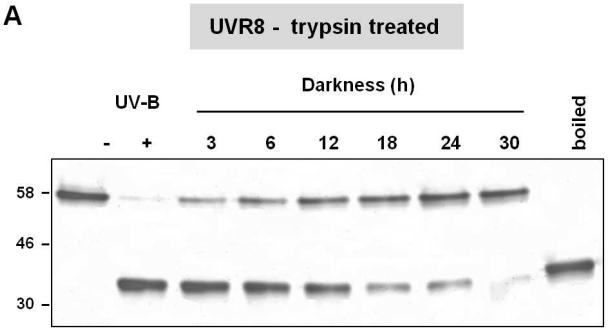

B

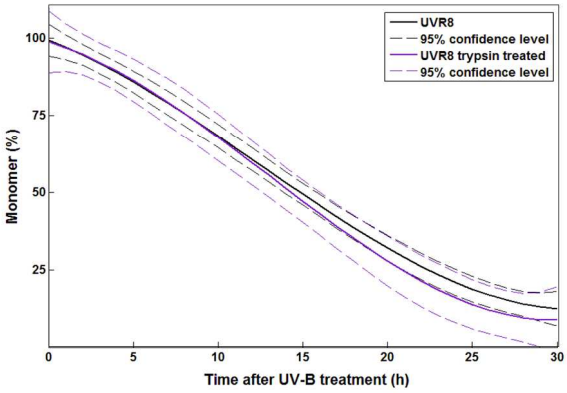

C

	50% monomer	R^2	Type of fit
UVR8 purified	15 h (+/- 1)*	0.98	cubic polynomial
UVR8 purified + trypsin	14.5 h (-2/ +1.5)*	0.95	cubic polynomial

* 95% confidence level

FIGURE 5-7: The in vitro regeneration rate of UVR8 is unaffected by the C-terminus.
(A) Coomassie stained SDS-PAGE of purified UVR8 protein digested with trypsin, exposed to 1.5 µmol m^{-2} s^{-1} UV-B for 1 h (UV-B +) and then transferred to darkness for the indicated times. Samples were analyzed without boiling on a 7.5% SDS-PAGE gel. A non-UV-B treated boiled sample is shown as a control. **(B)** Kinetics of the loss of UVR8 monomer in darkness following UV-B exposure. Data was obtained as described in Fig 5-2. **(C)** Time points when the monomer reached 50% are shown +/- the 95% confidence values at that point. The type of fit that produced a R^2 value closest to 1.0 was chosen. The R^2 value indicates how well the line fits the data points, where 1.0 would represent a perfect fit.

This observation indicates that the absence of the C27 region only negatively affects regeneration in intact cells, allowing the hypothesis that interaction of one or more proteins with the C27 region may be required to maximize the rate of regeneration. To test whether newly synthesised proteins that maximise the reversion process possibly interact with the C-terminus, the influence of CHX on dimer regeneration in *uvr8-2* plants was investigated. No considerable difference between CHX treated and untreated plants was observed (Fig 5-8). However the experiment was only carried out once and rather poor quality of the Western blots with the N-terminal UVR8 antibody that is required for the *uvr8-2* mutant limits the interpretation of this result. Unchanged kinetics of dimer regeneration in the *uvr8-2* mutant after CHX treatment could either mean that newly synthesised proteins are ineffective anyway, because they bind to the C-terminus which is not present, or proteins that facilitate reversion require functional UVR8 to be induced.

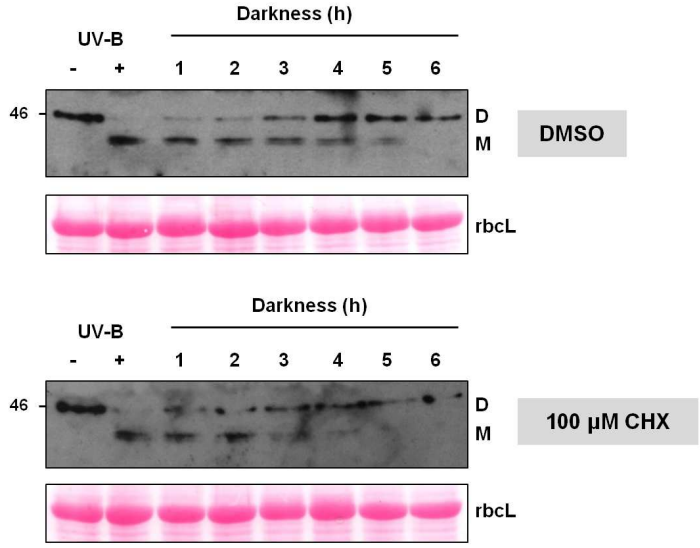

FIGURE 5-8: Protein synthesis is probably not required to maximize the rate of dimer regeneration if the C-terminus is absent. Immunoblots of whole cell extracts from *uvr8-2* plants probed with anti-UVR8 antibody (N-terminal). Plants were placed in medium containing 0.1% DMSO with or without 100 µM cycloheximide 1 h before exposure to 2.5 µmol m^{-2} s^{-1} UV-B for 3 h (UV-B +), and then transferred to darkness for the indicated times before extracts were prepared. Samples were prepared for electrophoresis without boiling and resolved on a 10% SDS-PAGE gel prior to immunoblotting. Ponceau staining of Rubisco large subunit (rbcL) is shown as a loading control.

5.6 COP1 is required for rapid dimer regeneration in vivo

To further investigate the kinetics of dimer regeneration, *cop1-4* mutant plants were analysed. The *cop1-4* allele belongs to the class of *cop1* mutants showing a weak phenotype (McNellis et al., 1994) due to the allele carrying a premature stop codon at position 288. The mutation is non-lethal since a truncated protein containing only the

N-terminal 282 amino acids lacking the WD40 repeats is expressed. Hence, lacking their UVR8 interaction domain (Cloix et al., 2012), interaction between UVR8 and COP1 is impaired in *cop1-4* mutant plants. As shown in Figure 5-9 A, *cop1-4* plants show normal UV-B induced UVR8 monomerisation after exposure to 2.5 µmol m^{-2} s^{-1} narrowband UV-B for 3 h. However, the rate of dimer regeneration in subsequent darkness is slower than in wild-type plants. Quantification of monomer loss reveals that about an extra hour is required to reach a 50% loss of monomer in *cop1-4* plants compared to wild-type (Fig 5-9 B and C). Thus the full length functional COP1 protein is required to maximize the rate of dimer regeneration in vivo.

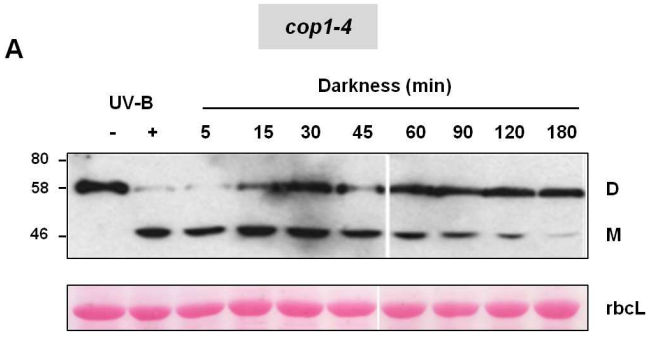

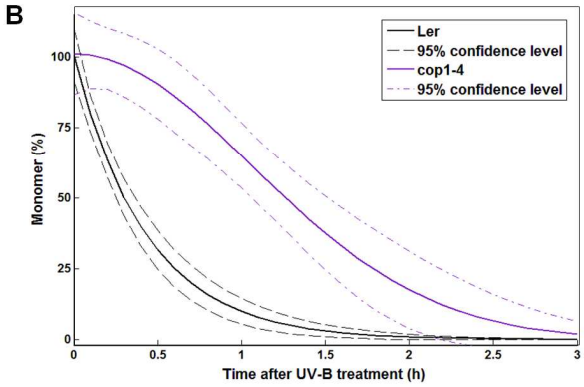

C

	50% monomer	R^2	Type of fit
Ler - in vivo	18 min (-3/ +4)*	0.94	exponential
cop1-4 - in vivo	75 min (-9/ +15)*	0.87	gaussian

* 95% confidence level

FIGURE 5-9: Rapid dimer regeneration in vivo requires intact COP1.
(A) Immunoblot of whole cell extract from *cop1-4* plants probed with anti-UVR8 antibody. Plants were exposed to 3 µmol m^{-2} s^{-1} UV-B for 3 h (UV-B +) and then transferred to darkness for the indicated times before extracts were prepared. Extract samples were prepared for electrophoresis without boiling and resolved on a 7.5% SDS-PAGE gel prior to immunoblotting. Ponceau staining of Rubisco large subunit (rbcL) is shown as a loading control. **(B)** Kinetics of the loss of UVR8 monomer in darkness following UV-B exposure. Data was obtained as described in Fig 5-2. **(C)** Time points when the monomer reached 50% are shown +/- the 95% confidence values at that point. The type of fit that produced a R^2 value closest to 1.0 was chosen. The R^2 value indicates how well the line fits the data points, where 1.0 would represent a perfect fit.

5.7 Discussion

5.7.1 Rapid regeneration of the UVR8 dimer by reversion of the monomer

Despite recent advances in determining the structure of UVR8 and important structural requirements to achieve the active signalling state of UVR8, not much is known so far about how the UV-B response is balanced and how overstimulation is prevented. Therefore, the study presented in this chapter focused on the question how the initial UV-B perceiving dimeric form of UVR8 is re-established once UV-B is no longer present.

In vivo, exposure to UV-B converts dimeric UVR8 into the monomer and the dimer is then fully regenerated in less than one hour of darkness (Fig 5-1 A). Furthermore, no change in the total amount of UVR8 over the monitored time course of monomerisation and regeneration can be observed. To address the two possibilities of dimer regeneration, namely degradation of the monomeric form combined with re-synthesis of the dimeric form or simple reversion of the monomer back to the dimer, the regeneration was analysed under the influence of the two inhibitors CHX and MG132. Treatment of wild-type plants with CHX does not prevent the regeneration of the dimer and also no change in the total amount of UVR8 over the duration of the experiment is detectable (Fig 5-3 A). The preincubation with CHX was evidently effective because it prevented the accumulation of CHS protein in response to the UV-B treatment. The fact that the dimer reappears completely in the presence of CHX indicates that UVR8 protein synthesis is not required for dimer regeneration.

If UVR8 protein synthesis can be ruled out as the way of dimer regeneration, degradation of the monomeric form is highly unlikely or even impossible for the signalling pathway to work in a cycle. In line with this, treatment of plants with MG132, a widely used inhibitor of proteasomal activity, has no effect on the disappearance of the UVR8 monomer during the regeneration process (Fig 5-4). Although MG132 evidently entered the cells, as shown by general accumulation of polyubiquitylated proteins, the total amount of UVR8 is not influenced which would be expected if the monomer was rapidly degraded via the proteasome and this pathway was impaired by the MG132 treatment. Nevertheless, it is not possible to rule out monomer degradation by other types of proteolysis, but the fact that the total amount of UVR8 remains constant throughout all the experiments presented in this study indicates that the protein is not subject to rapid turnover. This conclusion is consistent with previous studies showing that UVR8 is essentially constitutively expressed.

The protein is present in all plant tissues analysed to date (Rizzini et al., 2011) and its abundance is not affected by different light qualities (Kaiserli and Jenkins, 2007).

It can be concluded from the above experiments that reversion of the UVR8 monomer back to the dimer is the mechanism of dimer regeneration. The high stability of the protein could possibly allow photocycling between the dimeric and the monomeric forms resulting in a photoequilibrium regulated by the prevailing amount of UV-B present in a particular light environment. Such equilibrium is, for example, established between the inactive Pr and active Pfr forms of phytochromes in daylight (Chen et al., 2004). Further experiments are required to examine this proposed cycle more closely. A very interesting question is for example, if the dimeric and therefore inactive form of UVR8 is present in the nucleus as well as in the cytoplasm. So far, UV-B induced nuclear accumulation has been reported for UVR8 (Kaiserli and Jenkins, 2007) which supposedly is the monomeric form due to the presence of UV-B. However, no experimental data has been obtained yet on UVR8 moving out of the nucleus once UV-B is no longer present and whether the monomer or the dimer undergoes this movement or translocation.

Overall, the kinetics of dimer regeneration of UVR8 in vivo are comparable to regeneration kinetics of other photoreceptors, for example phototropins or phytochromes. Dephosphorylation of phototropins in vivo as well as regain of photosensitivity of membranes or whole cell extracts isolated following increasing dark periods after a blue light pulse was observed within periods of 20 to 30 min for maize (Palmer et al., 1993) or 60 to 90 min for oat (Salomon et al., 1997). Similarly, dark reversion of far red-absorbing phytochrome to red-absorbing phytochrome occurs quite rapidly in the dark during the first 30 minutes following initial phototransformation of the Pr form to the Pfr form (McArthur and Briggs, 1971).

5.7.2 The kinetics of dimer regeneration in vivo and in vitro

A very striking difference in respect to dimer regeneration is the time required for the process in vivo compared to in vitro. Reversion of the monomer back to the dimer in vitro is possible, but is a very slow process that takes up to 30 h to be completed (Fig 5-1 B). This is an incredibly long time period for a sessile plant that has to alter and adapt its gene expression profile to rather quickly changing environmental factors such as, for example, exposure to different levels of UV-B by changing weather conditions. In addition, dimer regeneration occurs with the same slow kinetics following exposure of plant extracts to UV-B (Fig 5-1 C). The observed slow reversion kinetics of purified protein in vitro could be due to structural reasons caused by the absence of interacting proteins that would

normally define the structure of the activated UVR8 monomer which might be required for subsequent rapid regeneration. Altered folding of parts of the protein that would constrain the rate of regeneration would most likely involve the flexible C-terminus. Since no difference in the rate of dimer regeneration between full length and trypsin treated truncated UVR8 is observed, the flexible C-terminus is not responsible for the slow regeneration behaviour in vitro (Fig 5-7 B).

The quick decay of the monomeric form observed in vivo suggests that in the plant a quick and efficient mechanism of regenerating the UVR8 dimer once UV-B is absent exists. An intact cellular environment is therefore required to maximize the rate of dimer regeneration, presumably because cellular compartmentalisation, as introduced above, or particular physiological processes are needed. The CHX experiment indicates that protein synthesis following UV-B exposure is required to facilitate rapid reversion from monomer to dimer. CHX treatment does not affect the total amount of UVR8 or prevents dimer regeneration, but the kinetics of monomer disappearance and dimer accumulation are slower. A likely scenario is that one or more proteins are synthesized in response to UV-B that facilitate reversion of the monomer. Also the involvement of chaperone proteins is conceivable. Chaperone proteins need sufficient amounts of ATP to function and addition of ATP to the plant cell extract might accelerate dimer regeneration during the in vitro experiment, if ATP is involved in the mechanism. Nevertheless, the rate of dimer formation in vivo in the presence of CHX is considerably faster than it is in vitro, so clearly protein synthesis is not the only factor required for rapid dimer regeneration.

5.7.3 The influence of COP1 on dimer regeneration

The role of COP1 in the UV-B response still remains poorly understood up to now. Despite it being a positive regulator of UVR8 mediated gene expression as shown in this study and before by others (Oravecz et al., 2006; Favory et al., 2009) its well characterized E3 ubiqutin ligase activity during photomorphogenesis (Lau and Deng, 2012) has so far not been reported to play a role in the UV-B response. As shown in Fig 5-9, the rate of dimer regeneration in the absence of COP1 is diminished but dimer regeneration is not abolished. This indicates that COP1 is involved in the process but it is not essential but rather fine-tunes and maximises the response. Moreover, COP1 is required for UV-B induction of many UVR8 regulated genes, so the absence of COP1 in the *cop1-4* mutant may impair synthesis of one or more components needed for rapid regeneration. The experimental data obtained does not allow to conclude whether COP1 directly affects the dimer regeneration via its ability to interact with the C-terminus of UVR8, or whether it indirectly affects a

process being required to synthesise one or more other proteins that facilitate the reversion. The second possibility seems to be supported if one compares the time that is required for 50% loss of the monomer in the *cop1-4* mutant and in plants treated with CHX which is 75 min and 60 min respectively. Nevertheless, regeneration of the dimer in *cop1-4* plants in vivo is still faster than in vitro, so additional so far uncharacterized factors are likely to maximize the rate of dimer regeneration.

5.7.4 The role of the C-terminus of UVR8 during the regeneration process

From the above described data, absence of the C-terminus of UVR8 shows the greatest impact on the rate of dimer regeneration in vivo. Deletion of the last 40 amino acids in the *uvr8-2* mutant as well as deletion of a stretch of 27 amino acids in the C-terminus causes the presence of considerable amounts of monomer four to six hours after the end of the UV-B treatment (Fig 5-5 and Fig 5-6 A). An unchanged rate of dimer regeneration is observed for the C-terminally truncated form in vitro which suggests that truncation of the C-terminus does not impair regeneration for structural reasons (Fig 5-7 B). The observation that the absence of the C-terminal region only affects regeneration in vivo allows the hypothesis that this region of UVR8 may interact with proteins that facilitate rapid reversion of the monomer. Two strong candidates for this are the RUP proteins that interact with the C27 region of UVR8 (Gruber et al., 2010; Cloix et al., 2012). Nothing is known so far about the effect of these two proteins on the rate of dimer regeneration. It has been shown that *RUP1* and *RUP2* transcripts are induced by UV-B in a COP1-, UVR8-, and HY5-dependent manner (Gruber et al., 2010). A second expression study of the RUP proteins or there also named EFO proteins indicates regulation of their transcript levels by the circadian clock showing high expression levels at night peaking at daybreak and declining during the day (Wang et al., 2011; see also 1.6). The results of these two studies only partially coincide and require further careful investigation of RUP protein levels under different light qualities and times of the day. Nevertheless, Gruber and co-workers (2010) showed that RUP gene activation is absent in the *cop1-4* mutant but dimer regeneration is only slowed down to some extent but is not completely prevented (Fig 5-9). RUP proteins should also not be expressed in the non-functional *uvr8-2* mutant; however loss of the C-terminus at the same time makes it difficult to explain the observed deceleration further. Moreover, RUP2-GFP can only be detected after about 4 h of exposure of the plants to UV-B but plants exposed to 3 h of UV-B show complete regeneration of the dimer already one hour after the end of the treatment. At the moment,

the present data is insufficient to understand whether RUP proteins play a role in UVR8 dimer regeneration. Future regeneration experiments with the r*up1* and *rup2* single and double mutants are planned and will provide valuable information about their involvement in the process.

It can also not be excluded that the slower kinetics of dimer regeneration in the *uvr8-2* and in the GFP-ΔC27UVR8 mutants result from their non-functionality. The induction of protein x facilitating the reversion might require functional UVR8 in addition to UV-B as seen for the RUP proteins. The slower reversion kinetics could therefore be due to the lack of protein x and not necessarily due to the lack of the C-terminus. To understand the role of the C-terminus in the regeneration process it will be important to identify more UVR8 interactors to be able to test whether their absence negatively affects the regeneration kinetics.

To conclude, the regeneration of the UVR8 dimer is very rapid in vivo and is accomplished by reversion of the monomer to the dimer. None of the above described experiments could identify a single component that completely prevented the reversion but each analysed condition contributed partially to the process. This suggests that the process of reversion from monomer to dimer is very complex and is facilitated by several factors allowing the photoreceptor to respond rapidly and sensitively to changes in ambient UV-B levels in sunlight.

6. BIOPHYSICAL ANALYSIS OF UVR8 PHOTORECEPTION

6.1 Introduction

The principal requirement of a photosensory protein is the presence of a light absorbing chromophore that undergoes chemical and structural changes upon light absorption. The apoprotein associated with the light activated chromophore modulates these photochemical aspects and at the same time constitutes the microenvironment that immediately responds to the photoinduced changes of the chromophore. This interplay between chromophore and apoprotein is an essential step in the signal-transduction process and has been characterized for the visible light photoreceptors over the past decades.

The crystallographic structure of UVR8 has revealed that UV-B photoreception by UVR8 does not rely on a bound chromophore (Christie et al., 2012; Wu et al., 2012). UVR8 is therefore fundamentally different from other photoreceptors in employing standard amino acid side chains instead of specialized chromophores for the initial photochemical event. As described in the Introduction and in Chapter 3, UV-B photoreception is mediated by excitonically coupled tryptophans at the dimer interface which are adjacent to arginines involved in forming dimer maintaining salt bridges. Photoreception results in the disruption of salt-bridges, causing dimer dissociation and initiates signalling. However, the precise mechanism of UV-B perception leading to changes in the photoreceptor has only been hypothesised so far without any experimental evidence (Christie et al., 2012; Wu et al., 2012). The purpose of the experiments presented in this chapter was to test the hypothesis that electron transfer may occur between the photoreceptive tryptophans and adjacent salt-bridging arginines leading to charge neutralization and thus dimer destabilization. Fourier transform infrared (FTIR) spectroscopy of purified UVR8 protein was employed to detect UV-B induced changes in the chemical structure of the amino acid side chains and the overall conformation of the protein. Changes in the local environment of the tryptophans were revealed by light-associated changes in tryptophan fluorescence. Finally, ultrafast transient absorption spectroscopy was used to gain first insights into the initial photochemistry of UVR8 and to test whether the formation of tryptophan radicals occurs as an intermediate step in UV-B photoreception. These approaches have created plenty of data in a short period of time about a so far entirely unknown process, making

analysis of the data and putting actual meaning behind them quite a challenge. Nevertheless, preliminary findings will be described and discussed in this Chapter.

6.2 FTIR spectroscopy reveals UV-B induced conformational changes in UVR8

The absorption of infrared radiation (IR) excites vibrational transitions of molecules when the frequencies of light and vibration are equal and when the molecular dipole moment changes during the vibration (Barth, 2007). The vibrating masses, the type of bond (single, double, triple) and the exact position of the bond influenced by electron withdrawing or donating effects of the intra- and intermolecular environment and by coupling with other vibrations determines the approximate position of an infrared absorption band (Barth, 2007). The vibrational spectrum of a protein therefore contains a wealth of information about its structure and conformation, its interaction with the environment and electronic properties. To be able to obtain detailed structural information from an FTIR spectrum, the number of groups that contribute to a spectrum must be reduced which is possible by recording light-induced difference spectra.

A light-minus dark difference spectrum of purified full length UVR8 protein is shown in Fig 6-1 A. The light-minus dark difference spectrum was obtained by subtracting an initially over one minute recorded dark state spectrum from the light activated protein spectrum recorded under continuous UV-B illumination over the duration of one minute. UVR8 shows prominent but weak signals all over the spectral range of 1750 to 1000 cm^{-1} but signals below 1300 cm^{-1} are difficult to assign due to poor signal to noise ratio in this region and are therefore not shown. The photoinduced reaction is complete under the chosen experimental conditions as tested by longer UV-B illumination periods resulting in similar spectra. The reaction is also reversible since qualitatively identical signals were obtained again after 24 to 48 h of dark recovery between the measurements. To possibly narrow down the number of bonds and groups that give rise to absorption in the difference spectrum UVR8 was treated with trypsin to remove the flexible C-terminus (Christie et al., 2012). However, the C-terminally truncated UVR8 protein displays essentially the same light induced difference spectrum as the full length protein suggesting that all observed signals originate from the protein core (Fig 6-1 A).

An FTIR spectrum comprises information about the infrared absorption of particular amino acid side chains and absorption of the protein backbone. The two most prominent signals of the protein backbone are the amide I band present around ~1650 cm^{-1} (1610-1700 cm^{-1}) and the amide II band at around ~1550 cm^{-1}. The more informative amide I band is caused

by carbonyl stretching vibrations of the peptide bond which are hardly affected by the nature of the side chains. It depends however on the secondary structure of the backbone and it is therefore the amide vibration that is most commonly used for secondary structure analysis (Barth, 2007).

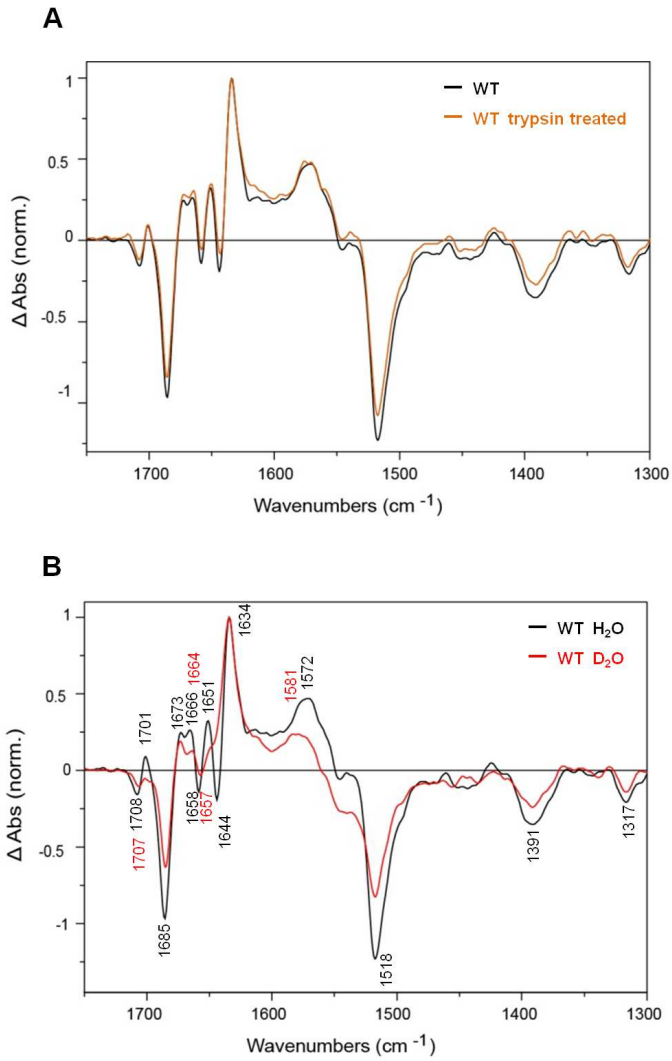

FIGURE 6-1: FTIR spectroscopy reveals UV-B induced conformational changes in UVR8. (A) Light (UV-B)-minus-dark difference FTIR spectra of full length wild-type UVR8 and trypsin treated wild-type UVR8. **(B)** Light (UV-B)-minus-dark difference FTIR spectra of wild-type UVR8 in H_2O and D_2O buffered medium. The major peaks are labelled with the respective maximum wavenumber observed in H_2O and D_2O.

Assignment of IR absorption bands to specific chemical bonds and groups is possible by studying model compounds, chemical modifications of cofactors or ligands, isotopic labelling of amino acids or by site-directed mutagenesis (Barth, 2007). The last two approaches are suitable for UVR8 and were therefore pursued in the following experiments. One way of labelling protein is by H/D exchange. For this purpose, protein samples were lyophilized and resuspended in D_2O which exchanges the accessible hydrogens of the protein including the main-chain peptide group NH and the side-chain protons bound to N, O and S atoms of polar groups by deuteriums (Englander et al., 1996). It should be noted, that carbon bound hydrogens do not exchange easily and are therefore not affected. For UVR8, most signals of the light-induced difference spectrum are

surprisingly indifferent to H/D exchange (Fig 6-1 B). Especially secondary structure changes, which are reflected by the change in absorption of the amide groups, usually show strong H/D influenced IR absorbance between 1600 and 1700 cm^{-1}. The most prominent D-induced shift is observed for the band at 1651 (+) cm^{-1}, which is reduced to only a small shoulder of the peak at 1634 (+) cm^{-1}. This frequency region might be attributed to turn and loop structures of the protein. Another detectable H/D sensitive contribution is the broad positive peak centred around 1572 cm^{-1} which up shifts by approximately 10 cm^{-1} if UVR8 is deuterated. This is a characteristic feature of the asymmetric stretching vibrations of the carboxylate groups of glutamates or aspartates. Additionally, the negative peak at 1708 cm^{-1} shows a slight downshift of about 1 cm^{-1} in the deuterated sample which might be attributed to changes in amide side chains of asparatates or glutamates.

6.3 FTIR spectra of UVR8 salt bridge mutants

The observed difference bands in the amide I range indicate overall UV-B induced conformational changes in the UVR8 structure. However, definite assignments of bands to contributions of specific amino acid side chains were not possible by analysis of the wild-type protein alone. Ideally, an IR signal due to a specific amino acid is missing when this amino acid has been selectively replaced and the band can then be assigned to the mutated amino acid. The hypothesised electron transfer from the UV-B perceiving tryptophan pyramid to the adjacent arginines might be associated with proton transfer. Salt bridge forming amino acids should therefore show a change in their protonation state upon UV-B induced monomerisation. To test this, light induced difference spectra of UVR8 mutants with point mutations in the essential R286-D107 and D96 salt bridge were recorded.

Remarkably, the two constitutive monomeric mutants, $UVR8^{D96N/D107N}$ and $UVR8^{R286A}$ showed no light induced difference signals (data not shown); although $UVR8^{D96N/D107N}$ is functional in plants (Chapter 4) and the fluorescence behaviour of $UVR8^{R286A}$ suggests UV-B-induced transitions (Fig 6-5 E). Based on this observation, one can reason that the difference spectra most likely correspond to structural differences between dimer and monomer and the process of monomerisation is essential for generation of the signal.

The single aspartic acid mutants $UVR8^{D96N}$ and $UVR8^{D107N}$ are still able to undergo a dimer to monomer shift and therefore showed light induced difference signals (Fig 6-2 A and B). The broad peak observed for wild-type UVR8 centred at 1572 cm^{-1} is reduced and slightly altered in its shape in the $UVR8^{D107N}$ mutant and therefore might support the

assignment of this peak to a carboxylate vibration of aspartates. However, this peak is unaltered in the UVR8^{D96N} mutant. A possible explanation for this might be that although both aspartates are possibly expected to show light induced changes due to the breaking of the salt bridges upon monomerisation, the molecular environment of D96 in the monomer is similar to its environment in the dimer, while D107 experiences a changed environment in the monomer causing alteration of the signal. A second band that might be attributed to changes in vibrations of carboxyl groups of aspartates is the one at 1391 cm^{-1} which is shifted in both mutants, once up and once down. Subtle changes between the spectra of the two mutants and wild-type are also present in the spectral region around 1705 cm^{-1}. However, the signal to noise ratio in this part of the spectrum is very low and therefore hinders an assignment of the bands.

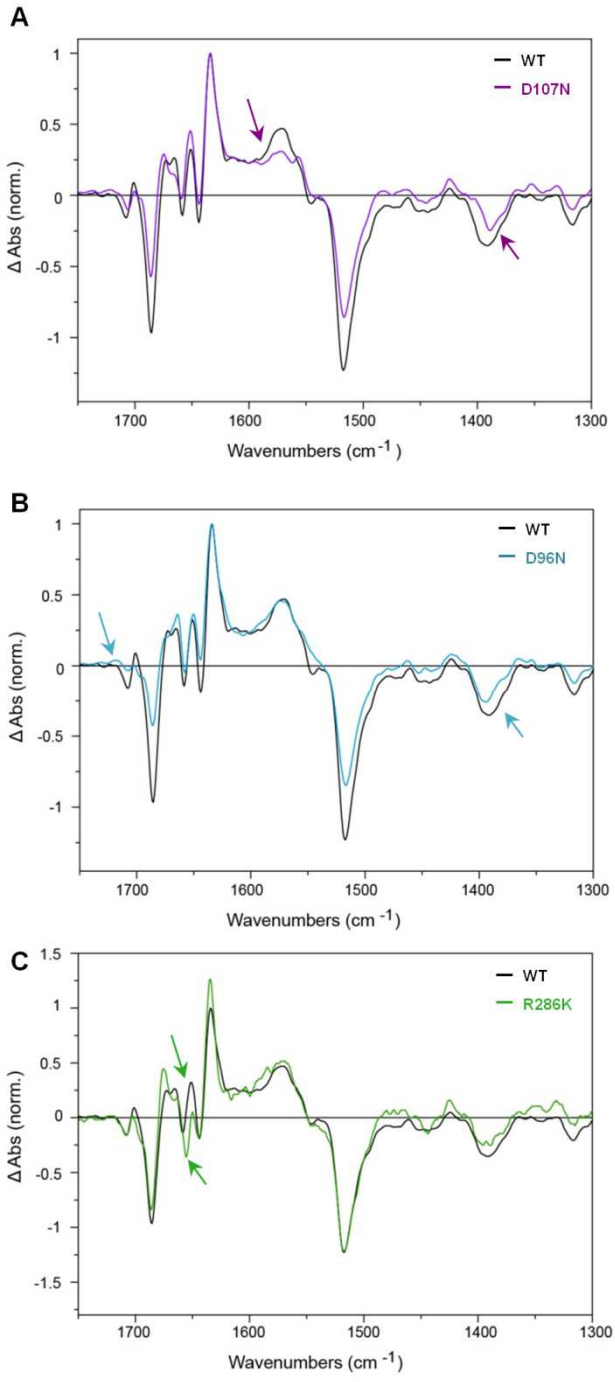

FIGURE 6-2: Dimeric UVR8 salt bridge mutants and wild-type UVR8 show comparable light-minus-dark difference FTIR spectra. (A) Light (UV-B)-minus-dark difference FTIR spectra of wild-type UVR8 and UVR8^{D107N}. **(B)** Light (UV-B)-minus-dark difference FTIR spectra of wild-type UVR8 and UVR8^{D96N}. **(C)** Light (UV-B)-minus-dark difference FTIR spectra of wild-type UVR8 compared to UVR8^{R286K}. The arrows point to the most pronounced differences between the spectra of wild-type and of the three mutants.

Finally, light-induced difference spectra of another dimeric salt bridge mutant UVR8^{R286K} were recorded (Fig 6-2 C). Again, the spectrum looks very similar to the one of the wild-type protein but features a slightly downshifted band at 1655 cm^{-1} and a very small positive band at 1649 cm^{-1}. Therefore this signal might be assigned to the changed environment of the arginine/lysine side chain upon monomerisation. Both side chains usually feature absorbance in this region but the small differences in the signal only allow a remote assignment of the bands. In general, the proposed specific assignment of any of the bands at that point is rather speculative and has to be established further in the future.

6.4 UV-B induced changes in UVR8 fluorescence

Another way of gaining information about conformational changes of a protein is by utilizing intrinsic protein fluorescence. Of the three aromatic amino acids present in proteins, tryptophan is the most dominant intrinsic fluorophore and its fluorescence emission is highly sensitive to its local environment allowing to monitor conformational transitions, subunit association, substrate binding or denaturation by recording changes in the emission spectra (Lakowicz, 2006). A complicating factor in the interpretation of protein fluorescence is the presence of multiple fluorescent amino acids in most proteins. Especially for UVR8 with its exceptionally high number of aromatic residues (14W, 10Y and 8F), it is an impossible task to separate the spectral contributions of each tryptophan and also to some extent possible contributions of tyrosines. Additionally, the spectral properties of each residue are generally different due to the distinct environment of each residue. However, the absorption and emission spectra of tryptophan residues in proteins overlap at most wavelengths used for excitation and the observed changes in fluorescence can provide another fingerprint of the protein allowing comparison between wild-type and mutant forms.

Excitation of dark adapted wild-type UVR8 with 280 nm light produces an emission maximum at 327 nm (Fig 6-3 A and Table 6-1). Repeated excitation of the sample over an extended period of time causes a shift of the emission maximum to 335 nm. This red shift is completed after ~12 min under the UV-B fluence rate employed. Additionally, similar to what was observed by Wu and co-workers (2012), the fluorescence intensity at 335 nm rapidly increases by about two-fold within the first 20 min of UV-B illumination (excitation) and slowly starts to decrease after about 40 min until the completion of the experiment after two hours (Fig 6-3 B). However, at wavelengths greater than 450 nm, the emission intensity keeps rising slowly but constantly (data not shown). The same

experiment was undertaken with wild-type UVR8 preilluminated with UV-B and both the observed red shift as well as the initial increase in fluorescence is absent (Fig 6-3 C and D). The emission maximum remains unchanged at 335 nm over the recorded time. The wavelength of the emitted light is a well proven indicator of the environment of the fluorophore (Vivian and Callis, 2001). The observed red shift indicates that the position of the fluorophore has changed from being buried in the hydrophobic, "non-polar" core of the protein to being solvent exposed (polar environment). This is consistent with UV-B induced monomerisation and exposure of the tryptophan rich dimer interface to the solvent.

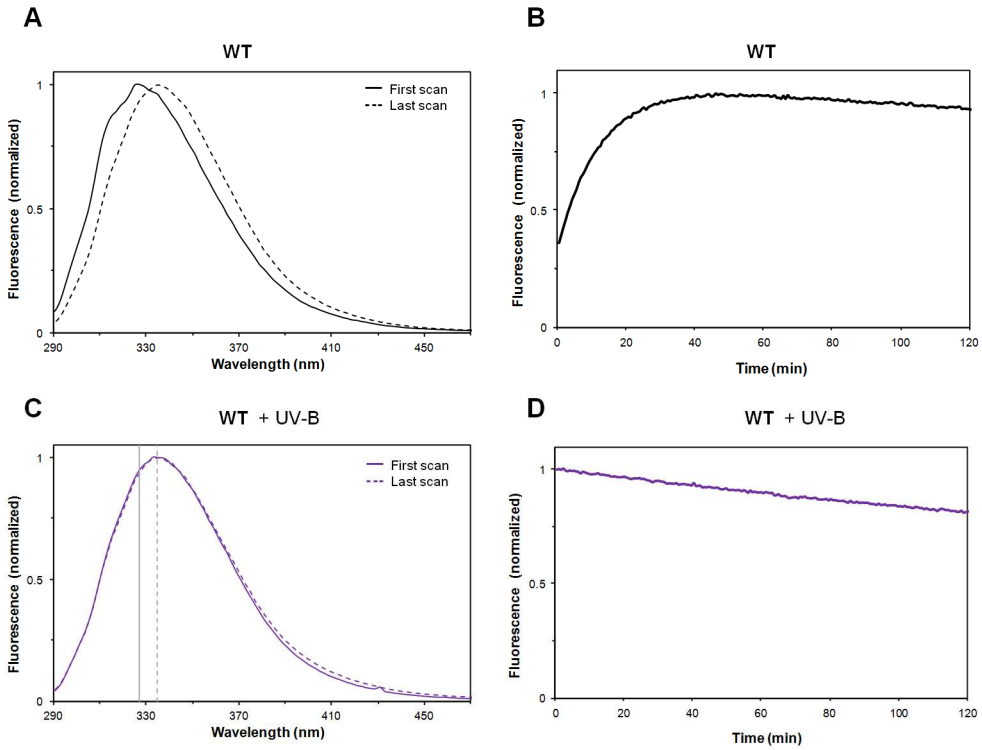

FIGURE 6-3: Monomerisation of wild-type UVR8 causes a red shift in its emission spectrum. (A) Emission spectrum of dark adapted dimeric wild-type UVR8 (solid line) compared to the emission spectrum of wild-type UVR8 after 200 subsequent excitations with 280 nm for 38 s resulting in complete monomerisation (dotted line). Complete monomerisation was tested by semi-native SDS-PAGE (data not shown). The emission maximum shifts from 327 nm to 335 nm. **(B)** Time resolved emission spectrum of wild-type UVR8 excited with 280 nm. The trace shows the emission of the sample at 335 nm. At time 0 the sample was dark adapted. **(C)** Emission spectrum of UV-B exposed wild-type UVR8 (solid line) compared to emission spectrum of UV-B exposed wild-type UVR8 after 200 subsequent excitations with 280 nm for 38 s (dotted line). The sample was exposed to UV-B for 10 min before start of the measurement to induce monomerisation. The emission maximum stays unchanged at 335 nm. The vertical lines indicate the emission maxima of dimer and monomer as shown in (A). **(D)** Time resolved emission spectrum of UV-B exposed wild-type UVR8. The trace shows the emission of the sample at 335 nm. The sample was exposed to UV-B for 10 min before start of the measurement to induce monomerisation. All spectra were normalised for better comparison.

In contrast to wild-type UVR8, the three analysed salt bridge mutants show differences in their fluorescence emission spectra, both in the maximum wavelength emission and in the development of fluorescence intensity. The constitutively monomeric mutant UVR8^{R286A} features an emission maximum at around 337 nm in the dark adapted state which shifts only slightly to about 339 nm within the first 20 min of the experiment (Fig 6-4 A and Table 6-1). The spectrum also loses its fine structure in the UV-B region and also becomes slightly narrower under prolonged UV-B exposure. The emission intensity increases by ~ 40% within the first 80 minutes and then reaches a plateau (Fig 6-4 B).

TABLE 6-1: Emission maxima of UVR8 wild-type and salt bridge mutants before and after exposure to UV-B (top) and after a dark recovery period of at least 24 h before a re-run of the experiment (bottom).

	λ_{max} Emission (nm)	
	- UV-B (first scan)	**+ UV-B (last scan)**
WT	327	335
R286A	337	339
D96N	333	333
D107N	331	335
WT rec	333	335
R286A rec	339	339
D107N rec	333	335

Next, the influence of the two aspartic acid mutations (D96N and D107N) on the protein fluorescence was analysed. Both mutants are still able to dimerize, but the dimer seems to be weakened compared to wild-type (Chapter 3). UVR8^{D96N} displays an already red shifted emission spectrum at the start of the time course compared to wild-type (Fig 6-4 C and Table 6-1). The emission maximum remains unchanged at 333 nm under prolonged UV-B excitation but becomes narrower on both sides along with a loss in fine structure on the blue side. The increase in fluorescence intensity is comparable to UVR8^{R286A} whereas the decrease towards the end of the experiment is hardly detectable (Fig 6-4 D). The emission spectrum of UVR8^{D107N} is further blue shifted at the start of the experiment than UVR8^{D96N} but not as much as the dimeric wild-type (Fig 6-4 E and Table 6-1). Prolonged UV-B illumination leads to a small shift in the emission maximum from 331 nm to about 333 to 335 nm. The precise maximum is difficult to determine since the peak is rather broad and the spectral resolution is limited. The spectrum becomes narrower in the UV-B region and

loses its fine structure. A small but clear rise in emission is also detected in the spectral region of about 420 nm. To define whether this rise is significant, measurements of this mutant have to be repeated since all data shown in Fig 6-4 are based on one-off runs of the experiments. Changes in the fluorescence intensity of UVR8^{D107N} over time resemble those of the wild-type protein with a fast increase by about two fold within the first 20 min followed by a slow decrease until completion of the experiment (Fig 6-4 F).

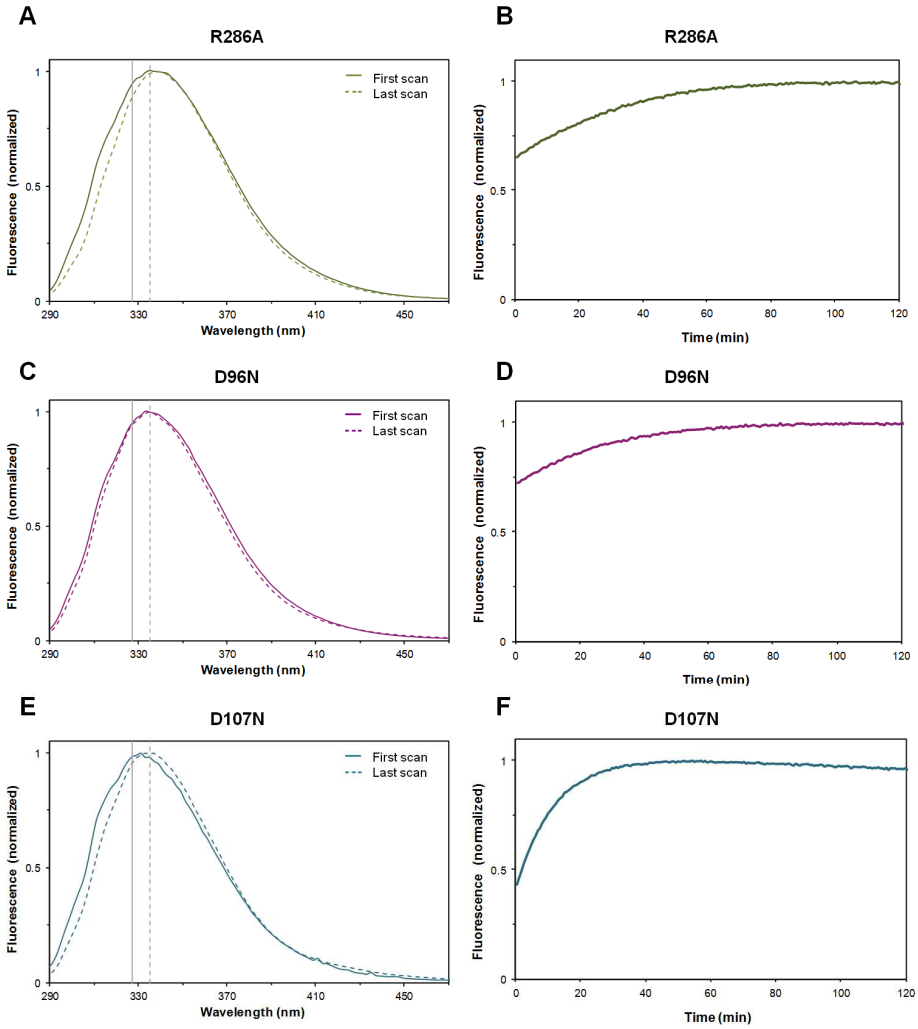

FIGURE 6-4: UVR8 salt bridge mutants show shifted emission spectra.
(A) Emission spectrum of dark adapted UVR8^{R286A} (solid line) compared to emission spectrum of UVR8^{R286A} after 200 subsequent excitations with 280 nm for 38 s (dotted line). The emission maximum shifts from 337 to 339 nm. The vertical lines indicate the emission maxima of wild-type dimer and monomer as shown in Fig 6-3. **(B)** Time resolved emission spectrum of UVR8^{R286A} with 280 nm excitation of the sample. The trace shows the emission of the sample at 339 nm. At time 0 the sample was dark adapted. **(C)** Emission spectrum of dark adapted UVR8^{D96N} (solid line) compared to emission spectrum of UVR8^{D96N} after 200 subsequent excitations with 280 nm for 38 s (dotted line). The emission maximum remains unchanged at 333 nm. **(D)** Time resolved emission spectrum of UVR8^{D96N} with 280 nm excitation of the sample. The trace shows the emission of the sample at 333 nm. At time 0 the sample was dark adapted. **(E)** Emission spectrum of dark adapted UVR8^{D107N} (solid line) compared to emission spectrum of UVR8^{D107N} after 200 subsequent excitations with 280 nm for 38 s (dotted line). The emission maximum shifts from 331 to 335 nm. **(F)** Time resolved emission spectrum of UVR8^{D107N} with 280 nm excitation of the sample. The trace shows the emission of the sample at 335 nm. At time 0 the sample was dark adapted.

To further characterize the fluorescence properties of UVR8 emission spectra of wild-type, UVR8^{D107N} and UVR8^{R286A} were recorded again after a dark recovery period of 36 h or 24 h respectively (Fig 6-5). If the experimental conditions allowed complete reversibility of UV-B induced monomerisation possibly associated with further conformational changes of the protein, the emission maximum should display its original maximum. However, for wild-type UVR8 as well as for UVR8^{D107N} this seems to be partially possible since the first spectrum after at least 24 h recovery is slightly blue shifted compared to the last spectrum recorded after prolonged UV-B illumination in the second experiment (Fig 6-5 A and C, Table 6-2). Additionally, some fine structure in the UV-B part of the emission spectrum is regained as well as the characteristic increase followed by a slow decrease of fluorescence intensity over time (Fig 6-5 B and D). The dimerisation state of wild-type UVR8 after the 36 h recovery period was also tested by semi-native SDS-PAGE revealing that about 50% of the protein had dimerised again. This recovery rate is much lower of what has been observed in Chapter 5 but is most likely due to the very low sample concentration required for fluorescence measurements, which will have a negative effect on regeneration of the dimer. Remarkably, the monomeric mutant UVR8^{R286A} shows no signs of a possible recovery since the emission maximum remains at 339 nm and also no changes in the fine structure can be observed after the recovery period followed by further UV-B illumination (Fig 6-5 E). Furthermore, no increase in the fluorescence intensity can be observed as in the first experiment. Instead, the intensity slowly decreases over the recorded time span (Fig 6-5 F) but the decrease is significantly less pronounced than in wild-type. To conclude, an in depth analysis of the intrinsic fluorescence data obtained for UVR8 is rather challenging to interpret at the moment but nevertheless these findings contribute to the overall picture of UV-B photoreception.

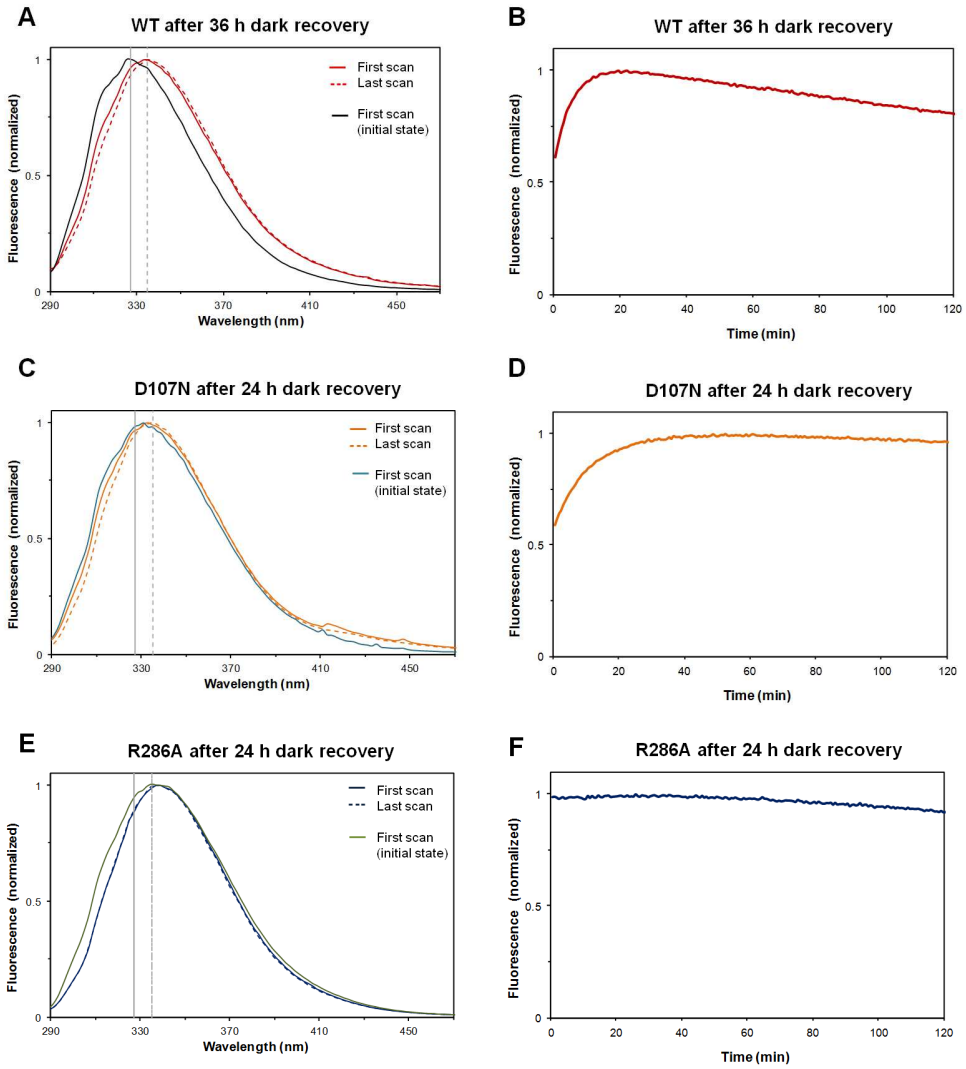

FIGURE 6-5: The shifted emission spectrum can be partially reversed after at least 24 h of dark recovery in wild-type UVR8 and UVR8^{D107N} but not in UVR8^{R286A}.
(A) Emission spectrum of 36 h dark recovered wild-type UVR8 (solid line) compared to emission spectrum of 36 h dark recovered wild-type UVR8 after 200 subsequent excitations with 280 nm for 38 s (dotted line). The emission maximum shifts from 333 to 335 nm. For comparison the initial emission spectrum of the sample of the first experiment is shown as well. The vertical lines indicate the emission maxima of dimer and monomer as shown in Fig 6-3. **(B)** Time resolved emission spectrum of 36 h dark recovered wild-type UVR8 with 280 nm excitation of the sample. The trace shows the emission of the sample at 335 nm. At time 0 the sample had completed 36 h dark recovery from the first experiment. **(C)** Emission spectrum of 24 h dark recovered UVR8^{D107N} (solid line) compared to emission spectrum of 24 h dark recovered UVR8^{D107N} after 200 subsequent excitations with 280 nm for 38 s (dotted line). The emission maximum shifts from 333 to 335 nm. **(D)** Time resolved emission spectrum of UVR8^{D107N} with 280 nm excitation of the sample. The trace shows the emission of the sample at 335 nm. At time 0 the sample had completed 24 h dark recovery from the first experiment. **(E)** Emission spectrum of 24 h dark recovered UVR8^{R286A} (solid line) compared to emission spectrum of 24 h dark recovered UVR8^{R286A} after 200 subsequent excitations with 280 nm for 38 s (dotted line). The emission maximum remains unchanged at 339 nm. **(F)** Time resolved emission spectrum of 24 h dark recovered UVR8^{R286A} with 280 nm excitation of the sample. The trace shows the emission of the sample at 339 nm. At time 0 the sample had completed 24 h dark recovery from the first experiment.

6.5 Ultrafast transient absorption spectroscopy of UVR8

To be able to understand how UV-B can induce monomerisation of UVR8 it is essential to understand the primary photophysics and photochemistry of the photoreceptor. Typically, initial events after photon absorption occur in less than 1 ns and therefore ultrafast spectroscopy has to be applied to picture those very early steps in photoreception. Since photoreceptor proteins can be triggered by a short flash of light, the functional protein dynamic can be studied over a wide span of timescales down to femtosecond resolution (Kennis and Groot, 2007). In this way, energy migration within the system as well as the formation of new chemical species such as charge-separated states can be tracked in real time.

In collaboration with Dr. John Kennis (Biophysics Group VU Amsterdam, LaserLab Europe) ultrafast transient absorption spectroscopy studies of UVR8 were initiated. To excite UVR8, a 266 nm pump pulse was generated by third harmonic generation to trigger the photoreaction. The energy of the resulting 266 nm excitation beam was determined to be between 500 and 600 nJ. The excitation (or pump) pulse promotes a fraction (0.1% to tens of percent depending on the type of experiment) of the molecules in the sample to an electronically excited state. To prevent multiple excitations at one spot the sample was continuously circulated with a flow cell. A weak probe pulse, that has such a low intensity that multiphoton/multistep processes are avoided during probing, is sent through the sample with a delay (τ) in respect to the pump pulse. The probe pulse was then focused into a spectrograph and was dispersed on a detector between 355 and 660 nm. A difference absorption spectrum was calculated, i.e., the absorption spectrum of the excited sample minus the absorption spectrum of the sample in the ground state (ΔA). By changing the time delay τ between the pump and the probe and recording a ΔA spectrum at each time delay, a ΔA profile as a function of τ and wavelength λ, $\Delta A(\lambda, \tau)$ was obtained (Berera et al., 2009).

The biggest challenge of a time-resolved spectroscopic experiment is the thorough analysis of the very large amount of data present in the generated $\Delta A(\lambda, \tau)$ datasets. The collected data has to be broken down into a relatively small number of components and spectra which is done by global and target analysis techniques (van Stokkum et al., 2004). However, such an analysis has been undertaken by our collaborators but is still ongoing and beyond what can be presented in this Chapter. Nevertheless, valuable information could be extracted by analysis of the absorption spectra for a given time point at different wavelengths (ΔA) and analysis of single kinetic traces (evolution of one wavelength over time) which will be presented in the next section.

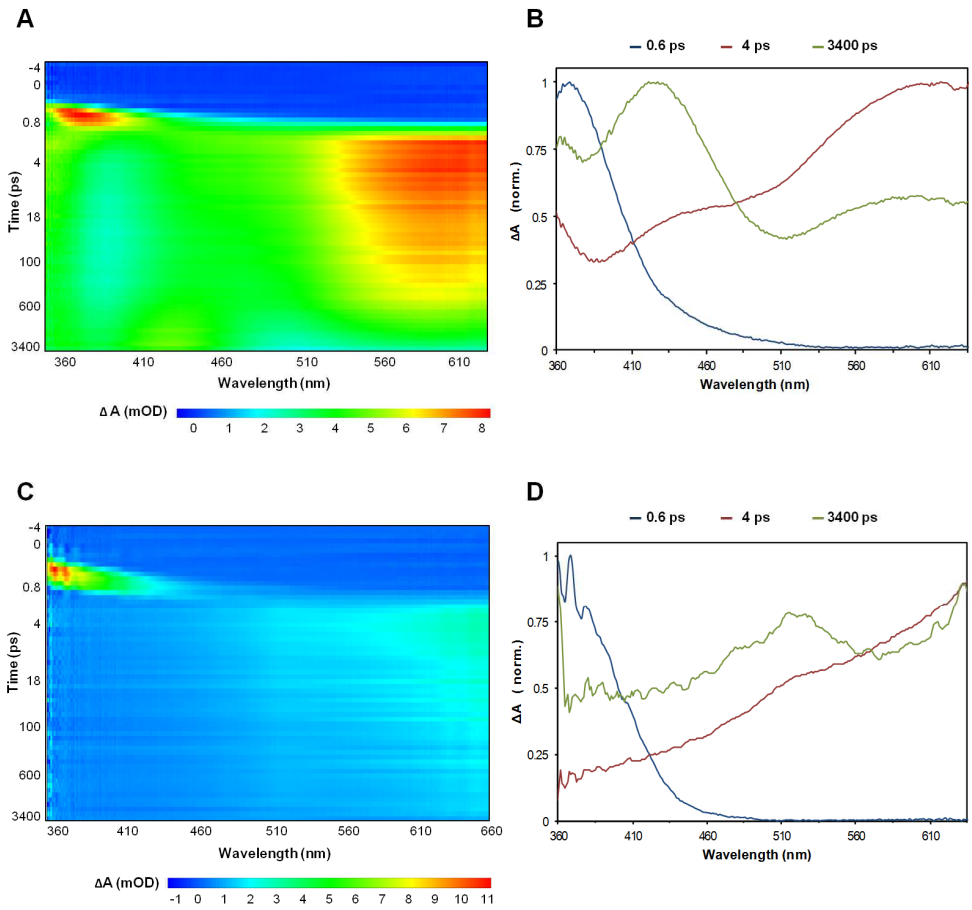

FIGURE 6-6: Excitation of tryptophan in solution with 266 nm pulses leads to formation of a photoproduct with an absorption band at 425 nm.
(A) Two dimensional map of time- and wavelength-resolved transient absorption data of tryptophan in 50 mM Tris-HCl pH 7.5, 150 mM NaCl and 1 mM β-mercaptoethanol after excitation by 40 fs 266 nm pulses. **(B)** Normalized time-resolved absorption spectra for 0.6, 4 and 3400 ps extracted from the dataset shown in (A). The final non-decaying spectrum (green) shows a discrete peak at 425 nm characteristic of a photoproduct. **(C)** Two dimensional map of time- and wavelength-resolved transient absorption data of 50 mM Tris-HCl pH 7.5, 150 mM NaCl and 1 mM β-mercaptoethanol after excitation by 40 fs 266 nm pulses. **(D)** Normalized time-resolved absorption spectra for 0.6, 4 and 3400 ps extracted from the dataset shown in (C) to show the artefact that is due to solvated electron species.

As reference for the measurements of UVR8 and to establish the experimental setup, transient absorption spectra of tryptophan in solution were recorded (Fig 6-6 A and B). At all time delays and wavelengths, the observed signal is positive. Excited state absorption (ESA) of tryptophan is responsible for the peak centred around 375 nm at 0.6 ps (Fig 6-6 B). Within a few picoseconds a broad absorption rises in the red and an absorption band centred at 450 nm is attributed to an ESA, which clearly appears as a shoulder in the 420 to 470 nm range. At later delays towards the end of the time range of the experiment (3.4 ns), a significant increase of absorption is observed at 425 nm, while the UV ESA at wavelengths below 370 nm and the red one at 550 to 625 nm both decay. These findings are in agreement with studies by Sharma et al. (2010) and Leonhard et al. (2010). The absorption band centred at 425 nm is attributed to the primary photoproduct of tryptophan

responsible for fluorescence quenching. This photoproduct which accumulates up to 6 ns after excitation most likely displays a protonated indole, possibly in a triplet state (Leonhard et al., 2010). It has to be noted that at 266 nm excitation, the buffer/water itself displays a rather pronounced signal, probably a solvated electron species (Fig 6-6 C). This is visible in the raw data as a clear offset directly after excitation (Fig 6-6 D). The absorption peak centred at 370 nm decays within 0.9 ps and gives rise to a red absorbing species with a maximum of 2.5 mOD at 2 ps after excitation (Fig 6-6 C). Generally, this artefact can be taken as species immediately formed in the instrument response function which does not completely decay on the timescale of the experiment but notably gives an overall weaker signal than the studied samples.

Next, transient absorption states of the dark adapted dimeric wild-type UVR8 protein were recorded. Comparison between the raw data obtained for tryptophan in solution and UVR8 reveals clear differences between the two samples (Fig 6-6 A, 6-7 A and C). For UVR8, the signal is also always positive but the main signal is situated at about 370 nm and decays within the time frame of the experiment. The spectrum obtained after 0.6 ps may be assigned to some pulse follower artefact similar to the buffer data or to a fast relaxing species, similar to tryptophan in solution (Fig 6-7 B). Subsequently, a broad absorption over the whole measured wavelength range rises but with a discrete absorption band at 375 nm. This spectrum is clearly different from the one obtained for tryptophan in solution in respect to the ratio between absorption in the UV and the blue part of the spectrum. For UVR8, the intensity is highest for the UV wavelengths. The final non-decaying spectrum recorded at 3.4 ns after excitation is clearly distinct from the previous ones and displays a rather broad peak at 450-460 nm. The shape looks similar to what has been observed for the primary photoproduct formed by tryptophan but is clearly red shifted. The spectrum is noisier than for tryptophan in solution due to experimental restraints caused by slow regeneration of UVR8 after excitation but similar unstructured absorbance is observed ‘framing’ the main peak. Furthermore, the discrete blue shoulder at 360 nm seems to be absent in UVR8 in the final non-decaying spectrum. To be able to monitor the oligomerisation state of UVR8 during the experiment, a fraction of the sample was taken after each scan (63 time points, ~3 min) and its fluorescence maximum was measured. Only two scans were possible on the dimer sample before a clear red shift of the fluorescence spectrum indicated monomerisation of the protein.

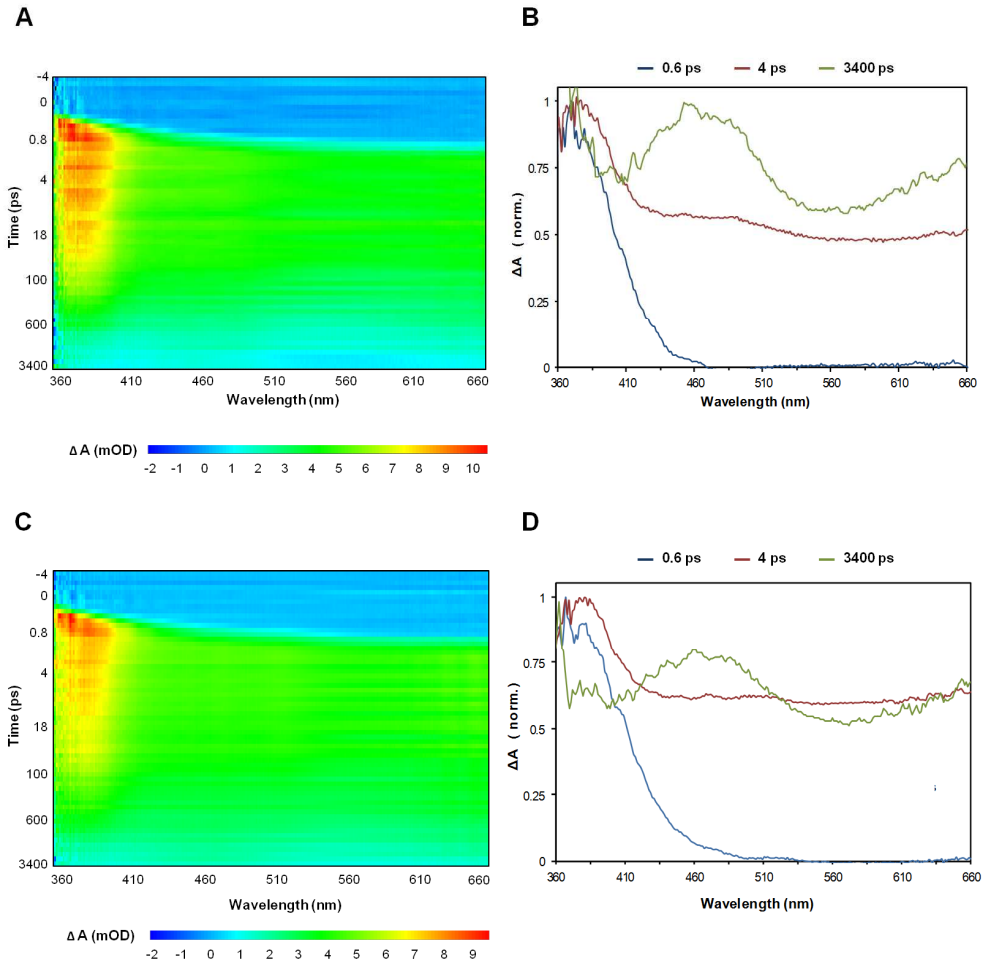

FIGURE 6-7: Excitation of the UVR8 dimer and monomer with 266 nm pulses generates a long lived photoproduct. (A) Two dimensional map of time- and wavelength-resolved transient absorption data of dimeric wild-type UVR8 after excitation by 40 fs 266 nm pulses. **(B)** Normalized time-resolved absorption spectra for 0.6, 4 and 3400 ps extracted from the dataset shown in (A). The final non-decaying spectrum (green) features a broad absorbance centered around 450 nm. **(C)** Two dimensional map of time- and wavelength-resolved transient absorption data of monomeric wild-type UVR8 after excitation by 40 fs 266 nm pulses. **(D)** Normalized time-resolved absorption spectra for 0.6, 4 and 3400 ps extracted from the dataset shown in (C). The final non-decaying spectrum (green) is shifted by about 10 nm to the red compared to the UVR8 dimer.

Time-resolved absorption spectra recorded on the monomeric wild-type UVR8 protein look very similar to what has been seen for the dimeric form (Fig 6-7 C and D). A direct comparison of the two final non-decaying species suggests that the peak observed at 450-460 nm in the dimer undergoes a small red shift and is centred rather at 470 nm in the monomer (Fig 6-8 A). However, the broadness of the peaks hinders the precise assignment of the maxima and therefore this observation needs further experimental proof. Also the ratio between the peak and the red unstructured absorbance seems to be smaller in the monomer than in the dimer. Another small difference between dimer and monomer is revealed by comparison of the two kinetic traces of the samples at 460 nm (Fig 6-8 B). On the longer time scales (1 to 2 ns) a faster decay of the absorption of the dimer over the

monomer seems to be present. In the earlier times, the differences lie within the signal to noise ratio.

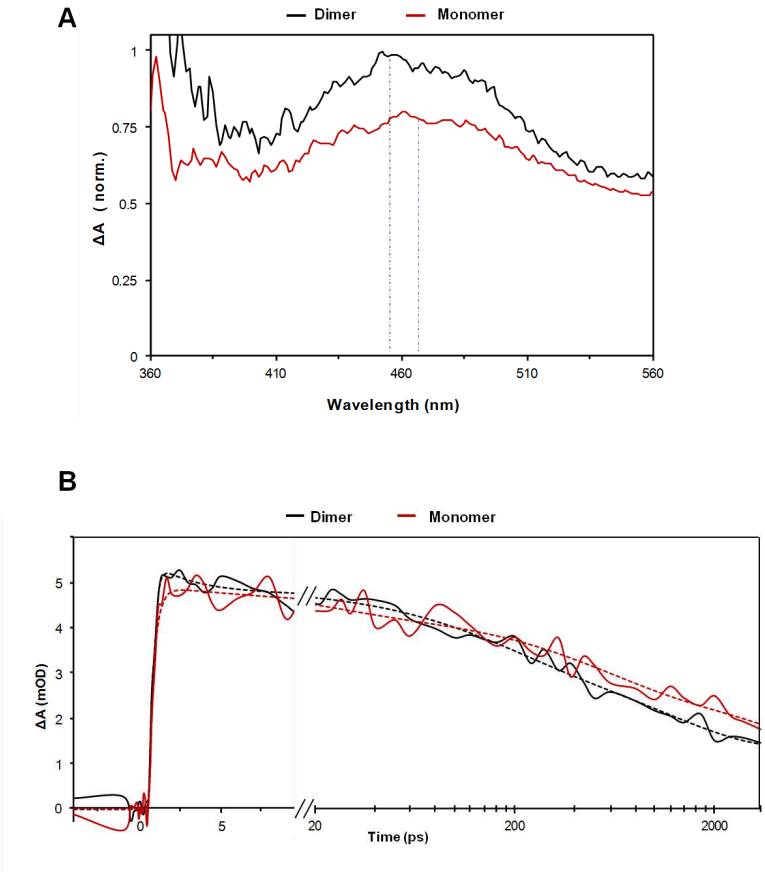

FIGURE 6-8: Comparison of the formed photoproduct between UVR8 wild-type dimer and monomer. (A) Normalized time-resolved absorption spectra recorded at 3400 ps after excitation with 266 nm for dimeric and monomeric wild-type UVR8. A small shift of about 10 nm to the red is visible between the two forms. **(B)** Kinetic trace at 460 nm of dimeric and monomeric wild-type UVR8. A faster decay of absorption can be observed in the dimer over the monomer on the longer time scales. The dotted lines represent the best fit of the data.

Overall, these preliminary results of the time resolved absorption spectroscopy demonstrate that the implemented experimental setup with the 266 nm excitation pulse allows analysis of initial steps of UVR8 photoreception. The fact that differences in the absorption spectra between monomer and dimer, even if very subtle, are visible encourages the follow-up and extension of these measurements.

6.6 Discussion

6.6.1 Detection of photoinduced changes in UVR8

Being able to express and purify recombinant UVR8 protein in *E. coli* in sufficient amounts has opened the way to study photobiophysical aspects of the photoreceptor. Structural and mechanistic parameters, determination of quantum yields and energetics as well as very early stages in signal transduction have especially been characterized for flavin based photosensors by utilizing FTIR spectroscopy and transient absorption spectroscopy (Losi, 2007). FTIR spectroscopy has also shown to be a very informative method to study the structure-function aspects in photosensitive proteins like bacteriorhodopsin (Rothschild, 1992) or photosynthetic reaction centres (Nabedryk, 1996). In fact, changes in the hydrogen bonding of even a single water molecule can be detected by FTIR spectroscopy, leading to elucidation of its functional importance (Kandori, 2004).
FTIR spectroscopy was therefore undertaken with UVR8 with the aim of identifying the catalytically important side chains and to deduce their environmental and structural changes as well as overall conformational changes of the receptor induced by UV-B. Overall, the obtained UV-B induced difference spectra of UVR8 can be regarded as a characteristic fingerprint of the conformational change taking place during photoreception. Two key observations of these initial experiments are that the signals seem to originate from the core of the protein (Fig 6-1 A) and most likely correspond to structural differences between monomer and dimer since no difference signal could be obtained for constitutively monomeric mutants, even if one of them is functional in transgenic Arabidopsis lines.
The particular assignment of absorption bands of the presented spectra is hampered by the fact that overlapping bands limit the information that can be deduced from a spectrum. For example, most known vibrational features of tryptophan residues can be found all over the spectral region that was analysed (Barth, 2007). Unfortunately, the direct comparison between spectra recorded in H_2O and D_2O revealed that the overall shape of the band pattern in the region of 1700 to 1300 cm^{-1} did not change much upon deuteration (Fig 6-1 B). Likewise, the studied mutants only showed subtle changes compared to wild-type which complicates tentative band assignments even further (Fig 6-2). Of the many amino acid side chain absorption bands, polar amino acids display the strongest absorption coefficients and therefore cause the most pronounced signals due to vibration of the polar groups (Barth and Zscherp, 2002). The high abundance of polar amino acids in UVR8, especially at the dimer interface, where structural and chemical changes are expected

during UV-B perception, therefore poses a great challenge on the interpretation of UVR8 FTIR spectra. Absorbance of most of the polar groups overlaps with the amide I band of the polypeptide backbone (1610-1700 cm^{-1}) which is the region of the UVR8 difference spectrum that shows the most pronounced peaks. To be able to differentiate between these signals, further experiments are required. One possibility is to either uniformly label the protein with ^{13}C or ^{15}N (Haris et al., 1992), label all amino acids of one type or even site-directed labelling of one particular amino acid to induce shifts of certain bands (Sonar et al., 1994). For example the labelling of backbone carbonyls with ^{13}C shifts the amide band by 36 to 38 cm^{-1} to lower wavenumbers, possibly allowing identification of then no longer overlapping signals (Haris et al., 1992). Also, time-resolved IR spectroscopy is a powerful tool that can reveal many of the dynamic structural details of chromophores involved in photobiological reactions and can reveal the response of those parts of the protein that are affected by the ongoing reactions (Groot et al., 2007). Such future approaches will contribute to our understanding of structure-function relationships of UVR8 and hopefully will elucidate how aromatic amino acids can act as intrinsic chromophores and induce signalling.

6.6.2 Changes in the local environment of tryptophans during UV-B photoreception

The detailed analysis of intrinsic protein fluorescence is a challenging task due to the complexity of tryptophan fluorescence. The presence of multiple fluorophores especially in UVR8 makes it almost impossible to allocate observed changes to certain residues or fluorophores. The actual situation is even more complex since tryptophan displays complex spectral properties due to the presence of two overlapping electronic states, ^1L_a and ^1L_b (Lakowicz, 2006). It is now accepted that even for single-tryptophan proteins the emission often contains multiple spectral contributions due to either multiple conformations or the intrinsic heterogeneity of tryptophan itself (Lakowicz, 2006).

UV-B perception is clearly coupled with chemical and/or conformational changes around the chromophore since excitation with UV-B causes a red shift of the emission spectrum of UVR8 wild-type protein (Fig 6-3). The maximum wavelength of tryptophan emission is sensitive to its local environment ranging from 308 nm in azurin, a copper-containing enzyme from denitrifying bacteria to 355 nm for example in glucagon (Vivian and Callis, 2001). The red shift indicates that the chromophore, which is formed by the tryptophan pyramid, is no longer buried in a “non-polar” environment but becomes solvent exposed in the process of UV-B induced monomerisation. The observed variability of maximum

emission wavelengths among the salt bridge mutants compared to wild-type demonstrates the sensitivity of tryptophan fluorescence to its local environment (Fig 6-4). Small motions of the amino-acid side chains or backbone due to the introduced mutation can result in changes in tryptophan emission and some of these motions may occur during the excited-state lifetime. The already slightly red shifted emission spectra of dark adapted UVR8^{D96N} and UVR8^{D107N} compared to wild-type strengthen the observation of a weakened dimer as described in Chapter 3. A weakened dimer is expected to expose the chromophore/fluorophore, which is normally shielded through the effect of dimerisation, more to solvent creating a more polar environment and therefore altering the emission properties of the tryptophans. The further red shifted emission spectrum of the monomeric mutant UVR8^{R286A} confirms that in a monomer the chromophore/fluorophore is solvent exposed and that the rather drastic mutation of R286 to alanine also alters the arrangement of the tryptophans in the pyramid resulting in a different emission maximum. The presence of UV-B induced changes in the emission maximum of this mutant suggests that UV-B perception is still somehow possible. This ties in with the results for this mutant obtained from limited proteolysis experiments where differences in the banding pattern before and after UV-B exposure also suggest UV-B responsiveness even if the mutation leads to a non-functional form of UVR8 in vivo (Chapter 4). It is, however, remarkable, that this mutant has lost the ability to recover from the UV-B response back to the dark state since the emission maximum does not shift back nor does the increase in emission reoccur after a sufficient recovery period (Fig 6-5).

The initial increase of emission measured at 335 nm followed by a slow decrease in emission after prolonged UV-B exposure of the protein has been reported before for UVR8 (Fig 6-3; Wu et al., 2012). There, the emission maximum is reached earlier, but this is most likely due to higher excitation energies, which are not clearly stated by Wu and co-workers. The authors also rather insufficiently attribute the rise of emission to saturation of UV-B perception and the decrease of the signal to fluorescence quenching (Wu et al., 2012). Nevertheless, this method allowed them to identify W285 and W233 as the main chromophores since these mutants no longer showed an increase in fluorescence induced by UV-B. This is in agreement with what has been reported by Christie et al. (2012), where far-UV CD spectroscopy was used as the method of choice to determine the main chromophores. The variability of fluorescence lifetimes and quantum yields of tryptophan residues in proteins is affected by several factors such as quenching by proton transfer from nearby charged amino groups or by electron acceptors such as protonated carboxyl groups or by resonance energy transfer among tryptophan residues (Lakowicz, 2006).

These interactions are strongly dependent on distance, especially the rate of electron transfer, which decreases exponentially with distance and therefore UV-B induced changes in UVR8 conformation are responsible for changes in the emission properties. Different conformations of a protein may each display a different quantum yield. For UVR8, the emission intensities of the monomer are higher (raw data, not shown). However, it should be noted that the red shift of the emission spectrum that has been attributed to monomerisation is completed earlier then when the maximum of emission is reached. This suggests that UVR8 once it has reached its monomeric form undergoes further changes which are responsible for the rise of emission. Whether this effect is functionally important or only due to an in vitro artefact remains to be investigated more closely.

To summarize, the currently limited understanding of the UV-B perception mechanism impedes a detailed analysis of UVR8 intrinsic fluorescence. However, these findings might hopefully supplement and tie up with observations from future experiments and are one way of monitoring changes in the local environment of the chromophore.

6.6.3 The primary events of UV-B perception in UVR8

The initial photochemical events of blue light photoreceptors including BLUF (blue light sensing using FAD), LOV and CRY proteins have been extensively studied and have revealed events such as proton-coupled electron transfer and intersystem crossing and have defined roles for tryrosines and tryptophans as intrinsic electron donors (Gauden et al., 2006; Kennis et al., 2003; Giovani et al., 2003). Those blue-light photoreceptors utilize flavin as chromophore and photoexcitation of flavins rapidly induces the formation of singlet and triplet excited states, which can induce direct electron transfer from nearby tryptophans or tyrosines as seen for cryptochromes and the related photolyases (Aubert et al., 2000; Zoltowski and Gardner, 2011). For UVR8, the initial situation is highly different due to its intrinsic chromophore. To address the hypothesis that electron transfer may occur between the photoreceptive tryptophans and adjacent salt-bridging arginines, ultrafast transient absorption studies of wild-type UVR8 and of tryptophan in solution have been performed.

One of the first objectives therefore was to determine whether a tryptophan radical is formed following a pulse of UV-B. The absorption maximum for tryptophan radicals is dependent on the local protein environment but can be attributed to the wavelength region between 500 and 600 nm (Solar et al., 1991; Miller et al.; 2003, Shafaat et al., 2010). The oxidation reaction of tryptophan is complex because it is often accompanied by the loss of a proton under physiological conditions (Solar et al., 1991). The broadness of the observed

signal after excitation with 266 nm makes it difficult to clearly assign a formed species to a photochemical event (Fig 6-7). The detection of a long-lived photoproduct at about 460 nm is so far the strongest indication that specific photochemistry is happening, and the 460 nm species may be related to the reaction coordinate that leads to monomerisation. The fact that a similar product, also slightly red shifted, is observed in the monomer as well does not mean that it is not coupled to the physiological reaction. It is not uncommon that 'dark' and 'light' states have similar primary photoproducts such as for example in BLUF domains (Mathes et al., 2012). Another indication for the successful establishment of a system with adequate excitation energy that can be used for further studies is the observed difference in the lifetimes of the formed species at 460 nm for dimer and monomer at the longer timescale (Fig 6-8). However, a detailed explanation of these findings will require further investigation. Future experiments should include measurements on a nanosecond to millisecond timescale on a flash photolysis set up to analyse what happens with the photoproduct absorbing at 460 nm, which currently does not decay within the experimental timescale of 3.4 ns.

A major difficulty that UVR8 poses on the pump-probe setup is its slow regeneration rate once it has been monomerised. Large amounts of protein are required to be able to accumulate and average a number of measurements on the dark state to improve the signal to noise ratio especially of the rather weak signal at 460 nm. Another difficulty of UVR8 that has already been mentioned in the discussion of UVR8 fluorescence properties is the exceptionally high abundance of tryptophans in the protein that restrain the assignment of an observed signal to a single residue. Transient absorption spectra of tryptophan mutants might allow a clearer assignment and uncover possible distinct peaks that are lost within the broad overall signal. A number of the conserved tryptophans seem to be not required for UVR8 function in plants (O'Hara and Jenkins, 2012) and a multiple tryptophan mutant, assuming no gross structural alterations are introduced by the mutation might be worth investigating.

It will be interesting to define a more precise role for the 'perimeter fence of tryptophan' and tyrosine residues present at the dimer interface that is proposed to shield the tryptophan pyramid from solvent. Possibly, the tyrosines could act as electron donors in a long range electron transfer process at the dimer interface. Electron transfer from tyrosine to a tryptophanyl radical has been demonstrated as an essential step in the process leading to the active form of photolyases (Aubert et al., 1999). Tyrosine radicals can be identified by their characteristic absorption spectra with a maximum at 410 nm. Additionally, the analysis of arginine mutants might shed further light on the UV-B reception mechanism

and might show whether the hypothesis of electron transfer between the tryptophan pyramid and the arginines can be sustained.

The biophysical experiments presented in this chapter can be regarded as an initial step towards elucidation of the UV-B perception mechanism and the primary events after light absorption. Even if the preliminary conclusions have to be confirmed and extended, the experimental conditions required for UVR8 for those methods have been established and can be exploited in the future.

7. FINAL DISCUSSION

7.1 Introduction

UV-B radiation is an integral component of natural sunlight with a strong impact on terrestrial ecosystems (Jansen et al., 1998; Paul and Gwynn-Jones, 2003). For plants, UV-B acclimation and UV-B stress tolerance is essential for survival and requires perception of UV-B radiation. Only recently, UVR8 has been identified as the UV-B photoreceptor in Arabidopsis (Rizzini et al., 2011). UVR8 specifically regulates the expression of numerous genes that underpin photomorphogenic responses to UV-B which ultimately lead to UV protection and acclimation (Ulm et al., 2004; Brown et al., 2005; Favory et al, 2009). Hence, *uvr8* mutant Arabidopsis plants, which fail to express these genes, are highly sensitive to elevated levels of UV-B (Kliebenstein et al., 2002; Brown et al., 2005). Although the importance of UVR8 and the transcriptional events necessary for plant survival are characterised (Kliebenstein et al., 2002; Brown et al., 2005), little is yet known about the structural properties of the photoreceptor itself, especially its mechanism of signal perception and its activation in response to UV-B. Therefore, a structure-function study of Arabidopsis UVR8 was carried out to extend our knowledge about the early events involved in UV-B perception and induction of UV-B mediated signalling of UVR8. Structure-function studies were accomplished in vivo as well as in vitro and revealed a number of key points in regard of the photochemistry, signal transduction and regulatory mechanisms of UVR8 which will be discussed in the following sections.

7.2 The salt bridge network and the tryptophan pyramid

In the absence of UV-B, UVR8 forms a highly stable homodimer that is considered to be the ground state of the photoreceptor (Rizzini et al., 2011; Heijde and Ulm, 2012). The crystal structure of UVR8 revealed that dimerisation is achieved via an extensive salt bridge network that spans across the dimer interface (Christie et al., 2012; Wu et al., 2012). The positively charged residues that participate in the cross-dimer salt bridges are almost exclusively arginines. Their presence in the evolutionarily conserved and repeated motif GWRHT, that comprises the postulated UV-B perceiving tryptophans, singled arginines out as first choice for a site-directed mutagenesis approach to investigate the importance of ionic interactions in maintaining the UVR8 dimer. Results obtained by size exclusion chromatography and far-UV CD spectroscopy of purified protein (Chapter 3) and RT-PCR

experiments to test UV-B induced *HY5* and *CHS* gene expression in generated transgenic Arabidopsis lines (Chapter 4) showed that R286 plays a major role in the UV-B perception mechanism of UVR8. R286 forms two central cross-dimer salt bridges via D96 and D107. Disruption of these salt bridges by either mutation of R286 to alanine or simultaneous replacement of the two aspartic acids by asparagines causes constitutive monomerisation of the photoreceptor. Interestingly, analysis of the two monomeric mutant proteins UVR8^{R286A} and UVR8$^{D96N/D107N}$ in vitro did not reveal major differences between the two mutants. However, in vivo, GFP-UVR8$^{D96N/D107N}$ is functional in the UV-B response whereas mutation of R286 to alanine leads to a non-functional form of the photoreceptor. These findings suggest that dimerisation is not essential for UV-B perception but nevertheless activation of the photoreceptor requires a positively charged residue in position 286. This ties in with the observed functionality of the UVR8^{R286K} mutant.

Constitutive monomerisation was only observed for one other salt bridge mutant, UVR8^{R338A}, although here higher ionic strength was necessary to shift the dimer-monomer equilibrium towards the monomer. In vivo, the mutation resulted in a non-functional form of UVR8. Disruption of various other cross-dimer salt bridges by mutation of arginine to alanine had less severe effects on dimerisation and functionality of the photoreceptor. Even if UVR8^{R146A} forms a destabilized dimer, its functionality is not impaired by the mutation. Similarly, dimerisation is still possible in the UVR8^{R200A} and the UVR8^{R354A} mutants (Wu et al., 2012). Those three salt bridges are situated distant from the postulated tryptophan perceiving pyramid, whereas R286 and R338 directly flank the remarkable arrangement of tryptophans. The close proximity and the coupling of arginines and tryptophans suggest a specific mechanism whereby photoreception leads to monomerisation. One major task for the future will be to understand the precise interplay between tryptophans and arginines during UV-B perception and to unravel the mechanism of cross-dimer salt bridge breaking. The proposed excited electron transfer from tryptophans to arginines leading to charge neutralisation (Christie et al., 2012) might also be coupled to excited state proton transfer which allows the tryptophan indole ring to carry a positive charge and thus to completely destroy the cation-π interactions which stabilise the salt bridge (Wu et al., 2012). Therefore Wu and co-workers hypothesize that D129, E182 and R234, which are located in close proximity to W233 and W285, might serve as proton donors. However, to be able to describe in detail which residues are involved in UVR8 signalling, an atomic resolution structure of the UV-B illuminated state is needed to reveal UV-B induced changes. Attempts to produce monomeric crystals of UVR8 have been made, but the ability of the

photoreceptor to revert back to the ground state in the absence of UV-B has impeded the process (unpublished data; Wu et al., 2012).

Light induced electron transfer has been described before as being crucial for photoreceptor activation. For the blue light photoreceptor cryptochrome, transient absorption spectroscopy has revealed that the primary light reaction involves intraprotein electron transfer through a chain of three conserved tryptophan residues (trp-triad) to the excited FAD cofactor (Giovani et al., 2003). However, a recent study by Li and co-workers (2011) has shown that mutation of all tryptophans in the triad in CRY2 resulted in loss of photoreduction activity in vitro but retained the physiological and biochemical activities in vivo. Even if the cryptochrome family has been discovered about 20 years ago, the photoreceptor's primary light reaction is still not understood (Liu et al., 2010). The complete elucidation of such a mechanism is a difficult and challenging undertaking and the above mentioned study shows that data obtained in vitro of recombinantly expressed protein has to be carefully assessed in vivo. The availability of in vivo data of a large number of transgenic Arabidopsis UVR8 mutant lines generated in this and previous studies (O'Hara and Jenkins, 2012) can be exploited in the future in combination with further biophysical studies to stepwise reveal the UV-B perception mechanism of UVR8.

7.3 UV-B induced monomerisation

The fact that the active signalling state of UVR8 is formed by the monomeric form of the protein clearly distinguishes UVR8 from other so far described dimeric photoreceptors, such as phytochromes, cryptochromes and phototropins, which remain in their dimeric conformation even if activated by light (Sharrock and Clack, 2004; Sang et al., 2005; Salomon et al., 2004). However, experimental evidence gathered so far is insufficient to explain how UV-B perception results in a functional monomer that can bind COP1 and initiate signalling. The data presented here suggest that there may be several steps involved: First, a conformational change resulting from photoreception because constitutive interaction between UVR8 and COP1, as seen with a number of the arginine mutants (Fig 4-4) still requires UV-B for activation of the UVR8 signalling pathway; second, a conformational change that alters/activates the C-terminus, as seen by limited proteolysis experiments, and finally monomerisation per se. Each of these appears necessary but neither is sufficient to initiate signalling. The constitutive interaction between the monomeric mutant GFP-UVR8$^{D96N/D107N}$ and COP1, which still requires UV-B for the induction of UVR8-mediated signalling, is the strongest evidence so far that

UV-B induces conformational changes beyond monomerisation. So far it has been difficult to assess the functional and non-functional constitutive monomers more closely, because methods that have been successful in analysing wild-type UVR8 such as far-UV CD spectroscopy or FTIR require dimer to monomer transitions to generate an informative signal, which is obviously absent in constitutively monomeric mutants. Similarly, tryptophan fluorescence signals are dominated by monomerisation effects making it difficult to distinguish overall monomerisation from structural and conformational changes arising from photochemical activity and from those in the C-terminus that presumably lead to COP1 binding and subsequent UVR8 function.

The discovery of the constitutively monomeric but still UV-B responsive functional mutant GFP-UVR8$^{D96N/D107N}$ poses the question whether monomerisation may be considered only as side effect of UV-B induced conformational changes especially of the C-terminus. Interestingly, preliminary structure-function studies of a UVR8 ortholog of lower plants show a similar behaviour in respect to monomerisation and functionality of the protein as observed for the Arabidopsis UVR8$^{D96N/D107N}$ mutant. Western Blot analysis of the UVR8 ortholog of *Physcomitrella patens* (A9RS92) expressed in yeast reveals constitutive monomerisation of the protein even in the absence of UV-B (Rizzini, Ph.D. thesis, 2010). Sequence comparison of the two orthologs shows that all residues that participate in the dimer maintaining salt bridge network of UVR8 in Arabidopsis are also present in the *P. patens* ortholog (Fig 4-1) and dimerisation is therefore theoretically possible based on the conserved protein sequence. As seen for the Arabidopsis UVR8$^{D96N/D107N}$ mutant, the possibly monomeric form of UVR8 of *P. patens* is able to complement the *uvr8-8/Pro$_{HY5}$:Luc*$^{+}$ mutant phenotype in stable transgenic Arabidopsis lines since UV-B responsiveness of the luciferase reporter driven by the *HY5* promoter could be detected (Rizzini, Ph.D. thesis, 2010). At present no data is available about the dimer-monomer state of the *P. patens* UVR8 in moss itself or the transgenic Arabidopsis lines expressing the UVR8 ortholog.

However, if the preliminary data of the yeast expression study can be confirmed in vivo, *P. patens* UVR8 will be a highly interesting ortholog for future studies and especially for elucidation of the UV-B perception mechanism. In general, relatively little is known so far about the molecular response of bryophytes to UV-B radiation. The *P. patens* genome encodes two UVR8 orthologs, two HY5 orthologs as well as several COP1 orthologs that constitute a multigene family (Richardt et al., 2007; Rensing et al., 2008; Wolf et al., 2010). The presence of these main players therefore theoretically allows UV-B signalling via the UVR8-COP1-HY5 pathway. A better understanding of the UV-B response and its

regulation in *P. patens* might provide a better understanding of the role of UVR8 dimerisation in Arabidopsis and other higher plants. Furthermore, due to its position in the evolutionary tree between aquatic algae and vascular plants, studies of UV-B photoreception of *P. patens* might also unravel the evolutionary aspects of UV-B tolerance and acclimation that laid the ground for land plant evolution. Comparison of the UVR8 ortholog of *P. patens* to the orthologs of UVR8 of two representatives of green algae, i.e. *Volvox carteri* and *Chlamydomonas reinhardtii*, reveals absence of the C-terminus in the latter two species. Presence of the C-terminus has been described as essential for COP1 binding to initiate UVR8 signalling (Cloix et al., 2012) and if UVR8 is functional in *V. carteri* and *C. reinhardtii*, this raises the question whether UVR8 can function via a so far unknown mechanism that does not require the C-terminus.

7.4 The UVR8-COP1 interaction

It has been shown in various ways that UVR8 and COP1 interact directly and specifically in a UV-B dependent manner (Favory et al., 2009; Rizzini et al., 2011). However, the UV-B specificity of the interaction gets lost if mutations of salt bridges either result in a destabilized, weakened UVR8 dimer or a constitutive monomer. Constitutive interaction of for example GFP-UVR8^{R286K} and GFP-UVR8^{D96N}, two destabilized dimers, with COP1 has been observed, but the interaction was insufficient to induce UVR8-mediated signalling in the absence of UV-B. To allow COP1 binding, the introduced point mutation at the interface must somehow alter the conformation of the C-terminus of UVR8 to expose its binding site. The most convincing explanation for this behaviour would be that destabilization of the dimer partially releases the C-termini from their inaccessibly dark state position, but they remain in their inactive conformation because UV-B is absent. However, SAXS experiments locate the missing C-termini at the distal ends of the dimer (Christie et al., 2012) suggesting no direct contact between the interface and the C-termini thus making it difficult to understand how opening up of the dimer interface influences the distant C-termini. The observation that COP1 can interact with destabilized dimers nevertheless supports the hypothesis that stable homodimerisation in the absence of UV-B is one mechanism that prevents uncontrolled interaction between UVR8 and COP1 which might negatively influence other COP1 mediated responses in the plant.

To further understand the direct interaction between UVR8 and COP1, two crucial points have to be investigated in the future. Firstly, the localisation and conformation of the C-terminus has to be defined for the dark state dimer and for the UV-B activated

monomeric form as already discussed in Chapter 4. Secondly, it will be important to narrow down the region of interaction between UVR8 and COP1 by identifying specific residues in the C27 region that are required for COP1 binding. Since COP1 interacts with a number of proteins in plants, it is not unlikely that motifs identified for the interaction in those proteins might be present in UVR8 as well. Holm and co-workers (2001), for example, identified a motif in HY5 and two other COP1-interacting proteins, STO and HOMOLOG OF STO (STH), that is responsible for interaction with the WD40 region of COP1 through both hydrophobic and ionic interactions. This motif (VPE/D-hydrophobic residue-G with several upstream negatively charged residues) is partly conserved in the C27 region of UVR8 (VPDETG with one upstream glutamate residue) and could be involved in the interaction with COP1. Interestingly, site-directed mutagenesis and subsequent yeast two-hybrid analysis of the HY5 and STO/STH mutants showed that the negatively charged glutamic or aspartic acid residue present in the conserved motif forms a salt bridge with a lysine residue in COP1 which is essential for the interaction (Holm et al., 2001). With respect to UVR8, the UV-B exposed interface would provide several residues that could participate in new salt bridges to either stabilise the activated C-terminus or also to mediate COP1 binding. So far it has not been investigated whether any kind of interaction between COP1 and the exposed dimer interface is formed, which though would have to be mediated by the C-terminus otherwise COP1 binding would be observed in GFP-ΔC27UVR8 mutant plants. One highly speculative scenario would be that COP1 becomes more or less clamped between the interface and the C-terminus in the UV-B activated monomer. Such a scenario would offer an explanation why the constitutively monomeric mutant GFP-UVR8^{R286A} is unable to bind COP1 in the absence of UV-B hypothesizing that the positive charge of R286 is required at the interface for the formation of a new salt bridge. In any case, more data has to be acquired to fully understand the structural requirements for the UV-B induced interaction between UVR8 and COP1 which is essential for the induction of gene expression by UVR8.

7.5 Integration of signals from different photoreceptors by COP1

COP1 does not only play a role in the UV-B response but also acts downstream of phytochromes and cryptochromes thus forming one of the central components of light signal transduction in plants. COP1 therefore enables crosstalk between the different photoreceptor responses and allows integration of the UVR8 signalling pathway with visible light photoreceptor pathways. It is remarkable that COP1 interacts with various

photoreceptors, but the molecular output of each interaction seems to be different (Lau and Deng, 2012). It is especially intriguing how COP1 can act as a positive regulator in the UV-B and phyB responses whereas it has long been known as a negative regulator of photomorphogenesis due to its E3 ubiquitin ligase activity (von Arnim et al., 1997). So far the specific function of COP1 in the UV-B response still remains elusive. COP1 is required in the nucleus to initiate signalling of the UVR8 pathway by direct interaction with the photoreceptor. COP1 is stabilised and accumulates in the nucleus following UV-B exposure in a UVR8-dependent manner, suggesting that COP1 is active in the nucleus (Favory et al., 2009). Nuclear accumulation of COP1 is also observed in white light supplemented with UV-B (Oravecz et al., 2006), which contrasts the previous dogma of COP1 nuclear exclusion in response to light and suggests that during the day, as soon as UV-B is present, COP1 starts to accumulate in the nucleus or rather remains in the nucleus. It has to be noted that nuclear enrichment of COP1 under supplemental UV-B is a rather slow process taking approximately 24 h, but it takes about the same time as nuclear exclusion in the dark-to light transition (Oravecz et al., 2006; von Arnim and Deng, 1994).

So far nothing is known about a potentially differential regulation of COP1 in the nucleus, which seems to be required under natural light conditions since HY5 protein can accumulate under UV-B, even though COP1 is present. The UV-B mediated interaction between UVR8 and COP1 implies that the physical association of the two proteins contributes to the specific activity of COP1 in UV-B signalling. One could hypothesise that interaction between UVR8 and COP1 represses the E3 ubiquitin ligase activity of COP1 and therefore HY5 protein can accumulate in the nucleus. This is supported by the fact that UVR8 and HY5 both bind to the WD40 domain of COP1 (Cloix et al., 2012; Holm et al., 2001) and depending on light conditions one might show higher affinity than the other. A direct competition between UVR8 and COP1 would be possible if the in motif HY5 that binds COP1 proves to be also essential for UVR8-COP1 interaction.

The recently discovered rapid down-regulation mechanisms of COP1 activity by cryptochromes (Lian et al., 2011; Liu et al., 2011; Zuo et al., 2011) highlights the importance of COP1 being part of a multimeric protein complex and also allows speculation whether a similar molecular mechanism of COP1 down-regulation can be assigned to the UV-B and also the phytochrome receptor pathway. Even if COP1 can ubiquitinate targets on its own in vitro, it forms a protein complex of about 700 kDa in vivo (Saijo et al., 2003). This indicates that additional protein components may be required to regulate COP1 function in vivo. Examples are the COP1 interacting SPA proteins, which have the ability to regulate the E3 ubiquitin ligase activity of the COP1 complex

since CRY1 mediated disruption of the SPA-COP1 interaction inhibits the activity of COP1 leading to accumulation of HY5 during de-etiolation (Lian et al., 2011; Liu et al., 2011). It will be interesting to determine how exactly SPA proteins modulate the activity of COP1 and whether UVR8 or other so far unidentified COP1 and UVR8 interactors can participate in a similar mechanism. One important aim for the future will be to integrate the knowledge about the various photoreceptor responses initiated by different light qualities to gain a complete picture of how light signalling pathways are controlled under natural sunlight when all light qualities are present.

7.6 Regeneration of the photoreceptor

A further important aspect of UVR8-signalling that was investigated in this study was how the initial dimeric state of the photoreceptor is regenerated once UV-B is no longer present to induce monomerisation. By applying inhibitors of protein synthesis and inhibitors of proteasomal degradation to Arabidopsis plants, it has been shown that the UVR8 dimer is not regenerated by rapid de novo synthesis following degradation of the monomer. Instead, regeneration occurs by reversion from the monomer to the dimer. Furthermore, regeneration of the UVR8 dimer happens much more rapidly in vivo than in vitro with illuminated plant extract or purified UVR8 suggesting that the presence of intact cells is required. This process enables the photoreceptor to respond rapidly and sensitively to changes in ambient UV-B levels in sunlight to regulate photomorphogenic responses. The regeneration process was considerably slowed down but not prevented in absence of the C-terminus possibly because the C-terminus might interact with proteins that facilitate rapid reversion of the monomer.

A recent publication on UVR8 shows that the reversion from monomer to dimer is even slower if the two RUP proteins, RUP1 and RUP2, are absent, suggesting that they play a major role in this process (Heijde and Ulm, 2013). To allow redimerisation, the UVR8-COP1 interaction must be broken. In the *rup1rup2* mutant, interaction between UVR8 and COP1 can be detected at least four hours after the end of the UV-B treatment, which coincides with the slower reversion rate of the mutant (Heijde and Ulm, 2013). Moreover, no interaction between UVR8 and COP1 can be detected in RUP2 overexpressor lines, suggesting that RUP1 and RUP2 negatively regulate the UVR8-COP1 interaction (Heijde and Ulm, 2013). It is unknown yet, whether COP1 is released solely because of UVR8 redimerisation or whether competition between COP1 and RUP1/RUP2 for binding sites in the C-terminus of UVR8 might play a role as well. Although the C27 region is both

necessary and sufficient for interaction with RUPs and COP1, the observation that RUPs can bind UVR8 independent of UV-B and thus in its dimeric form could be one indication that RUPs and COP1 might not interact with UVR8 via precisely the same binding site. To gain a better understanding of this process it will be necessary to fine-map the RUP-UVR8 interaction site within the C27 region as already suggested for COP1.

Reversion from the monomer to the dimer thus allows regeneration of the initial ground state and switches off signalling. Since it has been shown that UV-B induced UVR8-mediated signalling is possible in the constitutively monomeric mutant GFP-UVR8$^{D96N/D107N}$, the question arises how the inactive ground state is restored in this mutant. The currently available methods to monitor changes in the UVR8 protein are not sufficient to investigate what happens in a functional constitutively monomeric mutant once it is no longer exposed to UV-B. Presumably, the C-terminus has to return somehow into its inactive conformation and possible changes in the tryptophan chromophore have to be reversed as well. Further experiments are essential to investigate whether these processes can also be achieved in this mutant or if they require dimerisation of the photoreceptor.

7.7 Conclusions

The following main conclusions can be drawn from the data presented in this study:

1. Ionic interactions are the dominating force to maintain the UVR8 dimer.
2. The positive charge of R286 adjacent to the tryptophan pyramid is essential for UVR8 dimerisation and in vivo function.
3. R338 is also important for dimerisation and function.
4. Mutation of any of the tested cross-dimer salt bridges leads to a weakened and destabilized dimer.
5. UV-B reception and a functional UV-B response can be mediated by a constitutively monomeric form of UVR8.
6. Constitutive monomerisation is not sufficient for a UVR8-mediated response in the absence of UV-B.
7. Constitutive interaction between UVR8 and COP1 still requires UV-B for UVR8 function.
8. UV-B not only induces monomerisation but also induces conformational changes of the C-terminus which are essential for a UVR8-mediated response.
9. The local environment of the tryptophan pyramid changes during UV-B photoreception.

10. Formation of a long lived photoproduct is part of the primary response of UVR8 to UV-B.
11. The UVR8 dimer is regenerated by reversion of the monomer to the dimer.
12. Dimer regeneration is much quicker in vivo then in vitro and requires intact cells.
13. The C-terminus, COP1 and protein synthesis in response to UV-B is required to maximize the rate of dimer regeneration.

Based on these conclusions, the current model of UVR8 photoreception and signalling can be extended by a number of aspects (Fig 7-1). Future work will show whether some of the assumptions incorporated into the presented model prove to be correct or whether they have to be reconsidered.

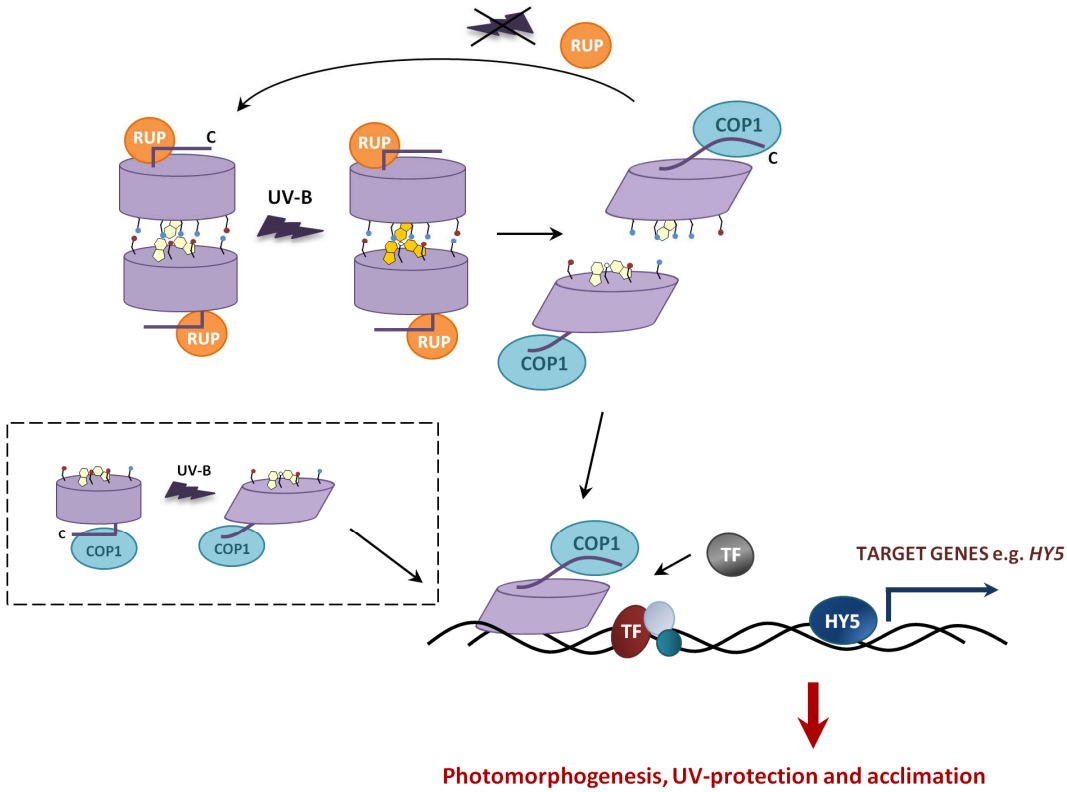

FIGURE 7-1: Proposed model of UVR8 photoreception and signalling.
UV-B is perceived by an excitonically coupled tryptophan pyramid (indicated by the three indole rings) which is in close contact to the cross-dimer salt bridges that maintain the UVR8 dimer in the dark state. Proposed electron transfer (yellow indole rings) between the tryptophans and adjacent arginines leads to charge neutralisation and destabilisation of the dimer. The photoreceptor undergoes conformational changes and exposes the C-terminus (C) leading to monomerisation. The UV-B activated monomer binds COP1. UVR8 associates with nucleosomes on chromatin in the region of target genes such as *HY5*. UVR8 is proposed to facilitate the activation or recruitment of transcription factors required for the UV-B induction of target genes that influence plant photomorphogenesis and lead to UV-protection and acclimation. Once UV-B is no longer present, the dimer is regenerated through reversion of the monomer. This process is mediated by RUP proteins, which can bind the UVR8 dimer as well as the monomer. **Box:** Perception of UV-B and initiation of signaling is still possible in a monomeric form of UVR8 (generated by mutation of the major salt bridge). Interaction with COP1 in the absence of UV-B is not sufficient for function.

7.8 Future Work

Even though our knowledge about the structure-function relationships of UVR8 in the UV-B signalling response has been extended by the data presented in this thesis and together with other published recent discoveries, many questions still need to be addressed in the future. Processes including the precise photochemistry and primary response of UVR8 to UV-B, subsequent signal transduction and especially regulatory mechanisms of the UV-B response have so far been insufficiently characterized and await further elucidation.

One main objective for future work on the structure-function studies of UVR8 will be to understand at the molecular level how UVR8 initiates signalling through interaction with COP1. To be able to define what conformational changes of the protein's C-terminus occur upon UV-B perception, at first the position and conformation of the C-terminus in the dark state dimer has to be determined. The best approach to examine the location of the C-terminus as well as conformational changes induced by photoreception will be by NMR spectroscopy studies of the protein. Solution NMR spectra of ^{15}N,^{13}C-labelled UVR8 samples will have to be recorded in the presence and absence of UV-B. This requires UV-B light delivery via fibre optics inside the NMR spectrometer which is possible, but not a standard feature of such instruments. Backbone resonance assignment of the C-terminal region will enable characterisation of the C-terminus dynamics through, for example, measurements of amide secondary chemical shifts, hydrogen exchange rates and ^{15}N relaxation parameters (Mittag and Forman-Kay, 2007). These measurements could identify which residues are highly dynamic and which associate with the globular core of UVR8. Furthermore it will be important to show how conformational changes produce an active monomer that can bind COP1. Therefore, once NMR spectroscopy has been established for wild-type UVR8, generation and comparison of atomic level structural data for some of the monomeric mutants generated in this study might reveal further information.

The number of known UVR8 interacting proteins is still very small and it is most likely that more downstream UV-B signalling components exist that directly associate with UVR8. Performance of a yeast two-hybrid screen under UV-B is one possibility to identify further UV-B dependent interactors. Further investigation of the binding site and binding conditions of the two RUP proteins is also required to better understand their role as negative regulators of the UV-B response and during the regeneration process. One of the first steps would be to narrow down the binding site of the RUPs as well as COP1 in the C27 region of UVR8. One possibility here would be the implementation of a synthetic

peptide array (Reineke et al., 2001). A series of peptides could be made from the C27 region in which each amino acid would sequentially be mutated to alanine. Those peptides would then be incubated with RUP or COP1 protein, either labelled with ^{35}S or with a tag that can be detected by an antibody. Subsequent autoradiography or immunoblotting should then reveal which alanine mutations prevent interaction of UVR8 with either COP1 or RUPs and the role of those residues could be examined further with various techniques, ultimately in vivo.

One aspect of UVR8 photoreception that has not been included in this study but also needs further investigation is the subcellular localisation of the photoreceptor. The precise mechanism of UV-B induced nuclear accumulation including the role of the N-terminus, and whether other proteins are involved has still not been established. Furthermore, BiFC experiments show that UVR8 can localise to discrete nuclear bodies/speckles (Favory et al., 2009) just like phytochromes and cryptochromes (Chen et al., 2003; Wang et al., 2001). Even if the general principles of nuclear body function and assembly are still largely unknown, their further investigation in respect to UVR8 is worthwhile. They might be involved in transcriptional regulation or might be associated with chromatin and could even serve as a hub for the interaction between the different light signalling pathways (van Buskirk et al., 2012). It is also unknown yet whether UVR8 plays a functional role in the cytoplasm or whether nucleo-cytoplasmic partitioning might play a role in the regeneration process.

Last, but not least, the in-depth elucidation of the molecular mechanism of UV-B reception via the tryptophan pyramid will provide a major challenge for biophysicists in the future. The proposed hypothesis of electron transfer between tryptophans and adjacent arginines needs to be tested further by spectroscopic methods and it will be interesting to see if any of the other conserved tryptophans play a role as well in the mechanism. Overall, future studies will hopefully reveal more unique and interesting details about UV-B photoreception by UVR8 and about the comprehensive control that sunlight exerts over plant growth and development.

APPENDIX

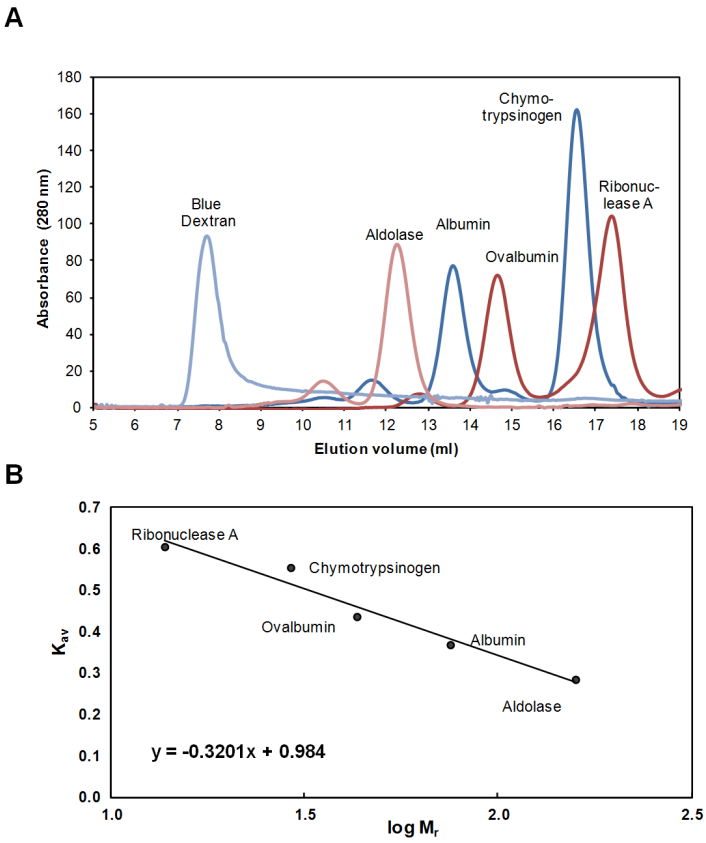

FIGURE A-1: Calibration curve for SEC column Superdex 200. (A) Elution profiles of aldolase, albumin, ovalbumin, chymotrypsinogen and ribonuclease A protein standards. Blue dextran was used to define the void volume of the column. **(B)** Sizes of UVR8 protein samples were calculated based on the calibration curve of the gel-phase distribution coefficient (K_{av}) vs. log of the molecular weight of the proteins : K_{av} ((V_e - V_o)/(V_c - V_o)) where V_o = column void volume, V_e = elution volume and V_c = geometric column volume.

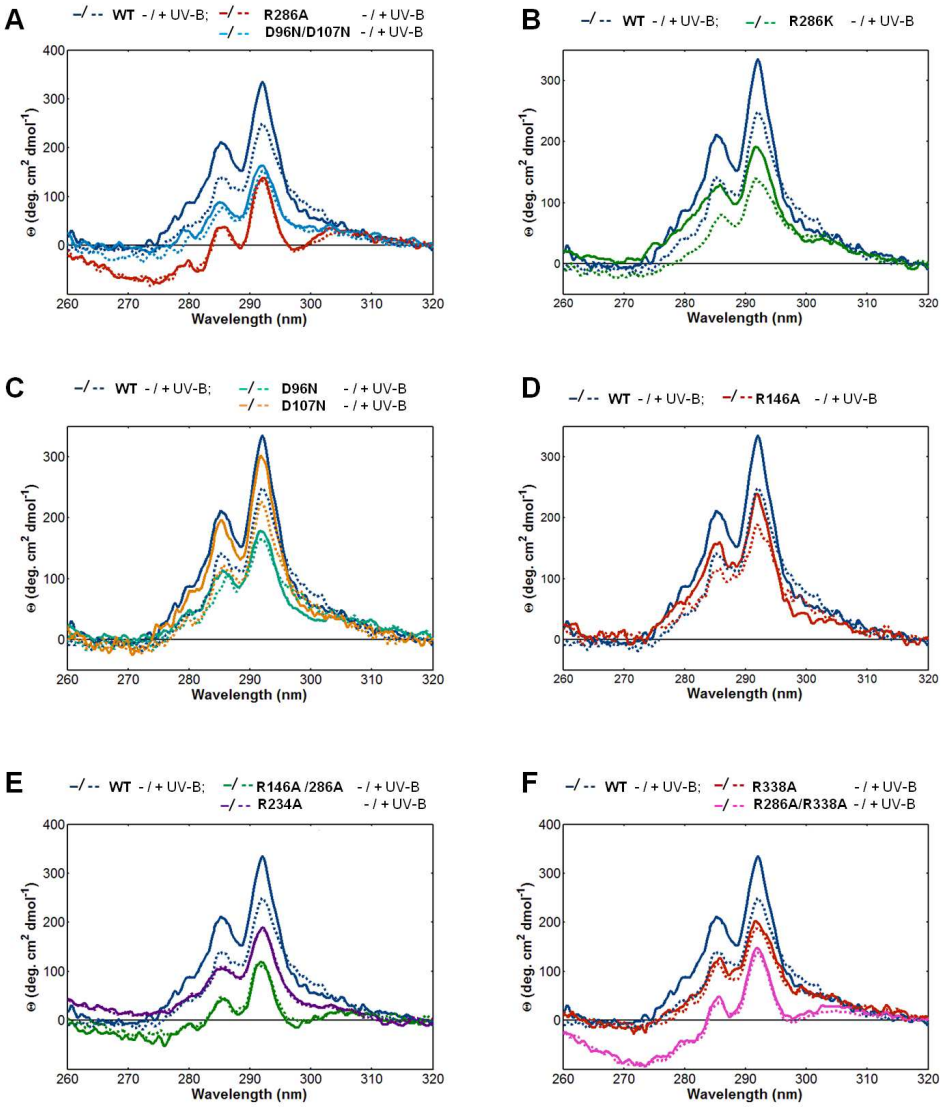

FIGURE A-2: Near-UV CD spectra of salt bridge mutants compared to wild-type UVR8. (A) Near-UV CD spectra of wild type UVR8 protein, $UVR8^{R286A}$ and $UVR8^{D96N/D107N}$ exposed or not (- UV-B, solid line) to 1.5 µmol m^{-2} s^{-1} narrowband UV-B for 1 h (+ UV-B, dotted line). **(B)** $UVR8^{R286K}$, **(C)** $UVR8^{D96N}$ and $UVR8^{D107N}$, **(D)** $UVR8^{R146A}$, **(E)** $UVR8^{R146A/R286A}$ and $UVR8^{R234A}$ and **(F)** $UVR8^{R338A}$ and $UVR8^{R286A/R338A}$ with same treatment as in (A).

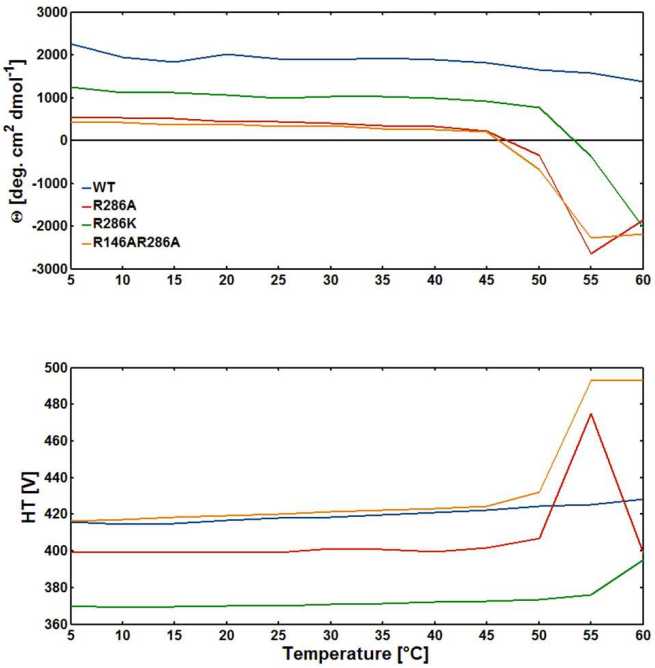

FIGURE A-3: Stability of wild-type UVR8 protein compared to dimeric mutant UVR8^{R286K} and monomeric mutants UVR8^{R286A} and UVR8$^{R146A/R286A}$. Thermal melt of UVR8 protein monitored by far-UV CD spectroscopy comparing the 234 nm peak characteristic of the exciton coupling between 5˚C and 60˚C.

REFERENCES

Ahmad M, Jarillo JA, Smirnova O, and Cashmore AR (1998) The CRY1 blue light photoreceptor of Arabidopsis interacts with phytochrome A in vitro. *Molecular Cell* 1:939-948.

Al-Sady B, Kikis EA, Monte E, and Quail PH (2008) Mechanistic duality of transcription factor function in phytochrome signaling. *Proc Natl Acad Sci USA* 105:2232-2237.

Andersson D, Carlson U, and Freskgard PO (2001) Contribution of tryptophan residues to the CD spectrum of the extracellular domain of human tissue factor. *European Journal of Biochemistry* 268:1118-1128.

Aubert C, Mathis P, Eker APM, and Brettel K (1999) Intraprotein electron transfer between tyrosine and tryptophan in DNA photolyase from Anacystis nidulans. *Proc Natl Acad Sci USA* 96:5423-5427.

Aubert C, Vos MH, Mathis P, Eker APM, and Brettel K (2000) Intraprotein radical transfer during photoactivation of DNA photolyase. *Nature* 405:586-590.

Ballaré CL, Barnes PW, and Flint SD (1995) Inhibition of hypocotyl elongation by ultraviolet-B radiation in de-etiolating tomato seedlings. *Physiologia Plantarum* 93:584-592.

Barta C, Kalai T, Hideg K, Vass I, and Hideg E (2004) Differences in the ROS-generating efficacy of various ultraviolet wavelengths in detached spinach leaves. *Functional plant biology* 31:23-28.

Barth A (2007) Infrared spectroscopy of proteins. *Biochimica et Biophysica Acta-Bioenergetics* 1767:1073-1101.

Barth A and Zscherp C (2002) What vibrations tell about proteins. *Quarterly Reviews of Biophysics* 35:369-430.

Batschauer A, Banerjee R, and Pokorny R (2007) Cryptochromes. In *Annual Plant Reviews Volume 30: Light and Plant Development* (eds. Whitelam GC and Halliday KJ), Blackwell Publishing Ltd: Oxford, UK, pp 17-48.

Beggs CJ, Stolzerjehle A, and Wellmann E (1985) Isoflavonoid formation as an indicator of UV stress in bean *(Phaseolus vulgaris* L.) leaves. *Plant Physiology* 79:630-634.

Berera R, van Grondelle R, and Kennis JTM (2009) Ultrafast transient absorption spectroscopy: principles and application to photosynthetic systems. *Photosynthesis Research* 101:105-118.

Bieza K and Lois R (2001) An Arabidopsis Mutant Tolerant to Lethal Ultraviolet-B Levels Shows Constitutively Elevated Accumulation of Flavonoids and Other Phenolics. *Plant Physiology* 126:1105-1115.

Boccalandro HE, Rossi MC, Saijo Y, Deng XW, and Casal JJ (2004) Promotion of photomorphogenesis by COP1. *Plant Molecular Biology* 56:905-915.

Bogan AA and Thorn KS (1998) Anatomy of hot spots in protein interfaces. *Journal of Molecular Biology* 280:1-9.

Bouly JP, Giovani B, Djamei A, Mueller M, Zeugner A, Dudkin EA, Batschauer A, and Ahmad M (2003) Novel ATP-binding and autophosphorylation activity associated with Arabidopsis and human cryptochrome-1. *European Journal of Biochemistry* 270:2921-2928.

Briggs WR and Christie JM (2002) Phototropins 1 and 2: versatile plant blue-light receptors. *Trends in Plant Science* 7:204-210.

Britt AB (2004) Repair of DNA damage induced by solar UV. *Photosynthesis Research* 81:105-112.

Britt AB, Chen JJ, Wykoff D, and Mitchell D (1993) A UV-sensitive mutant of Arabidopsis defective in the repair of pyrimidine-pyrimidone (6-4) dimers. *Science* 261:1571-1574.

Brosche M and Strid A (2003) Molecular events following perception of ultraviolet-B radiation by plants. *Physiologia Plantarum* 117:1-10.

Brosche M, Schuler MA, Kalbina I, Connor L, and Strid A (2002) Gene regulation by low level UV-B radiation: identification by DNA array analysis. *Photochemical & Photobiological Sciences* 1:656-664.

Brown BA and Jenkins GI (2008) UV-B signaling pathways with different fluence-rate response profiles are distinguished in mature Arabidopsis leaf tissue by requirement for UVR8, HY5, and HYH. *Plant Physiology* 146:576-588.

Brown BA, Cloix C, Jiang GH, Kaiserli E, Herzyk P, Kliebenstein DJ, and Jenkins GI (2005) A UV-B-specific signaling component orchestrates plant UV protection. *Proc Natl Acad Sci USA* 102:18225-18230.

Brown BA, Headland LR, and Jenkins GI (2009) UV-B Action Spectrum for UVR8-Mediated HY5 Transcript Accumulation in Arabidopsis. *Photochemistry and Photobiology* 85:1147-1155.

Brudler R, Hitomi K, Daiyasu H, Toh H, Kucho K, Ishiura M, Kanehisa M, Roberts VA, Todo T, Tainer JA, and Getzoff ED (2003) Identification of a new cryptochrome class: Structure, function, and evolution. *Molecular Cell* 11:59-67.

Butler WL, Norris KH, Siegelman HW, and Hendricks SB (1959) Detection, assay, and preliminary purification of the pigment controlling photoresponsive development in plants. *Proc Natl Acad Sci USA* 45:1703-1708.

Caldwell MM, Ballare CL, Bornman JF, Flint SD, Bjoern LO, Teramura AH, Kulandaivelu G, and Tevini M (2003) Terrestrial ecosystems increased solar ultraviolet radiation and interactions with other climatic change factors. *Photochemical & Photobiological Sciences* 2:29-38.

Caldwell MM, Bornman JF, Ballare CL, Flint SD, and Kulandaivelu G (2007) Terrestrial ecosystems, increased solar ultraviolet radiation, and interactions with other climate change factors. *Photochemical & Photobiological Sciences* 6:252-266.

Casati P and Walbot V (2003) Gene Expression Profiling in Response to Ultraviolet Radiation in Maize Genotypes with Varying Flavonoid Content. *Plant Physiology* 132:1739-1754.

Casati P and Walbot V (2004 a) Crosslinking of ribosomal proteins to RNA in maize ribosomes by UV-B and its effects on translation. *Plant Physiology* 136:3319-3332.

Casati P and Walbot V (2004 b) Rapid transcriptome responses of maize (*Zea mays*) to UV-B in irradiated and shielded tissues. *Genome Biology* 5:R16

Casati P, Campi M, Chu FX, Suzuki N, Maltby D, Guan SH, Burlingame AL, and Walbot V (2008) Histone acetylation and chromatin remodeling are required for UV-B-dependent transcriptional activation of regulated genes in maize. *Plant Cell* 20:827-842.

Casati P, Stapleton AE, Blum JE, and Walbot V (2006) Genome-wide analysis of high-altitude maize and gene knockdown stocks implicates chromatin remodeling proteins in response to UV-B. *Plant Journal* 46:613-627.

Cashmore AR, Jarillo JA, Wu YJ, and Liu DM (1999) Cryptochromes: Blue light receptors for plants and animals. *Science* 284:760-765.

Castillon A, Shen H, and Huq E (2007) Phytochrome Interacting Factors: central players in phytochrome-mediated light signaling networks. *Trends in Plant Science* 12:514-521.

Chaves I, Pokorny R, Byrdin M, Hoang N, Ritz T, Brettel K, Essen L-O, van der Horst GTJ, Batschauer A, and Ahmad M (2011) The Cryptochromes: Blue Light Photoreceptors in Plants and Animals. *Annual Review of Plant Biology* 62:335-364.

Chen H, Huang X, Gusmaroli G, Terzaghi W, Lau OS, Yanagawa Y, Zhang Y, Li J, Lee J-H, Zhu D, and Deng XW (2010) Arabidopsis CULLIN4-Damaged DNA Binding Protein 1 Interacts with CONSTITUTIVELY PHOTOMORPHOGENIC1-SUPPRESSOR OF PHYA Complexes to Regulate Photomorphogenesis and Flowering Time. *Plant Cell* 22:108-123.

Chen M, Chory J, and Fankhauser C (2004) Light signal transduction in higher plants. *Annual Review of Genetics* 38:87-117.

Chen M, Schwabb R, and Chory J (2003) Characterization of the requirements for localization of phytochrome B to nuclear bodies. *Proc Natl Acad Sci USA* 100:14493-14498.

Christie JM (2007) Phototropin blue-light receptors. *Annual Review of Plant Biology* 58:21-45.

Christie JM and Jenkins GI (1996) Distinct UV-B and UV-A blue light signal transduction pathways induce chalcone synthase gene expression in Arabidopsis cells. *Plant Cell* 8:1555-1567.

Christie JM, Arvai AS, Baxter KJ, Heilmann M, Pratt AJ, O'Hara A, Kelly SM, Hothorn M, Smith BO, Hitomi K, Jenkins GI, and Getzoff ED (2012) Plant UVR8 Photoreceptor Senses UV-B by Tryptophan-Mediated Disruption of Cross-Dimer Salt Bridges. *Science* 335:1492-1496.

Christie JM, Reymond P, Powell GK, Bernasconi P, Raibekas AA, Liscum E, and Briggs WR (1998) Arabidopsis NPH1: A Flavoprotein with the Properties of a Photoreceptor for Phototropism. *Science* 282:1698-1701.

Christie JM, Yang H, Richter GL, Sullivan S, Thomson CE, Lin J, Titapiwatanakun B, Ennis M, Kaiserli E, Lee OR, Adamec J, Peer WA, and Murphy AS (2011) Phot1 Inhibition of ABCB19 Primes Lateral Auxin Fluxes in the Shoot Apex Required For Phototropism. *Plos Biology* 9.

Clack T, Shokry A, Moffet M, Liu P, Faul M, and Sharrock RA (2009) Obligate Heterodimerization of Arabidopsis Phytochromes C and E and Interaction with the PIF3 Basic Helix-Loop-Helix Transcription Factor. *Plant Cell* 21:786-799.

Clackson T and Wells JA (1995) A hot-spot of binding-energy in a hormone-receptor interface. *Science* 267:383-386.

Cloix C and Jenkins GI (2008) Interaction of the Arabidopsis UV-B-specific signaling component UVR8 with chromatin. *Molecular Plant* 1:118-128.

Cloix C, Kaiserli E, Heilmann M, Baxter KJ, Brown BA, O'Hara A, Smith BO, Christie JM, and Jenkins GI (2012) C-terminal region of the UV-B photoreceptor UVR8 initiates signaling through interaction with the COP1 protein. *Proc Natl Acad Sci USA* 109:16366-16370.

Crosson S, Rajagopal S, and Moffat K (2003) The LOV domain family: Photoresponsive signaling modules coupled to diverse output domains. *Biochemistry* 42:2-10.

Crowley PB and Golovin A (2005) Cation-π interactions in protein-protein interfaces. *Proteins: Structure, Function, and Bioinformatics* 59:231-239.

Cui JS and Somerville RL (1993) The TyrR protein of *Escherichia coli*, analysis by limited proteolysis of domain-structure and ligand-mediated conformational changes. *Journal of Biological Chemistry* 268:5040-5047.

de Carbonnel M, Davis P, Roelfsema MRG, Inoue S-i, Schepens I, Lariguet P, Geisler M, Shimazaki K-i, Hangarter R, and Fankhauser C (2010) The Arabidopsis PHYTOCHROME KINASE SUBSTRATE 2 Protein is a Phototropin Signaling Element that regulates Leaf Flattening and Leaf Positioning. *Plant Physiology* 152:1391-1405.

Demarsy E and Fankhauser C (2009) Higher plants use LOV to perceive blue light. *Current Opinion in Plant Biology* 12:69-74.

Deng XW and Quail PH (1992) Genetic and phenotypic characterization of *cop1* mutants of *Arabidopsis thaliana*. *The Plant Journal* 2:83-95.

Devary Y, Gottlieb RA, Smeal T, and Karin M (1992) The mammalian ultraviolet response is triggered by activation of src tyrosine kinases. *Cell* 71:1081-1091.

Ding Z, Galvan-Ampudia CS, Demarsy E, Langowski L, Kleine-Vehn J, Fan Y, Morita MT, Tasaka M, Fankhauser C, Offringa R, and Friml J (2011) Light-mediated polarization of the PIN3 auxin transporter for the phototropic response in Arabidopsis. *Nature Cell Biology* 13:447-453.

Dong CH, Agarwal M, Zhang Y, Xie Q, and Zhu JK (2006) The negative regulator of plant cold responses, HOS1, is a RING E3 ligase that mediates the ubiquitination and degradation of ICE1. *Proceedings of the National Academy of Sciences* 103:8281-8286.

Englander SW, Sosnick TR, Englander JJ, and Mayne L (1996) Mechanisms and uses of hydrogen exchange. *Current Opinion in Structural Biology* 6:18-23.

Ensminger PA (1993) Control of development in plants and fungi by far-UV radiation. *Physiologia Plantarum* 88:501-508.

Favory JJ, Stec A, Gruber H, Rizzini L, Oravecz A, Funk M, Albert A, Cloix C, Jenkins GI, Oakeley EJ, Seidlitz HK, Nagy F, and Ulm R (2009) Interaction of COP1 and UVR8 regulates UV-B-induced photomorphogenesis and stress acclimation in Arabidopsis. *EMBO Journal* 28:591-601.

Feinbaum RL and Ausubel FM (1988) Transcriptional regulation of the *Arabidopsis thaliana* chalcone synthase gene. *Molecular and Cellular Biology* 8:1985-1992.

Fittinghoff K, Laubinger S, Nixdorf M, Fackendahl P, Baumgardt RL, Batschauer A, and Hoecker U (2006) Functional and expression analysis of Arabidopsis SPA genes during seedling photomorphogenesis and adult growth. *The Plant Journal* 47:577-590.

Fontana A, de Laureto PP, Spolaore B, Frare E, Picotti P, and Zambonin M (2004) Probing protein structure by limited proteolysis. *Acta Biochimica Polonica* 51:299-321.

Fontana A, Zambonin M, deLaureto PP, DeFilippis V, Clementi A, and Scaramella E (1997) Probing the conformational state of apomyoglobin by limited proteolysis. *Journal of Molecular Biology* 266:223-230.

Foyer CH, Descourvieres P, and Kunert KJ (1994) Protection against oxygen radicals: an important defence mechanism studied in transgenic plants. *Plant, Cell and Environment* 17:507-523.

Franklin KA and Quail PH (2010) Phytochrome functions in Arabidopsis development. *Journal of Experimental Botany* 61:11-24.

Frohnmeyer H and Staiger D (2003) Ultraviolet-B radiation-mediated responses in plants. Balancing damage and protection. *Plant Physiology* 133:1420-1428.

Frohnmeyer H, Loyall L, Blatt MR, and Grabov A (1999) Millisecond UV-B irradiation evokes prolonged elevation of cytosolic-free Ca^{2+} and stimulates gene expression in transgenic parsley cell cultures. *The Plant Journal* 20:109-117.

Fuglevand G, Jackson JA, and Jenkins GI (1996) UV-B, UV-A, and blue light signal transduction pathways interact synergistically to regulate chalcone synthase gene expression in Arabidopsis. *Plant Cell* 8:2347-2357.

Gardner KH and Correa F (2012) How Plants See the Invisible. *Science* 335:1451-1452.

Gauden M, van Stokkum IHM, Key JM, Luehrs DC, van Grondelle R, Hegemann P, and Kennis JTM (2006) Hydrogen-bond switching through a radical pair mechanism in a flavin-binding photoreceptor. *Proc Natl Acad Sci USA* 103:10895-10900.

Gilchrest BA, Eller MS, Geller AC, and Yaar M (1999) The pathogenesis of melanoma induced by ultraviolet radiation. *New England Journal of Medicine* 340:1341-1348.

Giovani B, Byrdin M, Ahmad M, and Brettel K (2003) Light-induced electron transfer in a cryptochrome blue-light photoreceptor. *Nat Struct Mol Biol* 10:489-490.

González Besteiro MA and Ulm R (2013) ATR and MKP1 play distinct roles in response to UV-B stress in Arabidopsis. *The Plant Journal*: doi: 10.1111/tpj.12095.

González Besteiro MA, Bartels S, Albert A, and Ulm R (2011) Arabidopsis MAP kinase phosphatase 1 and its target MAP kinases 3 and 6 antagonistically determine UV-B stress tolerance, independent of the UVR8 photoreceptor pathway. *The Plant Journal* 68:727-737.

Grefen C, Donald N, Hashimoto K, Kudla J, Schumacher K, and Blatt MR (2010) A ubiquitin-10 promoter-based vector set for fluorescent protein tagging facilitates temporal stability and native protein distribution in transient and stable expression studies. *Plant Journal* 64:355-365.

Grishina IB and Woody RW (1994) Contributions of tryptophan side chains to the circular dichroism of globular proteins: exciton couplets and coupled oscillators. *Faraday discussions*:245-262.

Groot ML, van Wilderen LJGW, and Di Donato M (2007) Femtosecond time-resolved and dispersed infrared spectroscopy on proteins. *Photochemical and Photobiological Sciences* 6:501-507.

Gruber H, Heijde M, Heller W, Albert A, Seidlitz HK, and Ulm R (2010) Negative feedback regulation of UV-B-induced photomorphogenesis and stress acclimation in Arabidopsis. *Proc Natl Acad Sci USA* 107:20132-20137.

Hahlbrock K and Grisebach H (1979) Enzymic controls in the biosynthesis of lignin and flavonoids. *Annual Review of Plant Physiology and Plant Molecular Biology* 30:105-130.

Haris PI, Robillard GT, Van Dijk AA, and Chapman D (1992) Potential of carbon-13 and nitrogen-15 labeling for studying protein-protein interactions using Fourier-transform infrared spectroscopy. *Biochemistry* 31:6279-6284.

Harper SM, Neil LC, and Gardner KH (2003) Structural basis of a phototropin light switch. *Science* 301:1541-1544.

Hattendorf DA, Andreeva A, Gangar A, Brennwald PJ, and Weis WI (2007) Structure of the yeast polarity protein Sro7 reveals a SNARE regulatory mechanism. *Nature* 446:567-571.

Headland LR (2009) UV-RESISTANCE LOCUS 8 and UV-B Specific Signaling in *Arabidopsis thaliana*. Ph.D. thesis, University of Glasgow.

Heijde M and Ulm R (2012) UV-B photoreceptor-mediated signalling in plants. *Trends in Plant Science* 17:230-237.

Heijde M and Ulm R (2013) Reversion of the Arabidopsis UV-B photoreceptor UVR8 to the homodimeric ground state. *Proc Natl Acad Sci USA*: doi:10.1073/pnas.1214237110.

Henriques R, Jang I-C, and Chua N-H (2009) Regulated proteolysis in light-related signaling pathways. *Current Opinion in Plant Biology* 12:49-56.

Hideg E, Barta C, Kalai T, Vass I, Hideg K, and Asada K (2002) Detection of Singlet Oxygen and Superoxide with Fluorescent Sensors in Leaves under Stress by Photoinhibition or UV Radiation. *Plant and Cell Physiology* 43:1154-1164.

Holm M, Hardtke CS, Gaudet R, and Deng XW (2001) Identification of a structural motif that confers specific interaction with the WD40 repeat domain of Arabidopsis COP1. *EMBO Journal* 20:118-127.

Holm M, Ma LG, Qu LJ, and Deng XW (2002) Two interacting bZIP proteins are direct targets of COP1-mediated control of light-dependent gene expression in Arabidopsis. *Genes & Development* 16:1247-1259.

Huang X, Ouyang X, Yang P, Lau OS, Li G, Li J, Chen H, and Deng XW (2012) Arabidopsis FHY3 and HY5 Positively Mediate Induction of COP1 Transcription in Response to Photomorphogenic UV-B Light. *Plant Cell* 24:4590-4606.

Inada S, Ohgishi M, Mayama T, Okada K, and Sakai T (2004) RPT2 is a signal transducer involved in phototropic response and stomatal opening by association with phototropin 1 in *Arabidopsis thaliana*. *Plant Cell* 16:887-896.

Indorf M, Cordero J, Neuhaus G, and Rodríguez-Franco M (2007) Salt tolerance (STO), a stress-related protein, has a major role in light signalling. *The Plant Journal* 51:563-574.

Izaguirre MM, Scopel AL, Baldwin IT, and Ballare CL (2003) Convergent Responses to Stress. *Plant Physiology* 132:1755-1767.

Jaedicke K, Lichtenthaeler AL, Meyberg R, Zeidler M, and Hughes J (2012) A phytochrome-phototropin light signaling complex at the plasma membrane. *Proc Natl Acad Sci USA* 109:12231-12236.

Jang IC, Henriques R, Seo HS, Nagatani A, and Chua NH (2010) Arabidopsis PHYTOCHROME INTERACTING FACTOR Proteins Promote Phytochrome B Polyubiquitination by COP1 E3 Ligase in the Nucleus. *Plant Cell* 22:2370-2383.

Jang IC, Yang JY, Seo HS, and Chua NH (2005) HFR1 is targeted by COP1 E3 ligase for post-translational proteolysis during phytochrome A signaling. *Genes & Development* 19:593-602.

Jansen MAK, Gaba V, and Greenberg BM (1998) Higher plants and UV-B radiation: balancing damage, repair and acclimation. *Trends in Plant Science* 3:243-243.

Jarillo JA, Capel J, Tang RH, Yang HQ, Alonso JM, Ecker JR, and Cashmore AR (2001) An Arabidopsis circadian clock component interacts with both CRY1 and phyB. *Nature* 410:487-490.

Jenkins GI (2009) Signal Transduction in Responses to UV-B Radiation. *Annual Review of Plant Biology* 60:407-431.

Jenkins GI, Long JC, Wade HK, Shenton MR, and Bibikova TN (2001) UV and blue light signalling: pathways regulating chalcone synthase gene expression in Arabidopsis. *New Phytologist* 151:121-131.

Jeong R-D, Chandra-Shekara AC, Barman SR, Navarre D, Klessig DF, Kachroo A, and Kachroo P (2010) Cryptochrome 2 and phototropin 2 regulate resistance protein-mediated viral defense by negatively regulating an E3 ubiquitin ligase. *Proc Natl Acad Sci USA* 107:13538-13543.

Jiang CZ, Yee J, Mitchell DL, and Britt AB (1997) Photorepair mutants of Arabidopsis. *Proc Natl Acad Sci USA* 94:7441-7445.

Jiang L, Wang Y, Li Q-F, Bjoern LO, He J-X, and Li S-S (2012) Arabidopsis STO/BBX24 negatively regulates UV-B signaling by interacting with COP1 and repressing HY5 transcriptional activity. *Cell Res* 22:1046-1057.

Jiao YL, Lau OS, and Deng XW (2007) Light-regulated transcriptional networks in higher plants. *Nature Reviews Genetics* 8:217-230.

Jordan BR (1996) The effects of ultraviolet-B radiation on plants: A molecular perspective. *Advances in Botanical Research* 22:97-162.

Kaiserli E (2007) Subcellular localisation and functional analysis of UVR8, a UV-B specific signalling component in *Arabidopsis*. Ph.D. thesis, University of Glasgow.

Kaiserli E and Jenkins GI (2007) UV-B promotes rapid nuclear translocation of the Arabidopsis UV-B-specific signaling component UVR8 and activates its function in the nucleus. *Plant Cell* 19:2662-2673.

Kaiserli E, Sullivan S, Jones MA, Feeney KA, and Christie JM (2009) Domain Swapping to Assess the Mechanistic Basis of Arabidopsis Phototropin 1 Receptor Kinase Activation and Endocytosis by Blue Light. *Plant Cell* 21:3226-3244.

Kalbina I, Li S, Kalbin G, Bjoern LO, and Strid A (2008) Two separate UV-B radiation wavelength regions control expression of different molecular markers in Arabidopsis thaliana. *Functional Plant Biology* 35:222-227.

Kami C, Lorrain Sv, Hornitschek P, Fankhauser C, and Marja CPT (2010) Chapter Two - Light-Regulated Plant Growth and Development. *Current Topics in Developmental Biology*, Academic Press, Vol 91, pp 29-66.

Kandori H (2004) Hydration switch model for the proton transfer in the Schiff base region of bacteriorhodopsin. *Biochimica et Biophysica Acta - Bioenergetics* 1658:72-79.

Kelly SM, Jess TJ, and Price NC (2005) How to study proteins by circular dichroism. *Biochimica Et Biophysica Acta-Proteins and Proteomics* 1751:119-139.

Kennis JTM and Groot ML (2007) Ultrafast spectroscopy of biological photoreceptors. *Current Opinion in Structural Biology* 17:623-630.

Kennis JTM, Crosson S, Gauden M, van Stokkum IHM, Moffat K, and van Grondelle R (2003) Primary Reactions of the LOV2 Domain of Phototropin, a Plant Blue-Light Photoreceptor *Biochemistry* 42:3385-3392.

Kim BC, Tennessen DJ, and Last RL (1998) UV-B-induced photomorphogenesis in *Arabidopsis thaliana*. *Plant Journal* 15:667-674.

Kim WY, Fujiwara S, Suh SS, Kim J, Kim Y, Han L, David K, Putterill J, Nam HG, and Somers DE (2007) ZEITLUPE is a circadian photoreceptor stabilized by GIGANTEA in blue light. *Nature* 449:356-360.

Kircher S, Kozma-Bognar L, Kim L, Adam E, Harter K, Schafer E, and Nagy F (1999) Light quality-dependent nuclear import of the plant photoreceptors phytochrome A and B. *Plant Cell* 11:1445-1456.

Kleine T, Lockhart P, and Batschauer A (2003) An Arabidopsis protein closely related to Synechocystis cryptochrome is targeted to organelles. *Plant Journal* 35:93-103.

Kliebenstein DJ, Lim JE, Landry LG, and Last RL (2002) Arabidopsis UVR8 regulates ultraviolet-B signal transduction and tolerance and contains sequence similarity to human Regulator of Chromatin Condensation 1. *Plant Physiology* 130:234-243.

Kucera B, Leubner-Metzger G, and Wellmann E (2003) Distinct ultraviolet-signaling pathways in bean leaves. *Plant Physiology* 133:1445-1452.

Kuwajima K, Garvey EP, Finn BE, Matthews CR, and Sugai S (1991) Transient intermediates in the folding of dihyrofolate-reductase as detected by far-ultraviolet circular-dichroism spectroscopy. *Biochemistry* 30:7693-7703.

Lakowicz JR (2006) *Principles of fluorescence spectroscopy*. Springer: New York. 3rd Ed.

Landry LG, Chapple CCS, and Last RL (1995) Arabidopsis mutants lacking phenolic sunscreens exhibit enhanced ultraviolet-B injury and oxidative damage. *Plant Physiology* 109:1159-1166.

Landry LG, Stapleton AE, Lim J, Hoffman P, Hays JB, Walbot V, and Last RL (1997) An Arabidopsis photolyase mutant is hypersensitive to ultraviolet-B radiation. *Proc Natl Acad Sci USA* 94:328-332.

Lau OS and Deng XW (2012) The photomorphogenic repressors COP1 and DET1: 20 years later. *Trends in Plant Science* 17:584-593.

Laubinger S, Fittinghoff K, and Hoecker U (2004) The SPA Quartet: A Family of WD-Repeat Proteins with a Central Role in Suppression of Photomorphogenesis in Arabidopsis. *Plant Cell* 16:2293-2306.

Leivar P and Quail PH (2011) PIFs: pivotal components in a cellular signaling hub. *Trends in Plant Science* 16:19-28.

Leivar P, Monte E, Al-Sady B, Carle C, Storer A, Alonso JM, Ecker JR, and Quail PH (2008) The Arabidopsis Phytochrome-Interacting Factor PIF7, together with PIF3 and PIF4, regulates responses to prolonged red light by modulating phyB levels. *Plant Cell* 20:337-352.

Leonard J, Sharma D, Szafarowicz B, Torgasin K, and Haacke S (2010) Formation dynamics and nature of tryptophan's primary photoproduct in aqueous solution. *Physical Chemistry Chemical Physics* 12:15744-15750.

Li JY, Oulee TM, Raba R, Amundson RG, and Last RL (1993) Arabidopsis flavonoid mutants are hypersensitive to UV-B irradiation. *Plant Cell* 5:171-179.

Li X, Wang Q, Yu X, Liu H, Yang H, Zhao C, Liu X, Tan C, Klejnot J, Zhong D, and Lin C (2011) Arabidopsis cryptochrome 2 (CRY2) functions by the photoactivation mechanism distinct from the tryptophan (trp) triad-dependent photoreduction. *Proc Natl Acad Sci USA* 108:20844-20849.

Lian HL, He SB, Zhang YC, Zhu DM, Zhang JY, Jia KP, Sun SX, Li L, and Yang HQ (2011) Blue-light-dependent interaction of cryptochrome 1 with SPA1 defines a dynamic signaling mechanism. *Genes & Development* 25:1023-1028.

Liscum E, Hodgson DW, and Campbell TJ (2003) Blue light signaling through the cryptochromes and phototropins. So that's what the blues is all about. *Plant Physiology* 133:1429-1436.

Liu B, Liu H, Zhong D, and Lin C (2010) Searching for a photocycle of the cryptochrome photoreceptors. *Current Opinion in Plant Biology* 13:578-586.

Liu B, Zuo Z, Liu H, Liu X, and Lin C (2011) Arabidopsis cryptochrome 1 interacts with SPA1 to suppress COP1 activity in response to blue light. *Genes & Development* 25:1029-1034.

Liu LJ, Zhang YC, Li QH, Sang Y, Mao J, Lian HL, Wang L, and Yang HQ (2008) COP1-Mediated Ubiquitination of CONSTANS Is Implicated in Cryptochrome Regulation of Flowering in Arabidopsis. *Plant Cell* 20:292-306.

Long JC and Jenkins GI (1998) Involvement of Plasma Membrane Redox Activity and Calcium Homeostasis in the UV-B and UV-A/Blue Light Induction of Gene Expression in Arabidopsis. *Plant Cell* 10:2077-2086.

Losi A (2007) Flavin-based Blue-light Photosensors: A Photobiophysics Update. *Photochemistry and Photobiology* 83:1283-1300.

Mackerness SAH, John CF, Jordan B, and Thomas B (2001) Early signaling components in ultraviolet-B responses: distinct roles for different reactive oxygen species and nitric oxide. *Febs Letters* 489:237-242.

Mackerness SAH, Surplus SL, Blake P, John CF, Buchanan-Wollaston V, Jordan BR, and Thomas B (1999) Ultraviolet-B-induced stress and changes in gene expression in *Arabidopsis thaliana*: role of signalling pathways controlled by jasmonic acid, ethylene and reactive oxygen species. *Plant Cell and Environment* 22:1413-1423.

Mas P, Devlin PF, Panda S, and Kay SA (2000) Functional interaction of phytochrome B and cryptochrome 2. *Nature* 408:207-211.

Mas P, Kim WY, Somers DE, and Kay SA (2003) Targeted degradation of TOC1 by ZTL modulates circadian function in *Arabidopsis thaliana*. *Nature* 426:567-570.

Mathes T, Zhu J, van Stokkum IHM, Groot ML, Hegemann P, and Kennis JTM (2012) Hydrogen Bond Switching among Flavin and Amino Acids Determines the Nature of Proton-Coupled Electron Transfer in BLUF Photoreceptors. *The Journal of Physical Chemistry Letters* 3:203-208.

McArthur JA and Briggs WR (1971) In Vivo Phytochrome Reversion in Immature Tissue of the Alaska Pea Seedling. *Plant Physiology* 48:46-49.

McKenzie RL, Bjoern LO, Bais A, and Ilyasd M (2003) Changes in biologically active ultraviolet radiation reaching the Earth's surface. *Photochemical & Photobiological Sciences* 2:5-15.

McNellis TW, von Arnim AG, Araki T, Komeda Y, Misera S, and Deng XW (1994) Genetic and molecular analysis of an allelic series of *cop1* mutants suggests functional roles for the multiple protein domains. *Plant Cell* 6:487-500.

Miller JE, Gradinaru C, Crane BR, Di Bilio AJ, Wehbi WA, Un S, Winkler JR, and Gray HB (2003) Spectroscopy and reactivity of a photogenerated tryptophan radical in a structurally defined protein environment. *Journal of the American Chemical Society* 125:14220-14221.

Mittag T and Forman-Kay JD (2007) Atomic-level characterization of disordered protein ensembles. *Current Opinion in Structural Biology* 17:3-14.

Moeglich A, Yang XJ, Ayers RA, and Moffat K (2010) Structure and Function of Plant Photoreceptors. *Annual Review of Plant Biology* 61:21-47.

Motchoulski A and Liscum E (1999) Arabidopsis NPH3: A NPH1 photoreceptor-interacting protein essential for phototropism. *Science* 286:961-964.

Nabedryk E (1996) Light-induced Fourier transform infrared difference spectroscopy of the primary electron donor in photosynthetic reaction centers. In *Infrared Spectroscopy of Biomolecules* (eds. Mantsch HH and Chapman D), Wiley-Lis: New York, pp 39-82.

Nagy F and Schaefer E (2002) Phytochromes control photomorphogenesis by differentially regulated, interacting signaling pathways in higher plants. *Annual Review of Plant Biology* 53:329-355.

Nakasako M, Zikihara K, Matsuoka D, Katsura H, and Tokutomi S (2008) Structural Basis of the LOV1 Dimerization of Arabidopsis Phototropins 1 and 2. *Journal of Molecular Biology* 381:718-733.

O'Hara A and Jenkins GI (2012) In Vivo Function of Tryptophans in the Arabidopsis UV-B Photoreceptor UVR8. *Plant Cell* 24:3755-3766.

Oravecz A, Baumann A, Mate Z, Brzezinska A, Molinier J, Oakeley EJ, Adam E, Schaefer E, Nagy F, and Ulm R (2006) CONSTITUTIVELY PHOTOMORPHOGENIC1 is required for the UV-B response in Arabidopsis. *Plant Cell* 18:1975-1990.

Osterlund MT, Hardtke CS, Wei N, and Deng XW (2000) Targeted destabilization of HY5 during light-regulated development of Arabidopsis. *Nature* 405:462-466.

Palmer JM, Short TW, Gallagher S, and Briggs WR (1993) Blue Light-Induced Phosphorylation of a Plasma Membrane-Associated Protein in Zea mays L. *Plant Physiology* 102:1211-1218.

Paul ND and Gwynn-Jones D (2003) Ecological roles of solar UV radiation: towards an integrated approach. *Trends in Ecology and Evolution* 18:48-55.

Rao MV, Paliyath C, and Ormrod DP (1996) Ultraviolet-B- and ozone-induced biochemical changes in antioxidant enzymes of *Arabidopsis thaliana*. *Plant Physiology* 110:125-136.

Reineke U, Volkmer-Engert R, and Schneider-Mergener J (2001) Applications of peptide arrays prepared by the SPOT-technology. *Current Opinion in Biotechnology* 12:59-64.

Renault L, Nassar N, Vetter I, Becker J, Klebe C, Roth M, and Wittinghofer A (1998) The 1.7 angstrom crystal structure of the regulator of chromosome condensation (RCC1) reveals a seven-bladed propeller. *Nature* 392:97-101.

Rensing SA, Lang D, Zimmer AD, Terry A, Salamov A, Shapiro H, Nishiyama T et al. (2008) The Physcomitrella Genome Reveals Evolutionary Insights into the Conquest of Land by Plants. *Science* 319:64-69.

Rice-Evans C, Miller N, and Paganga G (1997) Antioxidant properties of phenolic compounds. *Trends in Plant Science* 2:152-159.

Richardt S, Lang D, Reski R, Frank W, and Rensing SA (2007) PlanTAPDB, a Phylogeny-Based Resource of Plant Transcription-Associated Proteins. *Plant Physiology* 143:1452-1466.

Rizzini L (2010) UVR8: a plant UV-B photoreceptor. Ph.D. thesis, University of Freiburg.

Rizzini L, Favory JJ, Cloix C, Faggionato D, O'Hara A, Kaiserli E, Baumeister R, Schaefer E, Nagy F, Jenkins GI, and Ulm R (2011) Perception of UV-B by the Arabidopsis UVR8 Protein. *Science* 332:103-106.

Rockwell NC, Su YS, and Lagarias JC (2006) Phytochrome structure and signaling mechanisms. *Annual Review of Plant Biology* 57:837-858.

Rothschild K (1992) FTIR difference spectroscopy of bacteriorhodopsin: Toward a molecular model. *Journal of Bioenergetics and Biomembranes* 24:147-167.

Rozema J, van de Staaij J, Bjoern LO, and Caldwell M (1997) UV-B as an environmental factor in plant life: Stress and regulation. *Trends in Ecology and Evolution* 12:22-28.

Saijo Y, Sullivan JA, Wang HY, Yang JP, Shen YP, Rubio V, Ma LG, Hoecker U, and Deng XW (2003) The COP1-SPA1 interaction defines a critical step in phytochrome A-mediated regulation of HY5 activity. *Genes & Development* 17:2642-2647.

Salomon M, Zacherl M, Luff L, and Rudiger W (1997) Exposure of Oat Seedlings to Blue Light Results in Amplified Phosphorylation of the Putative Photoreceptor for Phototropism and in Higher Sensitivity of the Plants to Phototropic Stimulation. *Plant Physiology* 115:493-500.

Salomon M, Christie JM, Knieb E, Lempert U, and Briggs WR (2000) Photochemical and mutational analysis of the FMN-binding domains of the plant blue light receptor, phototropin. *Biochemistry* 39:9401-9410.

Salomon M, Lempert U, and Ruediger W (2004) Dimerization of the plant photoreceptor phototropin is probably mediated by the LOV1 domain. *Febs Letters* 572:8-10.

Sambrook J and Russell DW (2001) *Molecular Cloning: A Laboratory Manual*. Cold Spring Harbor Laboratory Press: New York, 3rd Ed.

Sancar A, Lindsey-Boltz LA, Uensal-Kacmaz K, and Linn S (2004) Molecular mechanism of mammalian DNA repair and the DNA damage checkpoints. *Annual Review of Biochemistry* 73:39-85.

Sang Y, Li QH, Rubio V, Zhang YC, Mao J, Deng XW, and Yang HQ (2005) N-terminal domain-mediated homodimerization is required for photoreceptor activity of Arabidopsis CRYPTOCHROME 1. *Plant Cell* 17:1569-1584.

Seki T, Hayashi N, and Nishimoto T (1996) RCC1 in the Ran Pathway. *Journal of Biochemistry* 120:207-214.

Seo HS, Watanabe E, Tokutomi S, Nagatani A, and Chua NH (2004) Photoreceptor ubiquitination by COP1 E3 ligase desensitizes phytochrome A signaling. *Genes & Development* 18:617-622.

Seo HS, Yang JY, Ishikawa M, Bolle C, Ballesteros ML, and Chua NH (2003) LAF1 ubiquitination by COP1 controls photomorphogenesis and is stimulated by SPA1. *Nature* 423:995-999.

Shafaat HS, Leigh BS, Tauber MJ, and Kim JE (2010) Spectroscopic Comparison of Photogenerated Tryptophan Radicals in Azurin: Effects of Local Environment and Structure. *Journal of the American Chemical Society* 132:9030-9039.

Shalitin D, Yang HY, Mockler TC, Maymon M, Guo HW, Whitelam GC, and Lin CT (2002) Regulation of Arabidopsis cryptochrome 2 by blue-light-dependent phosphorylation. *Nature* 417:763-767.

Sharma D, Leonard J, and Haacke S (2010) Ultrafast excited-state dynamics of tryptophan in water observed by transient absorption spectroscopy. *Chemical Physics Letters* 489:99-102.

Sharrock RA and Clack T (2004) Heterodimerization of type II phytochromes in Arabidopsis. *Proc Natl Acad Sci USA* 101:11500-11505.

Shinkle JR, Atkins AK, Humphrey EE, Rodgers CW, Wheeler SL, and Barnes PW (2004) Growth and morphological responses to different UV wavebands in cucumber (*Cucumis sativum*) and other dicotyledonous seedlings. *Physiologia Plantarum* 120:240-248.

Smith TF, Gaitatzes C, Saxena K, and Neer EJ (1999) The WD repeat: a common architecture for diverse functions. *Trends in Biochemical Sciences* 24:181-185.

Snellenburg JJ, Laptenok SP, Seger R, Mullen KM, and van Stokkum IHM (2012) Glotaran: A Java-Based Graphical User Interface for the R Package TIMP. *Journal of Statistical Software* 49:1-22.

Solar S, Getoff N, Surdhar PS, Armstrong DA, and Singh A (1991) Oxidation of tryptophan and N-methylindole by $N_3^{\cdot}$, Br_2^{-} and $(Scn)_2^{-}$ radicals in light- and heavy-water solutions. *Journal of Physical Chemistry* 95:3639-3643.

Sonar S, Lee CP, Coleman M, Patel N, Liu X, Marti T, Khorana HG, RajBhandary UL, and Rothschild KJ (1994) Site-directed isotope labelling and FTIR spectroscopy of bacteriorhodopsin. *Nat Struct Mol Biol* 1:512-517.

Stirnimann CU, Petsalaki E, Russell RB, and Mueller CW (2012) WD40 proteins propel cellular networks. *Trends in Biochemical Sciences* 35:565-574.

Stracke R, Ishihara H, Huep G, Barsch A, Mehrtens F, Niehaus K, and Weisshaar B (2007) Differential regulation of closely related R2R3-MYB transcription factors controls flavonol accumulation in different parts of the *Arabidopsis thaliana* seedling. *The Plant Journal* 50:660-677.

Strickland EH (1974) Aromatic contributions to circular dichroism spectra of proteins. *CRC Critical Reviews in Biochemistry* 2:113-175.

Suesslin C and Frohnmeyer H (2003) An Arabidopsis mutant defective in UV-B light-mediated responses. *Plant Journal* 33:591-601.

Taiz L and Zeiger E (2002) *Plant Physiology*. Sinauer Associates: Sunderland, MA. 3rd ed.

Takeda J and Abe S (1992) Light-induced synthesis of anthocyanin in carrot cells in suspension. IV. The action spectrum. *Photochem. Photobiol.* 56:69.

Tepperman JM, Zhu T, Chang H-S, Wang X, and Quail PH (2001) Multiple transcription-factor genes are early targets of phytochrome A signaling. *Proc Natl Acad Sci USA* 98:9437-9442.

Tossi V, Amenta M, Lamattina L, and Cassia R (2011) Nitric oxide enhances plant ultraviolet-B protection up-regulating gene expression of the phenylpropanoid biosynthetic pathway. *Plant, Cell & Environment* 34:909-921.

Ulm R (2006) UV-B perception and signalling in higher plants (Chapter 14). In: *Photomorphogenesis in plants and bacteria function and signal transduction mechanisms* (eds. Schaefer E and Nagy F). Springer: Dordrecht. 3rd ed.

Ulm R and Nagy F (2005) Signalling and gene regulation in response to ultraviolet light. *Current Opinion in Plant Biology* 8:477-482.

Ulm R, Baumann A, Oravecz A, Mate Z, Adam E, Oakeley EJ, Schaefer E, and Nagy F (2004) Genome-wide analysis of gene expression reveals function of the bZIP transcription factor HY5 in the UV-B response of Arabidopsis. *Proc Natl Acad Sci USA* 101:1397-1402.

van Buskirk EK, Decker PV, and Chen M (2012) Photobodies in Light Signaling. *Plant Physiology* 158:52-60.

van Stokkum IHM, Larsen DS, and van Grondelle R (2004) Global and target analysis of time-resolved spectra. *Biochimica et Biophysica Acta-Bioenergetics* 1657:82-104.

Vivian JT and Callis PR (2001) Mechanisms of tryptophan fluorescence shifts in proteins. *Biophysical Journal* 80:2093-2109.

Voegtli WC, Madrona AY, and Wilson DK (2003) The Structure of Aip1p, a WD Repeat Protein That Regulates Cofilin-mediated Actin Depolymerization. *Journal of Biological Chemistry* 278:34373-34379.

von Arnim AG and Deng XW (1994) Light inactivation of Arabidopsis photomorphogenic repressor COP1 involves a cell-specific regulation of its nucleocytoplasmic partitioning. *Cell* 79:1035-1045.

von Arnim AG, Osterlund MT, Kwok SF, and Deng XW (1997) Genetic and developmental control of nuclear accumulation of COP1, a repressor of photomorphogenesis in Arabidopsis. *Plant Physiology* 114:779-788.

Vuilleumier S, Sancho J, Loewenthal R, and Fersht AR (1993) Circular-dichroism studies of barnase and its mutants. *Biochemistry* 32:10303-10313.

Wade HK, Bibikova TN, Valentine WJ, and Jenkins GI (2001) Interactions within a network of phytochrome, cryptochrome and UV-B phototransduction pathways regulate chalcone synthase gene expression in Arabidopsis leaf tissue. *Plant Journal* 25:675-685.

Wang HY, Ma LG, Li JM, Zhao HY, and Deng XW (2001) Direct interaction of Arabidopsis cryptochromes with COP1 in light control development. *Science* 294:154-158.

Wang W, Yang D, and Feldmann KA (2011) EFO1 and EFO2, encoding putative WD-domain proteins, have overlapping and distinct roles in the regulation of vegetative development and flowering of Arabidopsis. *Journal of Experimental Botany* 62:1077-1088.

Wargent JJ, Gegas VC, Jenkins GI, Doonan JH, and Paul ND (2009) UVR8 in *Arabidopsis thaliana* regulates multiple aspects of cellular differentiation during leaf development in response to ultraviolet B radiation. *New Phytologist* 183:315-326.

Weidler G, zur Oven-Krockhaus S, Heunemann M, Orth C, Schleifenbaum F, Harter K, Hoecker U, and Batschauer A (2012) Degradation of Arabidopsis CRY2 Is Regulated by SPA Proteins and Phytochrome A. *Plant Cell* 24:2610-2623.

Weisshaar B and Jenkins GI (1998) Phenylpropanoid biosynthesis and its regulation. *Current Opinion in Plant Biology* 1:251-257.

Winkel BSJ (2006) The Biosynthesis of Flavonoids. *The Science of Flavonoids* (ed. by Grotewold E), Springer: New York, pp 71-95.

Wolf L, Rizzini L, Stracke R, Ulm R, and Rensing SA (2010) The Molecular and Physiological Responses of *Physcomitrella patens* to Ultraviolet-B Radiation. *Plant Physiology* 153:1123-1134.

Wu D, Hu Q, Yan Z, Chen W, Yan C, Huang X, Zhang J, Yang P, Deng H, Wang J, Deng X, and Shi Y (2012) Structural basis of ultraviolet-B perception by UVR8. *Nature* 484:214-219.

Xu C and Min J (2011) Structure and function of WD40 domain proteins. *Protein & Cell* 2:202-214.

Yamaguchi R, Nakamura M, Mochizuki N, Kay SA, and Nagatani A (1999) Light-dependent translocation of a phytochrome B-GFP fusion protein to the nucleus in transgenic Arabidopsis. *Journal of Cell Biology* 145:437-445.

Yan H, Marquardt K, Indorf M, Jutt D, Kircher S, Neuhaus G, and Rodriguez-Franco M (2011) Nuclear Localization and Interaction with COP1 Are Required for STO/BBX24 Function during Photomorphogenesis. *Plant Physiology* 156:1772-1782.

Yang HQ, Tang RH, and Cashmore AR (2001) The signaling mechanism of Arabidopsis CRY1 involves direct interaction with COP1. *Plant Cell* 13:2573-2587.

Yang HQ, Wu YJ, Tang RH, Liu DM, Liu Y, and Cashmore AR (2000) The C termini of Arabidopsis cryptochromes mediate a constitutive light response. *Cell* 103:815-827.

Yang JP, Lin RC, James S, Hoecker U, Liu BL, Xu L, Deng XW, and Wang HY (2005) Light regulates COP1-mediated degradation of HFR1, a transcription factor essential for light signaling in Arabidopsis. *Plant Cell* 17:804-821.

Yatsuhashi H, Hashimoto T, and Shimizu S (1982) Ultraviolet Action Spectrum for Anthocyanin Formation in Broom Sorghum First Internodes. *Plant Physiology* 70:735-741.

Yi CL and Deng XW (2005) COP1 - from plant photomorphogenesis to mammalian tumorigenesis. *Trends in Cell Biology* 15:618-625.

Yu JW, Rubio V, Lee NY, Bai S, Lee SY, Kim SS, Liu L, Zhang Y, Irigoyen ML, Sullivan JA, Zhang Y, Lee I, Xie Q, Paek NC, and Deng XW (2008) COP1 and ELF3 Control Circadian Function and Photoperiodic Flowering by Regulating GI Stability. *Molecular Cell* 32:617-630.

Yu X, Klejnot J, Zhao X, Shalitin D, Maymon M, Yang H, Lee J, Liu X, Lopez J, and Lin C (2007) Arabidopsis Cryptochrome 2 Completes Its Posttranslational Life Cycle in the Nucleus. *Plant Cell* 19:3146-3156.

Yu XH, Sayegh R, Maymon M, Warpeha K, Klejnot J, Yang HY, Huang J, Lee J, Kaufman L, and Lin CT (2009) Formation of Nuclear Bodies of Arabidopsis CRY2 in response to Blue Light is associated with its Blue Light-Dependent Degradation. *Plant Cell* 21:118-130.

Zoltowski BD and Gardner KH (2011) Tripping the Light Fantastic: Blue-Light Photoreceptors as Examples of Environmentally Modulated Protein-Protein Interactions. *Biochemistry* 50:4-16.

Zuo Z, Liu H, Liu B, Liu X, and Lin C (2011) Blue Light-Dependent Interaction of CRY2 with SPA1 Regulates COP1 activity and Floral Initiation in Arabidopsis. *Current biology* 21:841-847.